

**Groundwater Resources Program
Climate and Land Use Change Research & Development**

Simulation of Climate-Change Effects on Streamflow, Lake Water Budgets, and Stream Temperature Using GSFLOW and SNTEMP, Trout Lake Watershed, Wisconsin



Scientific Investigations Report 2013–5159

Cover image:

Looking northwest over the Long Term Ecological Research Lakes in the Trout Lake Watershed. (Photograph by Dr. Carl J. Bowser, University of Wisconsin-Madison, September 29, 1999)

Simulation of Climate-Change Effects on Streamflow, Lake Water Budgets, and Stream Temperature Using GSFLOW and SNTEMP, Trout Lake Watershed, Wisconsin

By Randall J. Hunt, John F. Walker, William R. Selbig, Stephen M. Westenbroek, and R. Steven Regan

Groundwater Resources Program
Climate and Land Use Change Research & Development

Scientific Investigations Report 2013–5159

U.S. Department of the Interior
U.S. Geological Survey

U.S. Department of the Interior
SALLY JEWELL, Secretary

U.S. Geological Survey
Suzette M. Kimball, Acting Director

U.S. Geological Survey, Reston, Virginia: 2013

For more information on the USGS—the Federal source for science about the Earth, its natural and living resources, natural hazards, and the environment, visit <http://www.usgs.gov> or call 1–888–ASK–USGS.

For an overview of USGS information products, including maps, imagery, and publications, visit <http://www.usgs.gov/pubprod>

To order this and other USGS information products, visit <http://store.usgs.gov>

Any use of trade, firm, or product names is for descriptive purposes only and does not imply endorsement by the U.S. Government.

Although this information product, for the most part, is in the public domain, it also may contain copyrighted materials as noted in the text. Permission to reproduce copyrighted items must be secured from the copyright owner.

Suggested citation:

Hunt, R.J., Walker, J.F., Selbig, W.R., Westenbroek, S.M., and Regan, R.S., 2013, Simulation of climate-change effects on streamflow, lake water budgets, and stream temperature using GSFLOW and SNTMP, Trout Lake Watershed, Wisconsin: U.S. Geological Survey Scientific Investigations Report 2013–5159, 118 p., <http://pubs.usgs.gov/sir/2013/5159/>.

Contents

Abstract.....	1
Introduction.....	2
Purpose and Scope	3
Site Description and Hydrologic Setting.....	3
GSFLOW Groundwater/Surface-Water Modeling Approach.....	3
Brief Description of Groundwater Model Construction	5
Brief Description of Surface-Water Model Construction	6
Considerations for Coupled Groundwater/Surface-Water Model Design.....	7
Considerations for Coupled Groundwater/Surface-Water Model Calibration.....	8
SNTEMP Temperature Model Description, Construction, and Calibration.....	9
Climate-Change Scenario Construction	10
Results and Discussion.....	12
GSFLOW Coupled Hydrologic Flow Model	12
SNTEMP Stream Temperature Model.....	16
Climate-Change Effects	19
Changes to Growing-Season Length.....	19
Changes to Basin-Scale Hydrologic Flows and Storage	20
Changes to Streamflow	22
Changes to Lake Water Budgets.....	25
Seepage Lakes	25
Drainage Lakes	25
Changes to Stream Temperature	31
GSFLOW and SNTEMP Limitations and Assumptions.....	32
Summary.....	33
Acknowledgments	33
References Cited.....	34
Appendix 1. Groundwater Model Construction.....	37
Appendix 2. Surface-Water Model Construction.....	45
Appendix 3. Model Calibration	55
Appendix 4. Temperature Model Construction and Calibration	75
Appendix 5. WEBB and LTER Data Collection (1991–2011)	85
Appendix 6. Calibration Results	89

Figures

1. Map showing location of Trout Lake Watershed in Wisconsin, showing streamflow-gaging stations and one miscellaneous measurement site	4
2. Diagram showing MODFLOW inset model of the Trout Lake area, calibration data-collection locations, and land-surface elevation	5
3. Map showing hydrologic response units generated for the Trout Lake PRMS model	7
4. Schematic showing conceptualization of sequentially linked calibration of separate uncoupled surface-water and groundwater models (modified from Hunt and others, 2009)	9
5. Graphs showing climate forcings from the Wisconsin Initiative on Climate Change Impacts (WICCI) downscaled data for 6 GCMs. The range of results for A1B and B1 emission scenarios represents all 6 GCMs; the range of the A2 emission scenario is from 5 GCMs.....	11
6. Graphs showing simulated flows for the Trout Lake Watershed (1999–2007). <i>A</i> , Daily overland flows. <i>B</i> , Log daily flows.....	14
7. Graph showing measured (symbols) and simulated (line) lake stages for two adjacent seepage lakes.....	15
8. Graph showing simulated watershed average lake precipitation and lake evaporation during 1999–2006	15
9. Graph showing basinwide simulated changes in volume of water stored in the unsaturated zone and rate of groundwater recharge	16
10. Graphs showing daily variation in simulated and observed daily mean stream temperatures in Stevenson, North, and Upper Allequash Creeks, April–September 2002.....	17
11. Graph showing comparison between simulated and observed daily mean stream temperatures for Stevenson, North, and Upper Allequash Creeks, April–September 2002.....	18
12. Graph showing difference between observed and simulated daily mean stream temperature in Stevenson, North, and Upper Allequash Creeks, April–September 2002.....	18
13. Graph showing climate-change-related change in growing-season length, defined as the difference between the date of the first killing frost in the fall and the date of the last killing frost in the spring	19
14. Graphs showing climate-change scenario results for simulations of precipitation form, snowpack, and snowmelt.....	20
15. Graphs showing climate-change scenario results for potential and actual evapotranspiration and the resulting watershedwide average soil moisture	21
16. Graph showing climate-change scenario results for watershedwide average recharge to the groundwater system.....	22

17. Graphs showing climate-change results for streamflow-gaging station 05357206, Allequash Creek Middle Site, showing total streamflow and base flow.....	22
18. Graphs showing climate-change results for streamflow-gaging station 05357215, Allequash Creek at County Highway M, showing total streamflow and base flow.....	23
19. Graphs showing climate-change results for streamflow-gaging station 05357225, Stevenson Creek at County Highway M, showing total streamflow and base flow.....	23
20. Graphs showing climate-change results for streamflow-gaging station 05357230, North Creek at Trout Lake, showing total streamflow and base flow.....	24
21. Graphs showing climate-change results for streamflow-gaging station 05357245, Trout River at Trout Lake, showing total streamflow and base flow	24
22. Graphs showing climate-change simulations for Crystal Lake showing net annual components of the hydrologic budget normalized by lake area and related annual lake stage	26
23. Graphs showing climate-change simulations for Big Muskellunge Lake showing net annual components of the hydrologic budget normalized by lake area and related annual lake stage	27
24. Graphs showing climate-change simulations for Sparkling Lake showing net annual components of the hydrologic budget normalized by lake area and related annual lake stage	28
25. Graphs showing climate-change simulations for Allequash Lake showing net annual components of the hydrologic budget normalized by lake area and related annual lake stage	29
26. Graphs showing climate-change simulations for Trout Lake showing net annual components of the hydrologic budget and normalized by lake area related annual lake stage	30
27. Graphs showing climate-change simulations showing annual average stream temperatures for Stevenson, North, and Upper Allequash Creeks	31

Tables

1. Selected General Circulation Models (GCMs) used to simulate future climate conditions.....	10
2. Selected emission scenarios used to simulate future climate conditions	11
3. Average areal precipitation and recharge rate for the Trout Lake model domain reported by the calibrated GSFLOW model.....	13
4. Analysis of fit between simulated and observed daily mean stream temperatures at calibration points in SNTMP for April through September 2002	16

Conversion Factors

Multiply	By	To obtain
Length		
centimeter (cm)	0.3937	inch (in.)
meter (m)	3.281	foot (ft)
kilometer (km)	0.6214	mile (mi)
Area		
square kilometer (km ²)	247.1	acre
square kilometer (km ²)	0.3861	square mile (mi ²)
Precipitation and flow rate		
centimeter per year (cm/yr)	0.3937	inch per year (in/yr)
inch per year (in/yr)	2.54	centimeter per year (cm/yr)
Hydraulic conductivity		
meter per day (m/d)	3.281	foot per day (ft/d)

Temperature in degrees Celsius (°C) may be converted to degrees Fahrenheit (°F) as follows:

$$^{\circ}\text{F}=(1.8\times^{\circ}\text{C})+32$$

Temperature in degrees Fahrenheit (°F) may be converted to degrees Celsius (°C) as follows:

$$^{\circ}\text{C}=(^{\circ}\text{F}-32)/1.8$$

Vertical coordinate information is referenced to the National Geodetic Vertical Datum of 1929 (NGVD 29).

The terms "altitude" and "elevation," as used in this report, refer to distance above the vertical datum.

Simulation of Climate-Change Effects on Streamflow, Lake Water Budgets, and Stream Temperature Using GSFLOW and SNTMP, Trout Lake Watershed, Wisconsin

By Randall J. Hunt, John F. Walker, William R. Selbig, Stephen M. Westenbroek, and R. Steven Regan

Abstract

Although groundwater and surface water are considered a single resource, historically hydrologic simulations have not accounted for feedback loops between the groundwater system and other hydrologic processes. These feedbacks include timing and rates of evapotranspiration, surface runoff, soil-zone flow, and interactions with the groundwater system. Simulations that iteratively couple the surface-water and groundwater systems, however, are characterized by long run times and calibration challenges. In this study, calibrated, uncoupled transient surface-water and steady-state groundwater models were used to construct one coupled transient groundwater/surface-water model for the Trout Lake Watershed in north-central Wisconsin, USA. The computer code GSFLOW (Groundwater/Surface-water FLOW) was used to simulate the coupled hydrologic system; a surface-water model represented hydrologic processes in the atmosphere, at land surface, and within the soil-zone, and a groundwater-flow model represented the unsaturated zone, saturated zone, stream, and lake budgets. The coupled GSFLOW model was calibrated by using heads, streamflows, lake levels, actual evapotranspiration rates, solar radiation, and snowpack measurements collected during water years 1998–2007; calibration was performed by using advanced features present in the PEST parameter estimation software suite.

Simulated streamflows from the calibrated GSFLOW model and other basin characteristics were used as input to the one-dimensional SNTMP (Stream-Network TEMPerature) model to simulate daily stream temperature in selected tributaries in the watershed. The temperature model was calibrated to high-resolution stream temperature time-series data measured in 2002. The calibrated GSFLOW and SNTMP models were then used to simulate effects of potential climate change for the period extending to the year 2100. An ensemble of climate models and emission scenarios was evaluated. Downscaled climate drivers for the period 2010–2100 showed increases in maximum and minimum temperature over the scenario period. Scenarios of future precipitation did not show a monotonic trend like temperature. Uncertainty in the

climate drivers increased over time for both temperature and precipitation.

Separate calibration of the uncoupled groundwater and surface-water models did not provide a representative initial parameter set for coupled model calibration. A sequentially linked calibration, in which the uncoupled models were linked by means of utility software, provided a starting parameter set suitable for coupled model calibration. Even with sequentially linked calibration, however, transmissivity of the lower part of the aquifer required further adjustment during coupled model calibration to attain reasonable parameter values for evaporation rates off a small seepage lake (a lake with no appreciable surface-water outlets) with a long history of study. The resulting coupled model was well calibrated to most types of observed time-series data used for calibration. Daily stream temperatures measured during 2002 were successfully simulated with SNTMP; the model fit was acceptable for a range of groundwater inflow rates into the streams.

Forecasts of potential climate change scenarios showed growing season length increasing by weeks, and both potential and actual evapotranspiration rates increasing appreciably, in response to increasing air temperature. Simulated actual evapotranspiration rates increased less than simulated potential evapotranspiration rates as a result of water limitation in the root zone during the summer high-evapotranspiration period. The hydrologic-system response to climate change was characterized by a reduction in the importance of the snow-melt pulse and an increase in the importance of fall and winter groundwater recharge. The less dynamic hydrologic regime is likely to result in drier soil conditions in rainfed wetlands and uplands, in contrast to less drying in groundwater-fed systems. Seepage lakes showed larger forecast stage declines related to climate change than did drainage lakes (lakes with outlet streams). Seepage lakes higher in the watershed (nearer to groundwater divides) had less groundwater inflow and thus had larger forecast declines in lake stage; however, groundwater inflow to seepage lakes in general tended to increase as a fraction of the lake budgets with lake-stage decline because inward hydraulic gradients increased. Drainage lakes were characterized by less simulated stage decline as reductions

in outlet streamflow offset losses to other water flows. Net groundwater inflow tended to decrease in drainage lakes over the scenario period.

Simulated stream temperatures increased appreciably with climate change. The estimated increase in annual average temperature ranged from approximately 1 to 2 degrees Celsius by 2100 in the stream characterized by a high groundwater inflow rate and 2 to 3 degrees Celsius in the stream with a lower rate. The climate drivers used for the climate-change scenarios had appreciable variation between the General Circulation Model and emission scenario selected; this uncertainty was reflected in hydrologic flow and temperature model results. Thus, as with all forecasts of this type, the results are best considered to approximate potential outcomes of climate change.

Introduction

Although groundwater and surface water are considered a single resource (for example, Leopold, 1974; Winter and others 1998), simulations involving this combined resource commonly do not explicitly couple the two systems. As a result, it is typical for simulations of the effects of climate variability on water resources to approximate just one of the two systems (for example, Zarriello and Ries, 2000; Ely, 2006), even though interaction of one with the other might be important. For example, a climate-change scenario can be as simple as applying some percentage reduction in the rate of steady-state groundwater recharge (for example, Cheng 1994); such a formulation, however, cannot account for either the inter-annual temporal characteristics of climate change or the feedback loops between the groundwater system and other hydrologic processes. Groundwater and surface-water models can be loosely linked outside of the models (for example, Hunt and Steuer, 2000; Steuer and Hunt, 2001); but often, only time-averaged/long-term simulations are tractable, and such simulations may not include enough inter-annual characteristics and related system dynamics to be useful for many water-resources questions. More computationally expensive coupled hydrologic models, on the other hand, can include various hydrologic feedback pathways and, therefore, can more fully encompass the processes and related dynamics that may augment or mitigate the effect of potential future hydrologic stress. These processes include the timing and rates of evapotranspiration, surface runoff, soil-zone flow, and interactions with the stream network, lakes, and groundwater system.

Coupled models can use a fully integrated approach (for example, three-dimensional Richards' equation) but require a much finer spatial grid and smaller time steps than typically are used to simulate saturated hydrologic flow systems (Markstrom and others, 2008). The high computational burden

and data requirements of fully integrated approaches limit their applicability for simulating watershed-scale flow over societally relevant time periods (years to tens of years or more). An efficient alternative to the fully integrated coupled-model approach is to simulate unsaturated flow, assuming that the dominant direction of flow within the unsaturated zone is vertical when averaged over the grid scale typical of a watershed model (Harter and Hopmans, 2004; Niswonger and others, 2006). By using this type of approximation, equations can be formulated to simulate flow and storage in the various regions of the watershed (that is, soil, unsaturated, and saturated zones) with the goal of attaining a compromise between computational efficiency and process accuracy.

This "coupled-regions" approach was implemented in the recently released software GSFLOW (Groundwater/Surface-water FLOW) (Markstrom and others, 2008). GSFLOW is an integration of the U.S. Geological Survey (USGS) Precipitation-Runoff Modeling System, PRMS (Leavesley and others, 1983; Leavesley and others, 2005), with versions of the USGS Modular Groundwater Flow Model MODFLOW-2005 (Harbaugh, 2005) and MODFLOW-NWT (Niswonger and others, 2011). In GSFLOW, separate equations are coupled to simulate (1) horizontal and vertical flow above land surface and through the soil zone, (2) gravity-driven, vertical flow through the unsaturated zone, and (3) three-dimensional groundwater flow through the saturated zone. GSFLOW uses physically based processes and empirical methods with user inputs of air temperature and snow/rain precipitation to simulate the distribution of precipitation into runoff, evapotranspiration, infiltration, groundwater flow, and surface-water flow. Because of its relative computational efficiency, GSFLOW can be applied to watershed-scale problems ranging from a few square kilometers to several thousand square kilometers and for time periods that range from months to several decades (Markstrom and others, 2008).

Decisions regarding the appropriate level of model simplification are facilitated by consideration of the model predictions of interest (Hunt and others, 2007; Simmons and Hunt, 2012). Such predictions often include not only water flows but also other societal relevant end-members that decision makers are charged with managing (Hunt and Wilcox, 2003; Hancock and others, 2009). The objectives for the model described herein included forecasts of the effects of climate-change scenarios on streamflow and stream temperature. Therefore, streamflow results from the coupled GSFLOW model were linked to an SNTMP model (Sream-Network TEMPerature; Bartholow, 1991), a steady-state, one-dimensional heat transport model that predicts daily mean and maximum temperatures as a function of stream distance and environmental heat flux. This approach allows propagation of potential temperature changes in the atmosphere to coldwater streams and associated fisheries.

Purpose and Scope

This report describes the construction, calibration, and scenario testing of a GSFLOW coupled groundwater and surface-water model and SNTTEMP model for the Trout Lake Watershed, north-central Wisconsin (Wis.), USA (fig. 1). The GSFLOW model simulates atmospheric, surface, and subsurface elements of the hydrologic cycle including rainfall, snowmelt, evapotranspiration, interflow, streamflow, base flow, and groundwater flow. Coupled groundwater/surface-water flow output was used to construct the stream-temperature model. The calibrated hydrologic/stream-temperature models were then used to simulate potential climate-change effects on streamflow, lake water budgets, and stream temperature.

The purpose of the study leading up to the report was to develop a quantitative tool to simulate historic, current, and potential future, streamflows and stream temperatures in the Trout Lake Watershed in Vilas County, Wis. (fig. 1). Because the streamflow and issues related to streamflow are a function of both groundwater and surface water, the focus is on a coupled groundwater/surface-water system. The coupled flow model outputs were linked to an associated stream-temperature model intended to inform questions related to stream ecology (for example, Hunt and others, 2006).

The report includes: (1) a brief description of construction and calibration of the coupled groundwater flow and surface-water flow model, (2) considerations required by coupled modeling as compared to uncoupled simulations, (3) construction and calibration of a stream-temperature model that uses results from the calibrated coupled groundwater/surface-water model, and (4) forecasts of stream and lake hydrologic changes and stream temperature for a set of potential climate scenarios. Appendixes are included to give a more extensive presentation of model construction and calibration approaches (appendixes 1-4), data-collection (appendix 5), and calibration results (appendix 6). The models were constructed by using daily or larger time increments; thus, “continuous” or “storm-mode” simulations of individual storm events were not in the scope of this work. In addition, because the tool is developed on the basis of watershed flows and not local hydraulic characteristics at any one location in the watershed, model results are reported as streamflow (discharge) and not local stream stage or flood peak.

Site Description and Hydrologic Setting

The Trout Lake Watershed (fig. 1) is in the Northern Highlands Lake District and is the site of the North Temperate Lakes Long Term Ecological Research (NTL-LTER) site (Magnuson and others, 2006) and the U.S. Geological Survey’s Trout Lake Water, Energy, and Biogeochemical

Budgets (WEBB) research watershed (Walker and Bullen, 2000). Groundwater-derived base flow in the region accounts for more than 80 percent of total streamflow (Gebert and others, 2011). Streams in the area are immature first- and second-order streams, with high flows dominated by spring snowmelt. The aquifer consists of 40 to 60 meters (m) of unconsolidated Pleistocene glacial deposits, mostly glacial outwash sands and gravel (Attig, 1985). Given land-surface elevations and groundwater heads, the unsaturated zone thickness ranges from 0 to about 50 m. Saturated horizontal hydraulic conductivities are estimated to average about 10 meters per day (m/d) (Okwueze, 1983; Hunt and others, 1998). Vertical anisotropy in hydraulic conductivity is relatively small, with the ratio of horizontal to vertical conductivity ranging from 4:1 to 8:1 at a scale of a couple of meters (Kenoyer, 1988). The lakes occupy depressions in the glacial deposits that may penetrate more than 80 percent of the aquifer thickness. Annual precipitation averages about 81.5 centimeters per year (cm/yr) (National Climatic Data Center, 2004); average groundwater recharge is estimated to be 27 cm/yr (Hunt and others 1998) and has been estimated to range from about 15 to 50 cm/yr at local areas within the watershed (Dripps and others 2006). Annual evaporation from the lakes is about 54 cm/yr (Krabbenhoft and others 1990; Wentz and Rose 1991). Lakes are well connected to the groundwater system, and many lakes are flowthrough lakes with respect to groundwater.

GSFLOW Groundwater/Surface-Water Modeling Approach

The models described herein have been constructed for use in future studies to address a variety of research problems including the effects of climate change on lakes, streams, and groundwater. Thus, the predictions of interest for this work can include (1) lake stages, (2) streamflow, (3) groundwater flux and its relation to lakes, (4) residence and travel times, and (5) lake-water stable isotope plume depth (Pint and others, 2003; Hunt and others, 2006). Groundwater and surface water are considered a single resource, and the groundwater/surface-water code used here is a fully coupled hydrologic model that includes hydrologic feedbacks and fully encompasses the processes and related dynamics that may augment or mitigate the effect of hydrologic stress. These processes include timing and rates of evapotranspiration, surface runoff, soil-zone flow, and interactions with the groundwater system. The code that implements these processes is called GSFLOW (Groundwater/Surface-water FLOW; Markstrom and others, 2008). Because a fully coupled model can have long runtimes, however, uncoupled models of the groundwater and surface-water system were constructed before the fully coupled model calibration, as described below.

4 Simulation of Climate-Change Effects Using GSFLOW and SNTMP, Trout Lake Watershed, Wisconsin

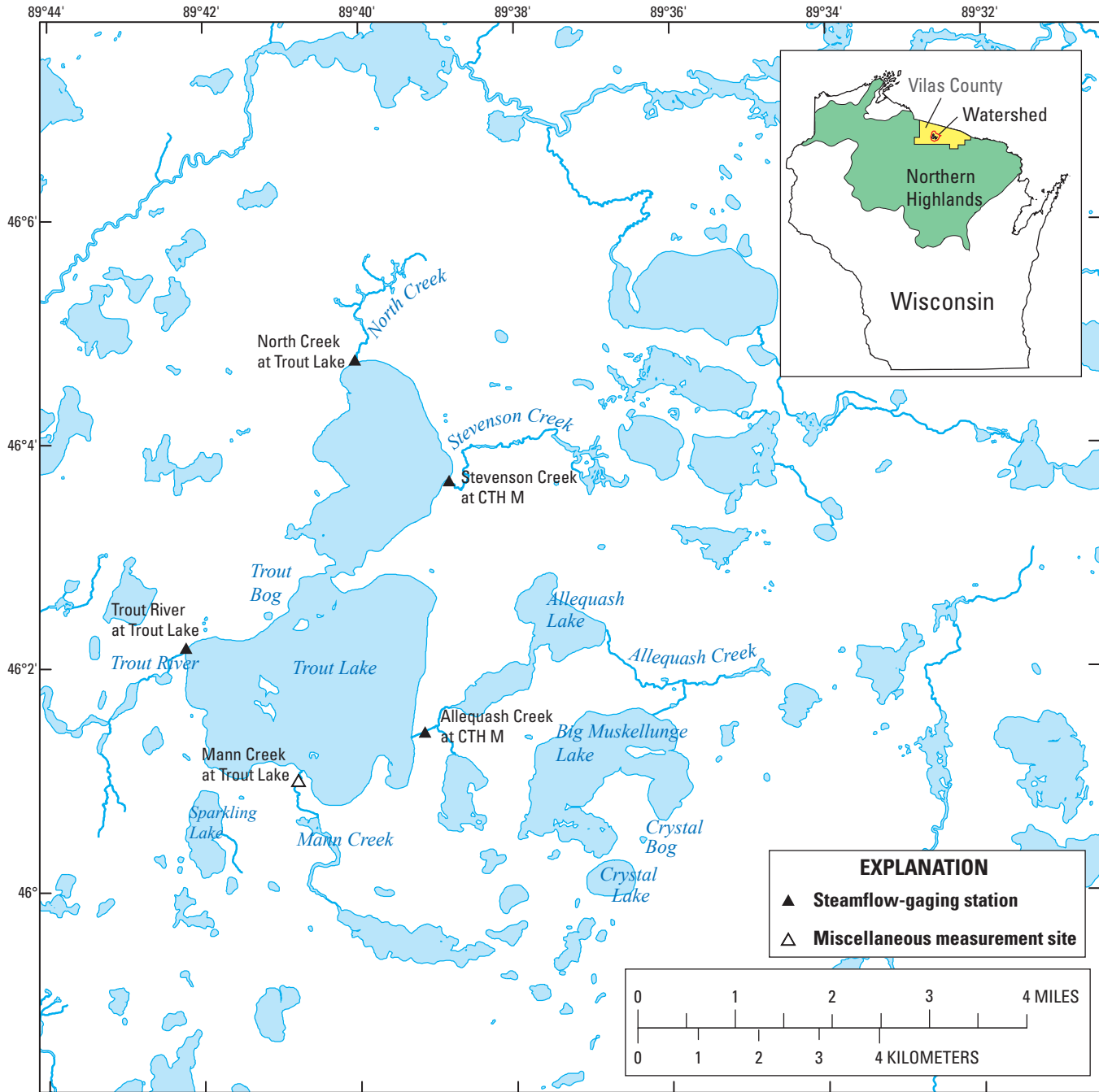


Figure 1. Location of Trout Lake Watershed in Wisconsin, showing streamflow-gaging stations and one miscellaneous measurement site.

Brief Description of Groundwater Model Construction

The Trout Lake Watershed has been the focus of several previous groundwater modeling studies (Cheng, 1994; Hunt and others, 1998; Anderson and Champion, 2000; Pint, 2002; Pint and others, 2003; John, 2005; Hunt and others, 2008; Muffels, 2008; Walker and others, 2009) that represent stages in the development and refinement of a watershed-scale groundwater model that has been used to address a variety of research problems, including the effects of climate change. We modified the model of Muffels (2008) and Hunt and others (2008); the groundwater model construction is described briefly here and in detail in appendix 1.

An inset MODFLOW-2005 (Harbaugh, 2005) finite-difference model was extracted from a regional analytic element model constructed for the Trout Lake area (Hunt and others, 1998). The regional model was used to assign constant flux boundary conditions along the perimeter of the inset model (fig. 2); the perimeter boundaries were set distant from the area of interest therefore the same analytic-element derived perimeter boundary conditions were used for all simulations. The inset grid consists of 230 rows and 240 columns, with each grid cell 75 m on a side. Model layering is the same as that of Muffels (2008): six layers, two for each of the glacial

sediment units of Attig (1985). The model was initially used in steady state for initial calibration and then used transiently for fully coupled model calibration. Hydraulic conductivity within the model domain was specified by using pilot points (Doherty, 2003) according to the design and layout of Muffels (2008). Parameterization of each aquifer layer was represented by 218 horizontal and 218 collocated vertical hydraulic conductivity pilot points, for a model total of 2,616 pilot points. In the inset model of the watershed, all streams inside the area of interest (defined here as “nearfield”) were simulated with the Streamflow Routing (SFR2) Package (Niswonger and Prudic, 2005), to allow accounting of streamflow. The Lake (LAK) Package (Merritt and Konikow, 2000) was used to simulate 30 nearfield seepage and drainage lakes. In the space outside the area of interest (defined as “farfield”), streams and lakes were simulated by means of the General Head Boundary (GHB) head-dependent flux boundary condition because GSFLOW does not support the River (RIV) Package commonly used in regional and uncoupled groundwater flow models. Simulation of recharge to the groundwater system is automatically derived from the surface-water-model soil zone to the Unsaturated Zone Flow (UZF) Package. The reader is referred to Harbaugh (2005) and Markstrom and others (2008) for detailed description of the MODFLOW packages used.

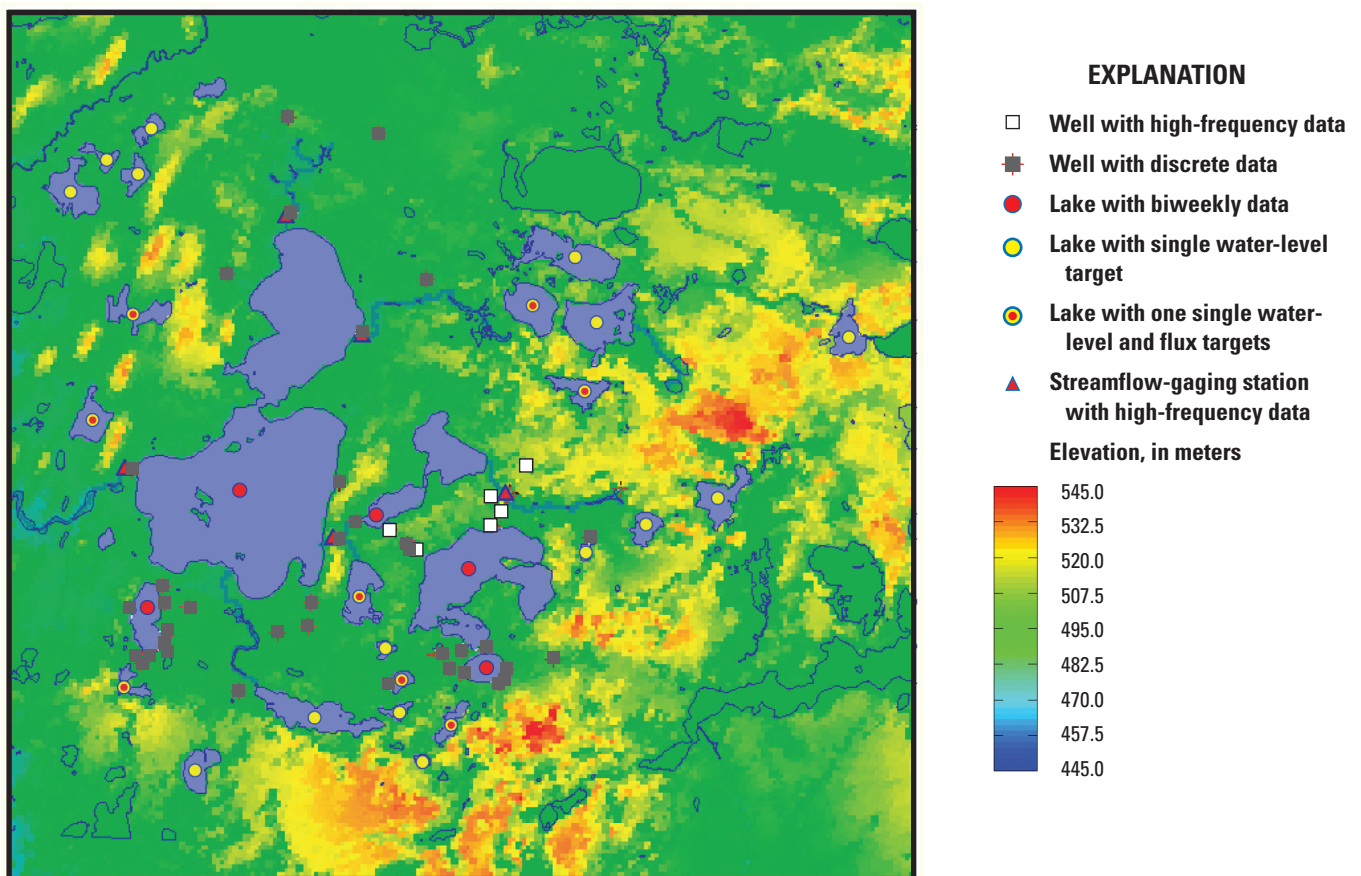


Figure 2. MODFLOW inset model of the Trout Lake area showing calibration data-collection locations and land-surface elevation.

Hunt and others (2008) note two capabilities of the UZF Package that are important for model calibration in general and the Trout Lake Watershed in particular. First, water that leaves the root zone is routed through the unsaturated zone to the water table rather than being directly applied to the water table. This approach allows simulation of lags and mixing between infiltration events leaving the root zone before becoming water-table recharge. Second, the UZF Package can generate and route runoff to surface-water features in areas where groundwater is at or near land surface or during periods when infiltration rates exceed the soil's ability to transmit the water. This capability allows for realistic simulations of groundwater/surface-water interaction dynamics and is superior to the overpressurizing of the groundwater system that can result from direct application of infiltration to the water table.

Brief Description of Surface-Water Model Construction

An initial surface-water model of the watershed was described in Markstrom and others (2012). An overview of current model construction and parameterization is given below; details are contained in appendix 2. Geographic Information System (GIS) datasets were used as the basis for generation of model subareas and parameters required by the surface-water model. The surface-water model domain was split into discrete subareas, known as hydrologic response units (HRUs). Each HRU is piecewise-constant; that is, it is considered internally homogeneous with respect to the physical characteristics assigned to it. Therefore, only one value for a given characteristic (for example, slope, vegetation, land use, or soil type) is specified for each HRU. The HRU configuration used in the Trout Lake model was generated by use of the GIS Weasel (Viger and Leavesley, 2007). A 30-m digital elevation model of Wisconsin (Gesch and others, 2002) was clipped, rotated, and resampled to coincide with the boundaries of the groundwater model grid (see appendix 2 for details on the grid rotation). Because the hydrologic system is dominated by groundwater flow, water-table altitudes were used, along with land-surface elevations, to construct the drainage network represented by the final distribution of HRUs.

The flow-direction grid generated by the GIS Weasel was processed to generate a stream network and an initial two-plane (right-bank/left-bank) HRU map. This process was repeated by using a water-table map derived from output from a MODFLOW model constructed previously for the study area (Muffels, 2008). The two-plane HRU maps were merged and further subdivided in lake and wetland areas to separate the near-stream areas from the upland areas. The result was a model consisting of 146 HRUs (fig. 3).

The PRMS model allows for surface flow to be routed to downslope HRUs and stream segments. Each connection between a pair of HRUs or between an HRU and a stream segment must be specified explicitly. These connections were generated by means of the GIS Weasel (Viger and Leavesley,

2007), using the flowlines derived from the land-surface topography. The resulting surface runoff routing diagram contains 145 connections. The PRMS model also allows for flow from an HRU groundwater reservoir to be routed to other groundwater reservoirs underlying adjacent HRUs by using modeler-specified routing connections. Similar to the surface-flow routing, the groundwater routing connections were generated by means of the GIS Weasel (Viger and Leavesley, 2007), using the flowlines derived from the water-table surface. The resulting groundwater flow-routing diagram contains 233 connections. This PRMS capability is not required in the fully coupled simulations because GSFLOW uses MODFLOW to simulate the groundwater flow system.

The PRMS model contains nearly 100 potential calibration parameter values that can be used to simulate user-identified features of a specific area of study, but not all parameters have the same importance. Initial parameter values were generated by means of the GIS Weasel (Viger and Leavesley, 2007). The GIS Weasel used a digital elevation model to generate HRUs and other physical model parameters such as slope and aspect; HRUs were intersected with nationwide soil and land-use GIS datasets to define HRU hydrologic characteristics. Because of the relative homogeneity of soils and geology in the Trout Lake Watershed, spatial variability of the soil-zone parameters that control runoff was simplified. HRUs were aggregated into eight subwatersheds and a far-field area (fig. 3). Initial parameter estimates derived by the GIS Weasel for each HRU were averaged over the subwatersheds, and each HRU within a subwatershed was then assigned the average initial value.

The PRMS model uses climate data as input to the hydrologic system; daily values of precipitation and temperature (maximum and minimum) are required inputs. Solar radiation based on a cloud-cover algorithm and potential evapotranspiration were calculated by the model and calibrated to observed data rather than specified as input into the model. The closest National Weather Service Cooperative (COOP) weather station is at Rest Lake (National Weather Service station ID 477092), approximately 10 km northwest of Trout Lake. However, to address issues of missing data and spatial variability of precipitation, data from five additional COOP weather stations were also input to the model (appendix 2). The temperature and precipitation data from the six weather stations were distributed to the HRUs by using an algorithm based on the inverse of distance from the HRU centroid and the location of each weather station (see appendix 2 for details). In a temperate climate, the growing season determines the period when evapotranspiration occurs. The beginning and end of the growing season for the calibration period were preprocessed by using an algorithm described in Christiansen and others (2011) and documented in Markstrom and others (2012). An assumed killing-frost temperature of -2.2 degrees Celsius ($^{\circ}\text{C}$), or 28 degrees Fahrenheit ($^{\circ}\text{F}$), was used for each HRU. During model calibration, the growing season beginning and end dates for each HRU were determined as average values for the calibration period.

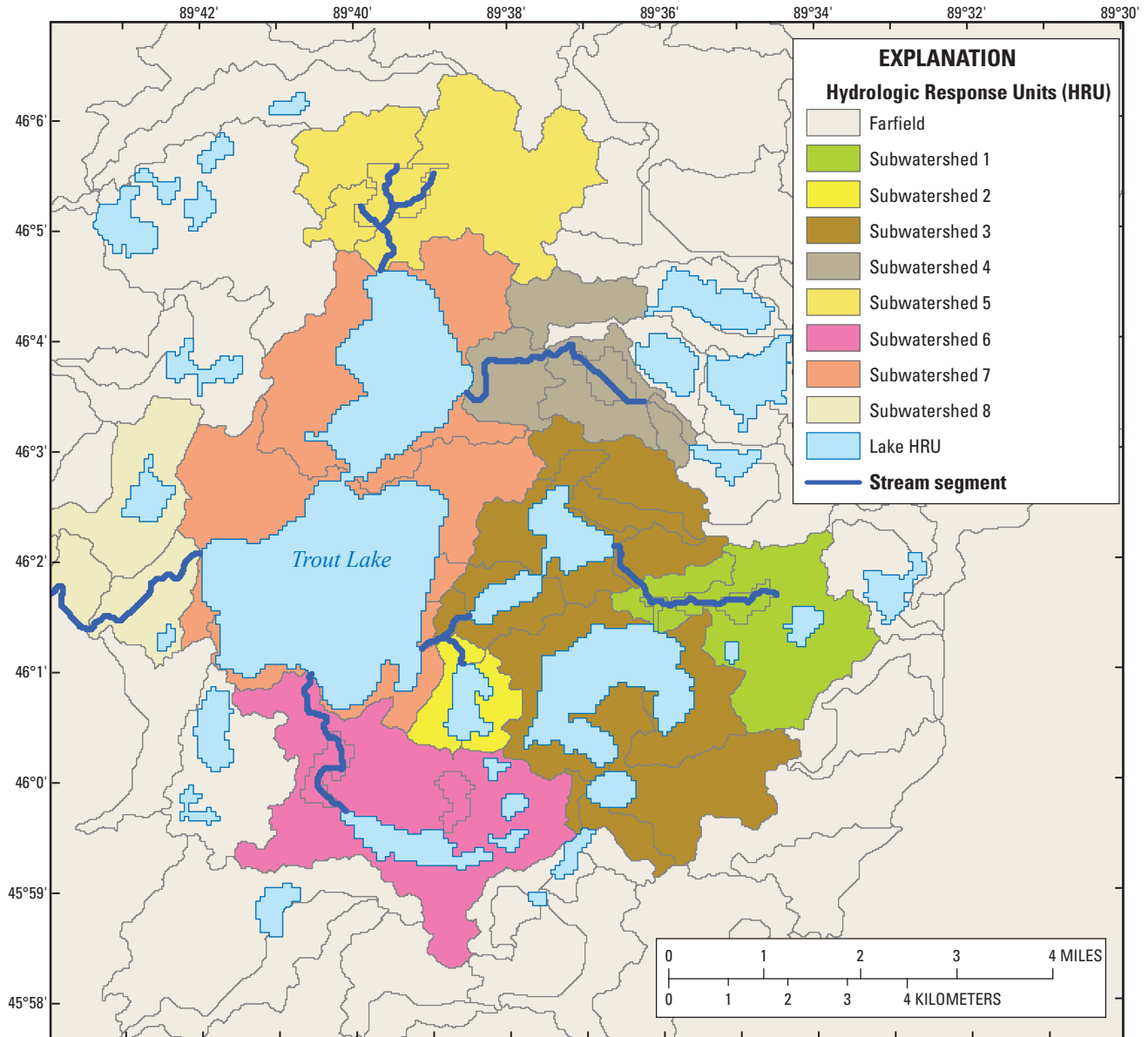


Figure 3. Hydrologic response units generated for the Trout Lake PRMS model; dark blue lines represent tributary streams to Trout Lake.

Considerations for Coupled Groundwater/Surface-Water Model Design

Many watershed numerical models are developed for mountainous areas and define the watershed of interest as that delineated by surface topography. Although such models are acceptable for many high-relief settings, they are problematic for many areas where the “groundwatershed” and surface watershed may not align (as described by Winter and others, 2003). In low-relief terrain such as that of the glaciated Midwest of the United States, surface-water and groundwater divides can differ from one another; such a misalignment of the groundwatershed and surface watershed was noted in the Trout Lake area by Hunt and others (1998). Therefore, unlike

uncoupled models, the simulated watershed of interest in a coupled model includes areas of both the surface watershed and groundwatershed. The groundwatershed, however, is not well known in most cases; thus, a larger groundwater-flow model is commonly used to solve for physically based perimeter boundaries for a smaller inset model of the groundwatershed.

The edges of the inset model should be sufficiently distant from the nearfield such that the area of interest is shielded from artifacts from the coarse regional representation of the flow system. This inset approach results in (1) an overall domain for the coupled model that is a rectangular grid typical of a MODFLOW model rather than the irregular shape typical of a surface-water model, and (2) a groundwater

domain that is larger than the surface watershed because the rectangular grid includes the entire groundwater and surface watershed for the watershed of interest, as well as areas not included in either but needed to simulate representative boundary conditions at the inset perimeter. This larger extent in itself is not problematic because GSFLOW is designed to simulate adjacent watersheds; however, this can confound simple representations of output because GSFLOW currently reports a total mass balance for the entire model domain. Thus, additional postprocessing may be required to fully distribute the total model flows between the watershed of interest and the remainder of the simulated area.

In addition to different spatial model domains, the timing and magnitude of transient response in the groundwater and surface-water systems also are different. The groundwater system can be thought of as a “low-pass filter” that removes much of the short-term transient dynamics and leaves the resilient long-term system dynamics, whereas the surface-water system is characterized by more high-frequency transience. As a result, potential problems can arise from choices of model simplification when the surface-water system is coupled to the groundwater system. Appropriate determination of salient simplification is especially important because only a small subset of the many parameters that may be employed by a surface-water (or coupled) model can be estimated on the basis of most streamflow calibration datasets (see, for example, Beven and Freer, 2001; Doherty and Hunt, 2009). There also may be concerns with surface-water datasets that contain measurement noise and redundant information because these types of datasets commonly include many more observations than a groundwater dataset—especially with respect to the temporal density of the observations (for example, Hunt and others, 2009).

Finally, the natural system has a hydrologic “memory” that retains the effects of antecedent climatic and hydrologic conditions that preceded the simulation start date. To account for the effect of conditions occurring before the simulated period of interest, a model initialization or “spin-up” period is used. During the spin-up period, representative model inputs are used to generate a dynamic equilibrium that is more representative of actual conditions at the start of the period of interest. The uncoupled surface-water (PRMS-only) mode of GSFLOW commonly uses a 1-year spin-up well suited for simulating observations with short hydrologic memory, such as snowpack accumulation (Hunt and others, 2009), which is completely reset to zero in temperate climates each year. The uncoupled surface-water model also uses linear groundwater reservoirs for simulating the groundwater system, which are also suited for a 1-year model spin-up.

The groundwater component of the fully coupled model, however, uses MODFLOW to represent subsurface storage. Many groundwater systems are characterized by a variably thick unsaturated zone and variable subsurface storage, thus

requiring longer spin-up periods. Indeed, if a calibration observation integrates multiple years (such as lakes that incorporate a range of transient fluxes over its residence time), it can take a multiple-year spin-up before the dynamics of the system are well represented in the model (Hunt and others, 2009). Thus, the goal for coupled model calibration is to have a sufficiently long spin-up such that parameter calibration does not simply reflect poor simulation of initial conditions. Long spin-up periods, however, add proportionally to the total run time of the coupled model.

Considerations for Coupled Groundwater/Surface-Water Model Calibration

Daily data for water years 1998–2007 (October 1, 1997 through September 30, 2007) (appendix 5) were used for all transient model calibration and were processed by the time-series processor TSPROC (Westenbroek and others, 2012); averages of measurements for these periods were used for calibration of the uncoupled steady-state groundwater model. All hydrologic models were calibrated by using the universal parameter estimation computer code PEST (Doherty, 2010a,b). The PEST optimization algorithm automatically adjusts coupled-model input parameters in a series of model runs. After each model run, simulated model outputs such as solar radiation, groundwater levels, vertical head gradients, and streamflows were automatically compared to observed equivalents measured in the field. Model runs continued until a best fit between simulated and measured targets was attained. Details on the calibration methodologies of the sequentially linked and coupled models are provided in appendix 3, and results of each calibration exercise are given in appendix 6. A brief overview of coupled model-calibration considerations follows.

Coupled simulations have run times that are much longer than if only an uncoupled groundwater or surface-water model is used. In many cases, forward model run times can become limiting for practical calibration. Moreover, many of the coupled-model calibration parameters are primarily associated with one of the two systems and therefore would seem to be appreciably informed by uncoupled runs. Therefore, the hope is that insight can be gained from an initial calibration of the faster, uncoupled run available from the “PRMS-only” and “MODFLOW-only” modes of GSFLOW (Markstrom and others, 2008). For the study described herein, this initial separate calibration of the uncoupled groundwater and surface-water models did not, however, provide a sufficiently accurate starting point for coupled model calibration because of mismatches in model structures, primarily with respect to the configuration of the recharge array. Therefore, a sequentially linked approach (Hunt and others, 2009) was employed (fig. 4).

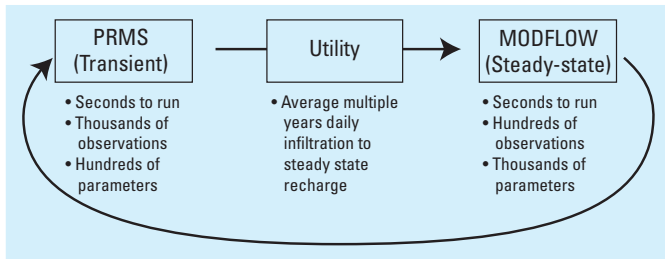


Figure 4. Conceptualization of sequentially linked calibration of separate uncoupled surface-water and groundwater models (modified from Hunt and others, 2009).

In the sequentially linked approach, transient PRMS-only results are translated by a software utility to create a steady-state infiltration/recharge array for the associated MODFLOW-only run. The translation occurs on the fly, and the PEST mode-run batch file includes calls for the PRMS-only, the translation utility, and MODFLOW-only programs sequentially. The resulting parameter-estimation formulation includes all surface-water transient observations (often in the thousands) and steady-state groundwater targets, as well as the majority of model parameters (also often in the thousands, especially with pilot points). Despite the inclusive nature of observations and parameters, the sequentially linked approach has run times much shorter than for the fully coupled model run. The respective optimal parameters are better starting points for calibration of the fully coupled model because the PRMS-only discretization directly informs the MODFLOW-only recharge/infiltration array. The Trout Lake sequentially linked calibration consisted of 2,768 adjustable parameters (appendix 3). This calibration was followed by final calibration in which most of the 2,768 parameters were fixed at their optimal values determined from sequentially linked calibration, and a subset of parameters important for water exchange between the groundwater and surface-water system (168 parameters) was estimated by using the fully coupled GSFLOW model.

SNTMP Temperature Model Description, Construction, and Calibration

A stream-temperature model was developed to use coupled flow model output to simulate daily mean stream temperatures at select tributaries to Trout Lake. This section briefly describes the model framework, data collection and synthesis, and calibration procedures for the stream-temperature model; appendix 4 provides a more extensive description.

The instream-water-temperature model SNTMP (Bartholow, 1991) was used to simulate stream temperatures in a subset of streams that drain into Trout Lake. SNTMP is a

one-dimensional heat-transport model that uses a successive steady-state approach to simulate daily mean and maximum temperatures as a function of stream distance and environmental heat flux. A heat-transport equation describes the downstream movement of heat energy in the water and actual exchange of heat energy between the water and its surrounding physical environment (Theurer and others, 1984). Net heat flux is calculated by using inputs describing meteorology, hydrology, stream geometry, and shade setting for a dendritic network of mainstem and tributary stream segments that compose the stream system of interest. The Trout Lake stream system was represented by three main tributaries: North Creek, Stevenson Creek, and Upper Allequash Creek (upstream of Allequash Lake). Each stream was discretized into two or more segments. Physical, meteorological, and hydrological characteristics of each segment are constant over the segment. Therefore, each stream segment assumes uniform width, groundwater accretion rate, and topographic and riparian vegetation conditions. Each stream segment requires a physical description of stream geometry, hydrology, and shading variables. Meteorological variables are considered more global in nature and were applied to all stream segments equally. In SNTMP, it is assumed that all input data, including meteorological and hydrological variables, can be represented by 24-hour averages (Bartholow, 1991). Many of the model input parameters were taken from published data sources; additional field data were collected to characterize the meteorological, hydrological, and stream-temperature parameters (see appendix 4).

An SNTMP model is composed of component modules that can be categorized into three broad categories of stream geometry, meteorology, and hydrology. Stream-geometry data consist of the network layout of the main stem and all tributaries, site elevations, stream widths, Manning's n values, and shade estimates. The width of the stream segment represents an average and was assumed to remain constant for all values of flow. Manning's n values were assumed to apply to all values of flow; estimates were initially based on reported ranges for natural channels and were varied during calibration of the model. Stream-shading parameters, such as vegetation height and density, were specified by using initial values measured in the field then adjusted during calibration. Meteorological data consist of measured solar radiation, air temperature, relative humidity, wind speed, and cloud cover. SNTMP uses only one set of meteorological data, which is applied to all stream segments. Air temperature, cloud cover, dust coefficients, and ground reflectivity were taken from existing published values (appendix 4). Default values were used for all other meteorological variables required by SNTMP. Hydrologic data consist of stream discharge and water temperatures. SNTMP requires both upstream discharge and temperature data for each modeled stream segment. For SNTMP calibration, daily mean discharge data were based on coupled GSFLOW simulation output or supporting measured discharge data when available. All future scenarios were run with GSFLOW simulated flows. Mean groundwater temperatures

were specified by using the shallow groundwater temperatures reported by Hunt and others (2006). Although measured at a single location within each stream, the measured groundwater temperatures were applied equally across each stream segment in the model. The time period April through September 2002 was selected for model calibration because it spans the longest continuous water temperature and discharge datasets at multiple locations throughout North, Stevenson, and Upper Allequash Creeks during the GSFLOW model-calibration period. After data processing and formatting for the SNTMP model, calibration consisted of fitting simulated daily mean stream temperatures to observations in the field. Calibration was achieved by trial-and-error adjustment of SNTMP input variables until agreement was reached between simulated and measured calibration locations.

Climate-Change Scenario Construction

Multiple General Circulation Models (GCMs) were used to obtain a range of potential future climatic conditions. Daily precipitation and temperature output from six GCMs documented in the Intergovernmental Panel on Climate Change (IPCC) Fourth Assessment Special Report on Emission Scenarios (2007) were considered (table 1). For each GCM, one current and three future scenarios were used (table 2). The GCM output was downscaled for the Trout Lake area by the Wisconsin Initiative on Climate Change Impacts (WICCI) (2011), which is a more recent downscaled dataset than previous climate scenarios constructed for the watershed (for example, Walker and others, 2012). GCM potential future climate conditions were reformatted for input to the GSFLOW model.

Decisionmakers in the Trout Lake Watershed are commonly concerned with three hydrologic issues: (1) changes to streamflow and temperature, (2) changes in lake water resources, and (3) changes in soil moisture. Thus, reporting of the climate scenario results is focused on these three outputs.

Initial conditions used for assessing hydrologic changes were derived from the GSFLOW model calibrated to heads and flows collected during 1993–2007. For the WICCI climate scenarios, the first 20 years of the 1961–2100 simulation period were discarded to ensure that sufficient spin-up time was used to obtain a representation of dynamic equilibrium in the groundwater/surface-water systems.

The climate forcings for the six GCMs and the three emissions scenarios are depicted in figure 5, where solid lines represent the 10-year moving average across the six GCMs for each emission scenario and shaded areas represent the 10-year moving average of the maximum and minimum across the six GCMs for the three emissions scenarios. In general, all of the models show a substantial increase in maximum temperature (panel A, fig. 5) and minimum temperature (panel B, fig. 5), with a consistent, larger increase in minimum temperature compared to maximum temperature. The A2 scenario (table 2) tends to have the largest increase in temperature, followed by the A1B and finally the B1 scenario. The variability in temperatures shows a somewhat gradual increase over time, which represents increased uncertainty the farther the prediction is in the future. To update groundwater temperatures for climate-scenario simulations, a regression of air temperature to groundwater temperature was constructed whereby groundwater temperature in the lateral accretion term was estimated via linear regression analysis of measured air and shallow groundwater temperature during the calibration period (April–September 2002). Results of the regression showed strong correlation (coefficient of determination (R^2) values of 0.89, 0.86, and 0.89 for Stevenson, North, and Upper Allequash Creeks, respectively). This relation was then used to calculate future groundwater temperatures from potential future air-temperature increases provided by the GCMs/emission scenarios; all other temperature model parameters retained the calibrated values. The predicted climate trends for precipitation are more ambiguous than those for temperature, with more than ± 10 percent variability surrounding current precipitation rates throughout the scenario time period and slightly greater uncertainty towards the end of the scenario period.

Table 1. Selected General Circulation Models (GCMs) used to simulate future climate conditions.

Model abbreviation	Model identification	Organization
cccma_cgcm3_1	CGCM3.1(T47), 2005	Canadian Centre for Climate Modeling and Analysis, Canada
cnrm_cm3	CNRM-CM3, 2004	Centre National de Recherches Météorologiques, France
csiro_mk3_0	CSIRO-MK3.0, 2001	Commonwealth Scientific and Industrial Research Organization (CSIRO) Atmospheric Research, Australia
gfdl_cm2_0	GFDL-CM2.0, 2005	National Oceanic and Atmospheric Administration (NOAA) Geophysical Fluid Dynamics Laboratory (GFDL)
miroc3_2_medres	MIROC3.2(medres), 2004	Center for Climate Systems Research, National Institute for Environmental Studies and Frontier Research Center for Global Change, Japan
mri_cgcm2_3_2a	MRI-CGCM2.3.3, 2003	Meteorological Research Institute, Japan

Table 2. Selected emission scenarios used to simulate future climate conditions.

Scenario	Description
A1B	Rapid economic growth, global population peaking in mid-century and declining thereafter, and introduction of new and efficient technologies with a balance across all sources.
A2	Very heterogeneous world with self-reliance and preservation of local identities with gradual population growth, and slow regional economic growth and technological change.
B1	Convergent world with population change as described in the A1 scenarios with rapid changes towards a service and information economy with clean and resource-efficient technologies.

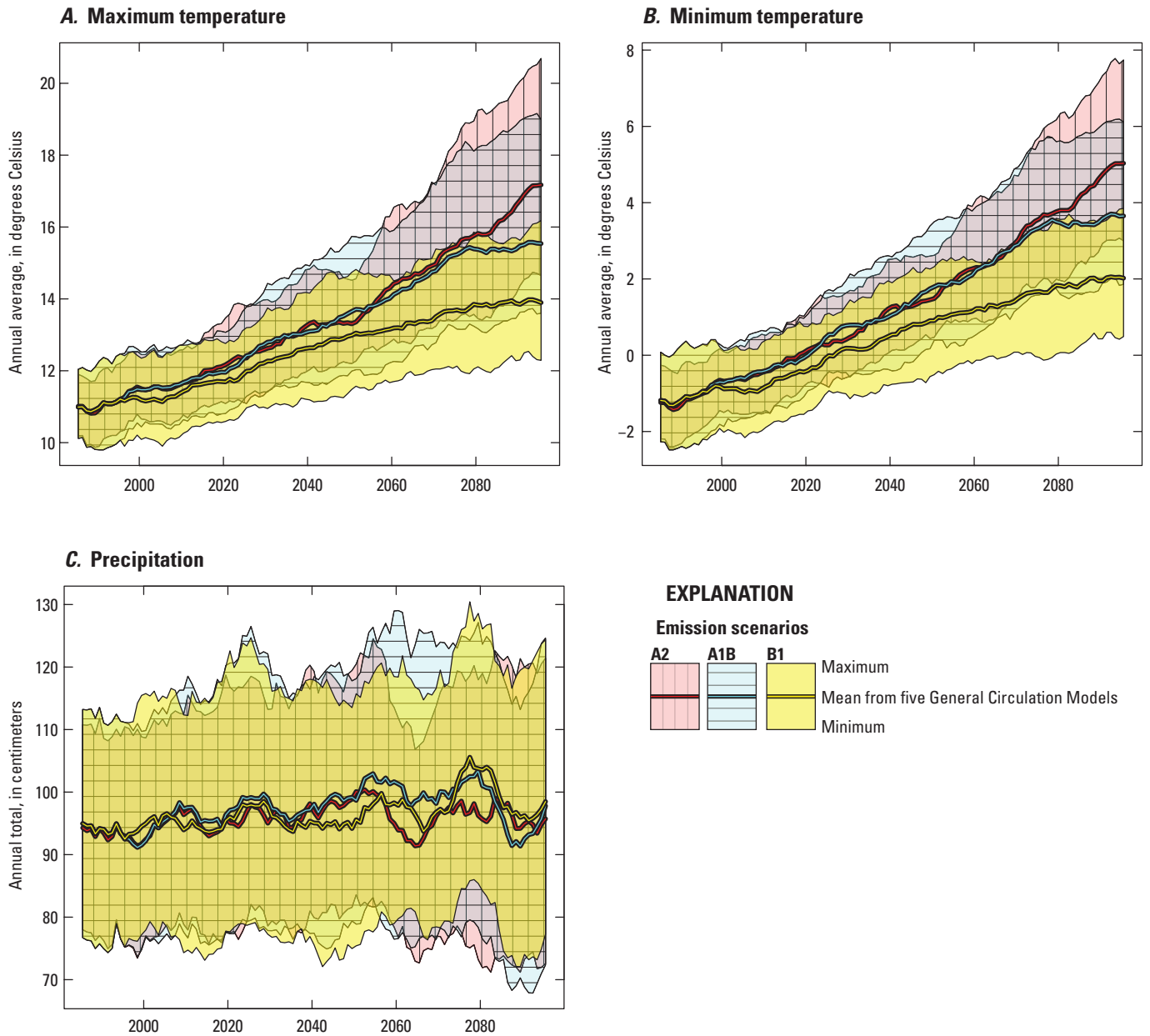


Figure 5. Climate forcings from the Wisconsin Initiative on Climate Change Impacts (WICCI) downscaled data for 6 GCMs. The range of results for A1B and B1 emission scenarios represents all 6 GCMs; the range of the A2 emission scenario is from 5 GCMs.

Climate-change effects on air temperatures are expected to affect timing and length of growing season (for example, Christiansen and others, 2011). The growing season affects the onset of evapotranspiration in the spring and plant senescence in the fall—dates required for simulation of potential changes to hydrologic flows. Similar to the calibration period calculation of growing season, the beginning and end dates of the growing season for the climate-change scenarios were preprocessed for each simulation year by using an algorithm described in Christiansen and others (2011) and documented in Markstrom and others (2012). An assumed killing-frost temperature of -2.2 degrees Celsius ($^{\circ}\text{C}$), 28 degrees Fahrenheit ($^{\circ}\text{F}$) was used for each HRU. During calibration, the growing season was determined as average values for the calibration period. In the climate-change scenarios, the growing season was determined for each year in the simulation period by using minimum temperature input for each specific GCM and emissions scenario. A preprocessing program was used to write a file of transpiration flags for each day for each HRU, indicating whether transpiration is on (flag=1) or off (flag=0). The GSFLOW model read the transpiration flags directly from the preprocessed file using the `climate_hru` module.

The effect of the climate-change scenarios on stream temperature was assessed by inputting GCM-derived changes to air temperature and associated GSFLOW-simulated streamflows into the calibrated SNTMP models for each stream. Each of the six GCM and three emission scenarios, with the exception of `cma_cgcm3_1` (A2 emission scenario omitted because of model run failure), provided average daily air temperature and solar radiation data necessary to compute an average daily stream temperature at the furthest downstream reach prior to entering Trout Lake. All other temperature-model parameters retained the calibrated values.

Results and Discussion

Detailed description, graphics, and tables of calibration results for each uncoupled model and the coupled model are described separately in appendix 6; only the most salient calibration results are repeated here for brevity.

GSFLOW Coupled Hydrologic Flow Model

Atmosphere-earth processes were well represented by observed solar radiation and potential evapotranspiration. Timing and magnitude of snowpack and high-resolution evaporation measurements from Sparkling Lake were well simulated

in the coupled GSFLOW model. The watershed outlet at the Trout River was well simulated, as were most tributary flows at measured locations. Long-term average lake stages were well simulated. Results of the study demonstrate the importance of spring snowmelt and late-fall recharge—time periods when plants are in senescence. During the summer months, when the plants are active, much of the water infiltrating into the soil is intercepted within the plant root zone. Snowmelt-period dynamics were also simulated less well than other times of the year. The lack of representative frozen-ground processes limits the coupled GSFLOW model's ability to simulate high snowmelt discharges. This discrepancy during snowmelt occurs even though the other times of the year are well simulated.

The calibrated model closely simulated most of the observed data used for groundwater calibration, including average heads, timing of head dynamics, average base flow, lake stage, depth of lake infiltrated water, and groundwater inflow to lakes. Simulated head time series generally show response timing and magnitudes similar to observed groundwater-system dynamics over the majority of the observed head dataset and a reasonable representation of the mean head. The range of variation in simulated groundwater levels and lake stages is systematically slightly lower than that in the observed data, reflecting spatial averaging over the nodal scale in addition to temporal daily averaging of climate drivers and soil-zone processes. Estimated aquifer hydraulic conductivities are similar to those from previous modeling of the Trout Lake Watershed, and the range of optimal anisotropy also agrees with values reported by others. The optimal uppermost sand and gravel (layers 1 and 2) renders as a mostly homogeneous unit (average $K_h = 9.5$ m/d, standard deviation = 3.4 m/d) and is consistent with spatial measurements made in the watershed. The middle unit of the aquifer sediments (layers 3 and 4, Wildcat sandy till of Attig, 1985) is even more homogeneous (average $K_h = 3.1$ m/d, standard deviation = 0.4 m/d). The bottom sand and gravel sediments (layers 4 and 5) have the highest hydraulic conductivities in the watershed and highest heterogeneity (average $K_h > 30$ m/d, standard deviation = 12 m/d), reflecting coarse sediments deposited when the glacial ice front was near the Trout Lake area (Attig, 1985). Average areal recharge over the model domain from the calibrated model for the 1999–2006 period is 42.6 cm/yr (16.8 inches per year (in/yr)) and ranges from 36 to 53 cm/yr (14 to 21 in/yr; table 3). The average recharge rate reported here is consistent with that calculated by using base-flow separation of streamflow-gaging station data (Gebert and others, 2011); the range of annual recharge rates is similar to those reported by Dripps (2003) and Dripps and others (2006).

Table 3. Average areal precipitation and recharge rate for the Trout Lake model domain reported by the calibrated GSFLOW model.

[cm/yr, centimeters per year; in/yr, inches per year]

Year	Precipitation (cm/yr)	Recharge rate (cm/yr)	Precipitation (in/yr)	Recharge rate (in/yr)
1999	104.0	45.6	40.9	18.0
2000	94.0	39.4	37.0	15.5
2001	96.8	42.3	38.1	16.7
2002	113.1	53.0	44.5	20.9
2003	86.0	44.2	33.9	17.4
2004	88.0	41.8	34.7	16.5
2005	87.6	36.2	34.5	14.2
2006	78.6	38.0	31.0	15.0

The coupled model output allows for detailed characterization of the groundwater and surface-water systems. The model spin-up period is not included, and discussion focuses on later times of the calibration period (2000–2007). For example, the holistic simulation of the water budget allows the distribution of land-surface/soil-zone flows to be visualized. The coupled model can report the distribution of overland flow between Hortonian overland flow (resulting from precipitation rates greater than the soil infiltration capacity; Horton, 1933) and saturation excess/Dunnian overland flow (generated by lack of subsurface storage in low-lying areas; Dunne and Black, 1970), plus groundwater seepage (fig. 6A). This distribution illustrates one defining characteristic of the Trout Lake Watershed: overland flow in the uplands (primarily Hortonian flow) is a relatively rare occurrence and is usually associated with snowmelt events (fig. 6A); however, some years are without an appreciable snowmelt event (1999 and 2000), and extreme summer rains can generate overland flow (for example, summer 2000). Water infiltrated out of the soil zone into the groundwater system is an order of magnitude higher than either overland flow component (fig. 6B)—a finding expected in a groundwater-dominated watershed with transmissive soils.

The 1999–2007 period is notable for its transition from conditions that were normal or wetter than normal (1999–2002) to drier conditions that resulted in low lake levels in seepage lakes throughout the watershed at the end of the simulation period (fig. 7).

Simulation of water budget for this period illustrates the interaction of factors that influence lake stage. First, an appreciable decrease to direct precipitation to the lake—the largest source of water to the lakes—occurred between 2002 and 2003 (fig. 8), with 1999–2002 values averaging about 102 cm/yr and 2003–6 values averaging about 85 cm/yr. During the same period, evaporation off the lakes increased slightly (fig. 8) from 73.5 to 74.5 cm/yr. However, the lake stages did not appreciably decline in 2003 (fig. 7) but lagged by about 2 years, reflecting the mitigating influence of the groundwater system.

The groundwater system is connected to the unsaturated zone (the layer below the soil zone but above the water table), and changes to precipitation at land surface are in turn buffered by antecedent water stored in the unsaturated zone. For example, multiple years of high precipitation (fig. 8) result in an increase in water stored in the unsaturated zone (2001, fig. 9), and a tipping point is reached where the recharge rate to the groundwater system becomes higher during wet conditions (2002, fig. 9). The appreciable decrease in precipitation at the surface in 2003 results in a net loss of water from the unsaturated zone in 2003 but less effect on groundwater recharge rates (fig. 9). This loss of storage in the unsaturated zone is partially replenished in years 2004–5, with reduction in groundwater recharge in subsequent years. This reduction in recharge, in turn, results in lower groundwater levels that serve to depressurize the groundwater/surface-water system—reducing the vertical gradients where groundwater flows into surface water and increasing vertical gradients where water flows out of surface water and into the groundwater system. This lagged response in the groundwater system manifests itself as lower lake levels in 2005 and 2006—two years after the first change in direct precipitation to the lake (fig. 7).

These interactions and mitigating effects underscore the power of a coupled simulation of the surface-water and groundwater systems. An uncoupled modeling approach could not capture, or constrain, the complex interplay of atmospheric drivers, unsaturated zone buffering, and lagged groundwater-system mitigation on lake stage changes.

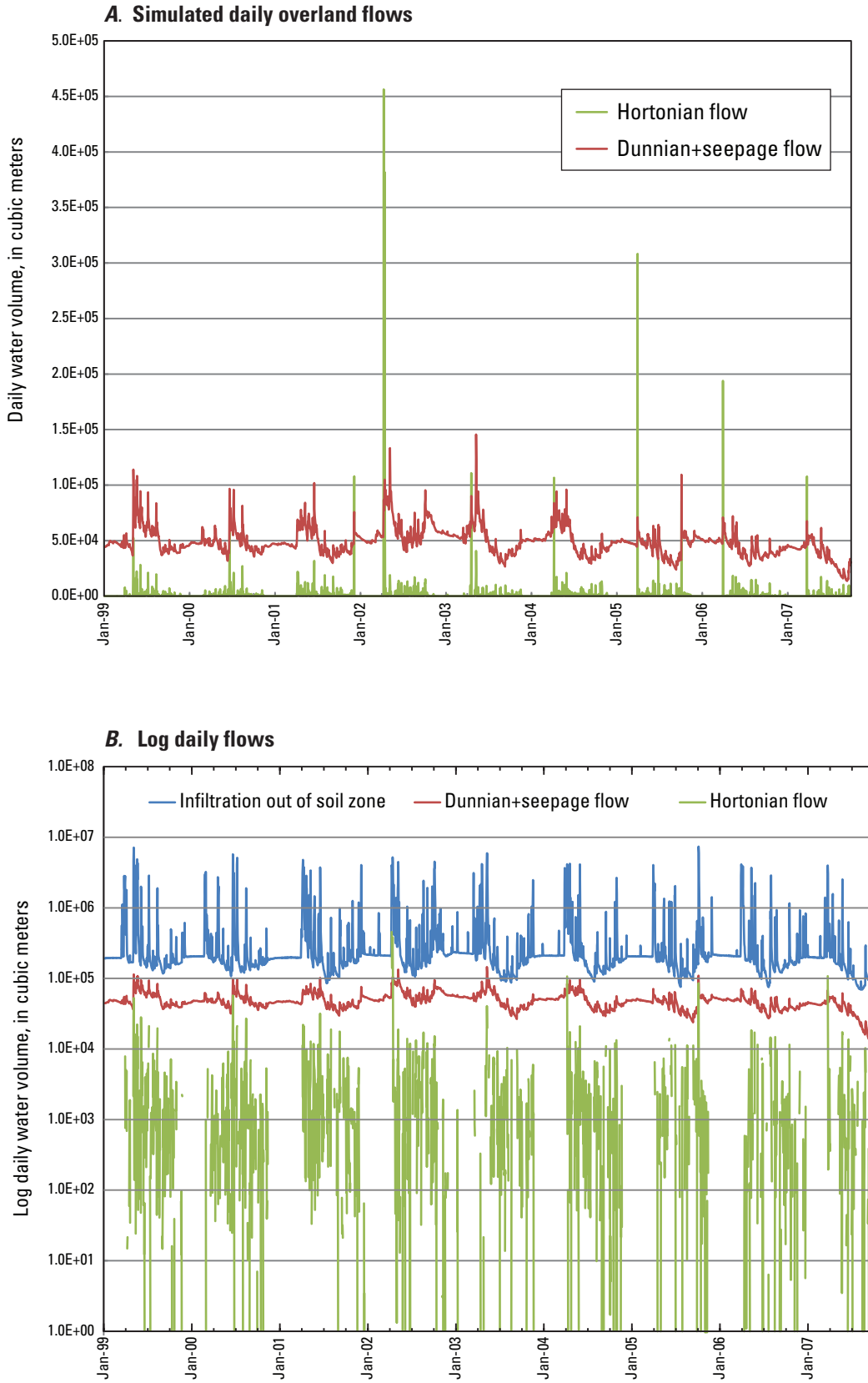


Figure 6. Simulated flows for the Trout Lake Watershed (1999–2007). *A*, Daily overland flows. *B*, Log daily flows.

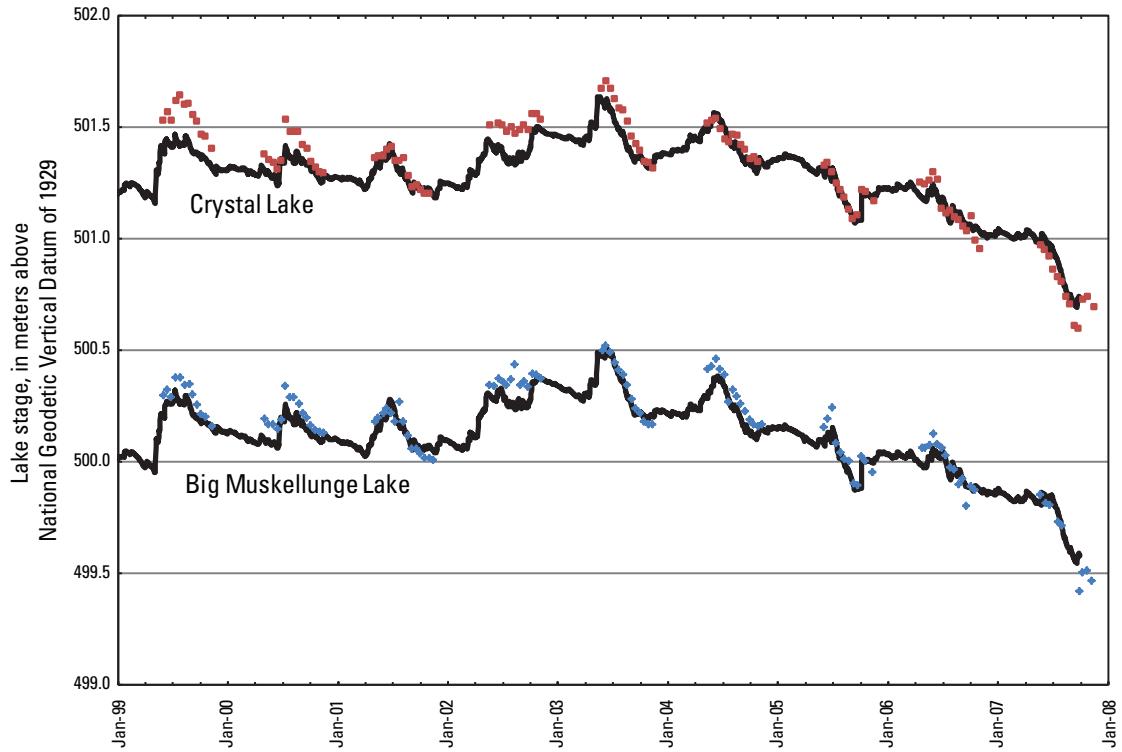


Figure 7. Measured (symbols) and simulated (line) lake stages for two adjacent seepage lakes.

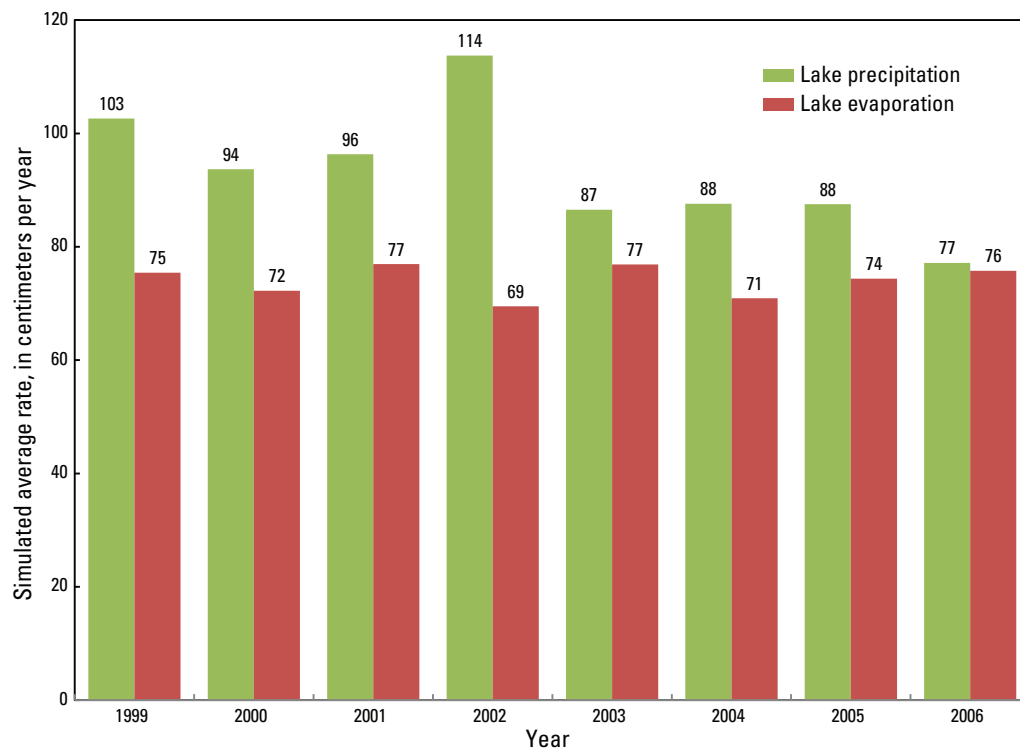


Figure 8. Simulated watershed average lake precipitation and lake evaporation during 1999–2006.

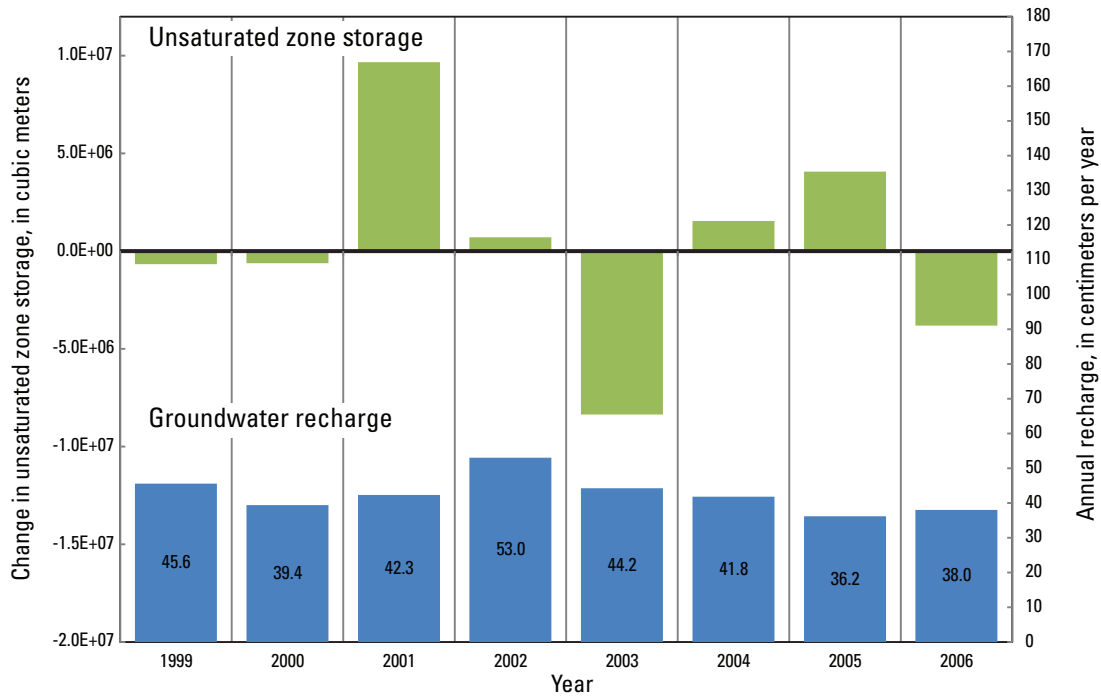


Figure 9. Basinwide simulated changes in volume of water stored in the unsaturated zone (green/upper) and rate of groundwater recharge (blue/lower).

SNTMP Stream Temperature Model

Relatively close agreement was obtained between simulated daily mean stream temperature simulations and observed stream temperature near North Creek, Allequash Creek, and Stevenson Creek locations (figs. 10 and 11). The larger range of annual stream temperature (observed range equal to approximately 25 °C) is better simulated than the daily range (observed range usually less than 1 °C). Although all SNTMP input variables were initially considered calibration parameters, the greatest change to simulated daily mean stream temperatures was effected by adjusting air temperature, streamflow, groundwater discharge, and groundwater temperature through lateral accretion. Of these four variables, air and groundwater temperature were both measured values, thus considered relatively well known and not adjusted during calibration. Similarly, although streamflow was not directly measured at all locations, it was considered well constrained by the calibrated flows simulated by the coupled GSFLOW model. Trial-and-error calibration was considered complete when three criteria were met: (1) high correlation between simulated and observed daily mean stream temperatures, (2) minimal difference between average simulated and average observed stream temperatures, and (3) minimal difference between individual daily mean simulated and observed stream temperatures.

When the complete 2002 time series is averaged at the calibration point within each creek, simulated and observed daily mean stream temperatures have mean errors (table 4, fig. 12) that are much smaller than the >20 °C temperature

range simulated (fig. 11). The overall trend of the time series is also well represented, as evidenced by a high correlation coefficient (table 4) illustrating that modeled stream temperatures respond similarly to fluctuations in air temperature, surface discharge, and so forth, as do measured stream temperatures, though not necessarily with the same magnitude. All three models generally tend to slightly underestimate stream temperature (negative mean error, table 4). In terms of model performance by day rather than entire period, the simple SNTMP model was less able to characterize the general system dynamics (percent days daily mean stream temperatures differed from observed temperatures by ±1 °C or more in table 4). Previous SNTMP studies on larger rivers suggest a calibration target of ±0.5 °C (Bartholow, 1989). North and Upper Allequash Creeks were slightly above the 0.5 °C threshold (table 4). Stevenson Creek had the greatest mean error at 1.4 °C, largely due to consistently underestimated stream temperatures during April through June.

Table 4. Analysis of fit between simulated and observed daily mean stream temperatures at calibration points in SNTMP for April through September 2002.

[°C, degrees Celsius]

Stream	Correlation coefficient	Mean error (°C)	Maximum error (°C)	Percent days ±1 °C
Stevenson	0.93	-1.4	-5.9	66
North	0.93	-0.6	-4.7	44
Upper Allequash	0.95	-0.6	-4.2	49

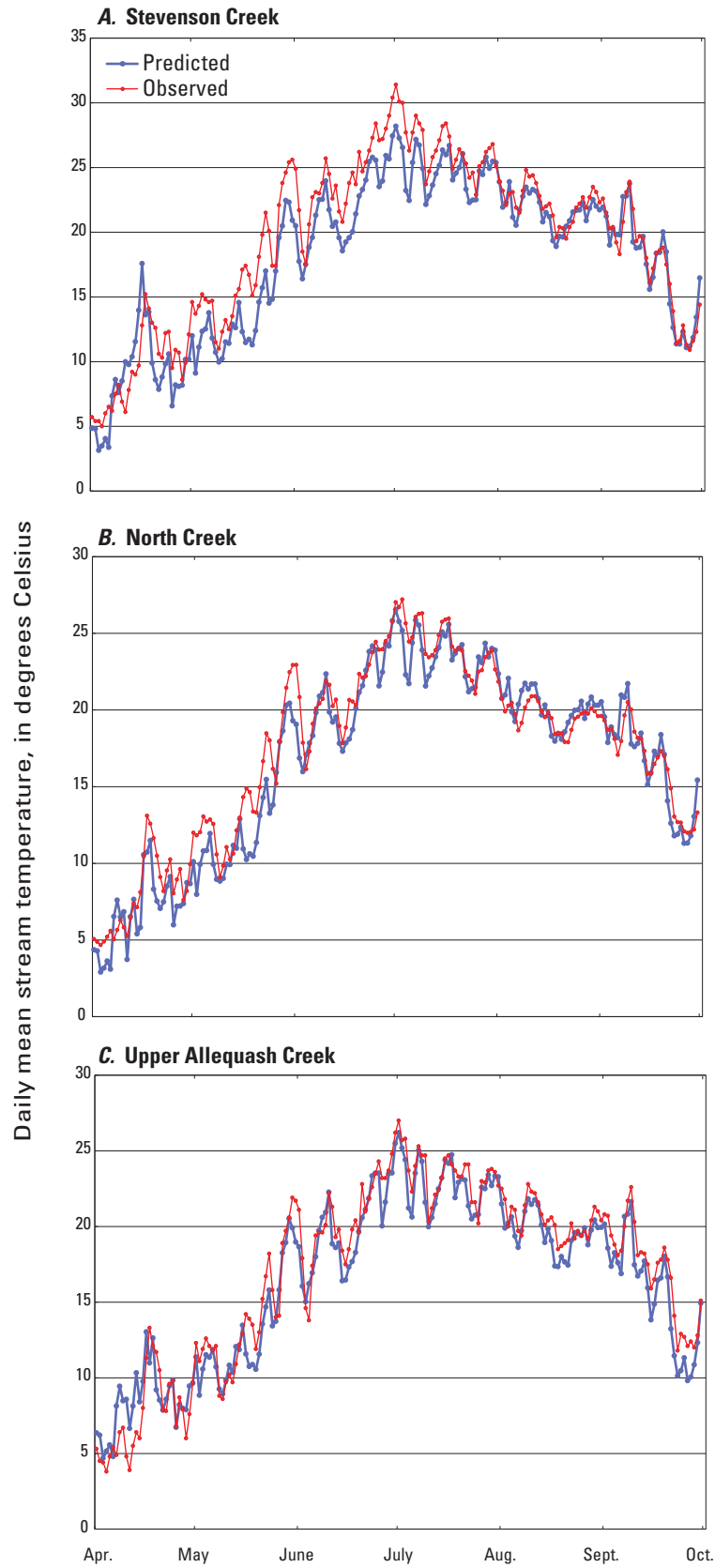


Figure 10. Daily variation in simulated and observed daily mean stream temperatures in Stevenson, North, and Upper Allequash Creeks, April–September 2002.

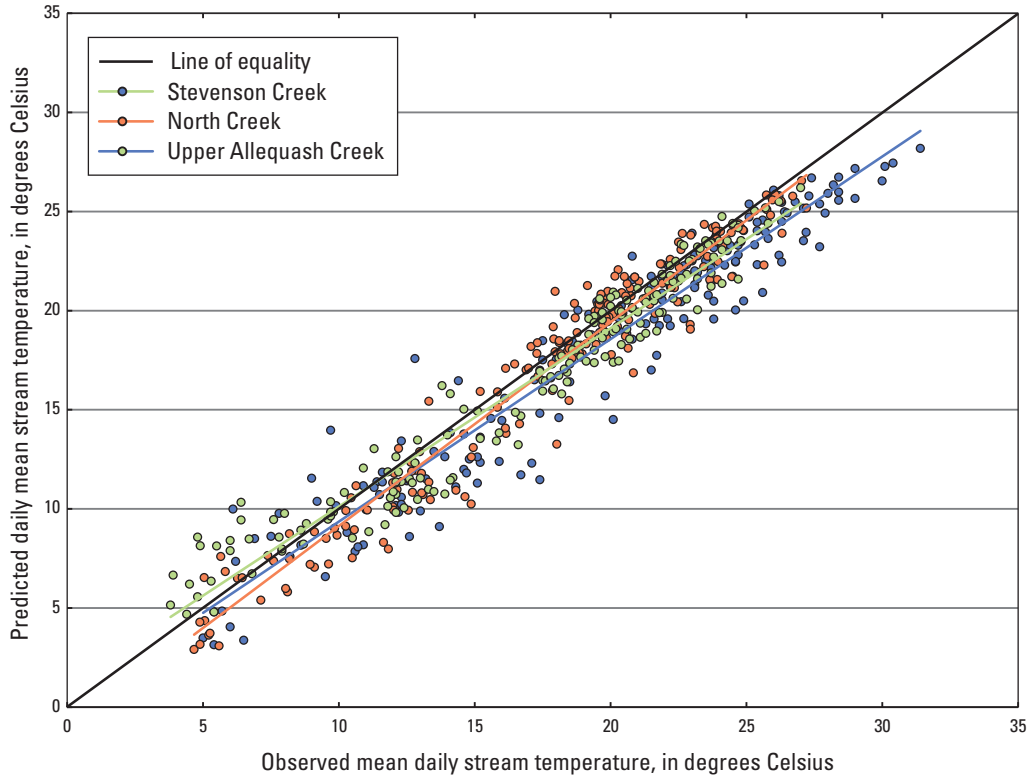


Figure 11. Comparison between simulated and observed daily mean stream temperatures for Stevenson, North, and Upper Allequash Creeks, April–September 2002. Colored lines reflect the resulting line for each site calculated from linear regression.

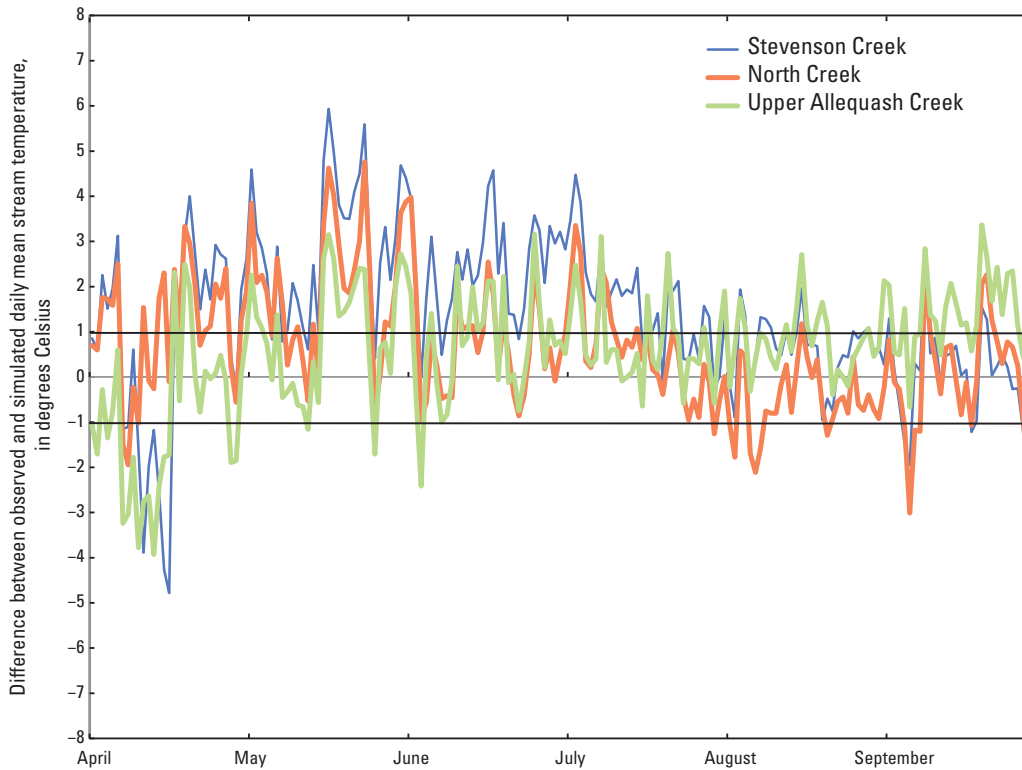


Figure 12. Difference between observed and simulated daily mean stream temperature in Stevenson, North, and Upper Allequash Creeks, April–September 2002.

Daily differences are generally greatest during April, May, and June (figs. 10 and 12)—months when air temperatures change by large magnitudes over short time periods. For example, average daily air temperature in one instance increased from approximately 14 to 22 °C within 24 hours (April 15–16, 2002). Similarly, a few days later, air temperature decreased from 14 to 3 °C (April 18–19, 2002). Air temperature exhibits less short-term variability in the warmer months of July, August, and September; accordingly, the fit between simulated and observed stream temperatures improves (figs. 10 and 12). The efficiency of transferring effects of rapid air-temperature change to stream temperature is expected to be only approximately simulated, given the relatively coarse stream-reach discretization and piecewise-constant daily time step of the model; that is, SNTMP is a successive steady-state model in which one assumes that all input data, including meteorological and hydrological variables, can be represented by 24-hour averages. This assumption is often appropriate for large river systems that tend to exhibit gradually varying temperatures over time, thereby containing sufficient heat capacity to mitigate large short-term variations in air temperature. However, the study streams simulated here are small, wetland-dominated streams.

Small adjustments to shading parameters had little effect on resulting model fits. Adjustments to stream width and groundwater temperature did facilitate closer fits to observed values; however, the parameter variations required for improved fit were not consistent with field observations of these parameters, so they were instead fixed at reasonable values for final calibration. The three streams being associated with wetlands may be a factor. Seasonal changes in streambed-surface albedo due to aquatic-vegetation growth later in the growing season could affect how the streambed adsorbs solar radiation. Water color in wetland streams that feed Trout Lake is generally a darker brown than in many comparable Wisconsin streams because of tannins derived from peat in the watershed. Houser (2006) has shown water color to significantly affect epilimnetic depth in a nearby northern-temperate lakes; darker water was warmer in response to more solar radiation being absorbed. Less adsorption of solar radiation would be consistent with streams becoming shallower and darker wetland streambeds becoming lighter (increased albedo) as aquatic vegetation becomes more established later in the growing season. Furthermore, using time series of hyporheic temperature profiles, Hunt and others (2006) show that peat sediments in wetland streams in the Trout Lake region are capable of having a relatively high insulative capacity. Albedo changes and increased insulation from peat sediments are processes that would be expected to be more appreciable on small streams than large ones. However, the confounding ability of these uncaptured processes diminishes as the dominant air-temperature driver increases later in the growing season.

Climate-Change Effects

Climate-change scenarios drove changes in GSFLOW and SNTMP model outputs, including a general ecohydrological driver (growing-season length), streamflow, lake hydrologic budget, and stream temperature. In the presentation of climate-change effects, the overall uncertainty in the forecasts increases in many instances (that is, the overall envelope of results from the three emission scenarios is wider). This effect is primarily due to differences in the underlying assumptions among the three emission scenarios used in the climate-change evaluation (table 2) that become increasingly important in the latter part of the simulations.

Changes to Growing-Season Length

As is expected given the increase in maximum and minimum air temperatures (figs. 5A and 5B), the length of the growing season generally lengthens on the order of weeks by 2100 for all emission scenarios (fig. 13), with the largest increases seen in the A1B and A2 scenarios (blue and red transparent areas, respectively, fig. 13). These values are comparable to those reported by Christiansen and others (2011) for the Trout Lake area, which used the same algorithm for calculating growing season but a different source for down-scaled GCM climate data.

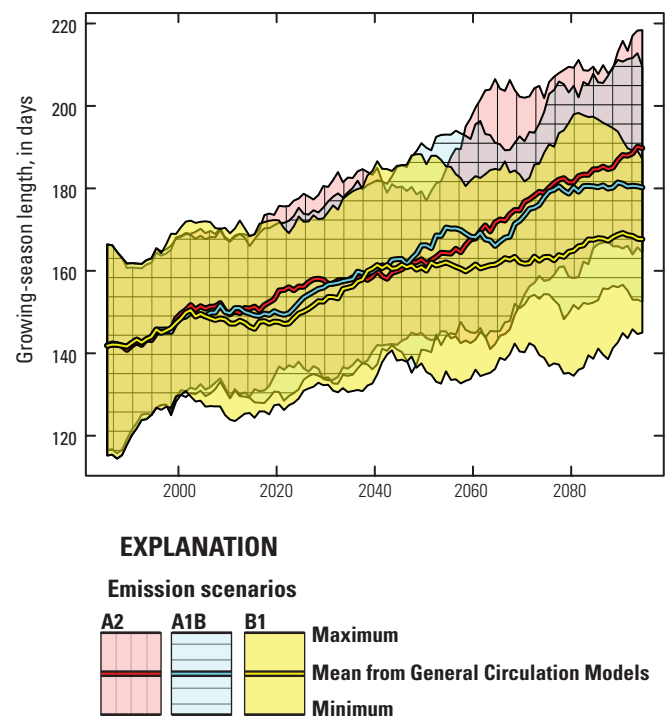


Figure 13. Climate-change-related change in growing-season length, defined as the difference between the date of the first killing frost in the fall and the date of the last killing frost in the spring.

Changes to Basin-Scale Hydrologic Flows and Storage

Although estimates of future total precipitation did not show strong trends in the GCMs evaluated here (fig. 5C), the distribution of precipitation between rainfall and snowfall does show appreciable potential change (figs. 14A and 14B), in which reductions in annual snowfall occur concurrently

with increases in annual rainfall. This combination is primarily a result of changes from late fall through winter, in which warmer temperatures result in more precipitation coming in the form of rainfall—during the period when snowfall currently dominates. This reduction in snowfall reduces the amount of precipitation banked as snowpack (fig. 14C), which in turn reduces the importance of snowmelt events (fig. 14D).

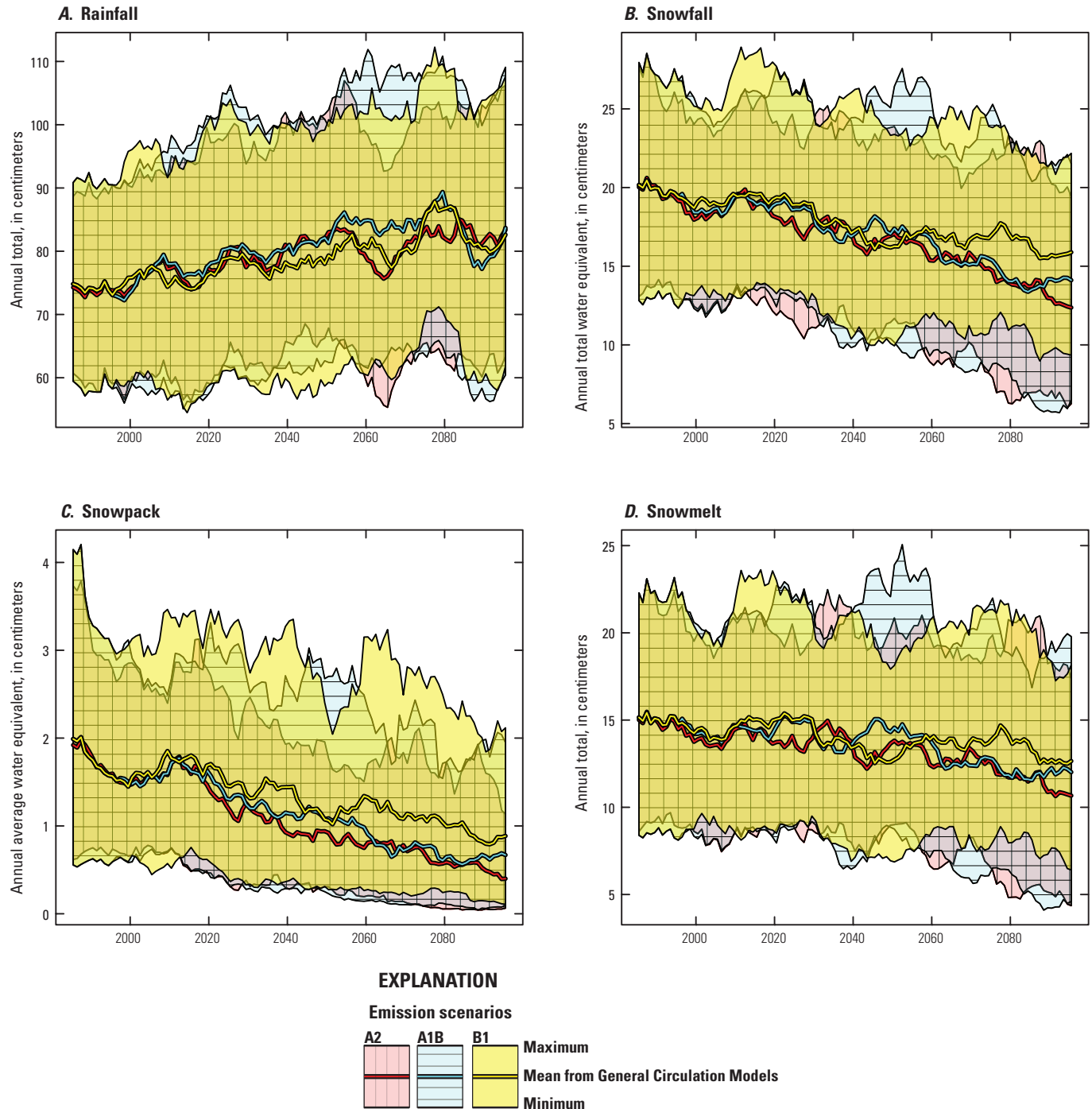


Figure 14. Climate-change scenario results for simulations of precipitation form, snowpack, and snowmelt.

Increases in temperature also increase the annual potential evapotranspiration amount (fig. 15A). Actual evaporation amounts (fig. 15B) show associated increases, but not to the same degree as potential evapotranspiration. The discrepancy between potential and actual evapotranspiration reflects water limitation in the soil zone during the summer periods when potential evapotranspiration is highest; that is, the potential is strong for evapotranspiration to occur, but water in the soil zone may not be available. The loss of soil moisture during

the increase in potential and actual transpiration is shown in decreases in the annual average soil moisture (fig. 15C). Average annual groundwater recharge (fig. 16) is less changed than the actual evapotranspiration and average annual soil moisture, reflecting the increase in rainfall during the winter months—a period of plant senescence. This result suggests a potential for general drying of rainfed ecosystems (such as bogs and ephemeral wetlands), with less relative drying occurring in ecosystems fed by the groundwater system (such as fens).

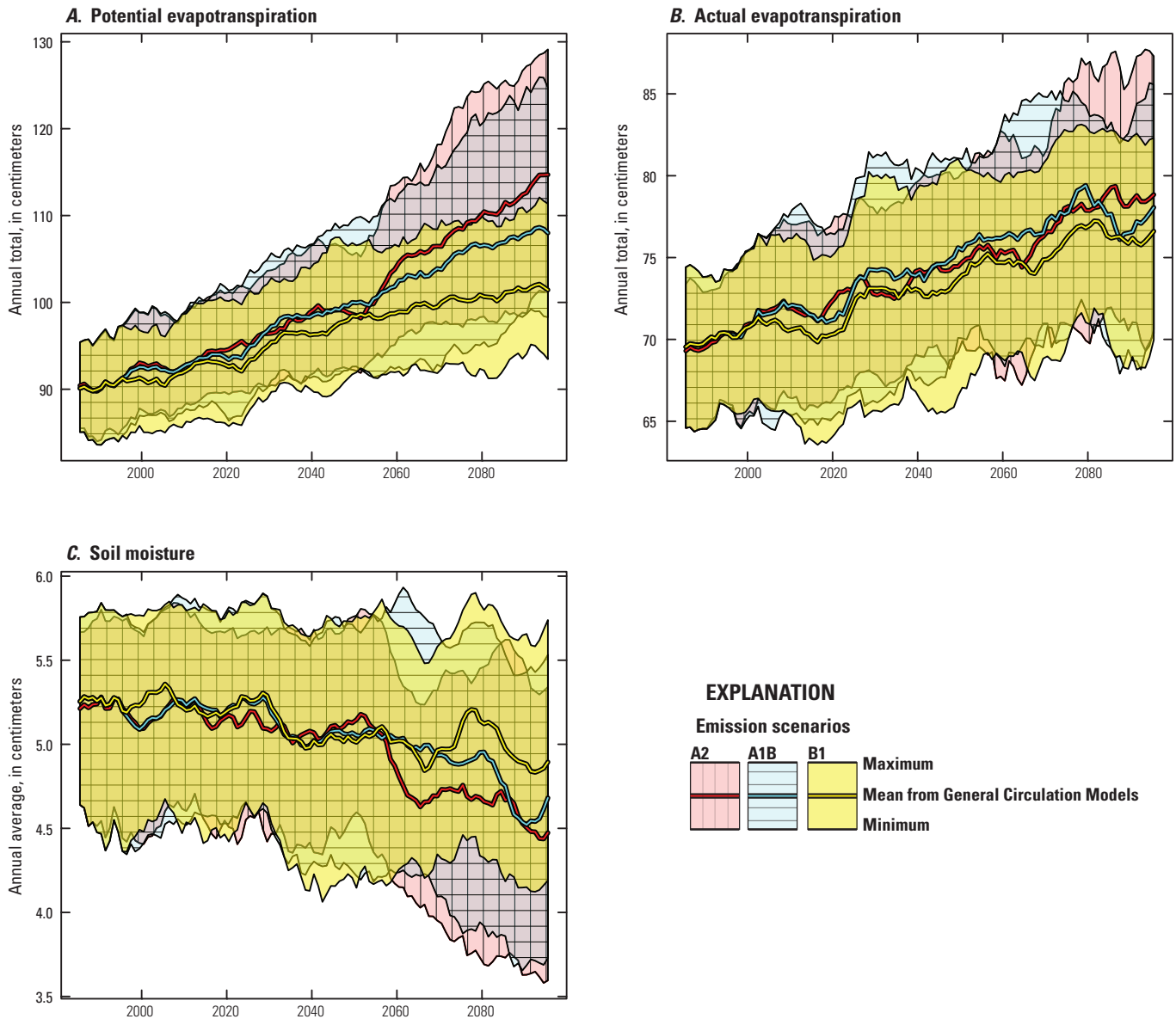


Figure 15. Climate-change scenario results for potential and actual evapotranspiration and the resulting watershedwide average soil moisture.

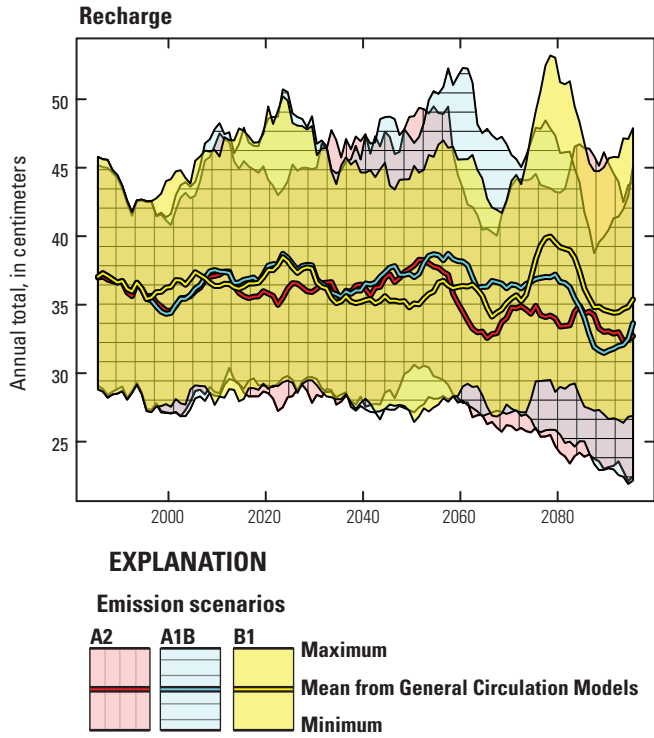


Figure 16. Climate-change scenario results for watershedwide average recharge to the groundwater system.

Changes to Streamflow

Changes in mid-century tributary streamflows and base flows (figs. 17–20) and watershed outlet flows (fig. 21) are generally not as large as the change to evapotranspiration (fig. 15). The agreement in response between streamflow and base flow, as well as the relatively smaller response to climate change, represents the importance of the groundwater system to the Trout Lake hydrologic system. Because increases in groundwater recharge resulting from increased winter rainfall are less available for soil-zone evapotranspiration, the net effect on annual flows is not as large as the increase in potential evapotranspiration in the summer months. Near the end of the 21st century, streamflows and base flows drop appreciably in two of the three emission scenarios (A1B, blue; A2, red). Whereas groundwater storage appears to mitigate some of the overall effects of climate change, decreases in a stream downgradient of a lake are comparable to changes in flow upgradient of the lake (for example, fig. 18 versus fig. 17), a pattern which demonstrates the lack of strong mitigating effect of surface-water storage on long-term climate-affected flows.

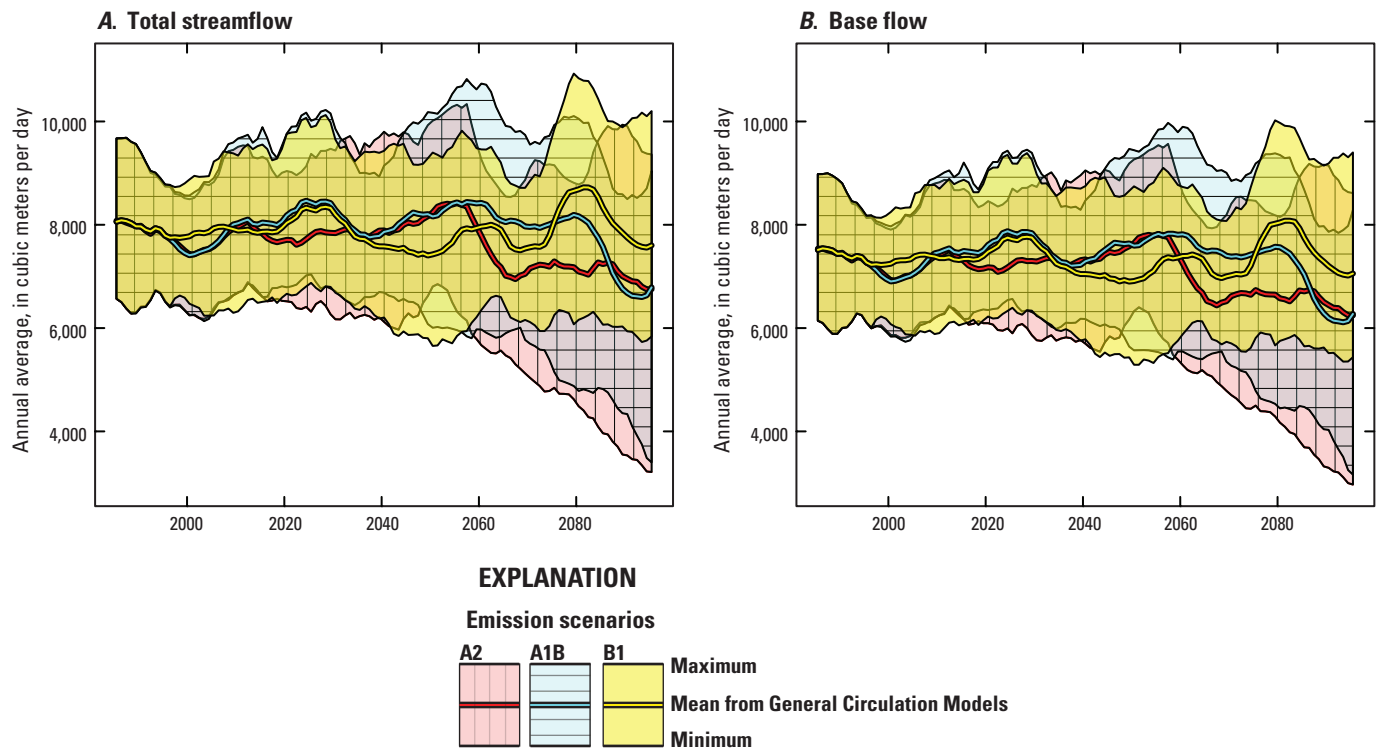


Figure 17. Climate-change results for streamflow-gaging station 05357206, Allequash Creek Middle Site, showing total streamflow and base flow.

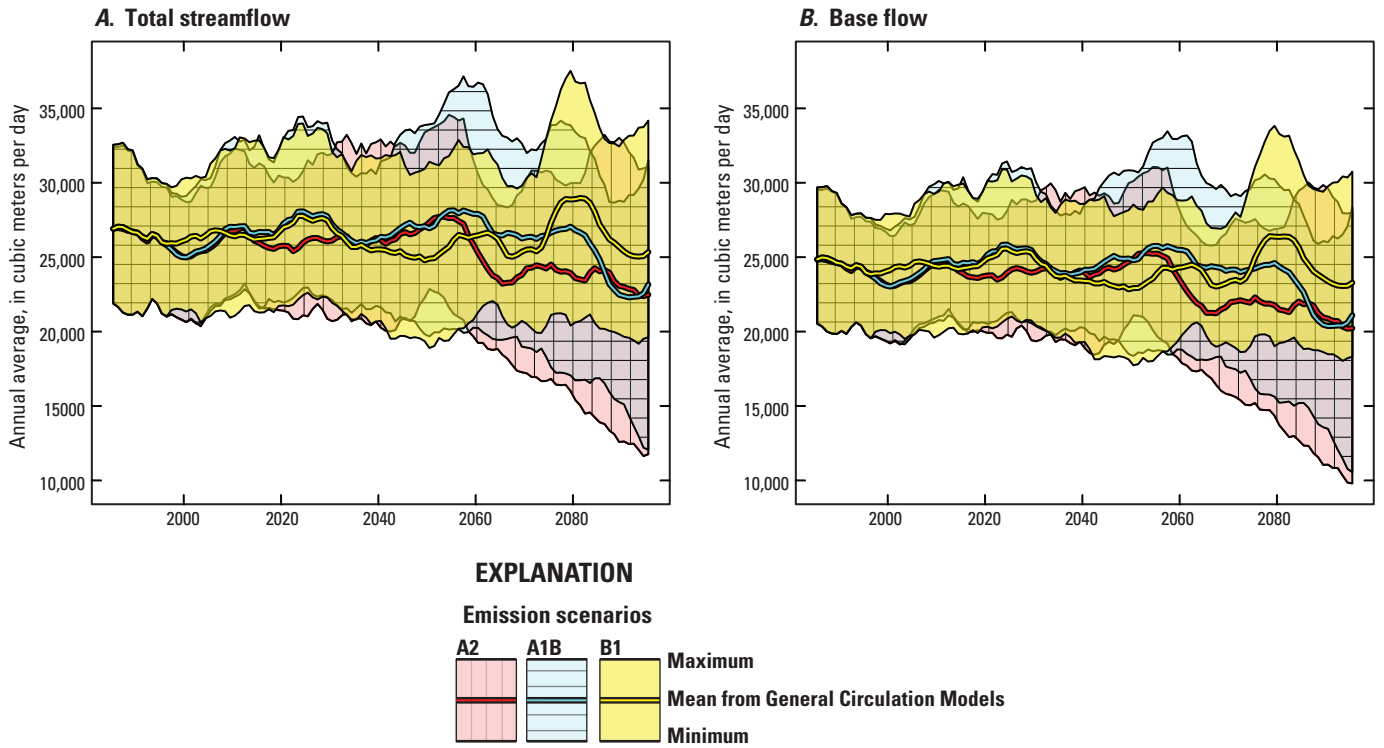


Figure 18. Climate-change results for streamflow-gaging station 05357215, Allequash Creek at County Highway M, showing total streamflow and base flow.

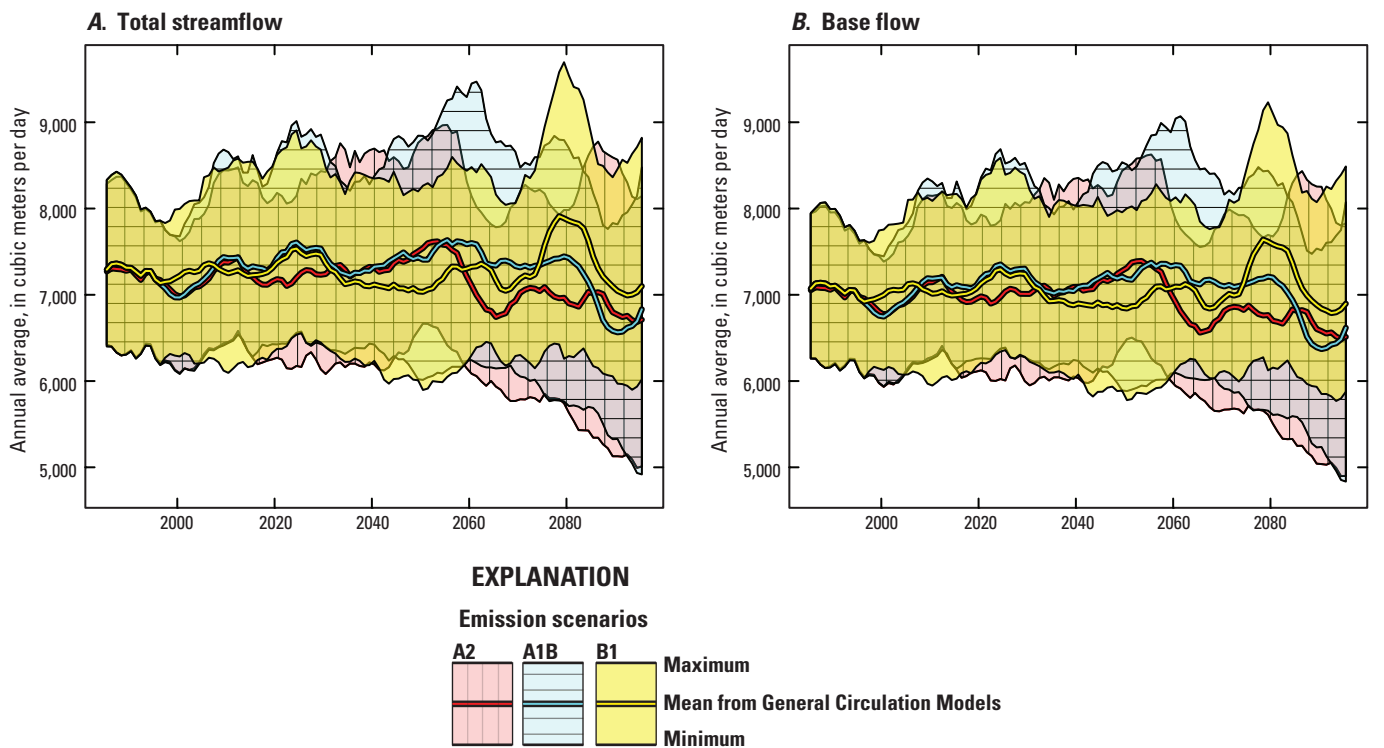


Figure 19. Climate-change results for streamflow-gaging station 05357225, Stevenson Creek at County Highway M, showing total streamflow and base flow.

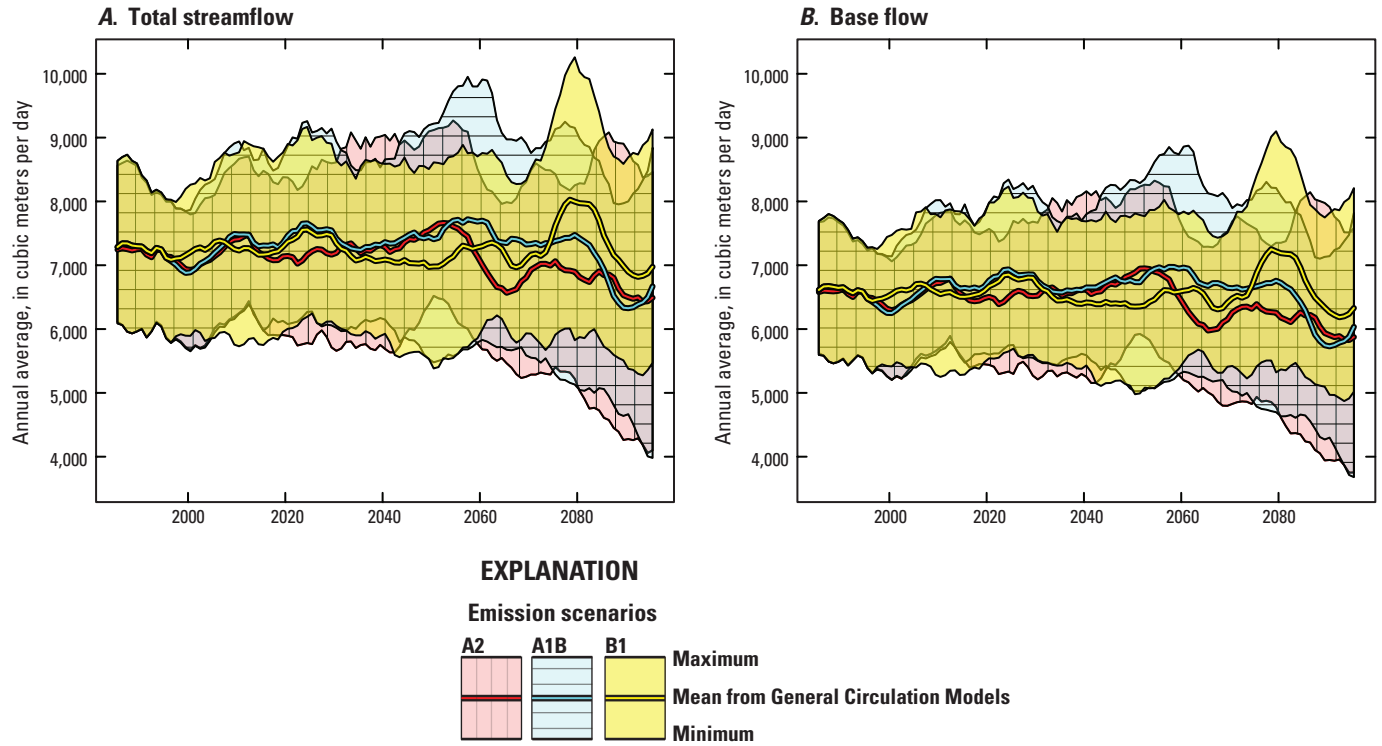


Figure 20. Climate-change results for streamflow-gaging station 05357230, North Creek at Trout Lake, showing total streamflow and base flow.

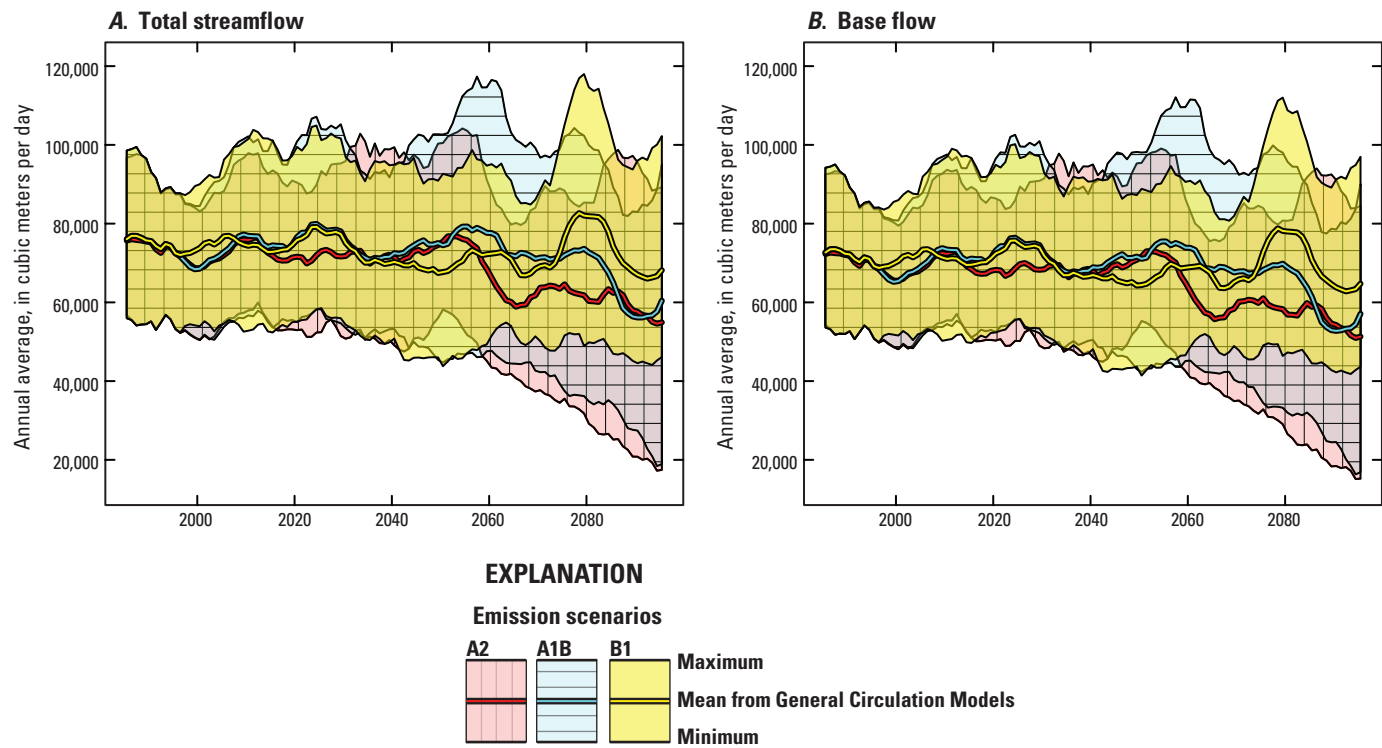


Figure 21. Climate-change results for streamflow-gaging station 05357245, Trout River at Trout Lake, showing total streamflow and base flow.

Changes to Lake Water Budgets

Climate-change effects on lake budgets will focus on a subset of 30 lakes simulated in the model domain and will first discuss seepage lakes (lakes with no appreciable surface water outlets) followed by drainage lakes (lakes with outlet streams).

Seepage Lakes

In the Trout Lake Watershed, there is a topographic gradient of lakes, from those high in the watershed near the groundwater divide to those lower in the watershed near the watershed outlet (for example, Cheng and Anderson, 1994). Results from three seepage lakes that span the watershed gradient include those from Crystal Lake (fig. 22) nearest the groundwater divide, Big Muskellunge Lake downgradient from Crystal Lake (fig. 23), and Sparkling Lake located lowest in the watershed nearest the Trout River (fig. 24). In all three seepage lakes, current positive net precipitation (that is, annual precipitation greater than annual lake evaporation) decreases over time (panel *A*), with largest decreases for the A1B (blue) and A2 (red) emission scenarios. Decreases in net precipitation are mitigated to some degree by increases in net groundwater inflows to the lakes (panel *B*), which in turn offset potential declines in lake stage (panel *D*). The mitigating effect of the groundwater system is most easily seen in comparison of the forecast stage decline for the lake highest in the watershed near the groundwater divide (on the order of 1 m, fig. 22) to that of the lake with the highest interaction with the groundwater system located lower in the watershed (on the order of 0.5 m, fig. 24 - note change in y-axis scale in fig. 24*D*). In all cases, the projected change in precipitation timing and magnitude (fig. 5*C*) does not result in surface runoff to the lakes (panel *C*, figs. 22–24). This is consistent with expected increases in potential and actual evapotranspiration (figs. 15*A* and 15*B*) and drier soil conditions (fig. 15*C*) throughout the watershed precluding soil-zone saturation and related surface runoff. As a result, it appears that the groundwater system will

be the primary storage called upon to offset increased lake evaporation resulting from projected climate warming. Such a change in water source can be expected to affect chemistry of the lake water (for example, Hurley and others, 1985; Anderson and Bowser, 1986), because groundwater inflows are characterized by higher alkalinity and higher dissolved solids/ion concentrations than precipitation sources. Moreover, increases in lake evaporation as a result of warmer air temperatures also will facilitate increases in dissolved solids in seepage lakes.

Drainage Lakes

In contrast to seepage lakes, drainage lakes are characterized by appreciable net surface-water flows (panel *C*, figs. 25 and 26, in which negative numbers represent surface-water outflows in excess of inflows to the lake). Surface-water outflows from a lake can have strong effects on a lake's water budget because they are hydrologically efficient (that is, have less resistance) compared to flows into and out of the groundwater system. With changing climate, the drainage lakes are forecast to undergo appreciable reductions in net surface-water outflows (less negative with increasing time). The reduction in surface-water outflows facilitates maintaining lake stages near current conditions (note change in y-axis scale in panel *D*, figs. 25–26), much closer than stages forecast for seepage lakes (panel *D*, figs. 22–24). However, reduction in stream-flow downstream from the lake may have ecological effects, the mitigation of lake-stage decline notwithstanding. Because stages in drainage lakes have relatively smaller changes in stage and the groundwater-system declines are lessened by increases in winter recharge, the hydraulic gradient between the groundwater system and drainage lakes is relatively less changed; thus, change in net groundwater-flux magnitude (panel *B*, figs. 25–26) is less than that for net surface-water flows. Net groundwater flows also appear to have a central tendency for slight decreases by 2100 as opposed to increases forecast for seepage lakes.

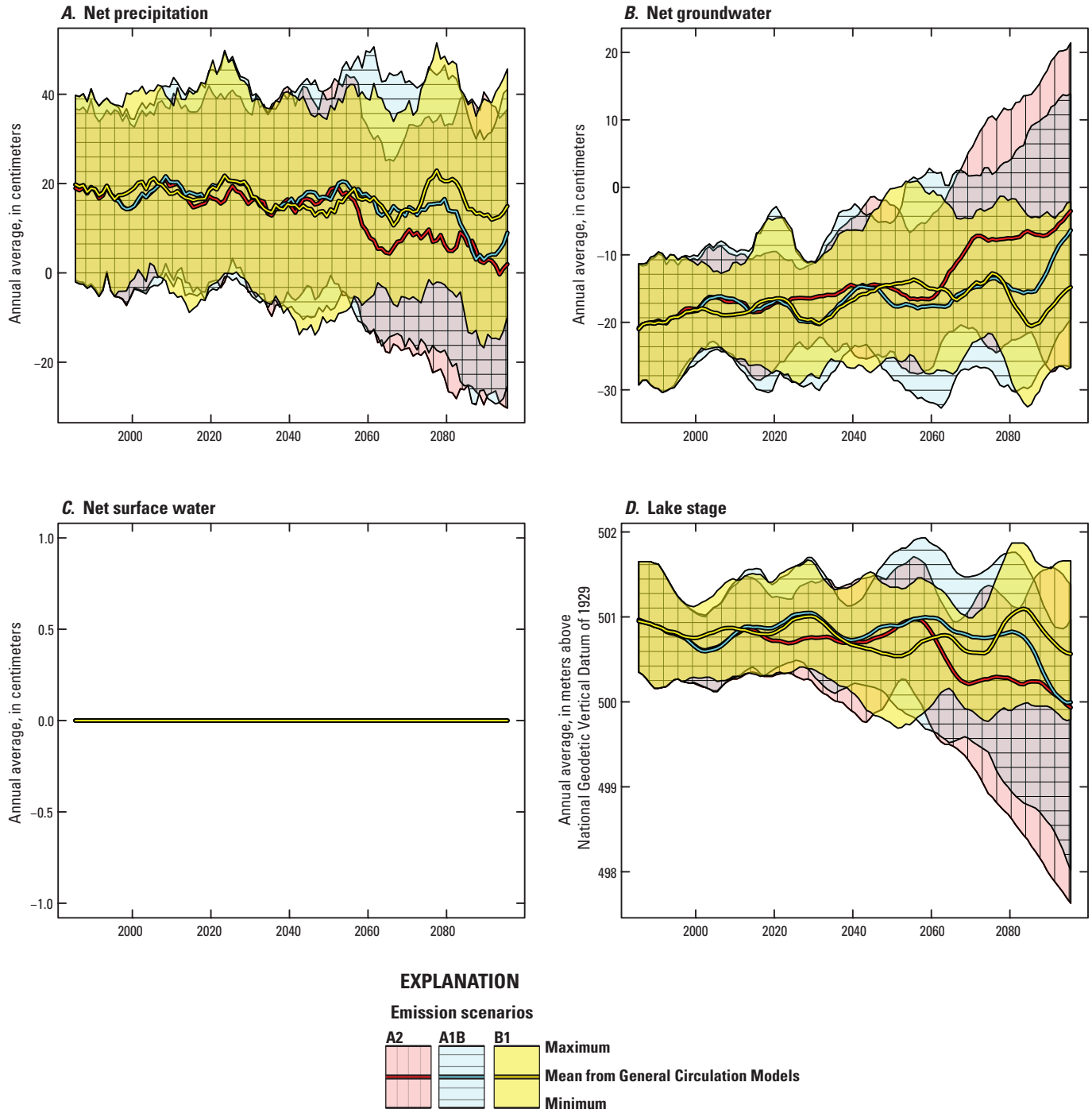


Figure 22. Climate-change simulations for Crystal Lake showing net annual components of the hydrologic budget normalized by lake area and related annual lake stage.

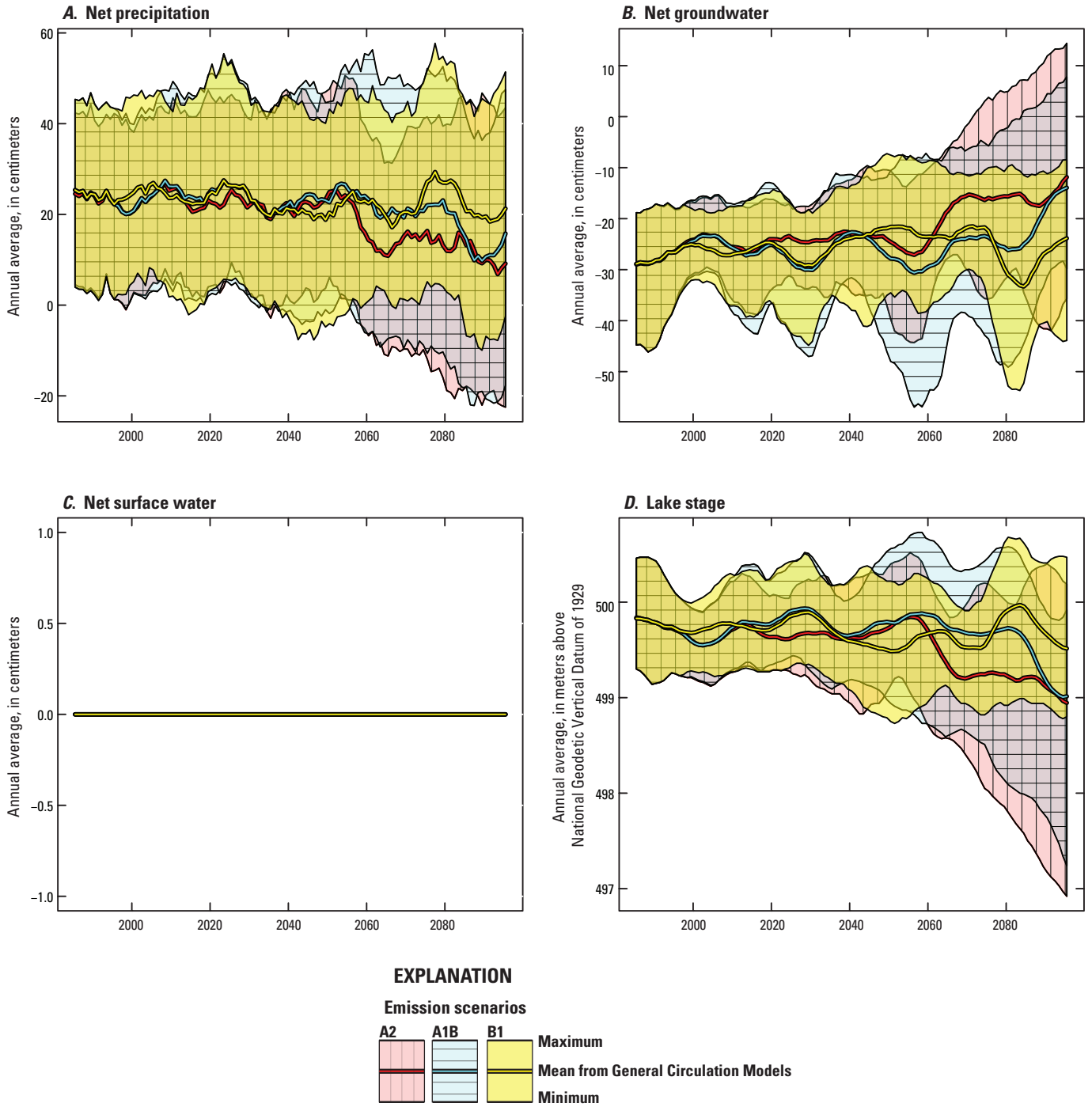


Figure 23. Climate-change simulations for Big Muskellunge Lake showing net annual components of the hydrologic budget normalized by lake area and related annual lake stage.

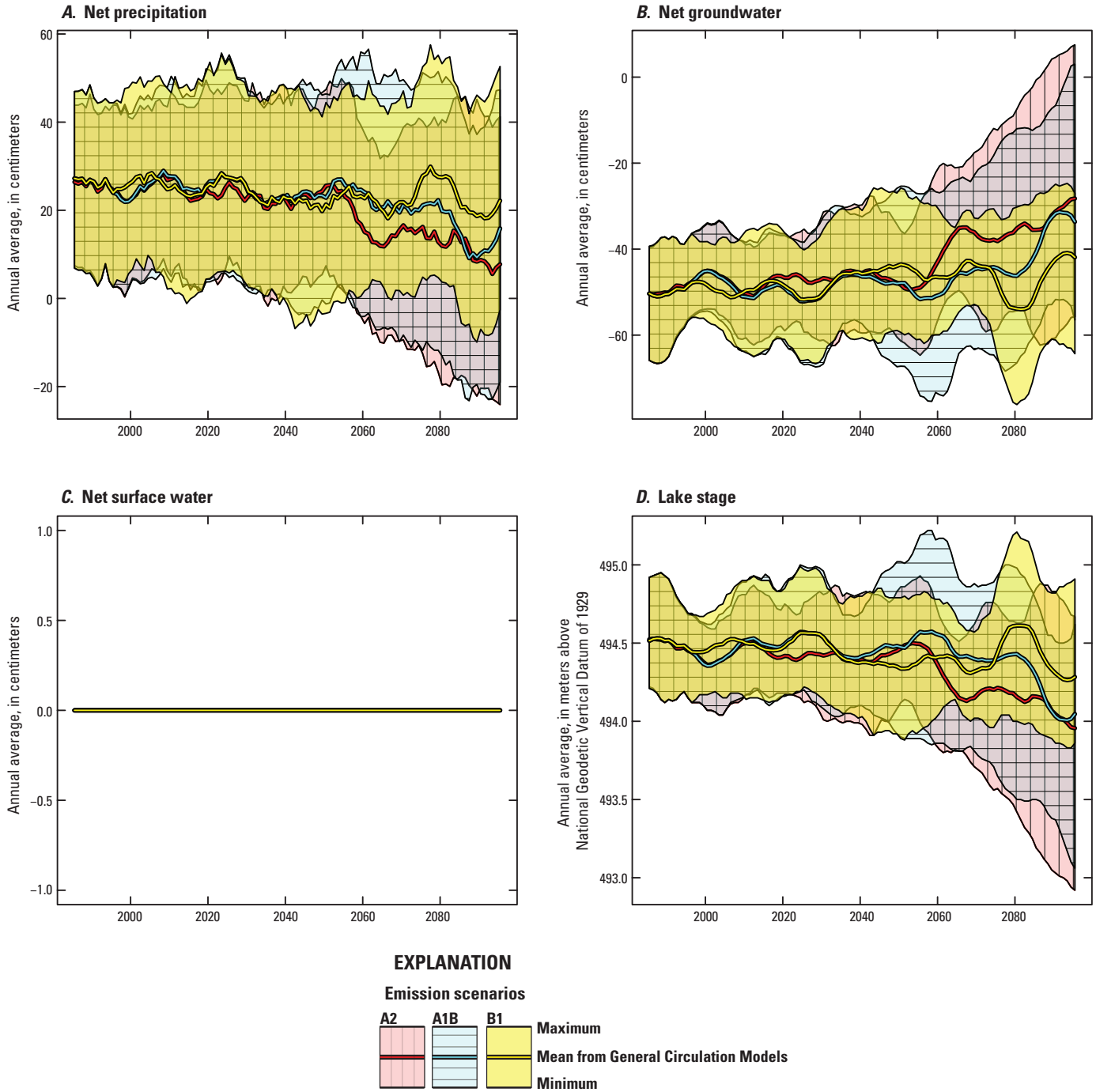


Figure 24. Climate-change simulations for Sparkling Lake showing net annual components of the hydrologic budget normalized by lake area and related annual lake stage.

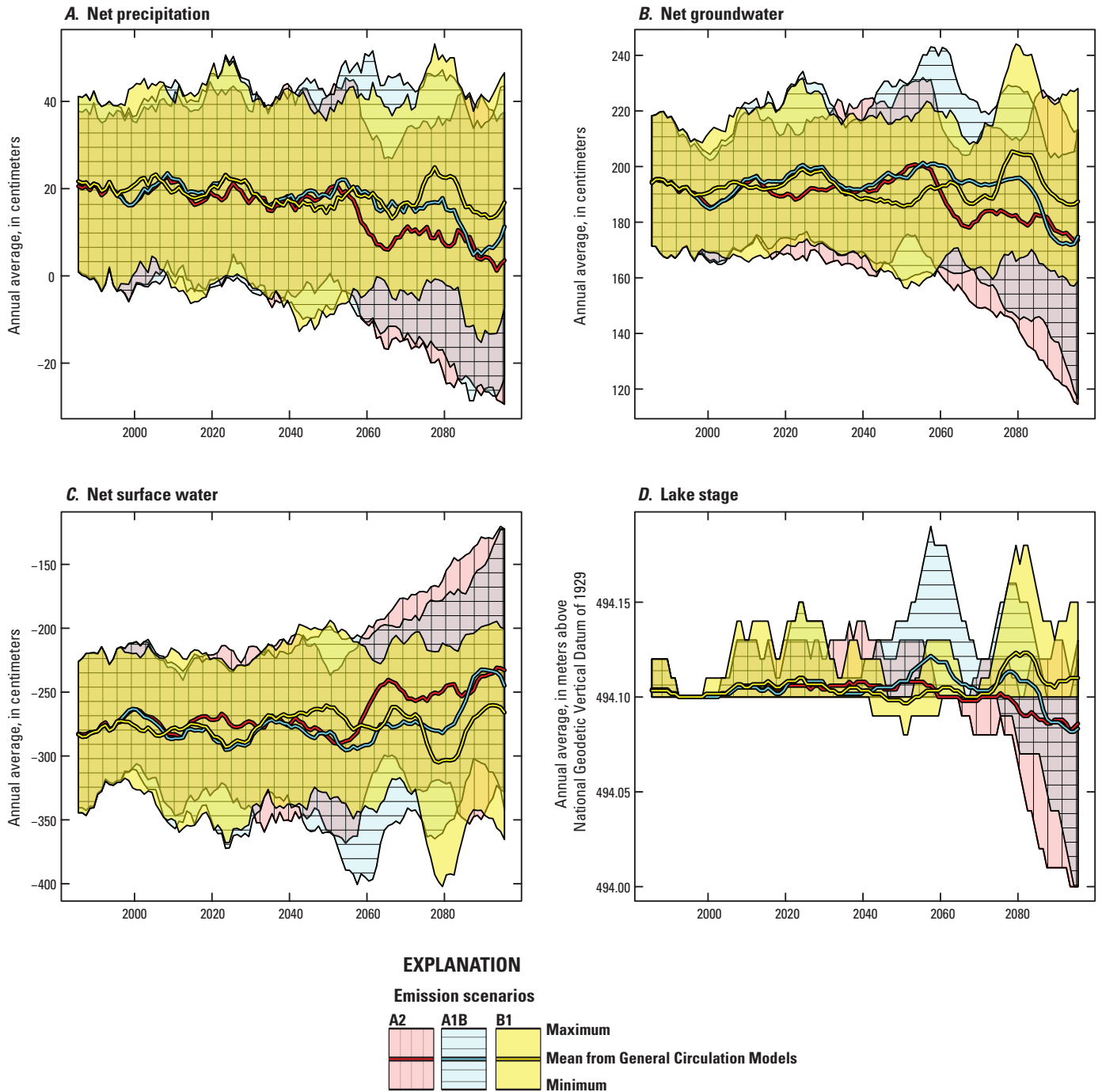


Figure 25. Climate-change simulations for Allequash Lake showing net annual components of the hydrologic budget normalized by lake area and related annual lake stage.

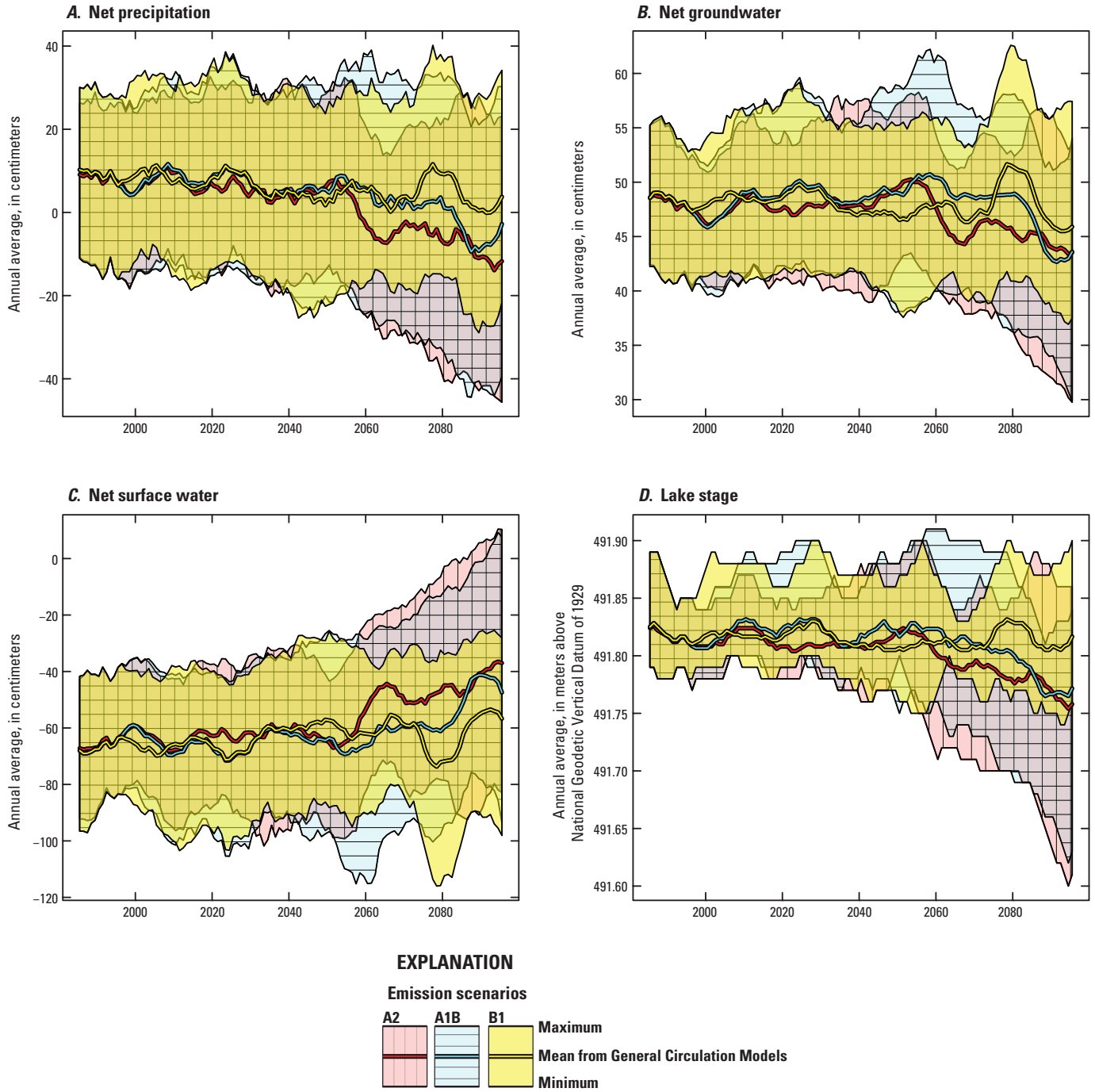


Figure 26. Climate-change simulations for Trout Lake showing net annual components of the hydrologic budget and normalized by lake area related annual lake stage.

Changes to Stream Temperature

All GCM models and scenarios result in a general increase in annual average stream temperatures over the 100-year simulation period (fig. 27). On the basis of the GCM scenario averages (solid lines in fig. 27), Upper Allequash Creek remains the coolest of the three streams and has the least amount of relative increase in annual average stream temperature (ranging from 1.0 to 2.2 °C depending on GCM emission scenario). North Creek and Stevenson Creek have larger relative increases in simulated stream temperatures,

ranging from 1.7 to 3.2 °C in Stevenson Creek and 1.4 to 2.9 °C in North Creek (fig. 27). Both the A2 (red) and A1B (blue) emission scenarios show the largest gains in average stream temperature. The B1 emission scenario shows relatively steady increases in average annual stream temperatures, but the rate of change is less than that of the other scenarios and gains over the 100-year period are the smallest. Similar to future forecasts of streamflow, stream temperature shows increasing variability (and thus uncertainty) across the scenarios as compared to current conditions (2000–2010) for all modeled streams.

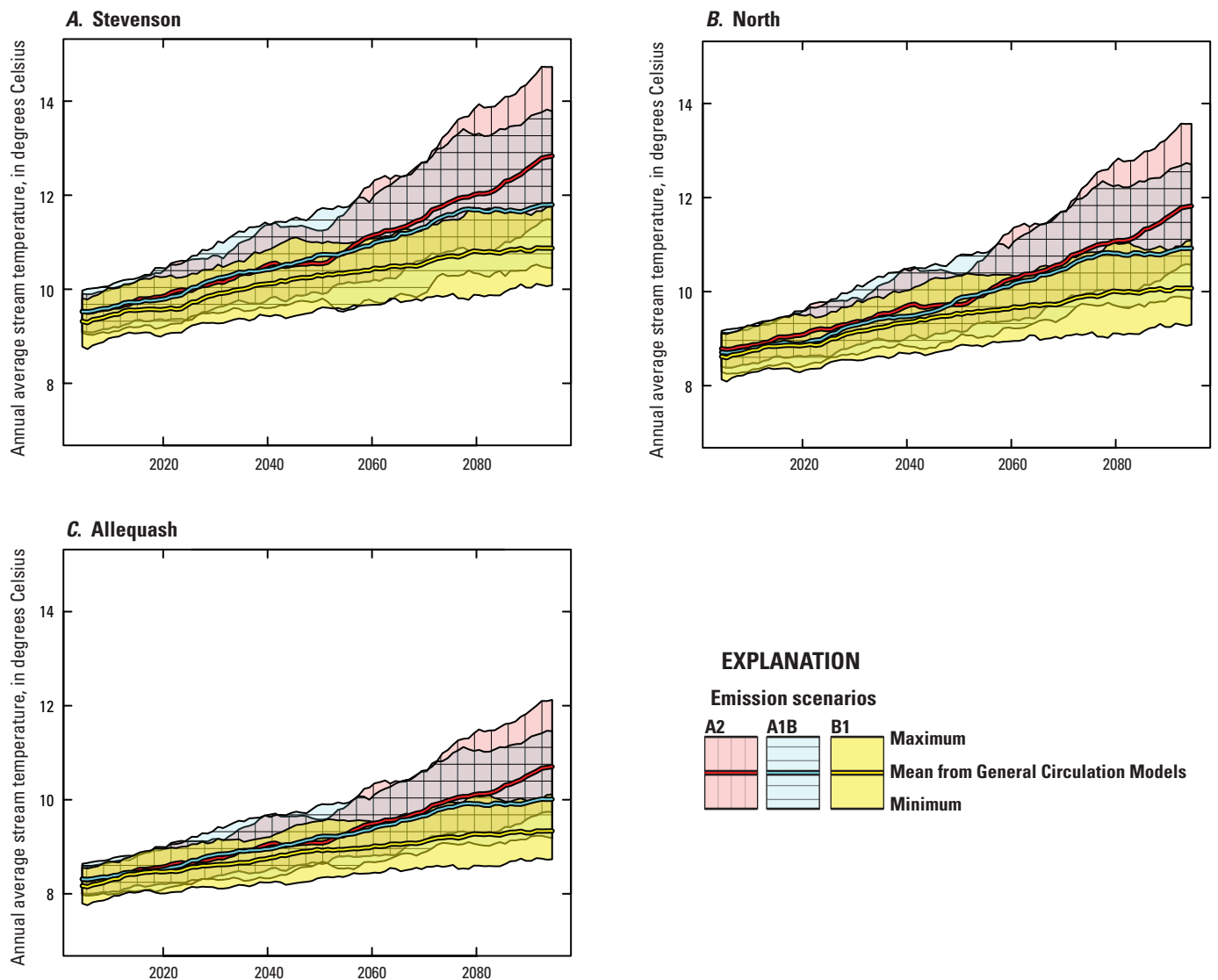


Figure 27. Climate-change simulations showing annual average stream temperatures for Stevenson, North, and Upper Allequash Creeks.

GSFLOW and SNTMP Limitations and Assumptions

Potential limitations of climate-change forecasts are well recognized (for example, Intergovernmental Panel on Climate Change, 2007) and thus are noted here but not expounded upon. Climate drivers used for the climate-change scenarios varied appreciably depending on the General Circulation Model (GCM) and emission scenario selected; this uncertainty was reflected in hydrologic-flow and temperature model results. Therefore, as with all forecasts of this type, the results are best considered to approximate potential outcomes of climate change.

Similar to all models, the Trout Lake hydrologic and temperature process-based models described here are simplifications of the natural world, with corresponding limitations in model simulation capability and forecast suitability. For example, the MODFLOW model discretization (cell size) is 75 m × 75 m; discretization of the PRMS surface-water model (hydrologic response unit, HRU) is even coarser. The conditions within the grid division (groundwater level, groundwater flow, evapotranspiration rate, soil moisture) are thus reduced to one average value for the entire model cell or HRU. Therefore, even though the resolution of the groundwater model grid is relatively high, the model would not be suitable for many site-scale or local headwater problems or issues without additional refinement.

Likewise, temporal simplifications were needed to develop tractable models used for this work. Models were constructed using daily or larger time increments; thus, partial-day (“continuous” or “storm-mode”) simulations of individual storm events were not in the scope of this work. Actual flood peaks that occur in the watershed due to intense rainfall on the partial-day timescale will not be reflected by this modeling on the daily timestep. Because of this averaging of partial-day stresses in the model, and the fact that the tool is developed by using watershed flows and not local hydraulic characteristics at any one location in the watershed, model results are reported in daily average streamflow (discharge) and not local stream stage or flood peak.

Although hydrologic parameters and aquifer and confining unit geometry in parts of the model area are generally not well known at smaller scales, data are more abundant and of better quality in some areas of the model domain (for example, the Allequash Creek Basin). As a result, properties that provide the best match between measured and simulated flows and groundwater levels primarily reflect conditions in these

data-rich parts of the watershed. Moreover, not all observed targets were given equal weight in the calibration; thus, all targets are not comparably simulated (appendix 6). Therefore, the GSFLOW model’s ability to simulate the Trout Lake system is variable, where some features (for example, primary LTER study lakes) are better represented than others (lakes on the periphery of the Trout Lake Watershed). Similarly, although the entire Trout Lake surface-water system is relatively well simulated, the streams with higher flows (Trout River, Allequash Creek) are better simulated than streams with lower streamflow (Stevenson Creek, North Creek). This underscores the model’s enhanced suitability to simulate large-scale bulk properties of the hydrologic system over smaller-scale property variation. The seasonal variability of solar radiation and potential evapotranspiration was based on existing national datasets; more contemporaneous local datasets would improve these crucial variables that influence many of the hydrologic processes in the model. Finally, the models are currently limited in their ability to simulate frozen-ground and lake-ice conditions. Therefore, simulated results may not capture all the short-term dynamics of the natural system during snow-melt periods.

Several assumptions and limitations are associated with in-stream temperature modeling. One of the biggest limiting factors is that SNTMP is a successive steady-state model and therefore can only represent changes over the minimum averaging period—in this case, 1 day. In other words, because the minimum averaging period is 1 day, the model cannot discern changes to stream temperature that occurred on an hourly scale. Consequently, changes in streamflow temperature cannot be well represented unless the change is gradually varying and sustained beyond the minimum averaging period. Another limiting assumption in SNTMP is homogenous and instantaneous mixing wherever two sources of water are combined; no dispersion or diffusion is represented in the model. Finally, all boundary conditions, similar to hydrologic conditions, are considered homogeneous and constant. This assumption has implications for the size of the network simulated for a single averaging period. Because the model is steady state, the water and associated thermal load must enter and exit within the 1-day averaging period. Given the relatively small geographical scale of the streams draining into Trout Lake and the velocity of the stream at base-flow conditions, the assumption of daily traveltime was likely violated only occasionally in this model during extremely high streamflow events. Nevertheless, potential for violations to this assumption may be important for some forecasts, such as reach-scale heat transport.

Summary

A calibrated transient surface-water model and a calibrated steady-state groundwater model were used to construct a single coupled transient groundwater/surface-water model for the Trout Lake Watershed in north-central Wisconsin, USA. The computer code GSFLOW was used to simulate the coupled hydrologic system; GSFLOW iteratively uses formulations of the PRMS surface-water model for hydrologic processes in the atmosphere, at land surface, and within the soil-zone, and a MODFLOW groundwater model for unsaturated-zone, saturated-zone, stream, and lake simulation. The coupled model was calibrated by using heads, streamflows, lake levels, actual evapotranspiration rates, solar radiation, and snowpack measurements collected during water years 1998–2007; calibration was done by use of advanced features in the PEST parameter-estimation software suite. Simulated streamflows from the calibrated GSFLOW model and other basin characteristics were used for SNTMP stream temperature simulations for selected tributaries in the watershed. The temperature model was calibrated to high-resolution stream temperature time-series data measured in 2002. The calibrated GSFLOW and SNTMP models were then used to simulate effects of potential climate change for the period 2010 to 2100. An ensemble of climate models and emission scenarios were evaluated. The results of this study can be summarized as follows:

- Separate calibration of the uncoupled groundwater and surface-water model did not provide a representative initial parameter set for coupled model calibration; however, a sequentially linked calibration, in which the uncoupled models were linked automatically by using utility software, provided a starting parameter set suitable for coupled-model calibration.
- Daily stream temperatures measured during 2002 were successfully simulated by using a 1-dimensional, steady-state SNTMP stream temperature model; the model fit was acceptable for a range of groundwater inflow rates into the streams.
- Downscaled climate drivers for the period 2010–2100 showed increases in maximum and minimum air temperature over the scenario period. Scenarios of future precipitation did not show a monotonic-like trend like temperature. Uncertainty in the climate drivers increased over time for both temperature and precipitation.
- Over the scenario period, growing-season length was simulated to increase by weeks, and both potential and actual evapotranspiration rates increased appreciably in response to increasing air temperature. Simulated actual evapotranspiration rates increased less than simulated potential evapotranspiration rates as a result

of water limitation in the root zone during the summer high-evapotranspiration period.

- The hydrologic-system response to climate change was characterized by a reduction in the importance of the snowmelt pulse and an increase in the importance of fall and winter groundwater recharge. The less dynamic simulated hydrologic regime is likely to result in drier soil conditions in rainfed wetlands and uplands and less drying in groundwater-fed systems.
- Averaging over an annual timeframe showed streamflows within the watershed being less affected by climate change than suggested by forecast increases in watershedwide evapotranspiration, owing to their strong connection to the groundwater system.
- Seepage lakes showed greater forecast stage declines related to climate change than drainage lakes. Seepage lakes higher in the watershed (nearer to groundwater divides) had less groundwater inflow and thus had larger forecast declines in lake stage. A seepage lake lower in the watershed had higher groundwater inflow and less forecast decline in lake stage. Groundwater inflow to seepage lakes tended to increase over time as lake stage declined.
- Drainage lakes responded with changes in outlet streamflow to offset losses to their water flows and were characterized by much smaller forecast stage declines. Net groundwater inflow tended to decrease in drainage lakes over the scenario period.
- Stream temperatures are expected to increase with climate change. The estimated increase in annual average temperature ranged from approximately 1 to 2 °C by 2100 in the high-groundwater-inflow stream and 2 to 3 °C in the stream with less groundwater inflow.
- The climate drivers used for the climate change scenarios varied appreciably between the General Circulation Model and emission scenario selected; this uncertainty was reflected in hydrologic-flow and temperature model results. Thus, as with all forecasts of this type, the results are best considered to approximate potential outcomes of climate change.

Acknowledgments

Roland Viger (USGS), Steven L. Markstrom (USGS), and David Prudic (USGS, retired) are acknowledged and thanked for their assistance in constructing early versions of models used in the project.

References Cited

- Anderson, M.P., and Bowser, C.J., 1986, The role of groundwater in delaying lake acidification: *Water Resources Research*, v. 22, p. 1101–1108.
- Anderson, M.P., and Champion, G.S., 2000, Assessment of impacts on groundwater/lake systems using MODFLOW with a lake package—Application to the Trout Lake Basin, northern Wisconsin: University of Wisconsin-Madison, Water Resources Institute, Groundwater Research Report WRI GRR 00-05.
- Attig, J.W., 1985, Pleistocene geology of Vilas County, Wisconsin: Wisconsin Geological and Natural History Survey Information Circular 50, 32 p.
- Bartholow, J.M., 1989, Stream temperature investigations—Field and analytical methods: U.S. Fish and Wildlife Service Instream Flow Information Paper No. 13, Biological Report 89(17), 139 p.
- Bartholow, J.M., 1991, A modeling assessment of the thermal regime for an urban sport fishery: *Environmental Management*, v. 15, no. 6, p. 833–845.
- Beven, K.J., and Freer, J., 2001, Equifinality, data assimilation, and uncertainty estimation in mechanistic modelling of complex environmental systems using the GLUE methodology: *Journal of Hydrology*, v. 249, nos. 1–4, p. 11–29.
- Cheng, Xiangxue, 1994, Numerical analysis of groundwater and lake systems with application to the Trout River Basin, Vilas County, Wisconsin: University of Wisconsin-Madison, Department of Geology and Geophysics, Ph.D. dissertation, 191 p.
- Cheng, Xiangxue, and Anderson, M.P., 1994, Simulating the influence of lake position on groundwater fluxes: *Water Resources Research*, v. 30, no. 7, p. 2041–2049.
- Christiansen, D.E., Markstrom, S.L., and Hay, L.E., 2011, Impacts of climate change on growing season in the United States: *Earth Interactions*, v. 15, no. 33, p. 1–17.
- Doherty, John, 2003, Groundwater model calibration using pilot points and regularization: *Ground Water*, v. 41, no. 2, p. 170–177.
- Doherty, John, and Hunt, R.J., 2009, Two statistics for evaluating parameter identifiability and error reduction: *Journal of Hydrology*, v. 366, p. 119–127, doi: 10.1016/j.jhydrol.2008.12.018.
- Doherty, John, 2010a, PEST, Model-independent parameter estimation—User manual (5th ed., with slight additions): Brisbane, Australia, Watermark Numerical Computing.
- Doherty, John, 2010b, Addendum to the PEST manual: Brisbane, Australia, Watermark Numerical Computing.
- Dripps, W.R., 2003, The spatial and temporal variability of groundwater recharge: University of Wisconsin-Madison, Department of Geology and Geophysics, Ph.D. dissertation, 231 p.
- Dripps, W.R., Hunt, R.J., and Anderson, M.P., 2006, Estimating recharge rates with analytic element models and parameter estimation: *Ground Water*, v. 44, no. 1, p. 47–55, doi:10.1111/j.1745-6584.2005.00115.x.
- Dunne, T., and Black, R.D., 1970, An experimental investigation of runoff production in permeable soils: *Water Resources Research*, v. 6, no. 5, p. 1296–1311.
- Ely, D.M., 2006, Analysis of sensitivity of simulated recharge to selected parameters for seven watersheds modeled using the precipitation-runoff modeling system: U.S. Geological Survey Scientific Investigations Report 2006–5041, 21 p.
- Gebert, W.A., Walker, J.F., and Hunt, R.J., 2011, Groundwater recharge in Wisconsin—Annual estimates for 1970–99 using streamflow data: U.S. Geological Survey Fact Sheet 2009–3092, 4 p.
- Gesch, D., Oimoen, M., Greenlee, S., Nelson, C., Steuck, M., and Tyler, D., 2002, The national elevation dataset: *Photogrammetric Engineering and Remote Sensing*, v. 68, p. 5–12.
- Hancock, P.J., Hunt, R.J., and Boulton, A.J., 2009, Preface—Hydrogeoeology, the interdisciplinary study of groundwater dependent ecosystems: *Hydrogeology Journal*, v. 17, no. 1, p. 1–4, doi:10.1007/s10040-008-0409-8.
- Harbaugh, A.W., 2005, MODFLOW-2005, the U.S. Geological Survey modular ground-water model—The ground-water flow process: U.S. Geological Survey Techniques and Methods, book 6, chap. A16 [variously paged].
- Harter, T., and Hopmans, J.W., 2004, Role of vadose zone flow processes in regional scale hydrology—Review, opportunities and challenges, *in* Feddes, R.A., de Rooij, G.H., and van Dam, J.C., *Unsaturated zone modeling—Progress, applications, and challenges*: Dordrecht, Boston, Kluwer Academic, p. 179–208.
- Horton, R.E., 1933, The role of infiltration in the hydrological cycle: *American Geophysical Union Transactions* v. 23, p. 479–482.
- Houser, J.N., 2006, Water color affects the stratification, surface temperature, heat content, and mean epilimnetic irradiance of small lakes: *Canadian Journal of Fisheries and Aquatic Sciences*, v. 63, no. 11, p. 2447–2455.

- Hunt, R.J., Anderson, M.P., and Kelson, V.A., 1998, Improving a complex finite-difference ground water flow model through the use of an analytic element screening model: *Ground Water*, v. 36, no. 6, p. 1011–1017.
- Hunt, R.J., Doherty, J., and Tonkin, M.J., 2007, Are models too simple? Arguments for increased parameterization: *Ground Water*, v. 45, no. 3, p. 254–262, doi:10.1111/j.1745-6584.2007.00316.x.
- Hunt, R.J., Doherty, J., and Walker, J.F., 2009, Parameter estimation and coupled groundwater/surface-water models—A PEST approach, in *Conference Proceedings from the 1st PEST Conference*, November 1–3, 2009, Potomac, Md.: Lulu Press, Inc., Raleigh, N.C., USA.
- Hunt, R.J., Prudic, D.E., Walker, J.F., and Anderson, M.P., 2008, Importance of unsaturated zone flow for simulating recharge in a humid climate: *Ground Water*, v. 46, no. 4, p. 551–560, doi:10.1111/j.1745-6584.2007.00427.x.
- Hunt, R.J., and Steuer, J.J., 2000, Simulation of the recharge area for Frederick Springs, Dane County, Wisconsin: U.S. Geological Survey Water-Resources Investigations Report 00–4172, 33 p.
- Hunt, R.J.; Strand, Mac; and Walker, J.F., 2006, Measuring groundwater-surface water interaction and its effect on wetland stream benthic productivity, Trout Lake Watershed, northern Wisconsin, USA: *Journal of Hydrology*, v. 320, p. 370–384.
- Hunt, R.J., and Wilcox, D.A., 2003, Ecohydrology—Why hydrologists should care: *Ground Water*, v. 41, no. 3, p. 289, doi:10.1111/j.1745-6584.2003.tb02592.x.
- Hurley, J.P., Armstrong, D.E., Kenoyer, G.J., and Bowser, C.J., 1985, Ground water as a silica source for diatom production in a precipitation-dominated lake: *Science*, v. 227, p. 1576–1578.
- Intergovernmental Panel on Climate Change, 2007, Summary for policymakers, in *Climate change 2007—The physical science basis*, Contributions of Working Group I to the Fourth Assessment Report of the Intergovernmental Panel on Climate Change: Cambridge and New York, Cambridge University Press, 18 p.
- John, Rahul, 2005, Simulating response rates and historical transience of surface water and groundwater—Trout Lake Basin, northern Wisconsin: University of Wisconsin-Madison, Department of Geology and Geophysics, M.S. thesis, 151 p.
- Kenoyer, G.J., 1988, Tracer test analysis of anisotropy in hydraulic conductivity of granular aquifers: *Ground Water Monitoring and Remediation*, v. 8, no. 3, p. 67–70, doi:10.1111/j.1745-6592.1988.tb01086.x.
- Krabbenhoft, D.P., Bowser, C.J., Anderson, M.P., and Valley, J.W., 1990, Estimating groundwater exchange with lakes—1. The stable isotope mass balance method: *Water Resources Research*, v. 26, no. 10, p. 2445–2453, doi:10.1029/WR026i010p02445.
- Leavesley, G.H., Lichty, R.W., Troutman, B.M., and Saindon, L.G., 1983, Precipitation-runoff modeling system—User’s manual: U.S. Geological Survey Water-Resources Investigation Report 83–4238, 207 p.
- Leavesley, G.H., Markstrom, S.L., Viger, R.J., and Hay, L.E., 2005, USGS Modular Modeling System (MMS)—Precipitation-Runoff Modeling System (PRMS) MMS-PRMS, in Singh, V., and Frevert, D., eds., *Watershed models*: Boca Raton, Fla., CRC Press, p. 159–177.
- Leopold, L.B., 1974, *Water—A primer*: San Francisco, W.H. Freeman Co., 172 p.
- Magnuson, J.J., Kratz, T.K., and Benson, B.J., eds., 2006, Long-term dynamics of lakes in the landscape—Long-term ecological research on north temperate lakes: New York, Oxford University Press, 400 p.
- Markstrom, S.L., Hay, L.E., Ward-Garrison, D.C., Risley, J.C., Battaglin, W.A., Bjerkle, D.M., Chase, K.J., Christiansen, D.E., Dudley, R.W., Hunt, R.J., Kocot, K.M., Mastin, M.C., Regan, R.S., Viger, R.L., Vining, K.C., and Walker, J.F., 2012, Integrated watershed scale response to climate change for selected basins across the United States: U.S. Geological Survey Scientific Investigations Report 2011–5077, 134 p.
- Markstrom, S.L., Niswonger, R.G., Regan, R.S., Prudic, D.E., and Barlow, P.M., 2008, GSFLOW—Coupled Ground-Water and Surface-Water Flow Model based on the integration of the Precipitation-Runoff Modeling System (PRMS) and the Modular Ground-Water Flow Model (MODFLOW-2005): U.S. Geological Survey Techniques and Methods, book 6, chap. D1, 240 p.
- Merritt, M.L., and Konikow, L.F., 2000, Documentation of a computer program to simulate lake-aquifer interaction using the MODFLOW ground-water flow model and the MOC3D solute-transport model: U.S. Geological Survey Water-Resources Investigations Report 00–4167, 146 p.

- Muffels, C.T., 2008, Application of the LSQR algorithm to the calibration of a regional groundwater flow model—Trout Lake Basin, Vilas County, Wisconsin: University of Wisconsin-Madison, M.S. thesis, 106 p.
- National Climatic Data Center, 2004, Climatology of the United States No. 20—Monthly station climate summaries, 1971–2000: Asheville, N.C., National Oceanic and Atmospheric Administration, 653 p.
- Niswonger, R.G.; Panday, Sorab; and Ibaraki, Motomu, 2011, MODFLOW-NWT, A Newton formulation for MODFLOW-2005: U.S. Geological Survey Techniques and Methods, book 6, chap. A37, 44 p.
- Niswonger, R.G., and Prudic, D.E., 2005, Documentation of the Streamflow-Routing (SFR2) Package to include unsaturated flow beneath streams—A modification to SFR1: U.S. Geological Survey Techniques and Methods, book 6, chap. A13, 51 p.
- Niswonger, R.G., Prudic, D.E., and Regan, R.S., 2006, Documentation of the Unsaturated-Zone Flow (UZF1) Package for modeling unsaturated flow between the land surface and the water table with MODFLOW-2005: U.S. Geological Survey Techniques and Methods, book 6, chap. A19, 74 p.
- Okwueze, E.E., 1983, Geophysical investigation of the bedrock and groundwater-lake flow system in the Trout Lake region of Vilas County, northern Wisconsin: University of Wisconsin-Madison, Department of Geology and Geophysics, Ph.D. dissertation, 130 p.
- Pint, C.D., 2002, A groundwater flow model of the Trout Lake Basin, Wisconsin—Calibration and lake capture zone analysis: University of Wisconsin-Madison, M.S. thesis, 123 p.
- Pint, C.D., Hunt, R.J., and Anderson, M.P., 2003, Flowpath delineation and ground water age, Allequash Basin, Wisconsin: *Ground Water*, v. 41, no. 7, p. 895–902.
- Simmons, C.T., and Hunt, R.J., 2012, Updating the debate on model complexity: *GSA Today*, v. 22, no. 8, p. 28–29, doi: 10.1130/GSATG150GW.1.
- Steuer, J.J., and Hunt, R.J., 2001, Use of a watershed-modeling approach to assess hydrologic effects of urbanization, North Fork Pheasant Branch Basin near Middleton, Wisconsin: U.S. Geological Survey Water-Resources Investigations Report 01–4113, 49 p.
- Theurer, F.D., Voos, K.A., and Miller, W.J., 1984, Instream water temperature model: U.S. Fish and Wildlife Service Instream Flow Information Paper 16, FWS/OBS-85/15 [variously paginated].
- Viger, R.J., and Leavesley, G.H., 2007, The GIS Weasel user's manual: U.S. Geological Survey Techniques and Methods, book 6, chap. B4, 201 p. (available at <http://pubs.usgs.gov/tm/2007/06B04/>).
- Walker, J.F., and Bullen, T.D., 2000, Trout Lake, Wisconsin—A Water, Energy, and Biogeochemical Budgets Program site: U.S. Geological Survey Fact Sheet 161–99, 4 p.
- Walker, J.F., Hunt, R.J., Hay, L.E., and Markstrom, S.L., 2012, Watershed scale response to climate change—Trout Lake Basin, Wisconsin: U.S. Geological Survey Fact Sheet 2011–3119, 6 p.
- Walker, J.F., Hunt, R.J., Markstrom, S.L., Hay, L.E., and Doherty, J., 2009, Using a coupled ground-water/surface-water model to predict climate-change impacts to lakes in the Trout Lake Watershed, Northern Wisconsin, *in* Webb, R.M.T., and Semmens, D.J., eds., Planning for an uncertain future—Monitoring, integration, and adaptation. Proceedings of the Third Interagency Conference on Research in the Watersheds: U.S. Geological Survey Scientific Investigations Report 2009–5049, p. 155–161.
- Wentz, D.A., and Rose, W.J., 1991, Hydrology of Lakes Clara and Vandercook in north-central Wisconsin: U.S. Geological Survey Water-Resources Investigations Report 89–4204, 24 p.
- Westenbroek, S.M., Doherty, J., Walker, J.F., Kelson, V.A., Hunt, R.J., and Cera, T.B., 2012, Approaches in highly parameterized inversion—TSPROC, A general time-series processor to assist in model calibration and result summarization: U.S. Geological Survey Techniques and Methods, book 7, chap. C7, 73 p.
- Wisconsin Initiative on Climate Change Impacts, 2011, Wisconsin's changing climate—Impacts and adaptation: Madison, Wis., Nelson Institute for Environmental Studies, University of Wisconsin-Madison and the Wisconsin Department of Natural Resources, 217 p.
- Winter, T.C., Harvey, J.W., Franke, O.L., and Alley, W.M., 1998, Ground water and surface water—A single resource: U.S. Geological Survey Circular 1139, 79 p.
- Winter, T.C., Rosenberry, D.O., and LaBaugh, J.W., 2003, Where does the ground water in small watersheds come from?: *Ground Water*, v. 41, no. 7, p. 989–1000, doi: 10.1111/j.1745-6584.2003.tb02440.x.
- Zarriello, P.J., and Ries, K.G., III, 2000, A precipitation-runoff model for the analysis of the effects of water withdrawals on streamflow, Ipswich River Basin, Massachusetts: U.S. Geological Survey Water-Resources Investigations Report 00–4029, 99 p.

Appendix 1. Groundwater Model Construction

Groundwater Model Construction	38
References Cited.....	44

Figures

1-1. Map showing Trout Lake Watershed model location.....	38
1-2. Map showing altitude of the impermeable bedrock surface used in MODFLOW and associated GSFLOW model.....	39
1-3. Hydrogeologic sections in Vilas County, Wisconsin.....	40
1-4. Hydrostratigraphic section showing associated model layering along B-B'	41
1-5. Map showing location of the 218 pilot points used in each layer	41
1-6. Map showing location of farfield surface-water features outside the Trout Lake area of interest simulated with the GHB Package, lakes simulated with the LAK3 Package in the nearfield area of interest, and nearfield streams simulated with the SFR Package	42
1-7. Map showing wetland areas adjacent to surface-water features	43

Groundwater Model Construction

The Trout Lake Watershed has been the focus of several modeling studies (Cheng, 1994; Hunt and others, 1998; Pint and others, 2003; Hunt and others, 2008) that represent stages in the development and refinement of a regional groundwater model. The model framework, boundary conditions, and conceptualization are described by Pint (2002). Traditional calibration targets (heads, fluxes) and nontraditional calibration targets (for example, lake groundwater inflow, depth of lake plume) are described by Pint (2002) and Hunt and

others (2005). The groundwater-model construction methods followed those described by Muffels (2008) and Hunt and others (2008). They included a telescopic mesh refinement of a regional analytic-element groundwater-flow model and automated regularized inversion calibration using a parameter-estimation program. Groundwater flow within the Trout Lake Watershed (fig. 1–1), was simulated by using MODFLOW2005 (Harbaugh, 2005). Particle tracking was performed by means of MODPATH (Pollock, 1994), and effective porosity was set equal to 0.29, after Krabbenhoft and Babiarz (1992).

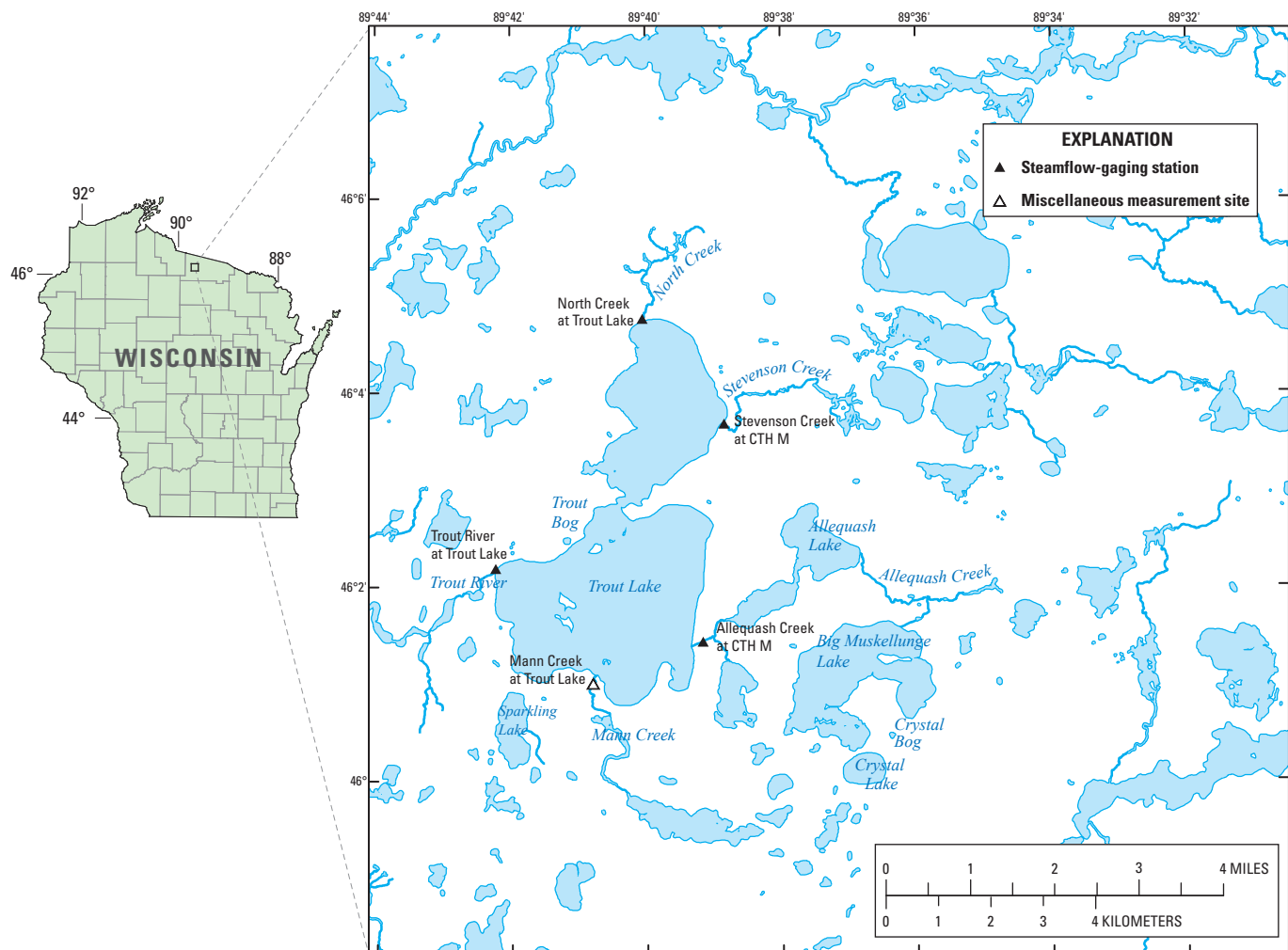


Figure 1–1. Trout Lake Watershed model location (from Hunt and others, 2008).

The three-dimensional, finite-difference model employs a grid comprising 230 rows and 240 columns with a uniform horizontal cell size of 75×75 meters (m) and six layers, which results in a model domain of 31,050 hectares (120 square miles). A two-dimensional analytic element (AE) model using GFLOW (Haitjema, 1995) was modified from an existing regional model of the Trout Lake area (Hunt and others, 1998) and was used to derive boundary conditions for the finite-difference model in accordance with the methods of Hunt and others (1998). Briefly, groundwater fluxes calculated

at the boundaries of the MODFLOW grid by the AE model were distributed to the six layers of the finite-difference model on the basis of layer transmissivity; these were then supplied to the model domain through MODFLOW's Well Package. The crystalline bedrock, assumed to be impervious, forms the bottom boundary of the model; although a horizontal model bottom was assumed in the regional analytic element model, the finite-difference model used a variable bottom (figs. 1–2 and 1–3). Recharge flux is specified across the water table, which forms the upper boundary of the groundwater model.

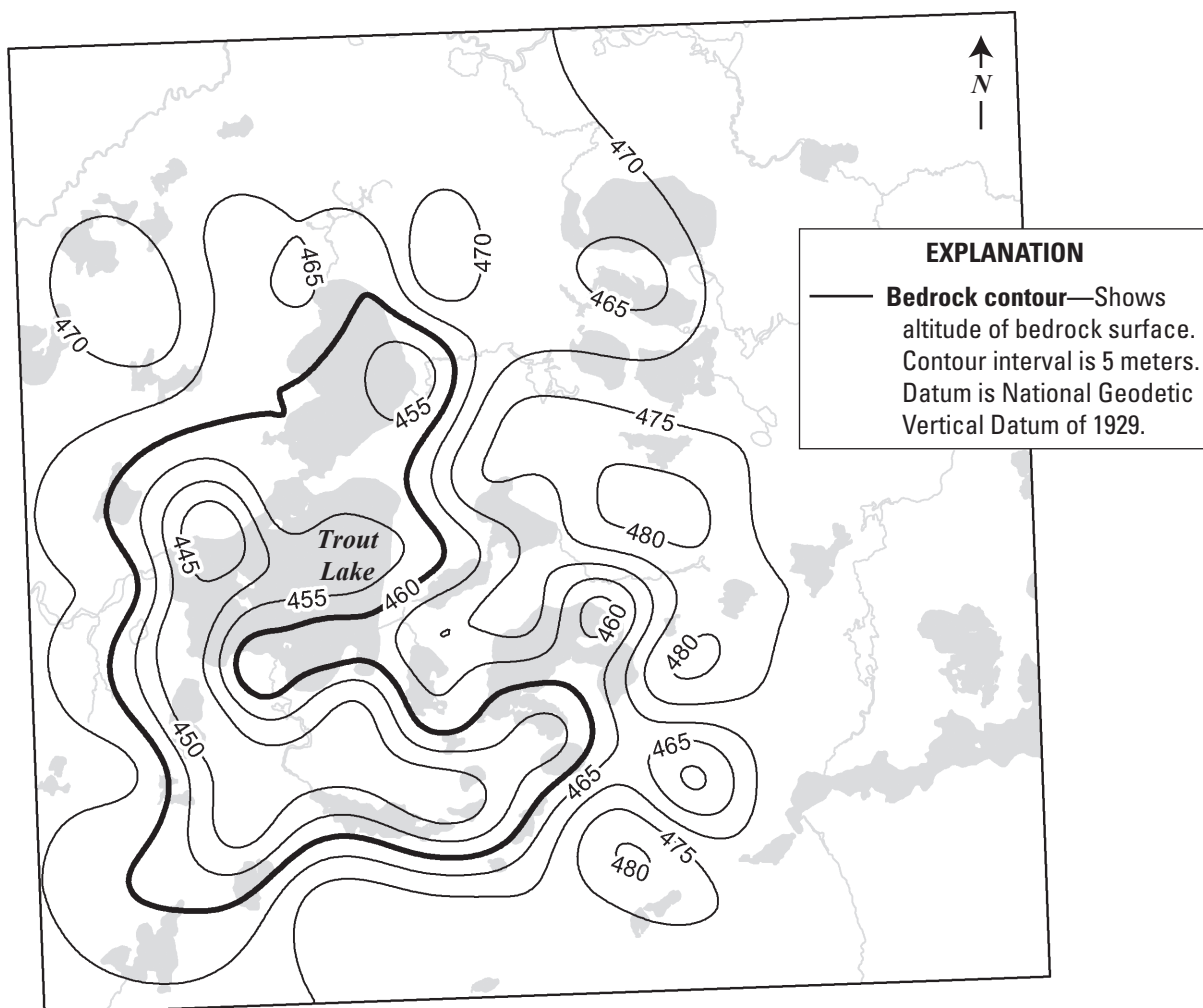


Figure 1–2. Altitude of the impermeable bedrock surface used in MODFLOW and associated GSFLOW model (from Muffels, 2008).

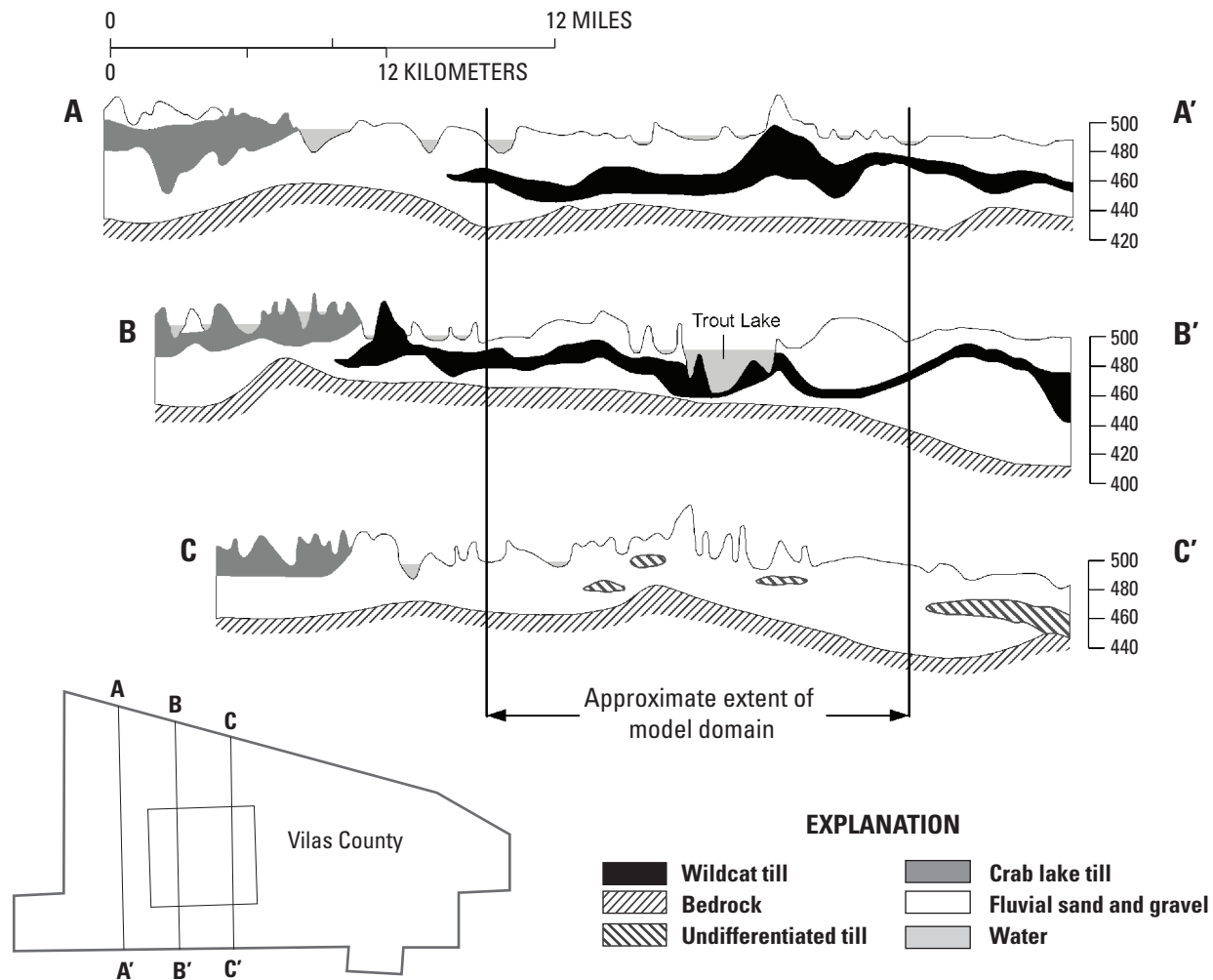


Figure 1-3. Hydrogeologic sections in Vilas County, Wisconsin, based on Attig (1985) and Muffels (2008). Legend and colors refer to glacial units reported by Attig (1985). Location of Vilas County is shown in figure 1-1.

Similar to Muffels (2008), the aquifer was represented in the model by using the stratigraphic conceptualization of Attig (1985), which distinguishes between glacial deposits (fig. 1-3) on the basis of glacial ice-front proximity. Stratigraphic units were converted to hydrostratigraphic units (fig. 1-4) by Muffels (2008); the layering and hydrostratigraphic assignments were unaltered in this model update. Hydrogeologic sections in Vilas County, Wisconsin, based on Attig (1985) and Muffels (2008). Legend and colors refer to glacial units reported by Attig (1985). Location of Vilas County is shown in figure 1-1.

Hydraulic conductivity within the model domain was specified by using pilot points (Doherty, 2003) in combination with the design and layout of Muffels (2008). The general goal of pilot-point use is to provide an intermediate alternative to two end-member approaches of parameterization: (1) cell-by-cell variability, whereby each model node can have a different value; and (2) a priori reduction/lumping of many nodes

into a small set of piecewise-constant homogeneous zones. In the pilot-point approach, parameter values are estimated at a number of discrete locations distributed throughout the model domain; cell-by-cell parameterization then takes place through spatial interpolation from the pilot points to the model grid or mesh. As applied in the Trout Lake model, pilot points were grouped to represent geologic continuity where it is believed to exist. Vertical-anisotropy pilot points were also specified at each horizontal hydraulic conductivity (K_h) pilot-point location. Therefore, each aquifer layer was represented by 218 horizontal-hydraulic-conductivity and 218 collocated vertical-anisotropy pilot points (fig. 1-5), for a total of 2,616 pilot points in the model domain. See Muffels (2008) for additional information regarding the pilot-point parameterization. Additional discussion of the application of pilot points is given in appendix 3 and the calibrated values of hydraulic conductivity resulting from the pilot point distribution are given in appendix 6.

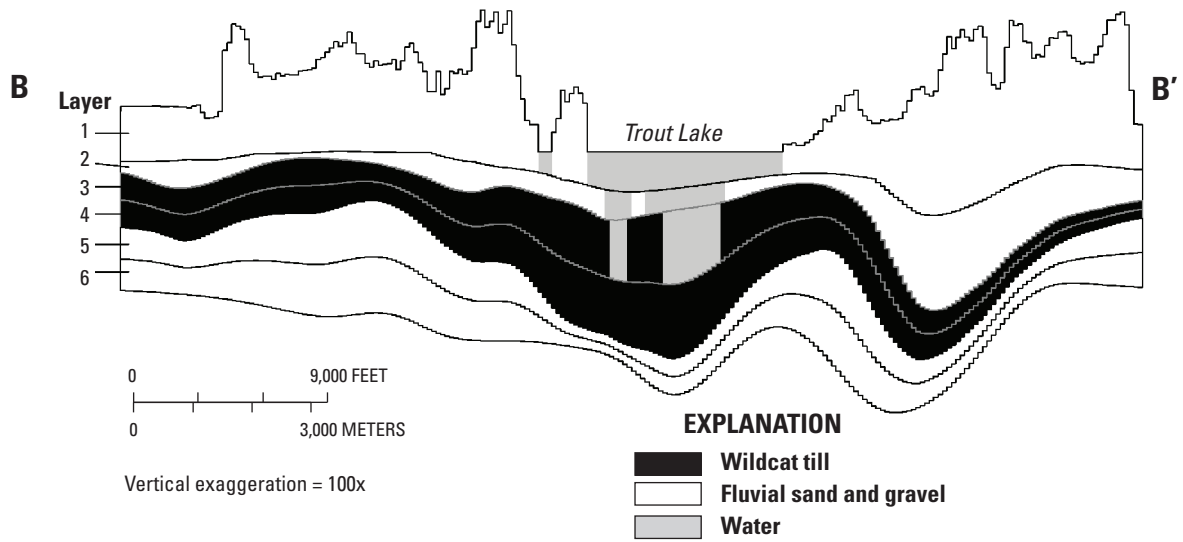


Figure 1-4. Hydrostratigraphic section showing associated model layering along B-B' (from Muffels, 2008).

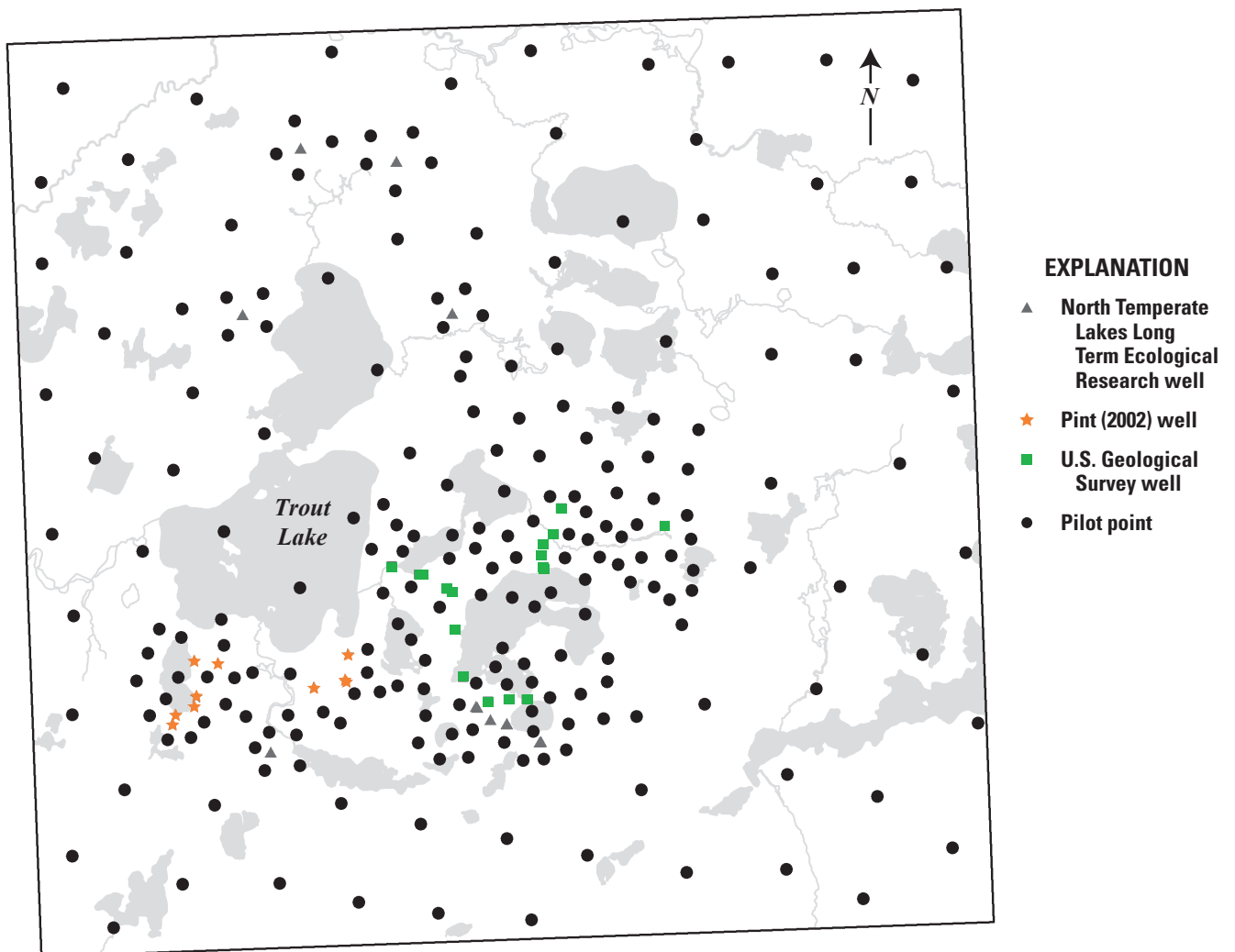


Figure 1-5. Location of the 218 pilot points used in each layer; K_h and K_v pilot points are colocated (from Muffels, 2008).

Thirty lakes within the Trout Lake Watershed or near its boundary are simulated by using the MODFLOW Lake Package (LAK: Merritt and Konikow 2000; updated by Markstrom and others, 2008; fig. 1–6), which calculates lake stages on the basis of volumetric water budgets. Simulating lake stages within the model is superior to specifying lake stages with constant-head nodes because it helps ensure that heads are not overly constrained in the immediate area of interest. Similarly, all streams inside the area of interest (defined here as “nearfield”) used the MODFLOW Streamflow Routing (SFR2) Package (Niswonger and Prudic, 2005), to allow accounting of streamflow. The SFR2 Package also limits the amount of water a stream can lose to the adjacent aquifer to the amount of water flowing in the stream. Streambed/lakebed sediments are assumed to have a uniform thickness of 1 m and a uniform vertical hydraulic conductivity. Outside the area of interest (defined here as “farfield”), streams and lakes were simulated with the MODFLOW General Head Boundary (GHB) Package (fig. 1–6).

Recharge to the model was simulated with the MODFLOW Unsaturated-Zone Flow (UZF) Package (Niswonger and others, 2006). Water leaving the soil zone (calculated by the PRMS model) was specified as “infiltration” to the top of the unsaturated zone. Recharge to the saturated zone was calculated by the UZF Package using specified unsaturated-zone properties, including the vertical saturated hydraulic conductivity of the soil (input variable VKS) and a parameter that describes the relation of hydraulic conductivity to soil moisture (a Brooks-Corey epsilon or EPS variable), as well as the transient loading of water specified by the time-varying infiltration (input variable FINF) rate. Unsaturated-zone thickness also is used by UZF to simulate recharge and is calculated by subtracting the simulated water-table elevation from the land-surface elevation that is specified by the top elevation (input variable TOP) in MODFLOW’s Layer Property Flow (LPF) Package. TOP is a critical parameter in the calculation of recharge within UZF, which differs from MODFLOW’s

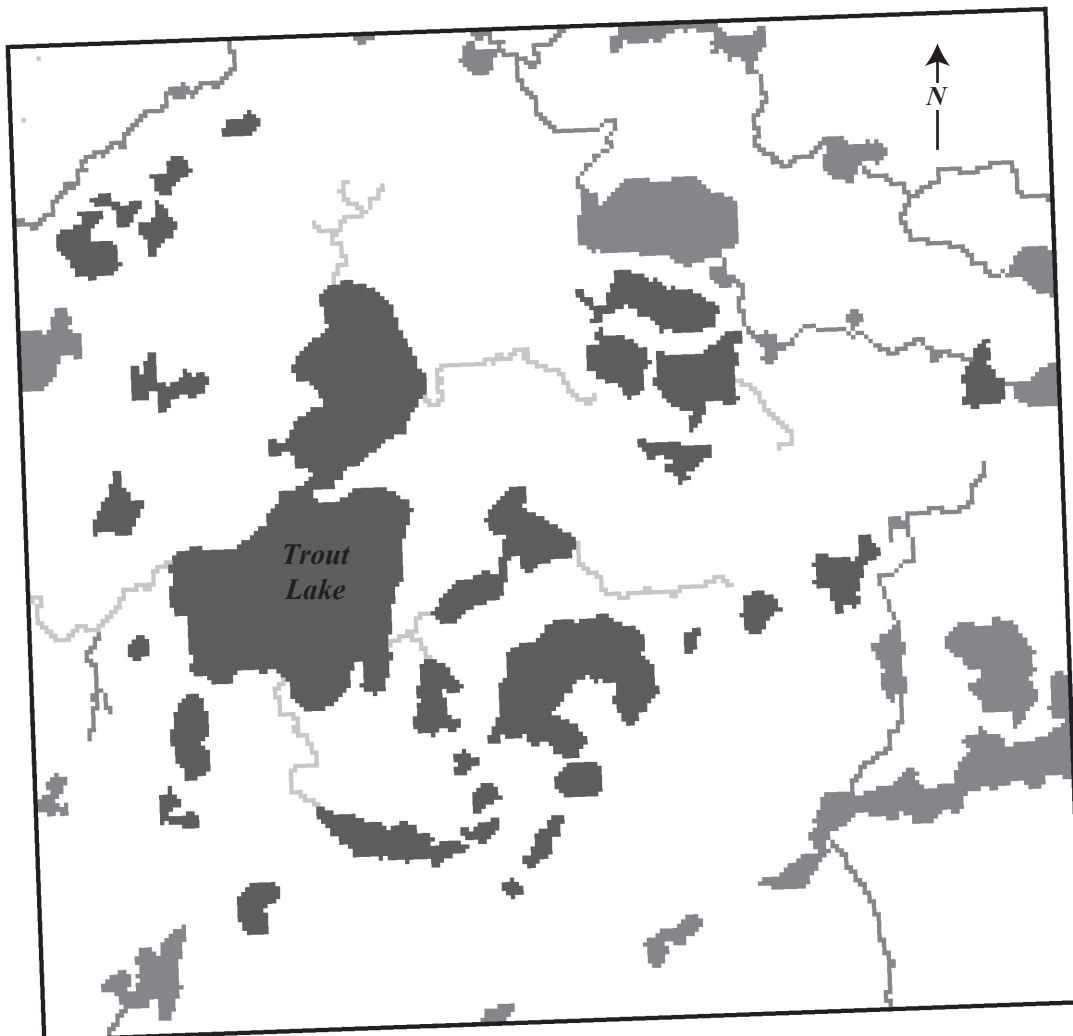


Figure 1–6. Location of farfield surface-water features outside the Trout Lake area of interest simulated with the GHB Package (dark gray), lakes simulated with the LAK3 Package in the nearfield area of interest (near black), and nearfield streams simulated with the SFR Package (light gray), from Muffels (2008).

Recharge (RCH) Package approach whereby the variable TOP for an unconfined top layer is commonly set to some arbitrary value because it is not used in most calculations of groundwater flow.

As described by Niswonger and others (2006), the UZF Package routes water through an assumed homogeneous unsaturated zone by using a one-dimensional kinematic wave approximation to Richards' equation that ignores capillary forces, and it can partition precipitation into evapotranspiration, runoff, unsaturated zone storage, and recharge. Two capabilities of the UZF Package are notable for model calibration. First, water that leaves the root zone is routed through the unsaturated zone to the water table rather than being directly applied to the water table. This allows simulation of lags and mixing between infiltration events leaving the root zone before becoming water-table recharge. Second, the UZF Package can generate and route runoff to surface-water features in areas where groundwater is at or above land surface, or during periods when infiltration rates exceed the soil's ability to transmit the water. This capability allows simulation of variable source areas for surface runoff generation. More representative simulations of variable source areas facilitate

more realistic simulations of groundwater/surface-water interaction dynamics. These areas represent potential variable source areas for surface-runoff generation when groundwater heads reach land surface and are therefore routed to LAK Package lakes or SFR Package streams in the model through the UZF Package IRUNBND array during the sequentially linked model calibration (see appendix 3). The fully coupled GSFLOW model does not use this explicit routing but instead routes overland flow by using surface-water cascades specified for the PRMS hydrologic response units. Streams within the watershed of interest are simulated with the SFR Package (light gray; fig. 1–6) and lakes are simulated with the LAK Package (black; fig. 1–6). Moreover, the ability to remove and route water to adjacent surface-water features is superior to the overpressurizing of the groundwater system that can result from direct application of infiltration to the water table (Hunt and others, 2008). Areas that generated overland runoff were in low-lying wetland areas adjacent to streams and lakes (fig. 1–7). Because the study watershed is relatively undeveloped, no other hydrologic features (for example, pumping wells, drain tiles) were included in the simulation.

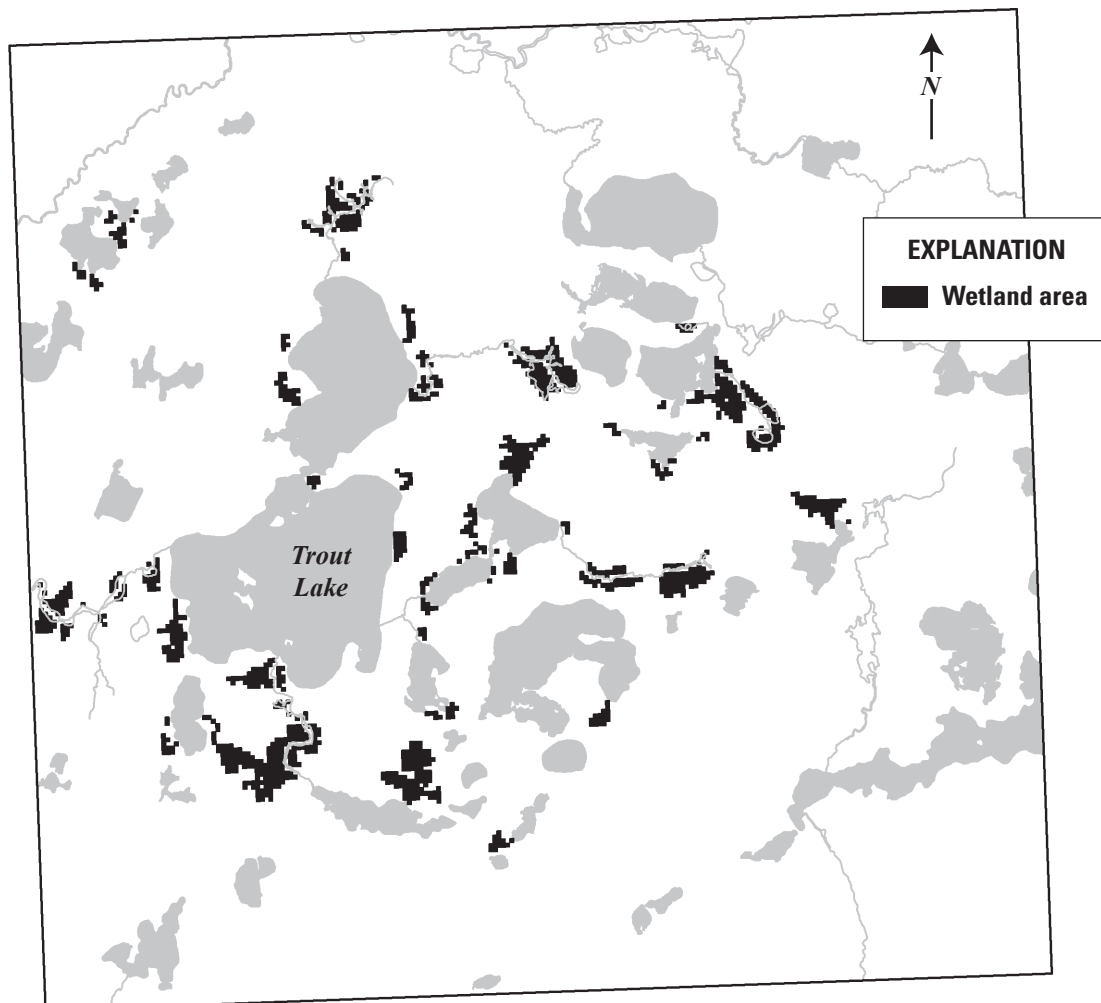


Figure 1–7. Wetland areas adjacent to surface-water features (black) from Muffels (2008).

References Cited

- Attig, J.W., 1985, Pleistocene geology of Vilas County, Wisconsin. Wisconsin Geological and Natural History Survey Information Circular 50, 32 p.
- Cheng, Xiangxue, 1994, Numerical analysis of groundwater and lake systems with application to the Trout River Basin, Vilas County, Wisconsin: University of Wisconsin-Madison, Department of Geology and Geophysics, Ph.D. dissertation, 191 p.
- Doherty, John, 2003, Groundwater model calibration using pilot points and regularization: *Ground Water*, v. 41, no. 2, p. 170–177.
- Haitjema, H.M., 1995, Analytic element modeling of groundwater flow: San Diego, Calif., Academic Press, 394 p.
- Harbaugh, A.W., 2005, MODFLOW-2005, the U.S. Geological Survey modular ground-water model—The Ground-Water Flow Process: U.S. Geological Survey Techniques and Methods, book 6, chap. A16 [variously paged].
- Hunt, R.J., Anderson, M.P., and Kelson, V.A., 1998, Improving a complex finite-difference ground water flow model through the use of an analytic element screening model: *Ground Water*, v. 36, no 6, p. 1011–1017.
- Hunt, R.J., Feinstein, D.T., Pint, C.D., and Anderson, M.P., 2005, The importance of diverse data types to calibrate a watershed model of the Trout Lake Basin, northern Wisconsin, USA: *Journal of Hydrology*, v. 321, nos. 1–4, p. 286–296, doi:10.1016/j.jhydrol.2005.08.005.
- Hunt, R.J., Prudic, D.E., Walker, J.F., and Anderson, M.P., 2008, Importance of unsaturated zone flow for simulating recharge in a humid climate: *Ground Water*, v. 46, no. 4, p. 551–560, doi:10.1111/j.1745-6584.2007.00427.x.
- Krabbenhoft, D.P., and Babiarz, C.L., 1992, The role of groundwater transport in aquatic mercury cycling: *Water Resources Research*, v. 28, no. 12, p. 3119–3128.
- Markstrom, S.L., Niswonger, R.G., Regan, R.S., Prudic, D.E., and Barlow, P.M., 2008, GSFLOW—Coupled Ground-Water and Surface-Water Flow Model based on the integration of the Precipitation-Runoff Modeling System (PRMS) and the Modular Ground-Water Flow Model (MODFLOW-2005): U.S. Geological Survey Techniques and Methods, book 6, chap. D1, 240 p.
- Merritt, M.L., and Konikow, L.F., 2000, Documentation of a computer program to simulate lake-aquifer interaction using the MODFLOW ground-water flow model and the MOC3D solute-transport model: U.S. Geological Survey Water-Resources Investigations Report 00–4167, 146 p.
- Muffels, C.T., 2008, Application of the LSQR algorithm to the calibration of a regional groundwater flow model—Trout Lake Basin, Vilas County, Wisconsin: University of Wisconsin-Madison, M.S. thesis, 106 p.
- Niswonger, R.G., and Prudic, D.E., 2005, Documentation of the Streamflow-Routing (SFR2) Package to include unsaturated flow beneath streams—A modification to SFR1: U.S. Geological Survey Techniques and Methods, book 6, chap. A13, 51 p.
- Niswonger, R.G., Prudic, D.E., and Regan, R.S., 2006, Documentation of the Unsaturated-Zone Flow (UZFI) Package for modeling unsaturated flow between the land surface and the water table with MODFLOW-2005: U.S. Geological Survey Techniques and Methods, book 6, chap. A19, 74 p.
- Pint, C.D., 2002, A groundwater flow model of the Trout Lake Basin, Wisconsin—Calibration and lake capture zone analysis: University of Wisconsin-Madison, M.S. thesis, 123 p.
- Pint, C.D., Hunt, R.J., and Anderson, M.P., 2003, Flowpath delineation and ground water age, Allequash Basin, Wisconsin: *Ground Water*, v. 41, no. 7, p. 895–902.
- Pollock, D.W., 1994, User's guide for MODPATH/MODPATH-PLOT, Version3—A particle tracking post-processing package for MODFLOW, the U.S. Geological Survey finite-difference ground-water flow model: U.S. Geological Survey Open-File Report 94–464, 249 p.

Appendix 2. Surface-Water Model Construction

Grid Rotation	46
Hydrologic Response Units	46
Surface-Water Routing	46
Parameterization of the Model	50
Climate Data Used for Model Forcing	50
Variation of Growing Season with Changing Temperatures	53
References Cited.....	53

Figures

2-1. Map showing subwatersheds used in assigning spatially variable parameter values to the individual hydrologic response units.....	47
2-2. Diagram showing overland-flow routing diagram generated for the Trout Lake Precipitation-Runoff Modeling System model.....	48
2-3. Diagram showing groundwater-flow routing diagram generated for the Trout Lake Precipitation-Runoff Modeling System model.....	49

Tables

2-1. Description of parameter types determined by the GIS Weasel that were not varied during calibration	51
2-2. National Weather Service Cooperative (COOP) weather stations used to provide input to the Precipitation-Runoff Modeling System (PRMS) model	52

This section contains additional detail regarding the development and initial parameterization of the PRMS surface-water model.

Grid Rotation

The 30-meter digital elevation model (DEM) of Wisconsin (Gesch and others, 2002) was clipped, rotated, and resampled to coincide with the boundaries of the groundwater-model grid. All of the gridded data used in this phase of the project were rotated about the lower left-hand coordinate of the MODFLOW grid (540680, 609772, Wisconsin Transverse Mercator 1983/1991 meters, Wisconsin State Cartographer's Office, 2009), with a rotation value of 2.1 degrees clockwise. Limitations in the ArcInfo grid format (ESRI, 2013) do not allow for grids to have any rotation in them relative to underlying projection coordinates. Because two of the tools used to assist in the parameterization of the PRMS model rely on the ArcInfo gridded data format, it was necessary to rotate the grids before further processing could occur.

Hydrologic Response Units

The surface-water modules included in the GSFLOW framework require that the model domain be split into discrete subareas, known as hydrologic response units (HRUs). Each HRU is assumed to be homogeneous with respect to hydrologic and physical characteristics such as slope, vegetation, land use, or soil type. The HRU configuration was generated by use of the GIS Weasel (Viger and Leavesley, 2007). Because the hydrologic system is dominated by groundwater flow, a combination of surface-elevation differences and

variations in the water table and lake elevations was used to construct the drainage network, which was then further subdivided into the final HRUs.

The GIS Weasel was used to process the DEM by filling depressions, thereby generating a flow-direction grid. The flow-direction grid was subsequently processed by use of the GIS Weasel's routines to generate a stream network and an initial two-plane HRU map. This process was repeated by using a water-table map derived from output from a MODFLOW model constructed previously for the study area (Muffels, 2008). The two-plane HRU maps were merged together and further subdivided with lake outlines and in wetland areas to separate the near-stream areas from the upland areas. The result was a model consisting of 146 HRUs (fig. 2-1).

Surface-Water Routing

The PRMS model allows for surface flow to be routed to downslope HRUs. Each connection between a pair of HRUs or between an HRU and a stream segment must be specified explicitly. These connections were generated by means of the GIS Weasel (Viger and Leavesley, 2007) using the flowlines derived from the land-surface topography. The resulting overland-flow routing diagram contains 145 connections (fig. 2-2).

In the complex low-relief terrain of the Trout Lake Watershed, the surface-water and groundwater divides can differ from one another. The PRMS model also allows for groundwater flow to be routed through the groundwater reservoirs underlying the HRUs by using a separate set of routing connections. The groundwater routing connections were generated by means of the GIS Weasel using the flowlines derived from the water-table surface. The resulting groundwater flow-routing diagram contains 233 connections (fig. 2-3).

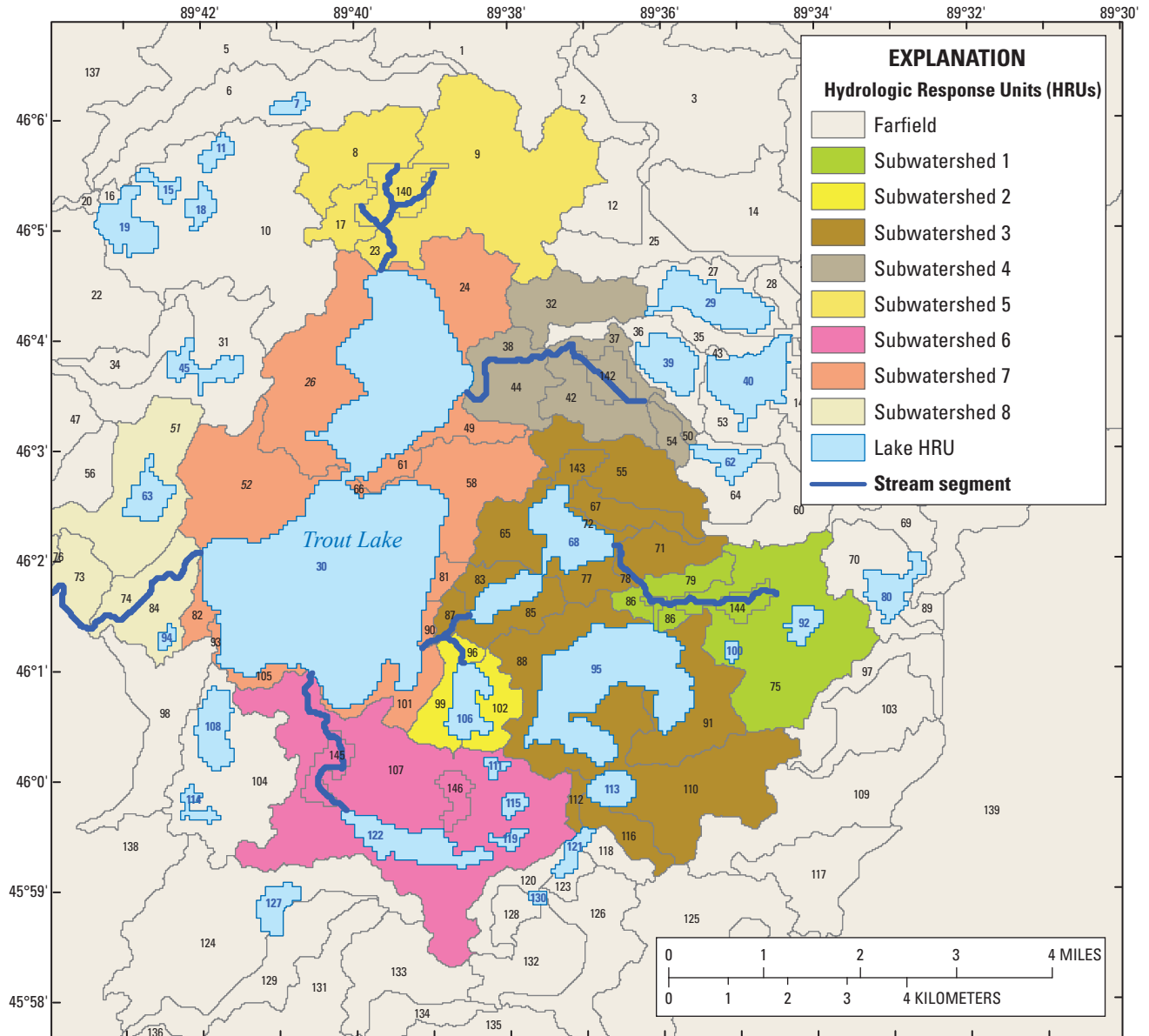


Figure 2-1. Subwatersheds used in assigning spatially variable parameter values to the individual hydrologic response units (HRUs).

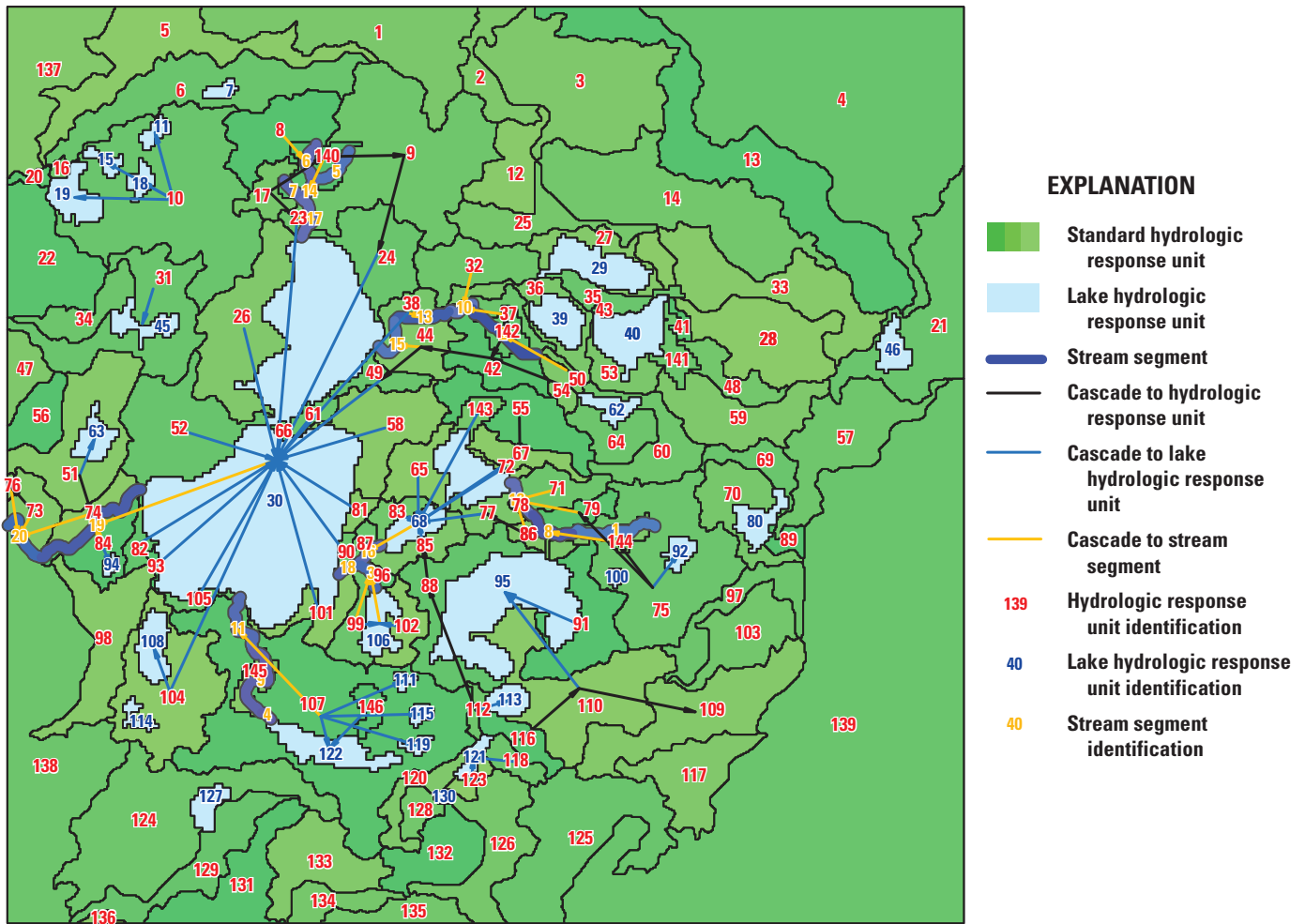


Figure 2-2. Overland-flow routing diagram generated for the Trout Lake Precipitation-Runoff Modeling System (PRMS) model.

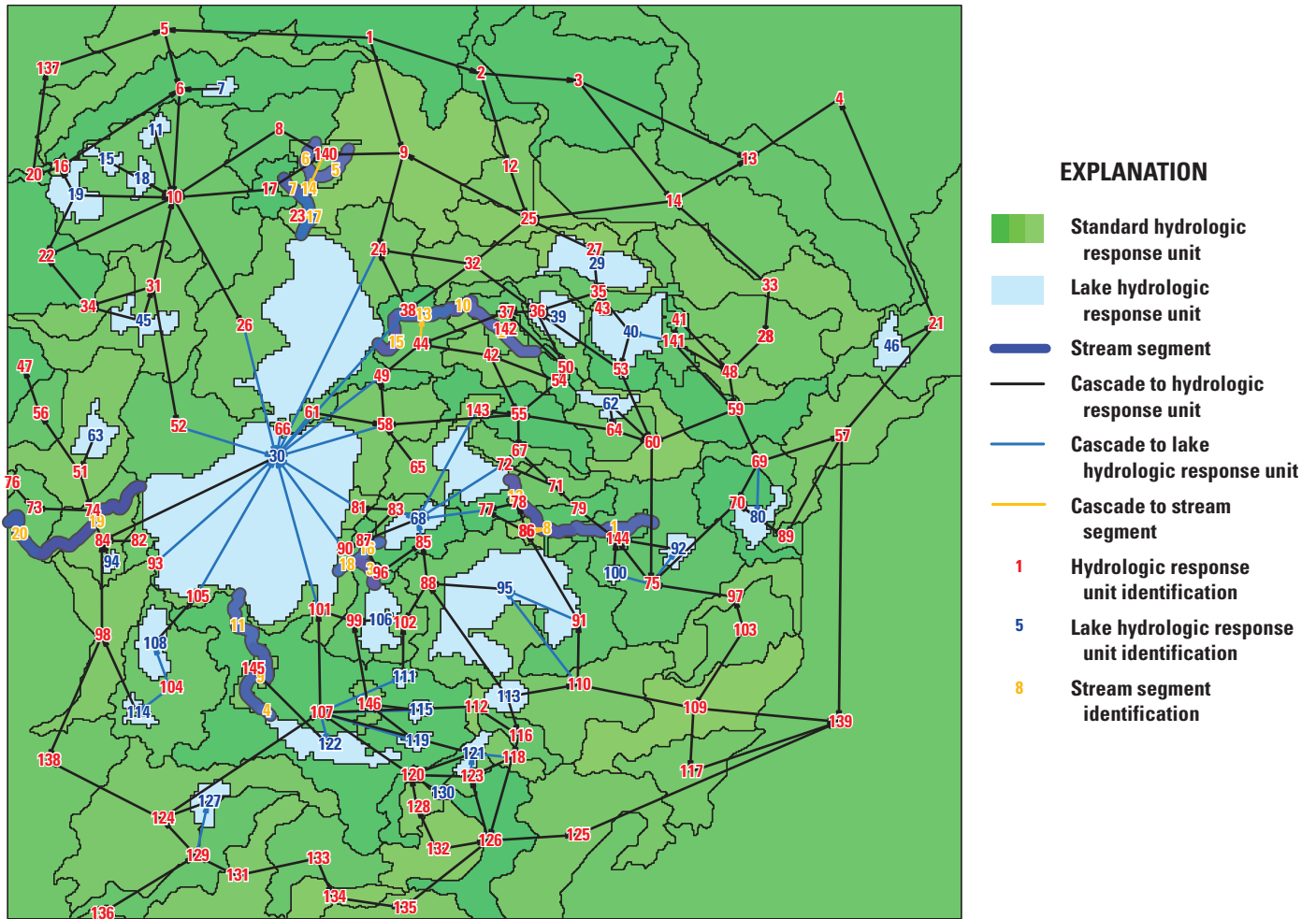


Figure 2-3. Groundwater-flow routing diagram generated for the Trout Lake Precipitation-Runoff Modeling System (PRMS) model.

Parameterization of the Model

The PRMS model contains hundreds of user-specified parameter values that can be used to tailor the model to the specific area of study. Some of these parameters are more important than others. This section contains a description of how some of the more important initial parameter values were derived.

Initial parameter values were generated by means of the GIS Weasel (Viger and Leavesley, 2007). The GIS Weasel has been developed to assist in generating model parameter values for PRMS and GSFLOW models; a project-specific digital elevation model is used to generate HRUs and other physical model parameters, whereas general, nationwide soils and land-use GIS datasets (Vogelmann and others, 2001; U.S. Department of Agriculture, 1994) are used to generate other parameter values.

The parameters that are needed to run the model can be divided into two groups. The first group describes physical characteristics of the watershed that are considered fixed and are not varied during model calibration. The second group describes parameters that can be estimated by using GIS datasets but are further adjusted during the calibration process. The parameters describing the physical characteristics that were not varied during model calibration are described in table 2–1.

Because of the relative homogeneous nature of the soils and geology in the Trout Lake Watershed, it was felt that detailed spatial variability of the soil-zone and of parameters that control runoff and groundwater flow was not warranted. Instead, the HRUs were aggregated into eight subwatersheds and a far-field area (fig. 2–1). The initial parameter estimates for each HRU derived by the GIS Weasel were averaged over the subwatersheds, and each HRU within a subwatershed was then assigned the average initial value.

Climate Data Used for Model Forcing

The PRMS model uses climate data as input to the hydrologic system. Daily values of precipitation and temperature (maximum and minimum) are required inputs. Values of solar radiation and potential evapotranspiration can be either input as specified data or calculated by the model. For this study, we chose to calculate these quantities using the cloud-cover solar-radiation algorithm (ccsolrad_prms; Markstrom and others, 2008, p. 162) and the Jensen-Haise formulation for potential evapotranspiration (potet_jh_prms module; Markstrom and others, 2008, p. 164).

The closest National Weather Service Cooperative (COOP) weather station is at Rest Lake (National Weather Service station ID 477092), approximately 10 km northwest

of Trout Lake. Although this single station might provide adequate input data for the model, in some cases there could be missing data that will cause the model to halt execution. In addition, the station is west of the model area, so it might not adequately represent the spatial variability of storms across the watershed. To address these difficulties, data from a total of six COOP weather stations were chosen for input to the model (table 2–2).

The temperature and precipitation data from the six weather stations were distributed to the HRUs by means of an algorithm based on the inverse of distance from the HRU centroid and each particular weather station. The weight for a station is computed as

$$w_n = (1.0 / d_n)^2 \quad (1)$$

where

w_n is the weight for station n , and
 d_n is the distance between the station n and the HRU-interpolation point.

The weights for a given HRU are determined by using the three nearest stations to each HRU.

Precipitation and maximum and minimum temperature values by HRU are calculated as

$$hru_ppt_{HRU}^m = \sum_{n=1}^3 (w_n \cdot precip_n) \quad (2a)$$

$$hru_tmax_{HRU}^m = \sum_{n=1}^3 (w_n \cdot tmax_n) \quad (2b)$$

$$hru_tmin_{HRU}^m = \sum_{n=1}^3 (w_n \cdot tmin_n) \quad (2c)$$

where

$hru_ppt_{HRU}^m$ is the average precip for time step m for a given HRU,
 $precip_n$ is the daily precip for station n ,
 $hru_tmax_{HRU}^m$ is the average maximum temperature for time step m for a given HRU,
 $tmax_n$ is the daily maximum temperature for station n ,
 $hru_tmin_{HRU}^m$ is the average minimum temperature for time step m for a given HRU,
 $tmin_n$ is the daily minimum temperature for station n , and
 w_n is the weight for station n calculated by equation 1.

Table 2–1. Description of parameter types determined by the GIS Weasel that were not varied during calibration.

[HRU, hydrologic response unit; precip, precipitation]

Name	Description	Model suggested values			Resulting values in the model		
		Default	Minimum	Maximum	Average	Minimum	Maximum
hru_area	HRU area	1	0.01	1E+9	525.46027	14.9	9278.2002
hru_percent_imperv	HRU percent impervious	0	0	0.99	0	0	0
hru_type	HRU type	1	0	3	1.20548	1	2
tmax_allrain	Precip all rain if HRU maximum temperature above this monthly value	40	0	90	52.4	52.4	52.4
tmax_adj	HRU maximum temperature adjustment	0	-10	10	0	0	0
tmin_adj	HRU minimum temperature adjustment	0	-10	10	0	0	0
cov_type	HRU cover type designation	3	0	3	2.38356	0	3
covden_sum	HRU summer vegetation cover density for major vegetation type	0.5	0	1	0.61465	0	0.88525
covden_win	HRU winter vegetation cover density for major vegetation type	0.5	0	1	0.41814	0	0.85869
snow_intcp	HRU snow interception storage capacity	0.1	0	5	0.03613	0.02	0.1
srain_intcp	HRU summer rain interception storage capacity	0.1	0	5	0.04979	0.04041	0.05
wrain_intcp	HRU winter rain interception storage capacity	0.1	0	5	0.02599	0.02	0.05
hru_deplcrv	Index number for snowpack areal depletion curve for each HRU	1	0	2	1	1	1
melt_force	Julian date to force snowpack to spring snowmelt stage	90	1	366	90	90	90
melt_look	Julian date to start looking for spring snowmelt	90	1	366	90	90	90
rad_trncf	HRU solar radiation transmission coefficient	0.5	0	1	0.13454	0.05171	0.21463
snarea_curve	Snow area depletion curve defined by 11 values for each curve	1	0	1	0.58318	0.05	1
snarea_thresh	HRU maximum threshold water equivalent for snow depletion	50	0	200	0.21866	0	0.515
tstorm_mo	Set to 1 if thunderstorms prevalent during month	0	0	1	0.41667	0	1
fastcoef_lin	HRU linear preferential-flow routing coefficient	0.1	0	1	0	0	0.00001
fastcoef_sq	HRU nonlinear preferential-flow routing coefficient	0.8	0	1	0	0	0.00001
pref_flow_den	HRU preferential-flow pore density	0	0	1	0	0	0
soil_moist_init	Initial values of water for soil zone of each HRU	3	0	20	1	1	1
soil_rechr_init	Initial value of water for soil recharge zone of each HRU	1	0	10	0.56507	0.5	1
soil_type	HRU soil type	2	1	3	1	1	1

Table 2–1. Description of parameter types determined by the GIS Weasel that were not varied during calibration.—Continued

[HRU, hydrologic response unit; precip, precipitation]

Name	Description	Model suggested values			Resulting values in the model		
		Default	Minimum	Maximum	Average	Minimum	Maximum
ssr2gw_exp	Coefficient to route water from subsurface to groundwater for each HRU	1	0	3	0.09635	0.09635	0.09635
ssstor_init	Initial storage in each gravity reservoir of each HRU	0	0	20	0	0	0
hru_aspect	HRU aspect	0	0	360	86.91781	0	315
hru_lat	HRU latitude	40	–90	90	40.61275	40.527	40.665
hru_slope	HRU slope	0	0	10	0.03652	0.00016	0.09925
ppt_rad_adj	Radiation reduced if basin precip above this monthly value	0.02	0	0.5	0.11097	0.11097	0.11097
radmax	Maximum fraction of potential solar radiation (decimal)	0.8	0.1	1	0.8	0.8	0.8
imperv_stor_max	HRU maximum impervious area retention storage	0	0	10	0.1	0.1	0.1
snowinfil_max	HRU maximum snow infiltration per day	2	0	20	1	1	1

Table 2–2. National Weather Service Cooperative (COOP) weather stations used to provide input to the Precipitation-Runoff Modeling System (PRMS) model.

Station number	Station name	Latitude (decimal degrees)	Longitude (decimal degrees)	Elevation (meters)
475516	Minocqua	45.886	–89.732	489
477480	St. Germain 2 East	45.907	–89.436	501
477092	Rest Lake	46.121	–89.876	491
476939	Rainbow Reservoir Tomahaw	45.834	–89.549	488
208680	Watersmeet 5 West	46.278	–89.174	485
472314	Eagle River	45.909	–89.253	501

Variation of Growing Season with Changing Temperatures

The growing season determines the period during which evapotranspiration from the vegetative portion of the HRUs can occur. It can be specified by two parameters: `spring_frost` and `fall_frost`. The `spring_frost` parameter specifies the date for each HRU that is the beginning of the growing season. Likewise, the `fall_frost` parameter specifies the date for each HRU that is the end of the growing season. Both parameters are calculated as a solar day, defined as the time in days since the winter solstice. The two frost parameters were preprocessed by means of an algorithm described in Christiansen and others (2011) and documented in Markstrom and others (2012). A killing-frost temperature of -2.2 degrees Celsius ($^{\circ}\text{C}$), 28 $^{\circ}\text{F}$, was used for each HRU. During model calibration, the frost parameters were determined as average values for the calibration period. During climate-change scenarios, the frost parameters were determined for each year in the simulation period by using minimum temperature input for each specific global circulation model (GCM) and emissions scenario.

A preprocessing program calculates the spring frost date and fall frost date for each calendar year for each HRU. The program then produces an input file for the model consisting of transpiration flags for each day for each HRU, indicating whether transpiration is on (`flag=1`) or off (`flag=0`). The GSFLOW model uses the `climate_hru` module to read the transpiration flags directly from the input file.

References Cited

- Christiansen, D.E., Markstrom, S.L., and Hay, L.E., 2011, Impacts of climate change on growing season in the United States: *Earth Interactions*, v. 15, no. 33, p. 1–17.
- Environmental Systems Research Institute (ESRI), 2013, “ESRI Grid Format,” ArcGIS Desktop Help, accessed August 21, 2013.
- Gesch, D., Oimoen, M., Greenlee, S., Nelson, C., Steuck, M., and Tyler, D., 2002, The national elevation dataset: *Photogrammetric Engineering and Remote Sensing*, v. 68, p. 5–12.
- Markstrom, S.L., Hay, L.E., Ward-Garrison, D.C., Risley, J.C., Battaglin, W.A., Bjerkle, D.M., Chase, K.J., Christiansen, D.E., Dudley, R.W., Hunt, R.J., Kocot, K.M., Mastin, M.C., Regan, R.S., Viger, R.L., Vining, K.C., and Walker, J.F., 2012, Integrated watershed scale response to climate change for selected basins across the United States: U.S. Geological Survey Scientific Investigations Report 2010–5077, 134 p.
- Markstrom, S.L., Niswonger, R.G., Regan, R.S., Prudic, D.E., and Barlow, P.M., 2008, GSFLOW—Coupled Ground-Water and Surface-Water Flow Model based on the integration of the Precipitation-Runoff Modeling System (PRMS) and the Modular Ground-Water Flow Model (MODFLOW-2005): U.S. Geological Survey Techniques and Methods, book 6, chap. D1, 240 p.
- Muffels, C.T., 2008, Application of the LSQR algorithm to the calibration of a regional groundwater flow model—Trout Lake Basin, Vilas County, Wisconsin: University of Wisconsin-Madison, M.S. thesis, 106 p.
- U.S. Department of Agriculture, 1994, State soil geographic (STATSGO) data base - data use information, (rev. ed.): Fort Worth, Texas, Natural Resources Conservation Service miscellaneous publication no. 1492, p. 212.
- Vogelmann, J.E., Howard, S.M., Yang, Limin, Larson, C.R., Wylie, B.K., Van Driel, Nick, 2001, Completion of the 1990s National Land Cover Dataset for the Conterminous United States from Landsat Thematic Mapper Data and Ancillary Data Sources: *Photogrammetric Engineering and Remote Sensing*, v. 67, no. 6, p. 650–662.
- Viger, R.J., and Leavesley, G.H., 2007, The GIS Weasel user’s manual: U.S. Geological Survey Techniques and Methods, book 6, chap. B4, 201 p. (available at <http://pubs.usgs.gov/tm/2007/06B04/>).
- Wisconsin State Cartographer’s Office, 2009, Wisconsin Coordinate Reference Systems, second edition: Madison, Wis., accessed September 21, 2011 at http://www.sco.wisc.edu/images/stories/publications/WisCoordRefSys_April2009.pdf.

Appendix 3. Model Calibration

Introduction.....	56
Time-Series Processing Approach.....	56
Observation Weights.....	56
Calibration Approach: PRMS-Only Model.....	57
Step 1—Solar Radiation, Potential Evapotranspiration, and Lake Evaporation.....	57
Step 2—Snowmelt.....	58
Step 3—Runoff, Infiltration, and Base Flow.....	60
Calibration Approach: Sequentially Linked Transient Surface-Water/Steady-State Groundwater Model.....	62
Pilot Points.....	66
Tikhonov Regularization.....	66
Singular Value Decomposition.....	68
Calibration Approach: Fully Coupled Surface-Water/Groundwater Model.....	68
References Cited.....	72

Figures

3-1. Schematic showing conceptualization of sequentially linked calibration of separate, uncoupled surface-water and groundwater models.....	62
3-2. Map showing locations of U.S. Geological Survey streamflow-gaging stations used to calibrate the model.....	63
3-3. Map showing simulated surface watershed of Hunt and others (1998) and names of surface-water features used in the model calibration.....	64
3-4. Map showing locations of groundwater-level measurements used as head targets for model calibration.....	65
3-5. Map showing pilot-point locations and links between pilot points used to apply preferred homogeneity Tikhonov regularization within each layer.....	67

Tables

3-1. Hydrologic processes associated with the individual steps in the calibration procedure.....	57
3-2. Parameter types used in step 1 of the calibration: solar radiation, potential evapotranspiration and lake evaporation.....	58
3-3. Parameter types used in step 2 of the calibration: snowmelt.....	59
3-4. Parameter types used in step 3 of the calibration: runoff, infiltration, and groundwater flow.....	61
3-5. Cascade parameters varied by PEST in step 3 of the calibration.....	60
3-6. PRMS parameter types estimated during calibration of the fully coupled GSFLOW model.....	70
3-7. MODFLOW parameter types estimated during calibration of the fully coupled GSFLOW model. Parameter names that represent a single parameter do not display minimum and maximum calibrated values.....	71

Introduction

The overall model-calibration strategy involved calibrating the PRMS-only and steady-state MODFLOW models independently as a first step. The transient PRMS model was then linked to the steady-state MODFLOW model in a sequential fashion to provide a revised set of soil-zone parameters and spatial distribution of hydraulic conductivity. Finally, the complete coupled model was calibrated to further refine the parameters. For parameters related to the PRMS model and associated parameters in the coupled model, a stepwise procedure was undertaken to isolate parameters controlling specific hydrologic processes (Hay and others, 2006).

Time-Series Processing Approach

In addition to issues of parameter insensitivity and correlation that affects coupled-model calibration (for example, Doherty and Hunt, 2009, 2010a), there are also concerns with the issue of measurement noise and redundant information in the observations used to calibrate these models. This is a primary concern here because surface-water datasets commonly include many observations, especially with respect to the temporal density of the observations within a spatially distributed network; many of these data carry redundant insight into the system, as well as contribute to the measurement noise that is encountered during calibration. In order to enhance the signal-to-noise ratio within our observation data, we employed a time-series processing approach to the time-series observations. In this approach, the raw observations were processed and distilled into characteristic aspects of the system (Walker and others, 2009). The simulated PRMS output was then processed in the same way as the raw observations and compared directly in the parameter-estimation process. We used the Time-Series Processor TSPROC (Doherty, 2008), modified to read the PRMS STATVAR and MODFLOW Gage (GAG) Package output files.

Observation Weights

In general, an estimate of uncertainty in the observations was the starting point for the weights for each observation group (w_g). The weight was assigned to be the reciprocal of the uncertainty for each group, which is defined by the standard deviation of the data (σ_g), thus

$$w_g = \frac{1}{\sigma_g} \quad (1)$$

where

w_g is the weight for a particular observation group, and

σ_g is the standard deviation of the uncertainty for the observations.

The uncertainties were estimated by using the coefficient of variation (standard deviation divided by the mean) and an average value for each observation group; thus, the weight is estimated as

$$w_g = \frac{1}{\mu_g CV_g} \quad (2)$$

where

CV_g is the coefficient of variation for the observation group, and

μ_g is the average value for the observation group.

For a log-transformed, normally distributed variable, the standard deviation in log space was determined by rearranging the equations relating log-space (y) moments to real space (x) (Miller and Freund, 1977):

$$\sigma_y = \sqrt{\log(1 + CV_x^2)} CV_x \quad (3)$$

where

CV_x is the coefficient of variation of the real-space observations, and

σ_y is the standard deviation of the log-space observations.

Because the groups contained observations at different time scales, the number of observations differed considerably within each group and from station to station. To compensate for the number of observations, the weights were adjusted to represent an equivalent number of annual observations for step 1 and monthly observations for step 3. This reasoning follows from the basic identity that the standard deviation of the mean from a random sample of size n is given by

$$\sigma_m = \frac{\sigma_g}{\sqrt{n}} \quad (4)$$

where

σ_m is the standard deviation of the mean of the observations,

σ_g is the standard deviation for the observation group, and

n is the sample size.

Because the weights are equal to the inverse of the standard deviation, the weight for a mean statistic becomes

$$w_m = \frac{1}{\sigma_m} = \frac{\sqrt{n}}{\sigma_g} = w_g \sqrt{n} \quad (5)$$

where

w_m is the resulting weight for the mean of the observation group, and

w_g is the base weight for the observation group (from equation 2).

Calibration Approach: PRMS-Only Model

The PRMS-only model was incrementally calibrated by means of the parameter estimation program PEST (Doherty, 2010a, 2010b) using singular value decomposition. Sequential steps were used in the calibration and are listed in table 3–1 (modified from Hay and others, 2006). Calibration efforts stayed within each step described below until all estimated parameters were within the bounds and appear to be reasonable for the hydrologic setting.

Table 3–1. Hydrologic processes associated with the individual steps in the calibration procedure.

Step	Hydrologic processes	Number	
		Parameters	Observation groups
1	Solar radiation, potential evapotranspiration, lake evaporation	42	3
2	Snowmelt	14	1
3	Runoff, infiltration, groundwater flow	104	20

Step 1—Solar Radiation, Potential Evapotranspiration, and Lake Evaporation

The first step in the parameter estimation process involved several parameters controlling incoming solar radiation, potential evapotranspiration, and lake evaporation. The main driver for several of the hydrologic processes simulated in the PRMS model (for example, snowmelt and evapotranspiration) is incoming solar radiation. If the model is able to simulate incoming solar radiation correctly, parameters specific to other processes will be more realistic and likely to fall within acceptable ranges. Likewise, simulating potential evapotranspiration correctly results in a more realistic simulation of infiltration, runoff, and groundwater-flow processes. Finally, simulating rather than specifying solar radiation allows for simulation of future climate conditions, where the amount of solar radiation is expected to differ from current or historic conditions (see appendix 2 for simulation method). Simulated values from other models, such as GCMs, could also be specified. The objective function for the calibration is defined as follows:

$$\phi = \sum_{i=1}^{Nobs} w_i^2 (S_i - O_i)^2 \quad (6)$$

where

- ϕ is the objective value being minimized,
- w_i is the weight used for observation i ,
- S_i is the simulated value for observation i ,

- O_i is the observed value for observation i , and
- $Nobs$ is the total number of observations used in the objective function.

For this step, parameters associated with solar radiation, potential evapotranspiration, and evaporation for Sparkling Lake were used in the objective function. The following calibration targets were processed:

1. Mean monthly solar radiation: Daily solar radiation for each month averaged across all years in the simulation period was used to capture the seasonal variation of solar radiation.
2. Mean monthly potential evapotranspiration: Daily potential evapotranspiration for each month averaged across all years in the simulation period was used to capture the seasonal variation of potential evapotranspiration.
3. Monthly Sparkling Lake evaporation: Daily actual evaporation was averaged for each month in the simulation period and used to capture the monthly and within-year variation in evaporation.

Mean monthly solar radiation observations were obtained from a dataset developed for the United States by Hay and others (2006). The dataset consists of mean monthly values estimated at a network of climate-station sites (Snotel Telemetry and National Weather Service) by using multiple regression analysis. The mean monthly values of solar radiation for the site closest to the centroid of the Trout Lake Watershed were used as the solar-radiation calibration target. Mean monthly potential evapotranspiration (PET) estimates were obtained from mean monthly PET maps derived from the free-water evaporation atlas of Farnsworth and others (1982). The mean monthly values were interpolated to the centroid of the Trout Lake Watershed to develop the PET calibration target. Because the model is relatively insensitive to the spatial component of the Jenson-Haise relationship (parameter `jh_coef_hru`), a single PET target was assumed. Daily estimates of evaporation from Sparkling Lake were obtained from Lenters and others (2005), and averaged for each month for the period 1992–98 to develop the lake evaporation target.

Parameters allowed to vary in this step included six parameters from the cloud-cover module (`ccsolrad_prms`; Markstrom and others, 2008, p. 162), two parameters from the potential evapotranspiration module (`potet_jh_prms` module; Markstrom and others, 2008, p. 164), and one parameter from the soil-zone module (`soilzone_prms`; Markstrom and others, 2008, p. 169). Three of the parameters (`ccov_slope`, `jh_coef` and `lake_evap_adj`) were allowed to vary by month, and six of the parameters (`ccov_intcp`, `crad_coef`, `crad_exp`, `radj_sppt`, `radj_wppt` and `jh_coef_hru`) were estimated as single values (table 3–2). The most sensitive and identifiable parameters (Doherty and Hunt, 2009) were the cloud-cover slope, the monthly Jenson-Haise coefficients, and the monthly `lake_evap_adj` coefficients. Most of the remaining terms remained relatively close to their default starting values (table 3–2).

Table 3–2. Parameter types used in step 1 of the calibration: solar radiation, potential evapotranspiration and lake evaporation.

[PET, potential evapotranspiration]

Name	Description	Model-suggested values			Calibrated values		
		Default	Minimum	Maximum	Average	Minimum	Maximum
ccsolrad_prms module							
ccov_intcp	Monthly intercept in temperature cloud cover relationship	1.83	0	5	5	5	5
ccov_slope	Monthly slope in temperature cloud cover relationship	–0.13	–0.5	–0.01	–0.04134	–0.05182	–0.02289
crad_coef	Coefficient in cloud cover-solar radiation relationship	0.4	0.1	0.7	0.49409	0.49409	0.49409
crad_exp	Exponent in cloud cover-solar radiation relationship	0.61	0.2	0.8	0.8	0.8	0.8
radj_sppt	Adjustment to solar radiation on precip day: summer	0.44	0	1	1	1	1
radj_wppt	Adjustment to solar radiation on precip day: winter	0.5	0	1	0.01333	0.01333	0.01333
potet_jh_prms module							
jh_coef	Monthly air temp coefficient: Jensen-Haise	0.014	0.005	0.06	0.01226	0.005	0.02746
jh_coef_hru	HRU air temp coefficient: Jensen-Haise	13	5	20	5.07067	5.07067	5.07067
soilzone_prms module							
lake_evap_adj	Monthly PET factor to adjust PET for each lake	1	0.005	1	0.86055	0.5	1.5

Step 2—Snowmelt

The second step of the parameter-estimation process involved parameters that control snow accumulation and melt throughout the watershed. The objective function for this group of parameters consisted of selected snowpack depths obtained from the Minocqua Dam COOP weather station (No. 475516) for the period October 1, 1999 to September 30, 2007 (MINOCQUA in table 2–2).

Parameters allowed to vary in this stage included 3 from the precipitation module (climate_hru, Steve Regan,

U.S. Geological Survey, written commun., May 2012), 1 from the interception module (intcp_prms; Markstrom and others, 2008, p. 165), and 10 from the snow computation module (snowcomp_prms; Markstrom and others, 2008, p. 166). Each of the parameters in table 3–3 was estimated as a single value. The most sensitive and identifiable parameters were tmax_all-snow, emis_noppt, den_max, adjust_snow, and den_init. Most of the remaining terms remained relatively close to their starting values (table 3–3).

Table 3–3. Parameter types used in step 2 of the calibration: snowmelt.

[ET, evapotranspiration; HRU, hydrologic response unit; precip, precipitation]

Name	Description	Model-suggested values			Calibrated values		
		Default	Minimum	Maximum	Average	Minimum	Maximum
climate_hru_prms module							
adjmix_rain	Monthly adjustment factor for rain in a rain/snow mix	1	0	3	1.35395	1.35395	1.35395
adjust_snow	Monthly downscaling fractional adjustment for snow for each HRU	0.01	–0.25	1	0.06988	–0.25	0.5
tmax_allsnow	Precip all snow if HRU maximum temperature below this value, in degrees Fahrenheit	32	–10	40	32.77165	32.77165	32.77165
intcp_prms module							
potet_sublim	Proportion of potential ET that is sublimated from snow surface	0.5	0.1	0.75	0.75	0.75	0.75
snowcomp_prms module							
albset_rna	Albedo reset: rain, accumulation stage, expressed as a decimal fraction	0.8	0	1	0	0	0
albset_rnm	Albedo reset: rain, melt stage, expressed as a decimal fraction	0.6	0	1	0.07764	0.07764	0.07764
albset_sna	Albedo reset: snow, accumulation stage, expressed as a decimal fraction	0.05	0.001	1	0.00351	0.00351	0.00351
albset_snm	Albedo reset: snow, melt stage, expressed as a decimal fraction	0.2	0.001	1	0.06607	0.06607	0.06607
cecn_coef	Monthly convection condensation energy coefficient	5	0	20	15.3375	15.3375	15.3375
den_init	Initial density of new-fallen snow, grams per cubic centimeter	0.1	0.01	0.5	0.0852	0.0852	0.0852
den_max	Average maximum snowpack density, grams per cubic centimeter	0.6	0.1	0.8	0.17371	0.17371	0.17371
emis_noppt	Emissivity of air on days without precipitation, expressed as a decimal fraction	0.757	0.757	1	0.91108	0.91108	0.91108
freeh2o_cap	Free-water holding capacity of snowpack, expressed as a decimal fraction	0.05	0.01	0.2	0.2	0.2	0.2
settle_const	Snowpack settlement time constant, expressed as a decimal fraction	0.1	0.01	0.5	0.12424	0.12424	0.12424

Step 3—Runoff, Infiltration, and Base Flow

The remaining step relies on processing daily streamflow data for the objective function targets. Data for water years 1998–2007 (October 1, 1997 to September 30, 2007) were used for the five long-term streamflow-gaging stations (fig. 1 main text; appendix table 5–1) available from the WEBB database (appendix 5); one additional gage with shorter record (Mann Creek, fig. 3–2) was also used. For all gages except the one on the Trout River, the data used were reduced to periods determined to be reliable for calibration. This step in the parameter-estimation process involved a group of parameters that control runoff, infiltration into the soil zone, and the rate and volume of flow from groundwater reservoirs to surface water. The following calibration targets were processed:

1. Log of daily streamflow: The natural log of daily streamflow was used to mitigate the undue influence of extremely high daily discharges.
2. Annual mean streamflow: This is the average streamflow for each water year during the simulation period and represents the streamflow portion of the annual hydrologic budget.
3. Monthly mean streamflow: This is the average streamflow for each month during the simulation and represents the total volume of streamflow for each month.
4. Monthly base flow: This is the average baseflow for each month during the simulation and represents the groundwater contribution to streamflow. Daily baseflow separations were computed by using the local minimum algorithm from the TSPROC time-series processor (Westenbroek and others, 2012). The time-series processor uses the U.S. Geological Survey's HYSEP algorithms for computing base flow (Sloto and Crouse, 1996).

Parameters allowed to vary in this step included two from the climate distribution module (climate_hru module; Steve Regan, U.S. Geological Survey, written commun., May 2012), two from the groundwater module (gwflow_casc_prms; Markstrom and others, 2008, p. 170), six from the soil-zone module (soilzone_prms; Markstrom and others, 2008, p. 169), and four from the runoff-generation module (srnoff_smidx_prms;

Markstrom and others, 2008, p. 168). One parameter (adjust_rain) was varied by month, two parameters (smidx_coef and smidx_exp) were estimated with single values, and the remaining parameters were varied by subwatershed (table 3–4). The most sensitive and identifiable parameters were gwsink_coef, gwflow_coef, adjust_snow, and adjust_rain. However, several other parameters were moderately sensitive and identifiable, including soil_moist_max and carea_max.

In addition to the parameters described in table 3–4, the fraction of water being routed among HRUs (as specified in the cascading-flow module) was adjusted during the calibration process for numerous connections. The hru_pct_up parameter describes the fraction of the upslope HRU that sends surface runoff to either a downslope HRU or stream segment. Final values determined through the calibration procedure are listed in table 3–5.

Table 3–5. Cascade parameters varied by PEST in step 3 of the calibration.

[HRU, hydrologic response unit]

Upslope HRU	Downslope HRU or segment	hru_pct_up
Cascades to HRUs		
75	92	0.100
75	144	0.050
84	94	0.005
104	108	0.038
110	95	0.075
112	113	0.100
Cascades to stream segments		
23	17	0.695
37	10	0.181
38	13	0.367
44	15	0.113
73	20	0.472
86	12	1.000
140	14	1.000
142	02	0.095

Table 3–4. Parameter types used in step 3 of the calibration: runoff, infiltration, and groundwater flow.

[GWR, groundwater reservoir; HRU, hydrologic response unit]

Name	Description	Model-suggested values			Calibrated values		
		Default	Minimum	Maximum	Average	Minimum	Maximum
climate_hru_prms module							
adjust_rain	Monthly downscaling fractional adjustment for rain for each HRU	0.01	–0.25	1	0.09447	–0.25	0.44873
adjust_snow	Monthly downscaling fractional adjustment for snow for each HRU	0.01	–0.25	1	0.06988	–0.25	0.5
gwflow_casc_prms module							
gwflow_coef	Groundwater routing coefficient for each GWR	0.015	0	1	0.1257	0.0026	0.7501
gwsink_coef	Groundwater sink coefficient for each GWR	0	0	1	0.06344	0.00000	0.56227
soilzone_prms module							
sat_threshold	Soil saturation threshold, above field-capacity threshold for each HRU, in inches	999	1	999	6.78082	6	12
slowcoef_lin	Linear gravity-flow reservoir routing coefficient for each HRU	0.015	0	1	0.16588	0.00001	0.32746
slowcoef_sq	Nonlinear gravity-flow reservoir routing coefficient for each HRU	0.1	0	1	0	0	0.00001
soil_rechr_max	Maximum value for soil recharge zone for each HRU, in inches	2	0	10	0.93202	0.06044	1.43793
soil2gw_max	Maximum value for soil-water excess to groundwater for each HRU, in inches	0	0	5	0.1928	0	0.33234
ssr2gw_rate	Coefficient to route water from subsurface to groundwater for each HRU	0.1	0	1	0.89838	0.11528	1.0
srunoff_smidx_prms module							
care_max	Maximum contributing area for each HRU, expressed as a decimal fraction	0.6	0	1	0.08468	0	1
smidx_coef	Coefficient in contributing area computations for each HRU	0.01	0.0001	1	0.10286	0.10286	0.10286
smidx_exp	Exponent in contributing area computations for each HRU	0.3	0.2	0.8	0.2	0.2	0.2
soil_moist_max	Maximum value of water for soil zone for each HRU, in inches	6	0	20	3.32745	0.4	5.02644

Calibration Approach: Sequentially Linked Transient Surface-Water/ Steady-State Groundwater Model

A sequentially linked model simulated the measured groundwater and surface-water system in the Trout Lake Watershed. Although GSFLOW allows simulation of fully coupled flow between the groundwater and surface-water systems, such simulations have run times much longer than if only the groundwater or surface-water system were simulated—run times that can become too long for practical calibration. Moreover, many of the model input parameters are primarily associated with one or the other of the two systems and thus are not appreciably more informed by fully coupled runs. As a result, appreciable initial calibration insight can be gained by using the faster, uncoupled runs. Therefore, initial calibration took advantage of “PRMS-only” and “MODFLOW-only” uncoupled modes of GSFLOW (Hunt and others, 2009). Rather than separate calibration of the uncoupled groundwater and surface-water models, a sequentially linked approach can be employed (fig. 3–1).

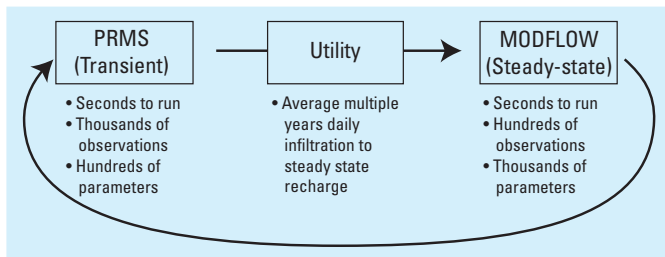


Figure 3–1. Conceptualization of sequentially linked calibration of separate, uncoupled surface-water and groundwater models (modified from Hunt and others, 2009).

In this approach, the transient PRMS-only run results are translated by a utility to create a steady-state infiltration/recharge array for the MODFLOW-only run. The translation occurs on the fly, and the PEST model run batch file includes all steps. The resulting parameter estimation includes all transient observations (often in the thousands), as well as all

model parameters (also often in the thousands, especially with pilot points), yet maintains run times much shorter than the fully coupled model run. Moreover, because the PRMS-only discretization directly informs the MODFLOW-only recharge/infiltration array, the respective optimal parameters are better starting points for calibration of the fully coupled model. This initial calibration was followed by final calibration where the majority of parameters were fixed at their optimal values from sequentially linked calibration, and a subset of parameters primarily important for simulating water exchange within the groundwater and surface-water system were estimated by using the fully coupled GSFLOW model (see section “Calibration Approach: Fully Coupled Transient Surface-Water Groundwater Model”).

The groundwater model was calibrated by using a parameter estimation program (PEST; Doherty, 2010a, 2010b). The sequentially linked PRMS-MODFLOW model calibration consisted of the following transient (PRMS) and steady-state (MODFLOW) targets:

1. Annual mean streamflow (PRMS), monthly base flow (PRMS), average base flows (MODFLOW), monthly mean streamflow (PRMS), and log of daily streamflow (PRMS) at locations in the watershed (fig. 3–2) for the period 1991–2000;
2. average lake stages (MODFLOW) for the period of record (lakes shown in fig. 3–3);
3. average head conditions (MODFLOW) as represented by groundwater levels (fig. 3–4) measured in July 2001, which are considered representative of average conditions during the period of record 1985–2001;
4. lake plume depth (MODFLOW) characterized by water stable isotope sampling (locations T1-70; T2-90, and T5-10 in fig. 3–4);
5. time of travel (MODFLOW) between Big Muskegon Lake and T1-70 (fig. 3–4); and
6. groundwater inflow into seepage lakes (MODFLOW) calculated by using a stable isotope mass-balance approach.

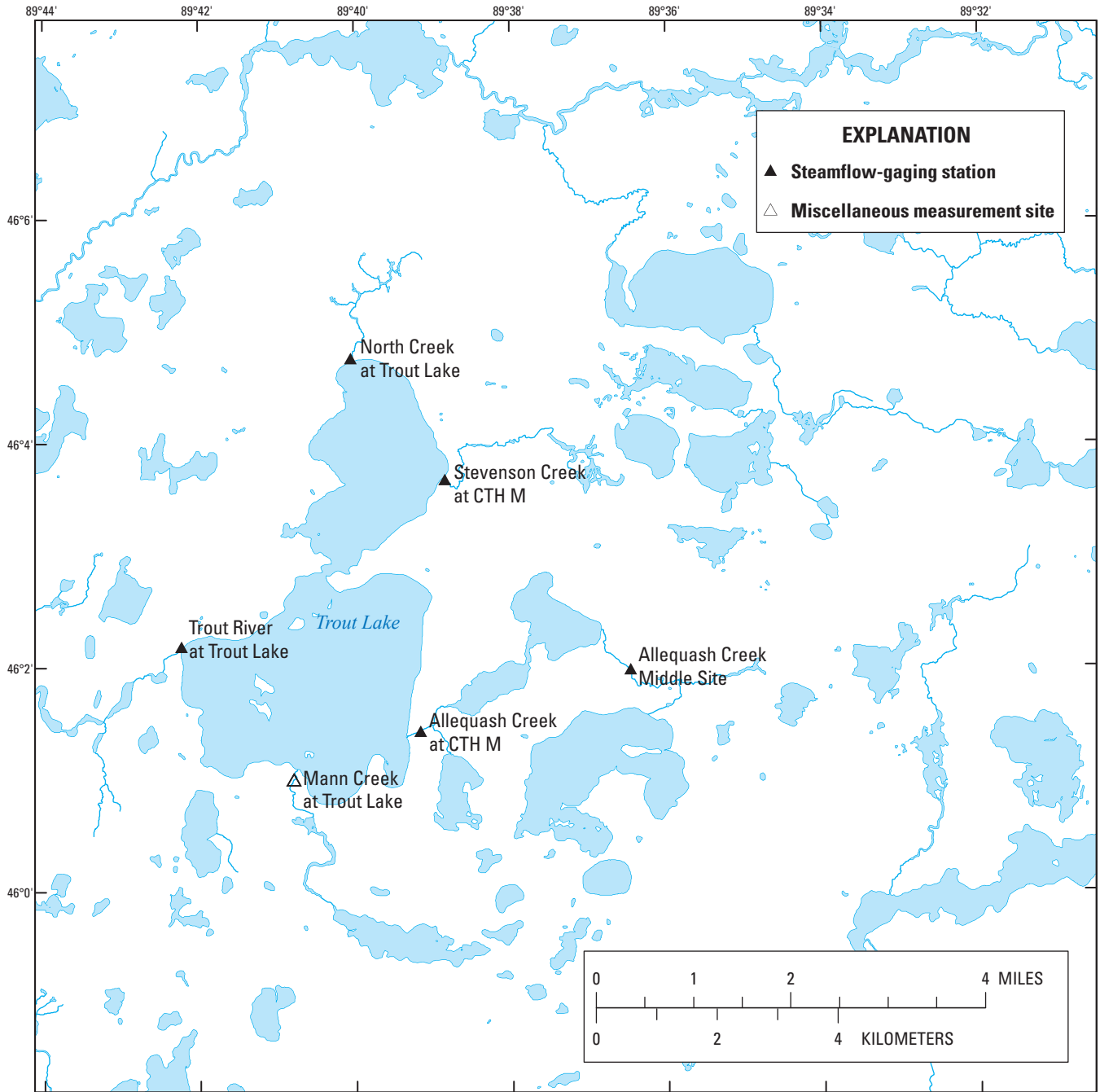


Figure 3-2. Locations of U.S. Geological Survey streamflow-gaging stations used to calibrate the model.

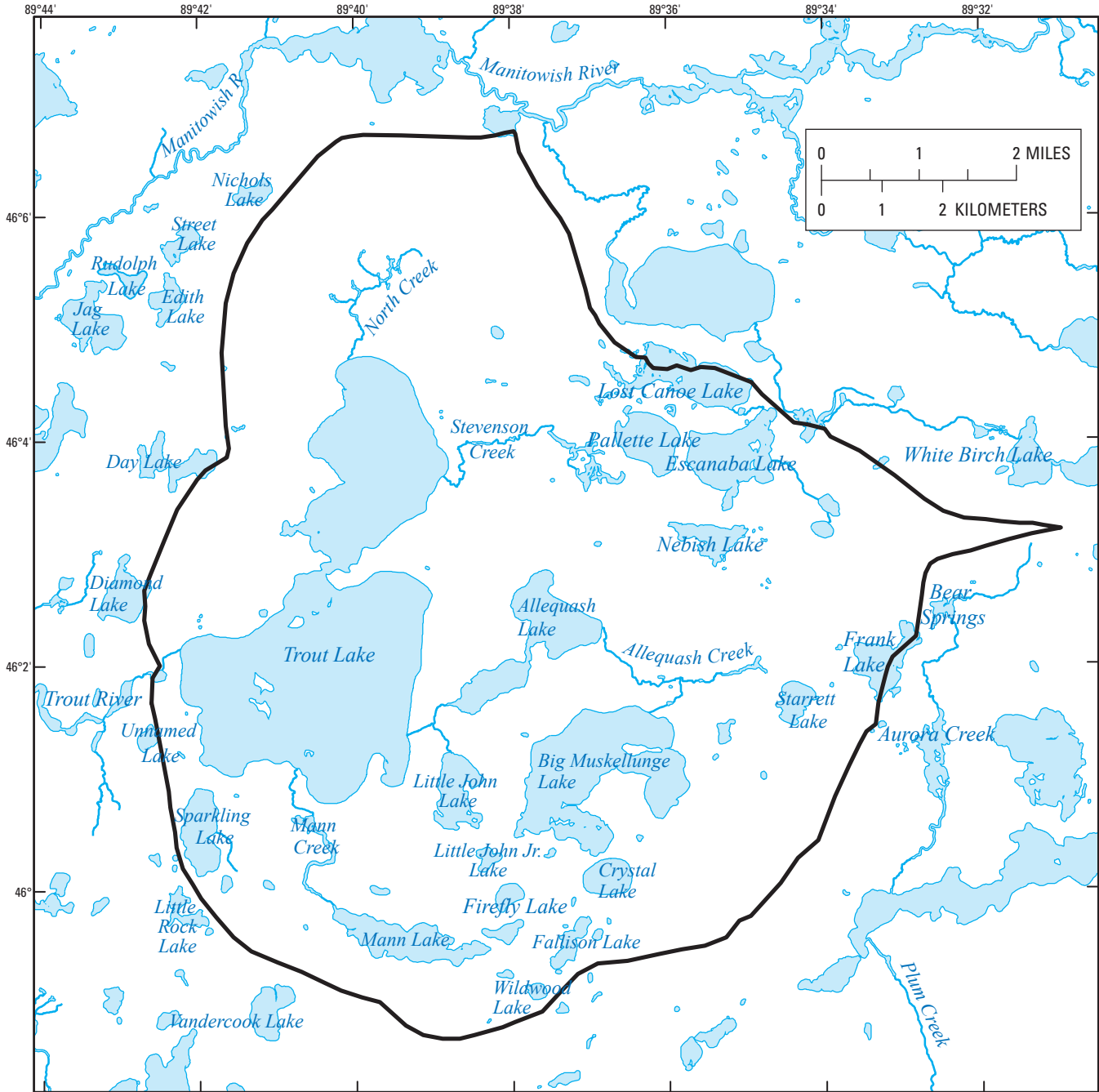


Figure 3-3. Simulated groundwater watershed (black line) of Hunt and others (1998) and names of surface-water features used in the model calibration (modified from Muffels, 2008).

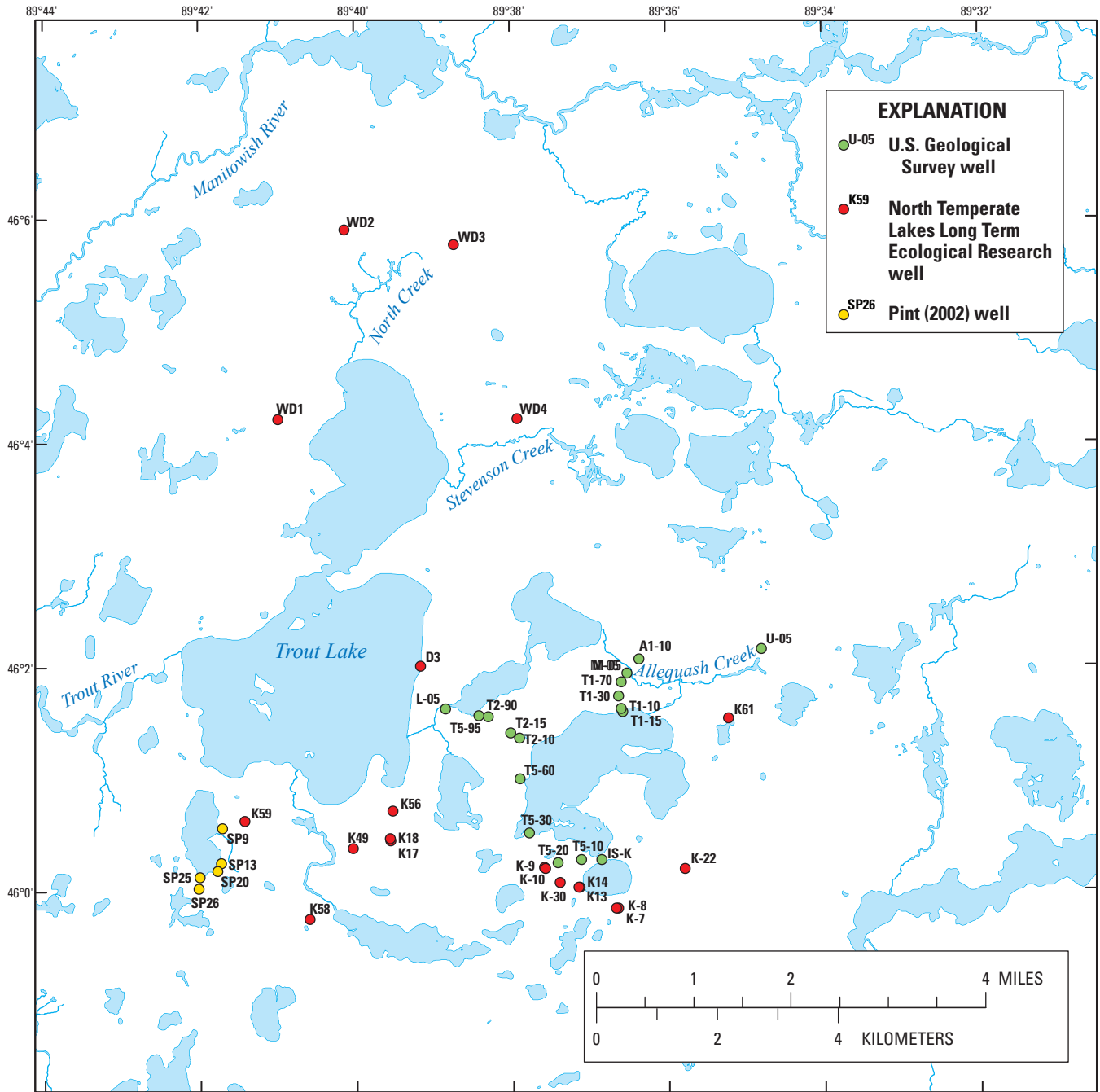


Figure 3-4. Locations of groundwater-level measurements used as head targets for model calibration.

Nonsynchronous measurements of head collected during July 2001 were used in order to maximize the number of calibration targets. This is considered acceptable because July 2001 was representative of average conditions as calculated from records of head in wells with longer datasets. Because lake stage and streamflow can be influenced by short-term transient events, average values of lake stage and streamflows were used for MODFLOW calibration. Additionally, estimates of groundwater fluxes to and from lakes (Ackerman, 1992), the depth of an oxygen isotope plume emanating from Big Muskellunge Lake as measured in three well nests (T1-70, T2-90, and T5-10, fig. 3–4), and traveltime between Big Muskellunge Lake and well T1-70 (fig. 3–4) estimated from chlorofluorocarbon (CFC) and tritium sampling (Walker and others, 2003) provided calibration targets.

The overall calibration approach used here is one of regularized inversion (Hunt and others, 2007; Doherty and Hunt, 2010b) and differs from traditional nonlinear regression parameter estimation by the use of (1) pilot points (Doherty, 2003; Doherty and others, 2010) in addition to a traditional parameter zone approach; (2) Tikhonov regularization (Tikhonov, 1963a, 1963b; Doherty, 2003; Doherty and Hunt, 2010b); and (3) singular value decomposition (Tonkin and Doherty, 2005; Hunt and others, 2007). Additional information regarding the overview of the advantages of using these more sophisticated tools for parameter estimation are discussed by Hunt and others (2007); the tools were applied in accordance with the guidelines given by Doherty and Hunt (2010b). A total of 2,768 adjustable parameter values were included in the sequentially linked calibration.

Pilot Points

A pilot-point approach (for example, fig. 3–5) allows for a parameterization approach that it is not “hardwired” as in a traditional zone approach (Hunt and others, 2007); moreover, adding parameters helps the calibration process extract more information from the calibration data. The result, however, is many more estimated parameter values than is typical in traditional model calibration, a situation that can lead to parameter insensitivity and correlation, which in turn lead to solution nonuniqueness and an ill-posed inverse problem. A number of mathematical approaches (“regularization” constraints) have been devised to create the conditions for uniqueness and to thereby stabilize the numerical-solution process. For brevity, these regularization strategies are reduced here into two

broad categories, soft-knowledge/Tikhonov regularization and subspace regularization, as performed by using singular value decomposition. Both regularization devices were used to obtain a tractable inverse problem in the Trout Lake model calibration. They are briefly described below; see Hunt and others (2007) and Doherty and Hunt (2010b) for more details.

Tikhonov Regularization

One measure of the quality of calibration is the extent to which geological information regarding the system modeled is expressed in the best-fit parameters estimated. Tikhonov regularization provides a vehicle for incorporation of this “soft” information into the calibration process at the same time as it provides a means for achievement of a unique solution to the inverse problem of model calibration. Understanding of a site can enter into the calibration process through definition of a preferred system condition (for example, preferred value such as “the hydraulic conductivity should have a value around 1 meter per day,” or preferred difference such as “the hydraulic conductivity should be uniform in this area”). The regularization process achieves this by supplementing the calibration observed dataset with a suite of pseudo observations, each of these pertaining to one or more parameters employed by the model. Collectively these provide a fallback position for parameters, or for relationships between parameters, in the event that little or no information resides in the observations in the calibration dataset. Where the information content of a calibration dataset is insufficient for unique estimation of certain parameters, or combinations of parameters, the fallback position prevails.

Apart from providing a fallback or default condition for parameters, and for relationships between them, Tikhonov regularization also provides constraints on the manner in which heterogeneity that is supported by the calibration dataset emerges in the estimated parameter field. If properly formulated, Tikhonov constraints facilitate only departures from background parameter fields that are geologically reasonable (that is, consistent with the modeler’s preferred condition). This approach filters out fields that may provide a good fit with the calibration dataset but at the expense of a credible estimated parameter field. Part of the art of formulating appropriate Tikhonov constraints for a particular parameter-estimation problem is to achieve good fit to measured data and reasonable parameters.

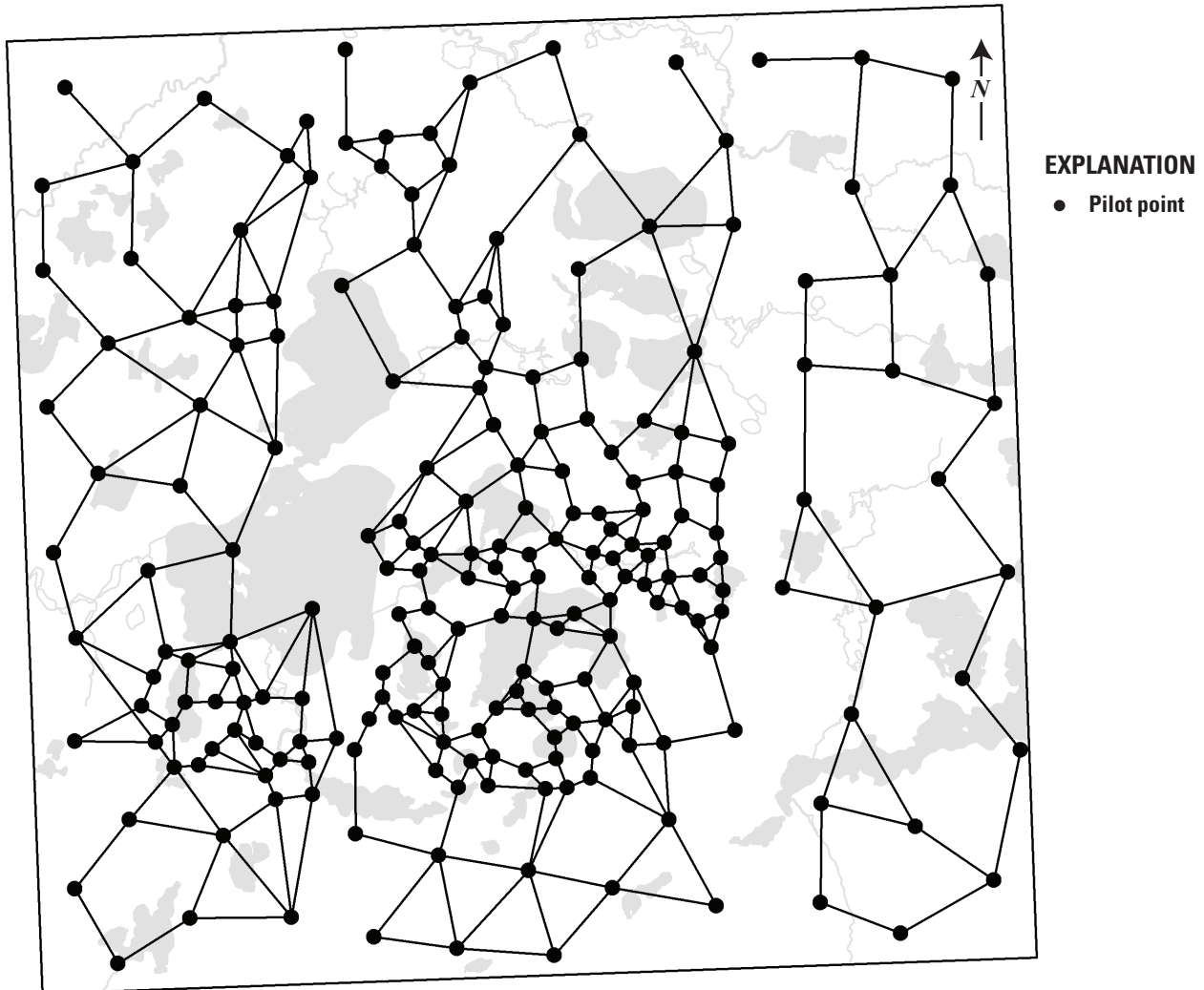


Figure 3-5. Pilot-point locations and links between pilot points used to apply preferred homogeneity Tikhonov regularization within each layer (from Muffels, 2008).

Soft-knowledge information was entered into the calibration by using Tikhonov regularization constraints. PEST adjusts the weights assigned to these equations such that all preferred conditions are seen as the objective function is minimized during the calibration process (see Doherty, 2003, 2010a). The inversion process thus becomes a dual constrained minimization process in which a regularization objective function specifying adherence to the preferred system condition encapsulated in the regularization constraints is minimized subject to the constraint that the measurement objective function adheres to its user-specified target (if this can be achieved). This target is set on the basis of measurement noise considerations. However, as described in detail by Fienen and others (2009) and Doherty and Hunt (2010b), the appropriate tradeoff is specified by the modeler via the PHIMLIM variable in PEST and often requires review during the calibration process. If the PHIMLIM variable is set too low, parameter fields

may become unrealistic as a result of fitting to noise; if set too high, parameter fields may fit the preferred condition too well, and the calibration process will fail to extract maximum information from the calibration dataset. The calibration used an established approach for setting PHILIM (Doherty and Hunt, 2010b, p. 20).

In the sequentially linked calibration, the Tikhonov regularization for horizontal conductivity pilot points (shown in fig. 3-5) consisted of preferred difference between pilot points set to zero, resulting in a preferred homogeneity soft-knowledge constraint. This is consistent with the high homogeneity reported for the area by Dripps (2003). The Tikhonov regularization for vertical anisotropy pilot points used a preferred value of approximately 1:3 ($K_v:K_h$) based on the tracer test of Kenoyer (1988) and previous modeling of Pint (2002) and Muffels (2008). A preferred value condition set at initial reasonable values was used for other model parameters.

Interregularization group weights adjustment also was activated (PEST variable IREGADJ=1; Doherty and Hunt, 2010b, p. 20); thus, the soft-knowledge importance between parameter types was adjusted during the calibration to ensure a similar relative importance of the parameter group soft-knowledge preferred conditions.

Singular Value Decomposition

In contrast to Tikhonov regularization, which adds information that expresses geological expertise to the calibration process to promote unique estimability of parameters, subspace methods subtract from the calibration process the need to estimate either individual parameters, or combinations of correlated parameters, that are inestimable on the basis of the current calibration dataset. These combinations are determined through undertaking singular value decomposition (SVD) of the weighted Jacobian matrix (see Moore and Doherty, 2005; Tonkin and Doherty, 2005). The Jacobian matrix encapsulates the sensitivities of model outputs corresponding to field measurements to all adjustable model parameters; each column of the Jacobian matrix contains the sensitivity of all model outputs for which there are corresponding field measurements to a single adjustable parameter. Individual parameters, or combinations of parameters, that are deemed capable of being estimated (these comprising the calibration solution space) are then estimated on the basis of the calibration dataset. Those parameters, and parameter combinations, that are deemed incapable of being estimated (these comprising the calibration null space) are not adjusted during calibration but rather retain their initial values.

The “SVD-assist” approach is an extension of the SVD approach that can provide gains in efficiency in solution of the inverse problem of model calibration. Prior to starting the calibration process, a set of superparameters is defined using sensitivities calculated from the full set of parameter values, then the full parameter space is reduced to a subset of the full set of base parameters by projecting base parameters onto a reduced set of axes composed of linear combinations of base parameters (Tonkin and Doherty, 2005). This reduction is easily obtained using an algorithm within PEST (for example, Doherty and Hunt, 2010b, p. 21). The resulting superparameters are linear combinations of the base parameters spanning the calibration solution space; their coefficients must be multiplied in order to achieve a calibrated set of “native” or “base” model parameters. In the case of the Trout Lake sequentially linked model, calibration involved 100 superparameters.

Calibration Approach: Fully Coupled Surface-Water/Groundwater Model

After the sequentially linked MODFLOW and PRMS models were constructed and calibrated, the MODFLOW and PRMS input files were slightly modified before the coupled model was run. Aquifer storage parameters and a second GSFLOW transient stress period were added to the optimal sequentially linked MODFLOW steady-state input file; therefore, steady-state MODFLOW simulations provided initial conditions for all transient GSFLOW runs. For the PRMS model, the `adjust_rain` and `adjust_snow` parameters were split into monthly components; monthly `lake_evap_adj` parameters were added for the five lakes with the most study, and additional surface-water cascades were added to allow adjustment of the amount of direct runoff into seepage lakes.

Whereas the sequentially linked calibration used representative steady-state heads for groundwater-model calibration, the fully coupled model is transient on a daily timestep. Therefore, the head time-series data measured during the study were included in coupled-model calibration and were processed by using the TSPROC utility (Westenbroek and others, 2012). The transient head data were used in the calibration via the following summary metrics:

1. **Average:** This is the average of the selected head time series for the period chosen and might be considered to represent the longer-term condition.
2. **Range:** This reports the range of all the values in the head time series for the period chosen and represents the system dynamics around the average condition.
3. **Time-Series Difference:** This reports the difference between the current value and the previous value in a time series and represents a “moving” drawdown that reflects the temporal dynamics of the time series.

Because the observed head data had a higher frequency than the daily timestep used in the coupled model, the observed data were summarized into daily average values before differencing. Transient lake-level data were available for five lakes at a biweekly frequency during the open-water periods. These data were processed with TSPROC with the same metrics used for the transient groundwater-head data described above. The targets derived from the streamflow time-series data were directly ported from the PRMS-only calibration.

Because forward run times were long, all parameters varied during the sequentially linked calibration could not be evaluated in the fully coupled model calibration. For example, more than 2,600 pilot points were used to estimate aquifer hydraulic conductivity in the sequentially linked calibration of the Trout Lake model, but only a subset of layer multipliers were included in the coupled model calibration. Thus, it is possible that undesirable artifacts from calibration of the uncoupled models may not be completely addressed in the coupled-model calibration. After some initial calibration tests, the final fully coupled model included only a subset of all possible model parameters (tables 3–6 and 3–7). The resulting 201 parameters estimated during the fully coupled calibration focused on (1) those parameters not specified in the steady-state MODFLOW-only calibration (for example, aquifer storage, unsaturated zone parameter surfdep), (2) those important for simulating the interface between the MODFLOW-only and PRMS-only model, and (3) those considered useful for calibration of coupled models (Jensen-Haise coefficient, saturated vertical hydraulic conductivity of the unsaturated zone). The fully coupled model calibration used singular value decomposition on the entire set of 201 base parameters. Of these 201 possible parameters, the information content of the multi-objective function observation data supported approximately 132 linear combinations (singular values) using a typical stability criterion (PEST variable EIGHTHRESH= 5.0E-07).

An important calibration issue became apparent during calibration of the fully coupled groundwater/surface-water model. Initially, all aquifer conductivity values were fixed at optimal values obtained during the sequentially linked calibration in order to reduce the number of parameters included in the long run times of the fully coupled model. However, initial calibrated GSFLOW Crystal Lake evaporation rates were appreciably higher than for other lakes in the watershed.

This was considered unreasonable because Crystal Lake is a sheltered, small, deep lake with short fetch and thus would be expected to have the same or lower evaporation rates than surrounding larger lakes. In what became the final fully coupled calibration, layer-wide multipliers for the lowest two layers were included as calibration parameters; these layers were chosen on the basis of parameter uncertainty analysis for Crystal Lake by Hunt and Doherty (2006). Increasing the calibration flexibility by including these additional hydraulic conductivity multipliers resulted in a slightly higher value of horizontal hydraulic conductivity in one of lower units (slight increase to the layer 5 multiplier 1.0 starting value; kh5mult in table 3–7) and slightly lower value layer 6 multiplier (decrease to 1.0 layer 6 multiplier; table 3–7). This relatively small change in the distribution of deeper layer transmissivity facilitated enhanced groundwater exchange and reduced the calibrated value for Crystal Lake evaporation to a more reasonable value.

The need for this additional calibration effort demonstrates the poor results that can potentially occur from not accounting for structural error within the model (in this case, misspecification of deep aquifer transmissivity distribution important for the Crystal Lake predictions of interest). Moreover, it underscores the importance of parameters that take on surrogate roles to address structural error (Doherty and Welter, 2010) in fully coupled models where many parameters are specified, and many processes and associated parameters are correlated with others. Therefore, the value of revisiting model conceptualization and calibration with the fully coupled GSFLOW model is demonstrated, even after improvements gained from sequentially linked calibration. Therefore, it is expected that fully coupled models will benefit from final calibration, even if the forward run times make the calibration computationally expensive.

Table 3–6. PRMS parameter types estimated during calibration of the fully coupled GSFLOW model.

[HRU, hydrologic response unit; potet, potential evapotranspiration]

Name	Description	Model-suggested values			Calibrated values		
		Default	Minimum	Maximum	Average	Minimum	Maximum
climate_hru_prms module							
adjust_rain	Monthly downscaling fractional adjustment for rain for each HRU	0.01	–0.25	1	0.13621	–0.25	0.5
adjust_snow	Monthly downscaling fractional adjustment for snow for each HRU	0.01	–0.25	1	0.15299	–0.25	0.5
soilzone_prms module							
lake_evap_adj	Monthly potet factor to adjust potet for each lake	1	0.005	1	0.74583	0.5	1.575
sat_threshold	Soil saturation threshold, above field-capacity threshold for each HRU	999	1	999	6.78082	6	12
slowcoef_lin	Linear gravity-flow reservoir routing coefficient for each HRU	0.015	0	1	0.21278	0.00001	0.34628
slowcoef_sq	Nonlinear gravity-flow reservoir routing coefficient for each HRU	0.1	0	1	0	0	0.00001
soil_rechr_max	Maximum value for soil recharge zone for each HRU, in inches	2	0	10	0.88442	0.05	4.80966
soil2gw_max	Maximum value for soil-water excess to groundwater for each HRU, in inches	0	0	5	0.02906	0	0.19243
ssr2gw_rate	Coefficient to route water from subsurface to groundwater for each HRU	0.1	0	1	0.86745	0.30331	1.01
srunoff_smidx_prms module							
carea_max	Maximum contributing area for each HRU, expressed as a decimal fraction	0.6	0	1	0.044	0	1
smidx_coef	Coefficient in contributing area computations for each HRU	0.01	0.0001	1	0.04215	0.04215	0.04215
smidx_exp	Exponent in contributing area computations for each HRU	0.3	0.2	0.8	0.2	0.2	0.2
soil_moist_max	Maximum value of water for soil zone for each HRU, in inches	6	0	20	3.16646	0.4	16.2656

Table 3–7. MODFLOW parameter types estimated during calibration of the fully coupled GSFLOW model. Parameter names that represent a single parameter do not display minimum and maximum calibrated values.

[m, meters; m/d, meters per day; m³/d, cubic meters per day]

Name	Description	Starting value	Lower bound	Upper bound	Calibrated values		
					Average	Minimum	Maximum
wetl strm_kv	Streambed vertical hydraulic conductivity for wetland tributary streams to Trout Lake (m/d)	1E-02	1E-10	1E10	1.36E-02	3.04E-03	1.99E-02
sandy strkv	Streambed vertical hydraulic conductivity for all nonwetland streams (m/d)	3	1E-10	1E10	2.592293		
kh5mult	Multiplier for layer 5 horizontal hydraulic conductivity array (dimensionless)	1.0	8E-01	1.E10	1.040898		
Kh6mult	Multiplier for layer 6 horizontal hydraulic conductivity array (dimensionless)	1.0	8E-01	1.E10	0.8129960		
lakebed leakance (non-profundal)	Lakebed leakance array; by lake (days-1)	Variable	1E-05	5E-01	3.90E-02	9.86E-05	5.00E-01
lakebed leakance (profundal)	Lakebed leakance array for deepest lakebed; one value for deep lakes (days-1)	2.9E-04	1E-05	5E-01	2.292E-04		
stream outflow for lake stage look up table	Streamflow value specified for given lake stage increment (m ³ /d)	Variable	Variable	Variable	Variable	Variable	Variable
storage	Confined aquifer storage (dimensionless)	8.9E-04	1E-05	1E-02	9.901E-04		
sy	Unconfined aquifer storage (specific yield)	0.27	0.1	0.3	0.2700		
surfdep	Land surface depression variable used to smooth UZF Package solution (m)	0.5	0.3	2	0.49689		
vksat multiplier	Multiplier applied to initial saturated vertical hydraulic conductivity used by UZF Package (dimensionless)	1	0.8	4	2.352756		

References Cited

- Ackerman, J.A., 1992, Extending the isotope based ($\delta^{18}\text{O}$) mass budget technique for lakes and comparison with solute based lake budgets: University of Wisconsin-Madison, M.S. thesis, 151 p.
- Doherty, John, 2003, Groundwater model calibration using pilot points and regularization: *Ground Water*, v. 41, no. 2, p. 170–177.
- Doherty, John, 2008, PEST surface water utilities: Brisbane, Australia, Watermark Numerical Computing and University of Idaho, 141 p., accessed September 28, 2011, at <http://www.pesthomepage.org/getfiles.php?file=swutils.pdf>.
- Doherty, John, 2010a, PEST, Model-independent parameter estimation—User manual (5th ed., with slight additions): Brisbane, Australia, Watermark Numerical Computing.
- Doherty, John, 2010b, Addendum to the PEST manual: Brisbane, Australia, Watermark Numerical Computing.
- Doherty, J.E., Fienen, M.F., and Hunt, R.J., 2010, Approaches to highly parameterized inversion—Pilot-point theory, guidelines, and research directions: U.S. Geological Survey Scientific Investigations Report 2010–5168, 36 p.
- Doherty, John, and Hunt, R.J., 2009, Two statistics for evaluating parameter identifiability and error reduction: *Journal of Hydrology*, v. 366, p. 119–127, doi: 10.1016/j.jhydrol.2008.12.018.
- Doherty, John, and Hunt, R.J., 2010a, Response to comment on “Two statistics for evaluating parameter identifiability and error reduction”: *Journal of Hydrology*, v. 380, p. 489–496, doi:10.1016/j.jhydrol.2009.10.012.
- Doherty, J.E., and Hunt, R.J., 2010b, Approaches to highly parameterized inversion—A guide to using PEST for groundwater-model calibration: U.S. Geological Survey Scientific Investigations Report 2010–5169, 60 p.
- Doherty, John, and Welter, David, 2010, A short exploration of structural noise: *Water Resources Research*, v. 46, W05525, 14 p., doi:10.1029/2009WR008377.
- Dripps, W.R., 2003, The spatial and temporal variability of groundwater recharge: University of Wisconsin-Madison, Department of Geology and Geophysics, Ph.D. dissertation, 231 p.
- Farnsworth, R.K., Thompson, E.S., and Peck, E.L., 1982, Evaporation atlas for the contiguous 48 United States: U.S. National Atmospheric and Oceanic Administration Technical Report NWS 33, 26 p., 4 pl.
- Fienen, M.N., Muffels, C.T., and Hunt, R.J., 2009, On constraining pilot point calibration with regularization in PEST: *Ground Water*, v. 47, no. 6, p. 835–844, doi: 10.1111/j.1745-6584.2009.00579.x
- Hay, L.E., Leavesley, G.H., Clark, M.P., Markstrom, S.L., Viger, R.J., and Umemoto, Makiko, 2006, Step wise, multiple objective calibration of a hydrologic model for a snowmelt dominated basin: *Journal of the American Water Resources Association*, v. 42, no. 4, p. 877–890.
- Hunt, R.J., Anderson, M.P., and Kelson, V.A., 1998, Improving a complex finite-difference ground water flow model through the use of an analytic element screening model: *Ground Water*, v. 36, no. 6, p. 1011–1017.
- Hunt, R.J., and Doherty, J., 2006, A strategy of constructing models to minimize prediction uncertainty, in *MODFLOW and More 2006—Managing Ground Water Systems. Proceedings of the 7th International Conference of the International Ground Water Modeling Center: Golden, Colo., Colorado School of Mines*, p. 56–60.
- Hunt, R.J., Doherty, John, and Tonkin, M.J., 2007, Are models too simple? Arguments for increased parameterization: *Ground Water*, v. 45, no. 3, p. 254–262, doi:10.1111/j.1745-6584.2007.00316.x.
- Hunt, R.J., Doherty, J., and Walker, J.F., 2009, Parameter estimation and coupled groundwater/surface-water models—A PEST approach, in *Conference Proceedings from the 1st PEST Conference, November 1–3, 2009, Potomac, Md.*
- Kenoyer, G.J., 1988, Tracer test analysis of anisotropy in hydraulic conductivity of granular aquifers: *Ground Water Monitoring and Remediation*, v. 8, no. 3, p. 67–70, doi:10.1111/j.1745-6592.1988.tb01086.x.
- Lenters, J.D., Kratz, T.K., and Bowser, C.J., 2005, Effects of climate variability on lake evaporation—Results from a long-term energy budget study of Sparkling Lake, northern Wisconsin (USA): *Journal of Hydrology*, v. 308, p. 168–195.
- Markstrom, S.L., Niswonger, R.G., Regan, R.S., Prudic, D.E., and Barlow, P.M., 2008, GSFLOW—Coupled Ground-Water and Surface-Water Flow Model based on the integration of the Precipitation-Runoff Modeling System (PRMS) and the Modular Ground-Water Flow Model (MODFLOW-2005): U.S. Geological Survey Techniques and Methods, book 6, chap. D1, 240 p.
- Miller, Irwin, and Freund, J.E., 1977, Probability and statistics for engineers: Englewood Cliffs, N.J., Prentice-Hall, 530 p.

- Moore, Catherine, and Doherty, John, 2005, The role of the calibration process in reducing model predictive error: *Water Resources Research*, v. 41, no. 5, W05020, 14 p.
- Muffels, C.T., 2008, Application of the LSQR algorithm to the calibration of a regional groundwater flow model—Trout Lake Basin, Vilas County, Wisconsin: University of Wisconsin-Madison, M.S. thesis, 106 p.
- Pint, C.D., 2002, A groundwater flow model of the Trout Lake Basin, Wisconsin—Calibration and lake capture zone analysis: University of Wisconsin-Madison, M.S. thesis, 123 p.
- Sloto, R.A., and Crouse, M.Y., 1996, HYSEP—A computer program for streamflow hydrograph separation and analysis: U.S. Geological Survey Water-Resources Investigations Report 96-4040, 46 p.
- Tikhonov, A.N., 1963a, Solution of incorrectly formulated problems and the regularization method: *Soviet Mathematics Doklady*, v. 4, p. 1035–1038.
- Tikhonov, A.N., 1963b, Regularization of incorrectly posed problems: *Soviet Mathematics Doklady*, v. 4, p. 1624–1637.
- Tonkin, M.J., and Doherty, John, 2005, A hybrid regularized inversion methodology for highly parameterized models: *Water Resources Research*, v. 41, no. 10, W10412, 16 p., doi:10.1029/2005WR003995.
- Walker, J.F., Hunt, R.J., Bullen, T.D., Krabbenhoft, D.P., and Kendall, Carol, 2003, Variability of isotope and major ion chemistry in the Allequash basin, Wisconsin: *Ground Water*, v. 41, no. 7, p. 883–894, doi:10.1111/j.1745-6584.2003.tb02431.x.
- Walker, J.F., Hunt, R.J., Doherty, J., and Hay, L., 2009, Processing time-series data to calibrate a surface-water model in small headwater watersheds, *in* Conference Proceedings from the 1st PEST Conference, November 1–3, 2009, Potomac, Md.: Lulu Publishing, Inc., Raleigh, N.C., USA.
- Westenbroek, S.M., Doherty, J., Walker, J.F., Kelson, V.A., Hunt, R.J., and Cera, T.B., 2012, Approaches in highly parameterized inversion—TSPROC, A general time-series processor to assist in model calibration and result summarization: U.S. Geological Survey Techniques and Methods, book 7, chap. C7, 73 p.

Appendix 4. Temperature Model Construction and Calibration

Introduction.....	76
Model Framework.....	76
Model Input and Calibration Data	76
Stream Geometry	81
Stream Shading.....	81
Meteorology.....	82
Hydrology	82
References Cited.....	83

Figures

4-1. Map showing location of stream segments used to represent three creeks in the Stream-Network TEMPerature (SNTEMP) model. <i>A</i> , North. <i>B</i> , Stevenson. <i>C</i> , Upper Allequash	77
4-2A. Map showing stream segment and node structure used to represent North Creek in the SNTEMP model	78
4-2B. Map showing stream segment and node structure used to represent Stevenson Creek in the SNTEMP model.....	79
4-2C. Map showing stream segment and node structure used to represent Upper Allequash Creek in the SNTEMP model.....	80

Tables

4-1. Stream-geometry characteristics for stream reaches described in the SNTEMP model	81
4-2. Stream-shading characteristics for stream reaches described in the SNTEMP model	82

Introduction

A stream temperature model was developed to predict daily mean and maximum stream temperatures at three selected main stems and associated tributaries of the Trout Lake stream network: North Creek, Stevenson Creek, and Upper Allequash Creek (fig. 4–1). This section describes the model framework, data collection and synthesis, and calibration procedures for the Trout Lake stream temperature model.

Model Framework

The instream water temperature model SNTemp (Stream-Network TEMPerature model – Bartholow, 1991), developed and supported by the U.S. Fish and Wildlife Service, was selected to predict stream temperatures in the Trout Lake stream network. A modified version of SNTemp called TRPA Stream Temperature for Windows (<http://trpafishbiologists.com/sindex.html>) provided a graphical user interface to simplify data entry and export. SNTemp is a steady-state, one-dimensional heat-transport model that predicts daily mean and maximum temperatures as a function of stream distance and environmental heat flux (Bartholow, 1991). A heat-transport equation describes the downstream movement of heat energy in the water and actual exchange of heat energy between the water and its surrounding physical environment (Theurer and others, 1984). Net heat flux is calculated by parameter inputs describing the meteorology, hydrology, stream geometry, and shade setting for a dendritic network of main-stem and tributary stream segments that drain into Trout Lake.

Model Input and Calibration Data

SNTemp is composed of several component modules that describe the physical setting of the study area. These modules can be broken into three broad categories of stream geometry, meteorology, and hydrology. In SNTemp, it is assumed that all input data, including meteorological and hydrological variables, can be represented by 24-hour averages (Bartholow, 1991). Many of the model input parameters, including meteorological and hydrological data, were taken from published, historical data sources. Daily mean stream temperatures based on unpublished data collected by Hunt and others (2006) were used as the target for SNTemp predictions. The calibration period was April–September 2002.

The Trout Lake stream network was split into 14 stream segments. Each segment represents uniform width, groundwater accretion rates, and relatively homogeneous topographic and riparian vegetation conditions with major transitions between segments. Each stream segment requires a physical description of stream geometry, hydrology, and shading variables. Meteorological variables are more global in nature and were applied to all stream segments universally. Figures 4–1 and 4–2 illustrate the geographic setting and conceptual model of the Trout Lake stream network used in SNTemp. This section documents the sources of both input and calibration data. After data processing and formatting for the SNTemp model, calibration consisted of fitting simulated daily mean stream temperatures to observations in the field. Calibration was achieved by trial-and-error adjustment of SNTemp input variables until minimal differences were achieved between simulated and measured downstream calibration locations.

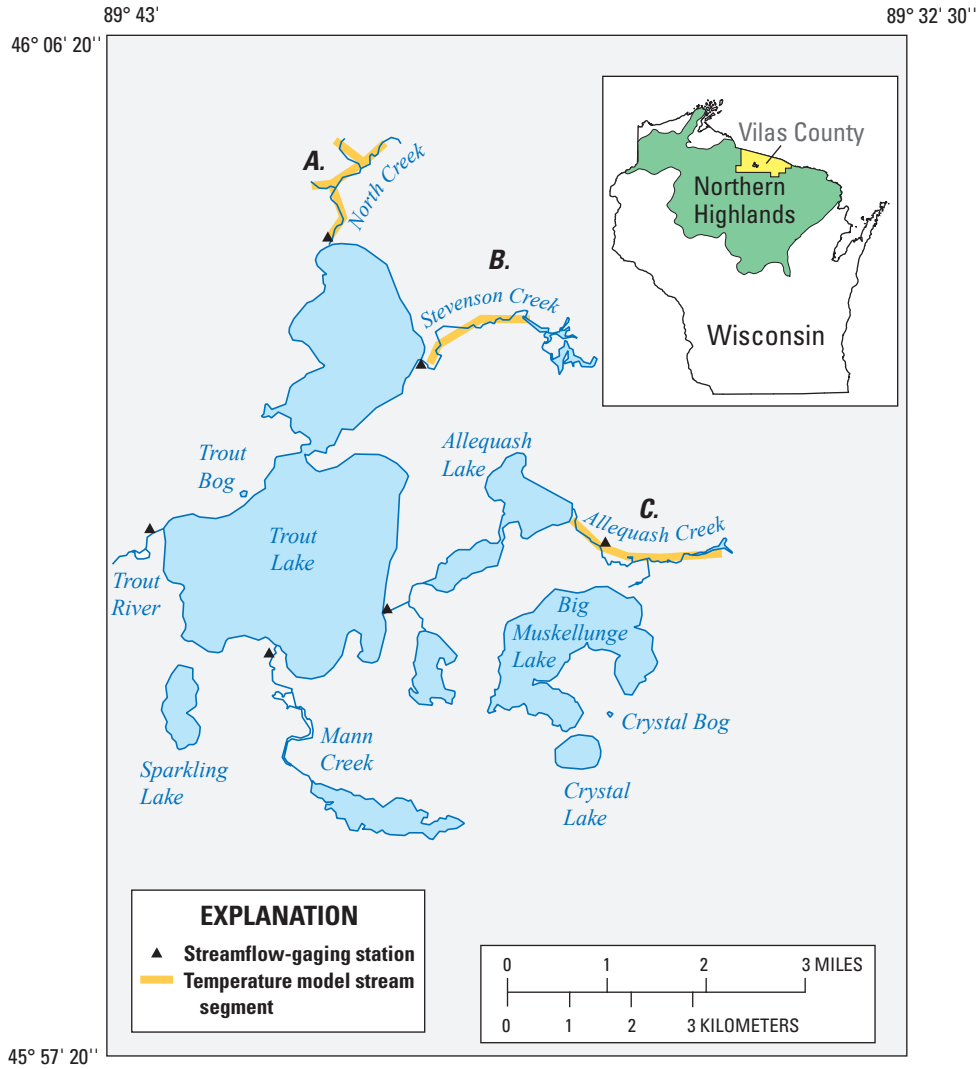


Figure 4-1. Location of stream segments used to represent three creeks in the Stream-Network TEMPerature (SNTemp) model. A, North. B, Stevenson. C, Upper Allequash.

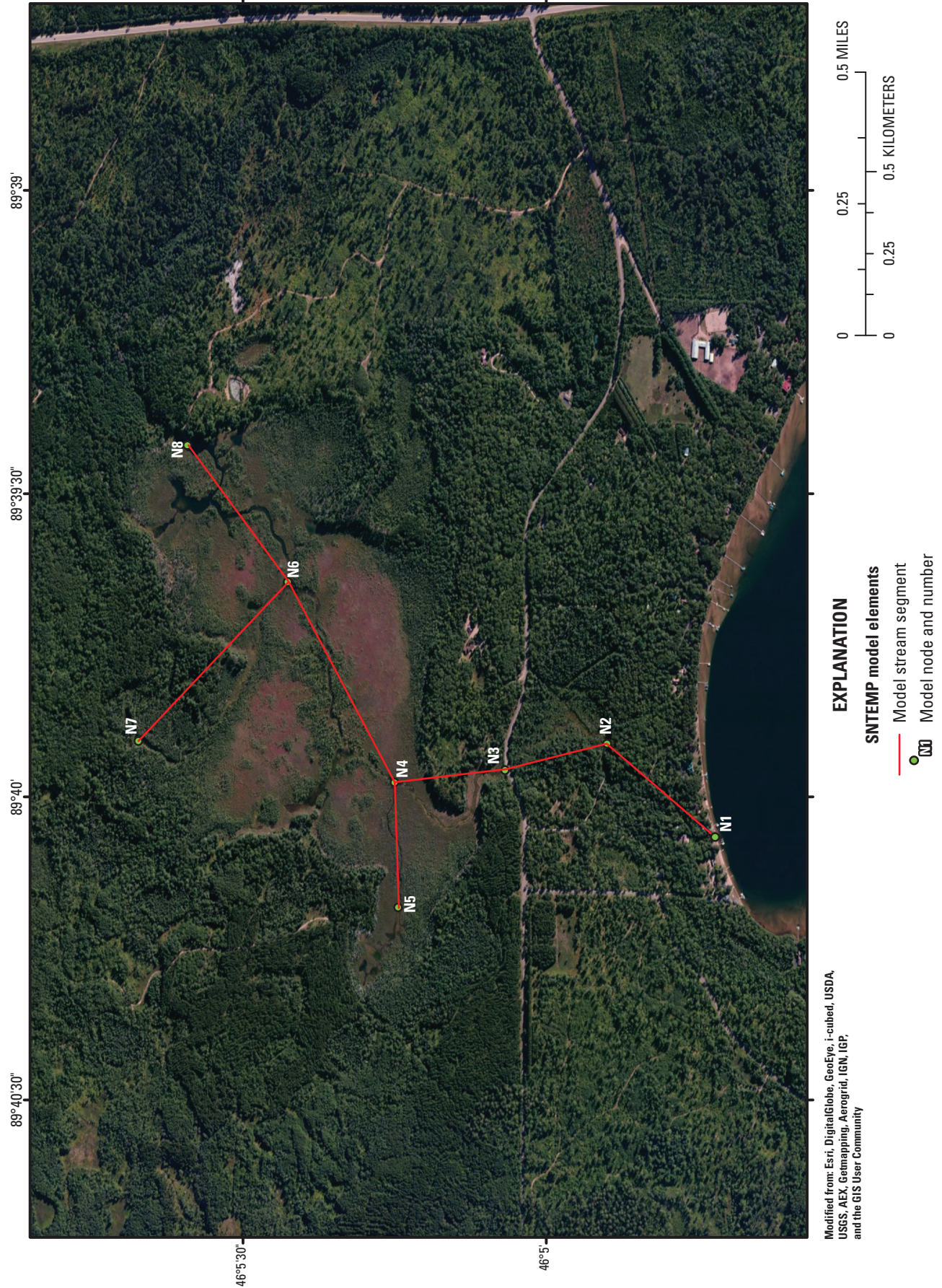


Figure 4-2A. Stream segment and node structure used to represent North Creek in the Stream-Network TEMPerature (SNTMP) model.

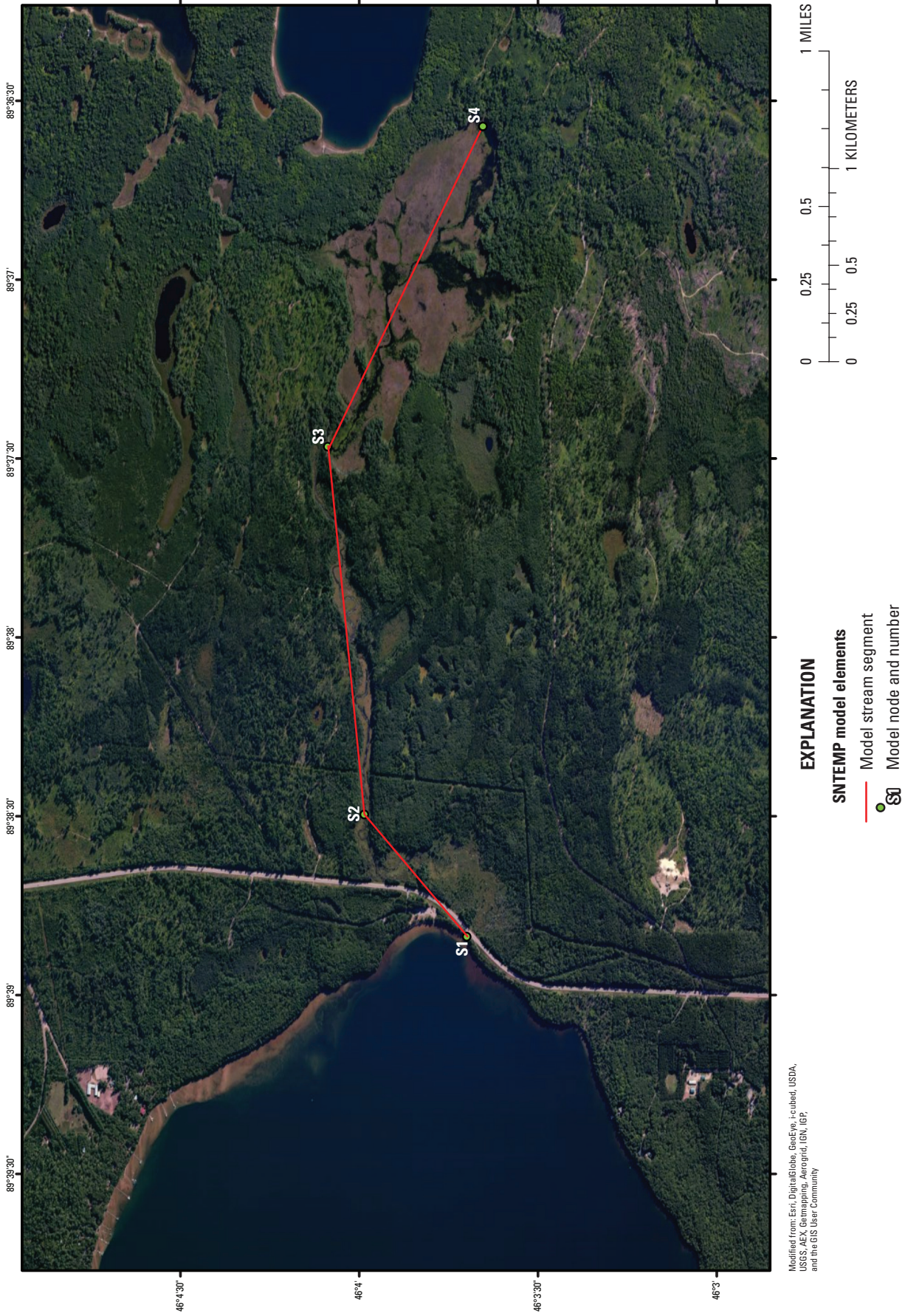


Figure 4-2B. Stream segment and node structure used to represent Stevenson Creek in the Stream_Network TEMPerature (SNTemp) model.

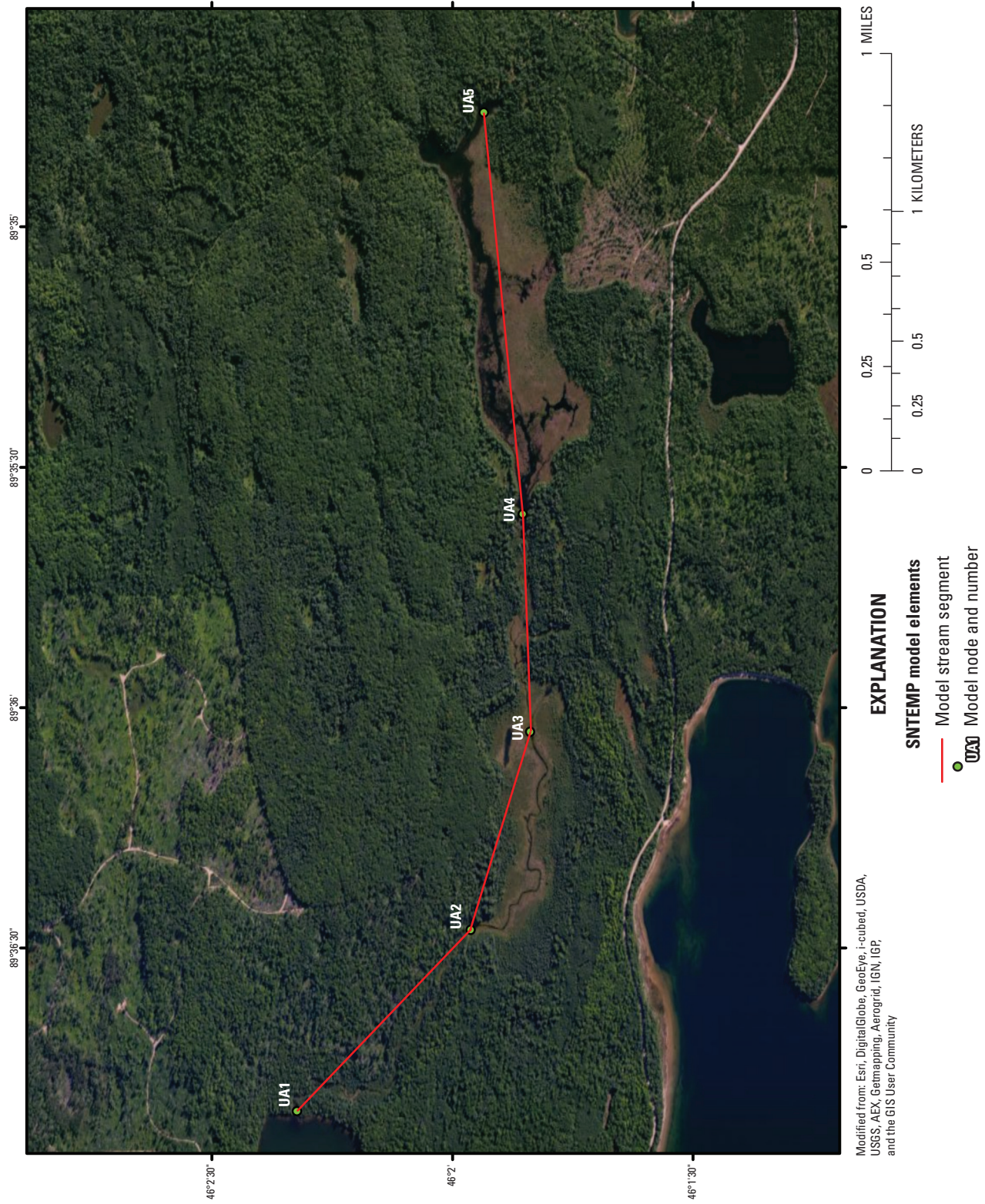


Figure 4-2C. Stream segment and node structure used to represent Upper Allequash Creek in the Stream_Network TEMPerature (SNTMP) model.

Stream Geometry

Stream-geometry data consist of the network layout of the main stem and all tributaries, site elevations, stream widths, and Manning's n values. Stream widths were measured at selected locations in the field then corroborated by using spatially rectified aerial photography for areas that were difficult to reach. SNTMP allows the user to describe stream width as a function of flow. Because the amount of information required to develop this relationship was beyond the scope of this project, it was assumed that the width of each stream segment remained constant with increasing flow. The thermal gradient applied to each reach made use of default values. Estimates of Manning's n values were based on reported ranges for natural channels (Gupta, 1989). Owing to the high degree of uncertainty associated with selecting an appropriate Manning's n value, each stream segment initially received that same value. Adjustments to Manning's n were made in order to calibrate the model. Elevation, latitude, longitude, and river kilometer locations were acquired through a global positioning system (GPS). Stream azimuth was determined

by using U.S. Geological Survey 1:24,000-scale topographic maps. Stream-geometry parameters for each stream reach described in the Trout Lake stream network models are listed in table 4–1.

Stream Shading

Topographic angle, vegetation offset from stream center, crown width, shade density, and riparian-vegetation height were measured throughout the summer of 2011 in accordance with methods described in Bartholow (1989) and Fitzpatrick and others (1998). Vegetation and topographic characteristics both were based on measurements taken at several random locations on the left and right banks of each stream segment then averaged to provide a single value for each stream-segment bank. Owing to the remote nature of the study area, shading values for some reaches were estimated by using a combination of onsite observations and spatially rectified aerial photographs. Stream-shading parameters for each stream reach described in the Trout Lake stream network models are listed in table 4–2.

Table 4–1. Stream-geometry characteristics for stream reaches described in the Stream-Network TEMPerature (SNTMP) model.

Stream name	Stream node		Latitude			Azimuth (degrees)	Manning's n	Width (meters)
	From	To	Degrees	Minutes	Seconds			
Stevenson Creek	S1	S2	46	2	30	50	0.035	3.70
Stevenson Creek	S2	S3	46	3	42	83	0.035	6.10
Stevenson Creek	S3	S4	46	3	42	110	0.035	30.0
North Creek	N1	N2	46	4	60	40	0.10	5.0
North Creek	N2	N3	46	4	60	-10	0.10	6.0
North Creek	N3	N4	46	4	60	-7	0.035	10.0
North Creek	N4	N5	46	4	60	-90	0.02	1.0
North Creek	N4	N6	46	3	60	60	0.035	12.0
North Creek	N6	N7	46	4	60	-45	0.035	1.0
North Creek	N6	N8	46	3	60	50	0.035	20.0
Upper Allequash	UA1	UA2	46	1	60	327	0.035	2.4
Upper Allequash	UA2	UA3	46	0	60	294	0.035	8.0
Upper Allequash	UA3	UA4	46	0	60	272	0.035	10.0
Upper Allequash	UA4	UA5	46	0	60	266	0.035	30.0

Table 4-2. Stream-shading characteristics for stream reaches described in the Stream-Network TEMPerature (SNTMP) model.

[m, meters; %, percent]

Stream name	Stream node		Vegetation characteristics						Topographic altitude (degrees)		Stream corridor width (m)	Stream center offset (m)
			Height (m)		Crowd width (m)		Density (%)		Left bank	Right bank		
			Left bank	Right bank	Left bank	Right bank	Left bank	Right bank				
Stevenson Creek	S1	S2	9.0	9.0	3	3	65	30	10	35	150	100
Stevenson Creek	S2	S3	9.0	9.0	3	3	40	40	25	25	45	0
Stevenson Creek	S3	S4	9.0	9.0	3	3	40	40	10	10	300	0
North Creek	N1	N2	7.5	7.5	4	4	75	75	75	75	5	0
North Creek	N2	N3	7.5	7.5	5	5	75	75	75	75	6	0
North Creek	N3	N4	9.0	9.0	4	4	75	75	10	30	150	75
North Creek	N4	N5	9.0	9.0	4	4	75	75	10	10	325	0
North Creek	N4	N6	9.0	9.0	3	3	75	75	7	7	400	0
North Creek	N6	N7	9.0	9.0	4	4	50	50	5	60	325	280
North Creek	N6	N8	9.0	9.0	3	3	75	75	7	7	375	0
Upper Allequash	UA1	UA2	8.0	8.0	3	3	75	75	35	35	25	0
Upper Allequash	UA2	UA3	9.0	9.0	4	4	30	30	10	10	230	0
Upper Allequash	UA3	UA4	12.0	12.0	4	4	75	75	40	40	30	0
Upper Allequash	UA4	UA5	12.0	12.0	4	4	75	75	20	5	3,050	-125

Meteorology

Meteorological data consist of air temperature, relative humidity, wind speed, and cloud cover. These variables are used by SNTMP to calculate solar radiation. The user can also directly enter solar radiation if data are available. A weather station at the Noble F. Lee Municipal airport in Woodruff, Wisconsin (Wis.) (<http://lter.limnology.wisc.edu/dataset/north-temperate-lakes-lter-meteorological-data-woodruff-airport>) was used for all daily mean temperature, humidity, and wind-speed data. Air temperature was verified for consistency by comparison to a nearby weather station in Minocqua, Wis. Cloud cover was estimated by using a calculated percent possible sunshine for Woodruff, Wis. (<http://aa.usno.navy.mil>). Dust coefficients and ground reflectivity were taken from published values described in Tennessee Valley Authority (1972; cited in Theurer and others, 1984). Dust coefficients were increased from 0.05 during the spring months of April and May to 0.06 for the remaining summer months. A ground reflectivity value of 0.08 was used for all stream segments to represent leaf-and-needle forest. Although solar-radiation data were available from areas outside the Trout Lake Watershed, better agreement between predicted and observed stream temperatures was achieved by using SNTMP-calculated values. Default values were used for all other meteorological variables required by SNTMP.

Hydrology

Hydrologic data input into SNTMP consists of stream discharge and water temperatures from both surface-water and groundwater sources. SNTMP requires both upstream discharge and temperature data for each modeled stream segment, with the exception of zero-flow headwaters. SNTMP allows the user to assume a zero headwater discharge, which then disregards any associated recorded temperature data because there is no streamflow. Daily mean discharge data used in the SNTMP model were obtained by using output from the calibrated version of the GSFLOW model described in this report. Headwater segments of Stevenson, Upper Allequash, and North Creeks were assumed to be zero-flow headwaters and thus did not require associated stream temperatures for model execution.

Stream and groundwater temperature data used for SNTMP model were based on measurements made by Hunt and others (2006) as part of the U.S. Geological Survey (USGS) Northern Temperate Lakes–Water, Energy and Biogeochemical Budgets (NTL–WEBB) project. Observed stream temperature values spanned approximately 25 degrees Celsius (°C) over the period simulated. Standard deviations of stream temperature data during the 2002 period ranged from 6.7 °C (Allequash Creek) to 8.4 °C (Stevenson Creek). Mean differences between daily maximum and minimum stream

temperature (April–September, 2002) ranged from 0.6 °C in April to 1.6 °C in July at Allequash Creek, 0.9 °C in August to 1.3 °C in May at Stevenson Creek, and 0.6 °C in August to 0.9 °C in May at North Creek. Shallow groundwater temperature was measured near the USGS streamflow-gaging stations in North, Stevenson, and Upper Allequash Creeks. Measurements were made approximately 15 centimeters (cm) below the streambed, with a measurement interval ranging between 1 and 3 hours. Mean groundwater temperatures reported by Hunt and others (2006) were, from lowest to highest, 10.3 °C (Allequash Creek), 11.8 °C (North Creek), and 12.6 °C (Stevenson Creek); standard deviations of the observed groundwater temperature data during this period were 4.0, 5.5, and 6.5 °C for Allequash Creek, North Creek, and Stevenson Creek, respectively (table 2; Hunt and others, 2006). Although deeper measurements of groundwater temperature were available, values from the shallow sensor were used because they were considered representative of the temperature of groundwater prior to entering the stream. Daily mean groundwater temperatures were computed from the measured instantaneous values of Hunt and others (2006) then applied to all reaches within their respective streams for the calibration period.

References Cited

- Bartholow, J.M., 1989, Stream temperature investigations—Field and analytical methods: U.S. Fish and Wildlife Service Instream Flow Information Paper No. 13, Biological Report 89(17), 139 p.
- Bartholow, J.M., 1991, A modeling assessment of the thermal regime for an urban sport fishery: *Environmental Management*, v. 15, no. 6, p. 833–845.
- Fitzpatrick, F.A., Waite, I.R., D’Arconte, P.J., Meador, M.R., Maupin, M.A., and Gurtz, M.E., 1998, Revised methods for characterizing stream habitat in the National Water-Quality Assessment Program: U.S. Geological Survey Water-Resources Investigations Report 98–4052, 67 p.
- Gupta, R.S., 1989, *Hydrology and hydraulic systems*: Englewood Cliffs, N.J., Prentice Hall, 739 p. (Reissued 1995, Prospect Heights, Ill., Waveland Press).
- Hunt, R.J.; Strand, Mac; and Walker, J.F., 2006, Measuring groundwater-surface water interaction and its effect on wetland stream benthic productivity, Trout Lake Watershed, northern Wisconsin, USA: *Journal of Hydrology*, v. 320, p. 370–384.
- Tennessee Valley Authority, 1972, Heat and mass transfer between a water surface and the atmosphere: Water Resources Research Lab, Report 14, 166 p.
- Theurer, F.D., Voos, K.A., and Miller, W.J., 1984, Instream water temperature model: U.S. Fish and Wildlife Service Instream Flow Information Paper No. 16, FWS/OBS-84/15 [variously paginated].

Appendix 5. WEBB and LTER Data Collection (1991–2011)

Introduction.....	86
Surface-Water Discharge	86
Groundwater/Surface-Water Temperature.....	86
Lake Water-Surface Elevation.....	86
Groundwater-Level Elevation	86
References Cited.....	87

Tables

5-1. Description of streamflow-gaging stations in the Trout Lake Watershed	86
5-2. Description of sites with continuous-record groundwater levels in the Trout Lake Watershed	87

Introduction

As a result of two long-term data-collection efforts—the U.S. Geological Survey Water, Energy and Biogeochemical Budgets (WEBB) Program and the University of Wisconsin Center for Limnology Long Term Ecological Research (LTER) site—rich datasets were available for model calibration. These datasets are described below.

Surface-Water Discharge

As part of the WEBB project, long-term streamflow-gaging stations were operated at five locations beginning in October of 1991 (fig. 3–2, appendix 3). Data collected at these locations can be found in USGS annual Water Data Reports or online at <http://wi.water.usgs.gov/data/index.html>. In addition, occasional streamflow measurements were made at the Mann Creek site. Brief station descriptions are given in table 5–1.

Table 5–1. Description of streamflow-gaging stations in the Trout Lake Watershed.

[--, not available]

Station number	Station name	Latitude (decimal degrees)	Longitude (decimal degrees)	Drainage area (square kilometers)
05357206	Allequash Creek Middle Site	46.03272847	–89.607925	9.84
05357215	Allequash Creek at County Highway M	46.0238395	–89.6529266	21.8
05357225	Stevenson Creek at County Highway M	46.0613392	–89.6473716	20.6
05357230	North Creek at Trout Lake	46.0786111	–89.6672222	9.27
05357239	Mann Creek at Trout Lake	46.01138889	–89.67583333	--
05357245	Trout River at Trout Lake	46.03550595	–89.7057066	120

Groundwater/Surface-Water Temperature

Groundwater and surface-water temperature measurements were made by Hunt and others (2006) as part of the U.S. Geological Survey's WEBB project during April–November 2002. Shallow groundwater temperature was measured near the mouth of North, Stevenson, and Upper Allequash Creeks. Measurements were made approximately 15 centimeters below the streambed at a measurement interval ranging between 1 and 3 hours. Although deeper measurements of groundwater temperature were available, values from the shallow sensor were used because they more closely reflected the temperature of groundwater prior to its entering the stream. For most all times measured, the upward gradient was relatively strong, so it is unlikely that the temperature was affected by interactions with the hyporheic zone.

Surface-water temperature was measured near the stream thalweg at a depth sufficient to prevent exposure to the atmosphere. Similar to groundwater, discrete measurements were made at approximately 1-hour increments. Daily mean temperatures were computed from the instantaneous values. Although much of the data were unpublished, site location and methods used to collect groundwater and surface-water temperature are detailed in Hunt and others (2006).

Lake Water-Surface Elevation

Time-series data of the elevation of five lake surfaces (Allequash, Big Muskellunge, Crystal, Sparkling, and Trout) were collected as part of the North Temperate Lakes LTER project. Lake levels are collected biweekly during the open-water period. Data were retrieved from the LTER online data archive (<http://lter.limnology.wisc.edu/datacatalog/search>).

Groundwater-Level Elevation

Time-series data of groundwater-level elevations were collected at six locations at 3-hour measurement intervals. The water levels were collected with unvented Solinst Leveloggers¹, and were compensated for atmospheric pressure fluctuations by using a barometric pressure transducer. These data are available through the Trout Lake WEBB Web site (http://wi.water.usgs.gov/webb/data_query.html). Recorded water levels were compared to hand measurements made approximately monthly; the differences between the observed and recorded values were used to adjust the recorded time series. Brief station descriptions are given in table 5–2, and are shown in appendix figure 3–4.

¹ Any use of trade, firm, or product names is for descriptive purposes only and does not imply endorsement by the U.S. Government.

Table 5–2. Description of sites with continuous-record groundwater levels in the Trout Lake Watershed.

Station number	Station name	Type	Well depth (meters)	Latitude (decimal degrees)	Longitude (decimal degrees)
460214089362101	Well A1-10	Water table	22.82	46.0372222	–89.6058333
460158089362801	Well M-05.1	Water table	9.39	46.0327778	–89.6077778
460138089363703	Well T1-15	Water table	5.49	46.0272222	–89.6102778
460152089363703	Well T1-70	Water table	7.32	46.0311111	–89.6102778
460125089380203	Well T2-15	Water table	7.01	46.0236111	–89.6338889
460134089382303	Well T2-90	Water table	7.52	46.0261111	–89.6397222

In addition, the North Temperate Lakes LTER project collects periodic water-level measurements in a network of wells in the Trout Lake Watershed. Data collected at a monthly time step were retrieved for 13 wells (D3, K7, K10, K18, K22, K30, K49, K59, K61 and WD1–4; appendix fig. 3–4) from the LTER online data archive (<http://lter.limnology.wisc.edu/datacatalog/search>).

References Cited

Hunt, R.J.; Strand, Mac; and Walker, J.F., 2006, Measuring groundwater-surface water interaction and its effect on wetland stream benthic productivity, Trout Lake Watershed, northern Wisconsin, USA: *Journal of Hydrology*, v. 320, p. 370–384.

Appendix 6. Calibration Results

PRMS-Only Calibration Results	91
Sequentially Linked MODFLOW-PRMS Calibration Results	91
Fully Coupled GSFLOW Calibration Results	101
References Cited	118

Figures

6-1. Graphs showing solar radiation, potential evapotranspiration, and lake evaporation calibration results for step 1 and snowpack results for step 2	92
6-2. Graphs showing calibration results for annual streamflow at the tributaries to Trout Lake	93
6-3. Graphs showing calibration results for monthly mean streamflow at the tributaries to Trout Lake	94
6-4. Graphs showing calibration results for streamflow at the Trout River outlet of Trout Lake	95
6-5. Graphs showing pilot-point-derived optimal horizontal hydraulic conductivity values, sequentially linked calibration	96
6-6. Graphs showing pilot-point-derived optimal vertical hydraulic conductivity values, sequentially linked calibration	97
6-7. Graph showing observed heads compared to heads simulated by the optimal sequentially linked model	99
6-8. Graph showing average observed lake stages from the primary Long-Term Ecological Research study lakes compared to steady-state lake stages simulated by the optimal sequentially linked model	99
6-9. Graph showing average observed lake stages from other lakes compared to steady-state lake stages simulated by the optimal sequentially linked model	100
6-10. Graph showing average observed streamflow compared to simulated streamflow	100
6-11. Graph showing lake-plume interface depth located by using stable isotopes of water (observed) compared to steady-state simulated lake plume interface depth by the optimal sequentially linked model	101
6-12. Graphs showing calibration results for 05357206, Allequash Creek at the middle site	102
6-13. Graphs showing calibration results for 05357215, Allequash Creek at Trout Lake	103
6-14. Graphs showing calibration results for 05357225, Stevenson Creek at Trout Lake	104
6-15. Graphs showing calibration results for 05357230, North Creek at Trout Lake	105
6-16. Graphs showing calibration results for 05357245, Trout River at Trout Lake outlet	106
6-17. Graphs showing calibration results for Long-Term Ecological Research (LTER) wells D3, K18, K49, and K59	107
6-18. Graphs showing calibration results for LTER wells WD1 and WD4	108
6-19. Graphs showing calibration results for LTER wells K7, K10, K22, and K30	109
6-20. Graphs showing calibration results for LTER wells K61, WD2, and WD3	110
6-21. Graphs showing calibration results for Water, Energy, and Biogeochemical Budgets (WEBB) wells M-05, A1-10, T1-15, and T1-70	111
6-22. Graphs showing calibration results for WEBB wells T2-15 and T2-90	112

6-23.	Graphs showing mean water levels	113
6-24.	Graphs showing range in water levels	114
6-25.	Graphs showing calibration results for lake levels of the Long-Term Ecological Research focus lakes	115
6-26.	Graph showing calibration results for lake level of Trout Lake	116
6-27.	Graphs showing mean lake levels for the Long-Term Ecological Research lakes and the remaining lakes in the model domain.....	116
6-28.	Graph showing calibration results for average groundwater inflow to selected lakes	117
6-29.	Graph showing ranges in lake levels for the Long-Term Ecological Research lakes.....	117

Tables

6-1.	Hydraulic conductivity and anisotropy after sequentially linked calibration	95
6-2.	Sequentially linked calibration statistics.....	98
6-3.	Aquifer hydraulic conductivity statistics after fully coupled model calibration	117

PRMS-Only Calibration Results

The results for step 1 of the calibration—solar radiation, potential evapotranspiration (ET), and lake evaporation—are given in figure 6–1. Where appropriate, the Nash-Sutcliffe coefficient of efficiency was included to provide a quantified estimate of the goodness of fit. The Nash-Sutcliffe coefficient is defined as follows:

$$NS = 1 - \frac{\sum(Q_o - Q_s)^2}{\sum(Q_o - \overline{Q_o})^2}$$

where

- NS is the Nash-Sutcliffe coefficient of efficiency,
- Q_o is observed streamflow,
- $\overline{Q_o}$ is the mean of the observed streamflow, and
- Q_s is simulated streamflow.

The coefficient ranges from $-\infty$ to 1; values close to 1 indicate a good fit. For a value of 0, the mean of the data is as good a predictor than the simulated values. For a value less than 0, the mean would provide a better estimate than the simulated values. The fits for solar radiation (fig. 6–1A) and potential ET (fig. 6–1B) are very close, and with the exception of the ice-cover period each year, the model is accurately reproducing the evaporation from Sparkling Lake (fig. 6–1C). The over-estimation during the winter period is not surprising because the model does not simulate a winter ice cover or account for sublimation from the snow on the ice. The results for step 2 of the calibration, snowpack, are given in figure 6–1D. The model does a reasonable job of reproducing the onset of the snowpack in the fall, the end of the snowpack in spring, and the general pattern of accumulation and ablation, but the individual target values do not match quite as well as with the previous targets. This is likely due to localized variations in snowpack depth. We selected a single HRU (number 58) to represent the data collected at the Minocqua Dam climatological station, and in addition to the distance from the station and the Trout Lake Watershed, the local conditions are likely different between HRU 58 and the Minocqua Dam station. However, on the basis of the results shown in figure 6–1D, the model is representing the overall variation in the snowpack in a reasonable fashion.

The results for step 3 of the calibration—surface-water runoff and soil infiltration—are shown in figures 6–2 through 6–4. Because the PRMS model was built specifically for a coupled GSFLOW model, we adjusted the parameters until we felt that the results represented a reasonable starting point

for the GSFLOW calibration. This was done partly because most of the parameters would have to be revisited during the GSFLOW model calibration and partly because the PRMS model uses a different set of processes than GSFLOW to represent groundwater flow. The results for annual streamflow at the tributary streams to Trout Lake (fig. 6–2) show a reasonable representation of the annual water budget across the four streams. The monthly streamflow plots for the tributary streams (fig. 6–3) reproduce the general seasonal patterns at the sites but are less robust in their ability to track the month-to-month variations in flow. This is not surprising, because most of the flow in the watershed is dominated by groundwater. The results for Trout River at Trout Lake (fig. 6–4), which is the outlet of the watershed, indicate that the overall annual budget of the watershed is being reproduced and that much of the seasonal variation of flow out of the lake is being reproduced with reasonable accuracy.

Sequentially Linked MODFLOW-PRMS Calibration Results

After the soft-knowledge and simulated best-fit trade-off was selected, the resulting parameter sets are reasonable given other work in the watershed (table 6–1). The optimal distribution for horizontal hydraulic conductivity (K_h) determined with the pilot points for the uppermost sand and gravel (layers 1 and 2) showed a mostly homogeneous unit (average $K_h = 9.5$ meters per day (m/d), standard deviation = 3.4 m/d). The middle unit (layers 3 and 4, Wildcat sandy till of Attig, 1985) was more homogeneous (average $K_h = 3.1$ m/d, standard deviation = 0.4 m/d). The bottommost sand and gravel sediments (layers 4 and 5) had the highest hydraulic conductivities in the watershed and the highest heterogeneity (average K_h greater than 30 m/d, standard deviation 12 m/d). The relatively higher values of the lowermost layers likely reflect coarse sediments deposited when the glacial ice front was close to the site area (Attig, 1985). Within layers, the high groundwater-discharge site of Hunt and others (2006) near the Allequash Creek Middle Site had the highest local conductivity, with (again) higher hydraulic conductivity in the lowermost unit. Vertical hydraulic conductivity was estimated as an anisotropy ratio (table 6–1) and was close to the preferred condition 3:1 $K_h:K_v$ ratio reported by Kenoyer (1988). Graphical depictions of the distributions of horizontal and vertical hydraulic conductivity are provided by layer in figures 6–5 and 6–6.

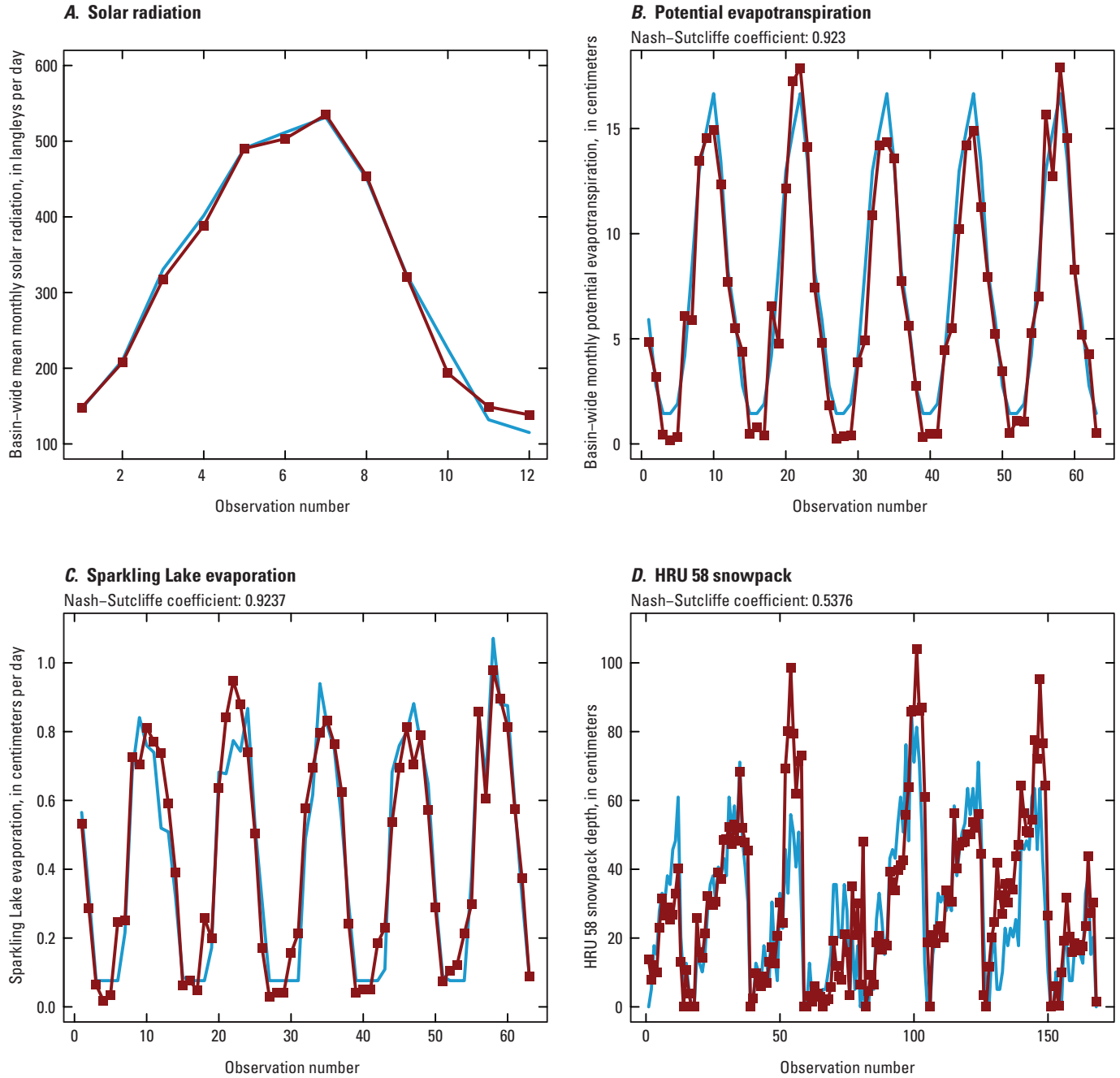


Figure 6-1. Solar radiation, potential evapotranspiration, and lake evaporation calibration results for step 1 (A–C) and snowpack results for step 2 (D). Blue lines and symbols are observed data; red lines and symbols are the PRMS-only model-simulated equivalent quantity. For figure readability and to facilitate comparison across figures, the x-axis shows the observation number as a temporally sequential order of the observation. The x-axis spans the 2001–7 calibration period and does not display gaps in the observed time series.

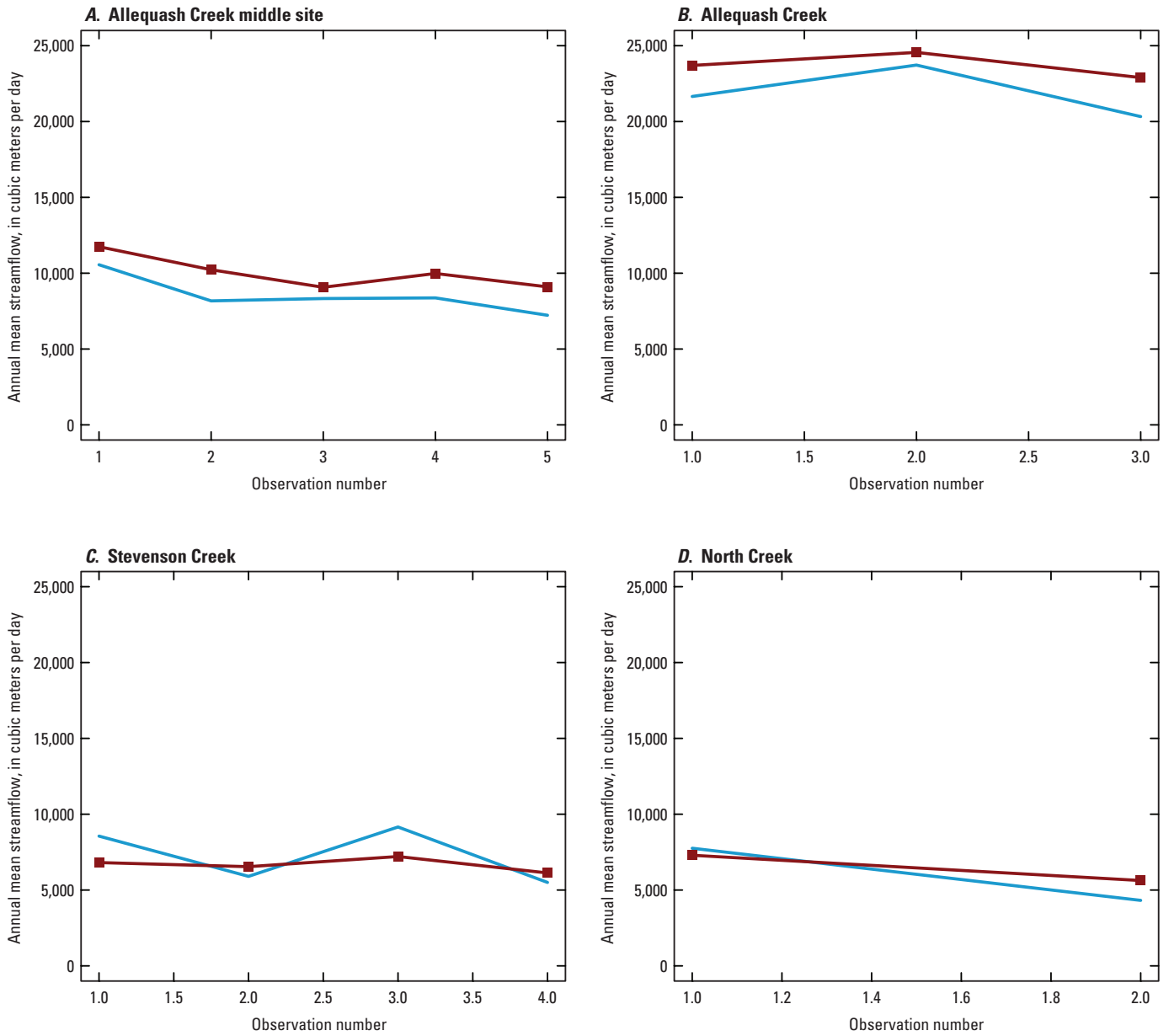


Figure 6–2. Calibration results for annual streamflow at the tributaries to Trout Lake. Blue lines and symbols are observed data; red lines and symbols are the PRMS-only model-simulated equivalent quantity. For figure readability and to facilitate comparison across figures, the x-axis shows the observation number as a temporally sequential order of the observation. The x-axis spans the 2001–7 calibration period and does not display gaps in the observed time series.

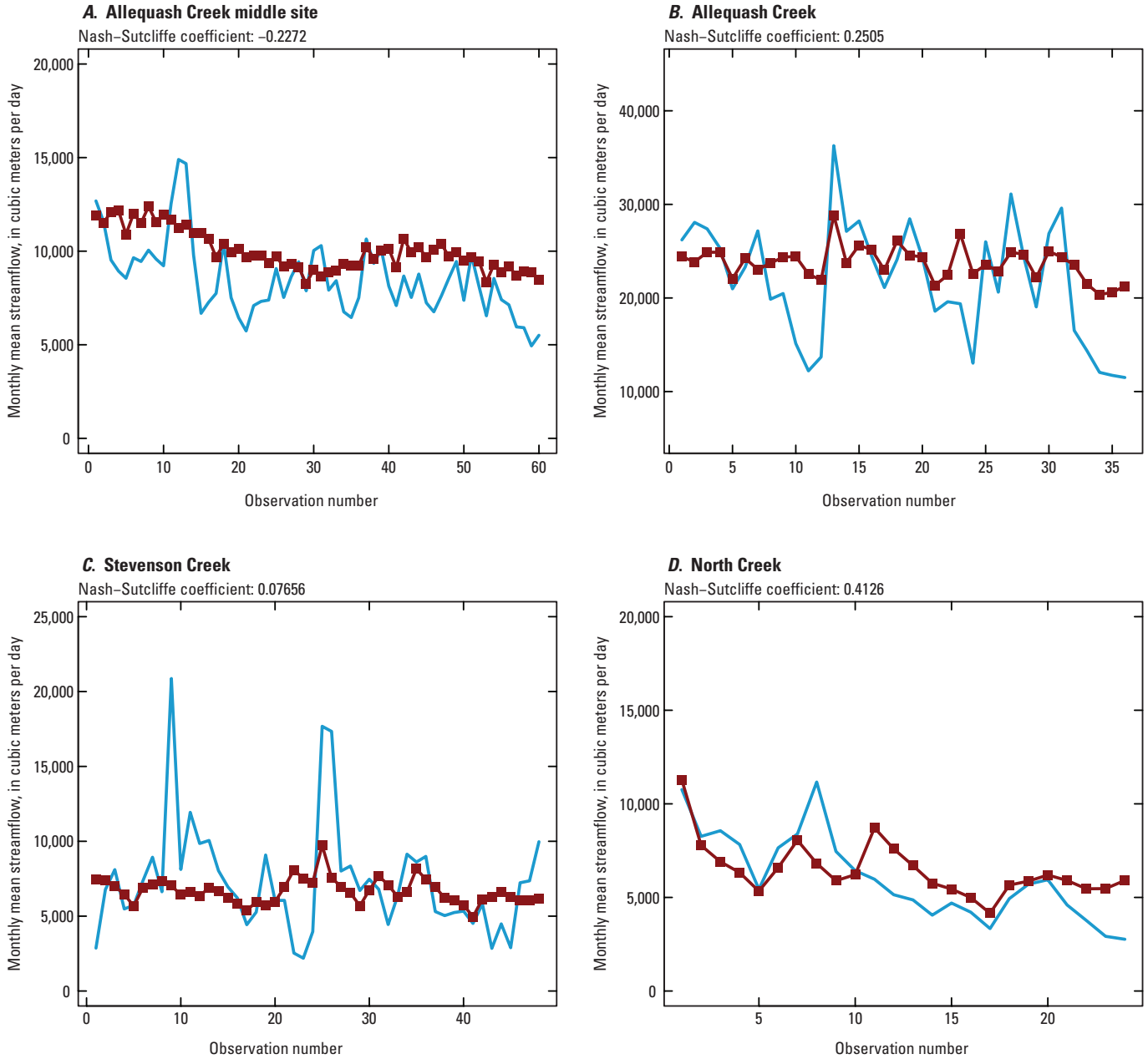


Figure 6-3. Calibration results for monthly mean streamflow at the tributaries to Trout Lake. Blue lines and symbols are observed data; red lines and symbols are the PRMS-only model-simulated equivalent quantity. For figure readability and to facilitate comparison across figures, the x-axis shows the observation number as a temporally sequential order of the observation. The x-axis spans the 2001–7 calibration period and does not display gaps in the observed time series.

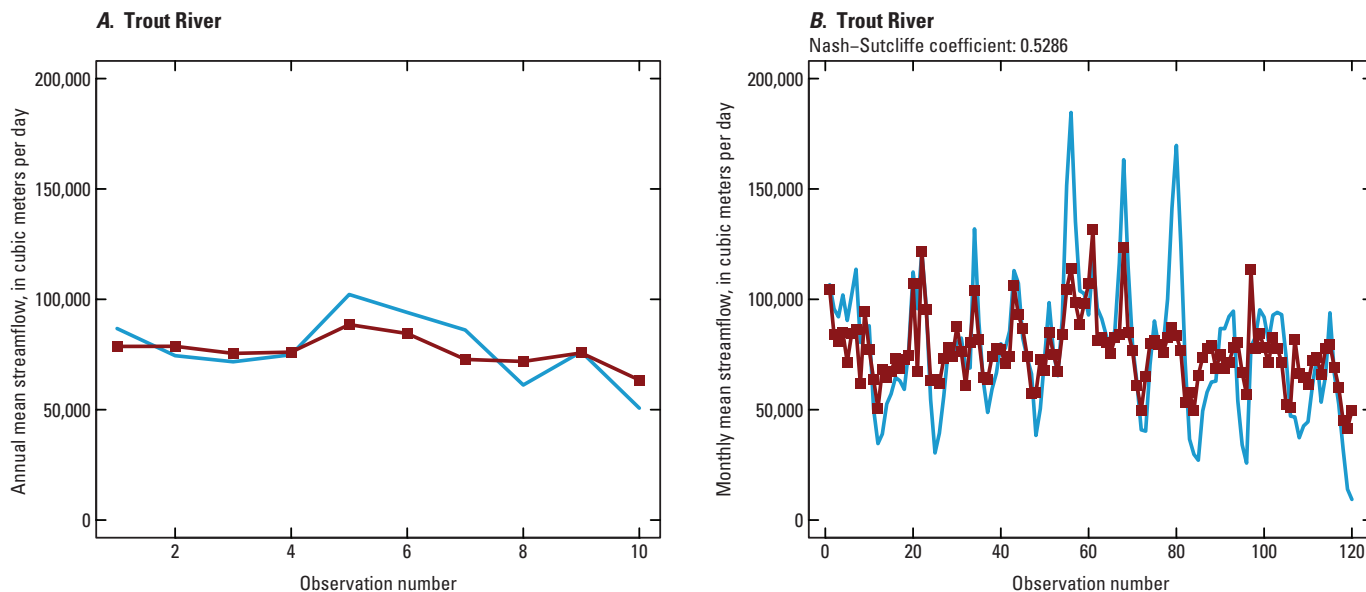


Figure 6-4. Calibration results for streamflow at the Trout River outlet of Trout Lake. *A*, Annual. *B*, Monthly mean. Blue lines and symbols are observed data; red lines and symbols are the PRMS-only model-simulated equivalent quantity. For figure readability and to facilitate comparison across figures, the x-axis shows the observation number as a temporally sequential order of the observation. The x-axis spans the 2001–7 calibration period and does not display gaps in the observed time series.

Table 6-1. Hydraulic conductivity and anisotropy after sequentially linked calibration.

[Min, minimum; max, maximum; std, standard; m/d, meters per day; K_h , horizontal hydraulic conductivity; K_v , vertical hydraulic conductivity]

	Current sequentially linked calibration (2013)				Previous MODFLOW modeling hydrostratigraphic equivalent Muffels (2008) 6-layer/pilot point values				
	Min (m/d)	Max (m/d)	Average (m/d)	Std deviation (m/d)	Min (m/d)	Max (m/d)	Average (m/d)	Std deviation (m/d)	Pint (2002) 4-layer/5-zone values (m/d)
Layer 1+2									
K_h	1.1	93.2	9.5	3.4	6.8	21.0	8.9	1.6	9.7–37
K_v	0.3	40.0	3.0	1.3	1.8	6.7	2.6	0.3	2.4–9.3
K_h/K_v			3.2				3.4		*4.0
Layer 3+4									
K_h	1.9	6.9	3.1	0.4	2.6	3.7	3.0	0.2	3.4
K_v	0.4	4.5	0.9	0.2	0.7	1.2	0.9	0.05	0.9
K_h/K_v			3.3				3.3		*4.0
Layer 5+6									
K_h	2.9	175.9	33.5	11.9	15.2	68.7	31.4	6.4	38.2
K_v	1.0	56.2	10.5	3.8	19.9	4.8	9.4	1.3	9.6
K_h/K_v			3.2				3.3		*4.0

*Assumed, not variable.

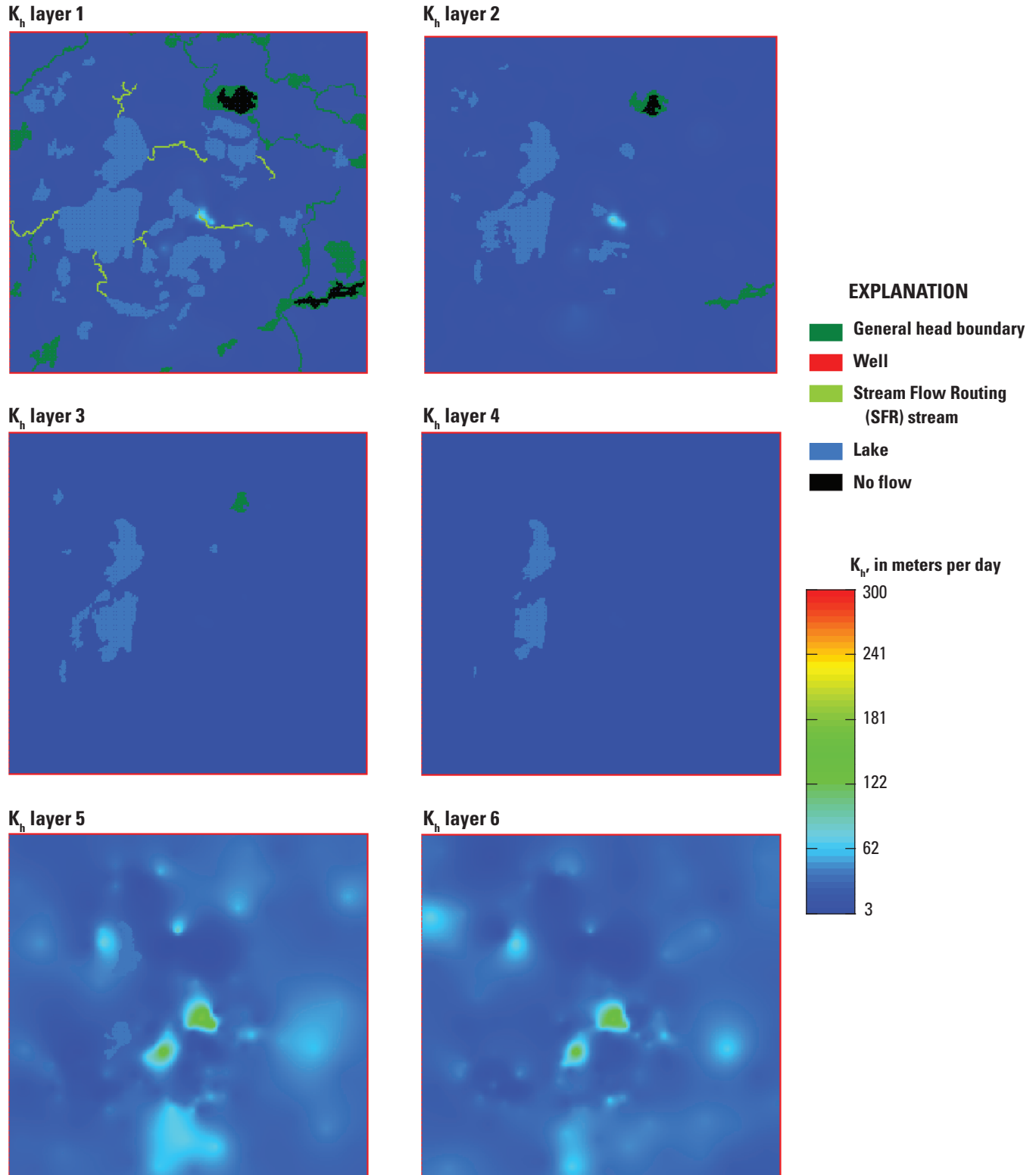


Figure 6–5. Pilot-point-derived optimal horizontal hydraulic conductivity (K_h) values, sequentially linked calibration.

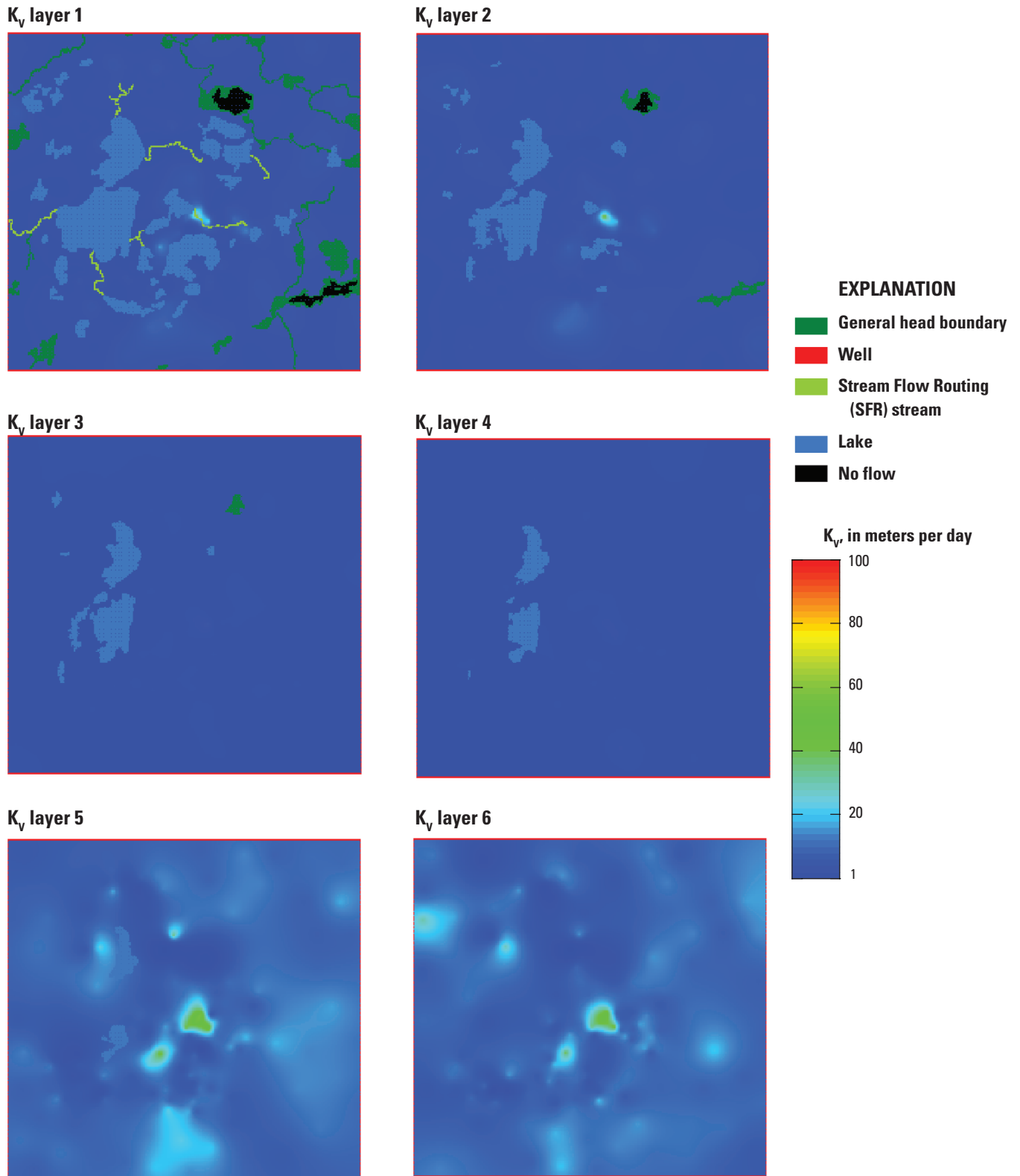


Figure 6–6. Pilot-point-derived optimal vertical hydraulic conductivity (K_v) values, sequentially linked calibration.

The sequentially linked model was able to adequately simulate the six different observation types; final calibration statistics are listed in table 6–2. Simulated heads tracked observed heads over the range of head values (fig. 6–7). Average stages of high important study lakes were well simulated (fig. 6–8), and other lake stages were reasonably simulated over a range of observed values (fig. 6–9). Average base flows for the tributary streams were simulated within measurement error (fig. 6–10). Less commonly used targets such as the depth of lake water plumes in the aquifer and traveltime were also well simulated (fig. 6–11 and table 6–2, respectively). Overall, the model fit to observed data is better than for previous modeling efforts in the watershed for a larger range of observation types, despite the higher number of targets and additional types of calibration constraints used. This improvement is attributed to the application of the highly parameterized approach as described by Doherty and Hunt (2010). Such highly parameterized approaches give increased flexibility through increased number of parameters, and this flexibility can result in tractable parameter estimation and reasonable optimal parameters through use of regularized inversion (Hunt and others, 2007; Doherty and Hunt, 2010).

Table 6–2. Sequentially linked calibration statistics. Error residual statistics or differences are calculated as observed minus simulated value.

[m, meters; LTER, Long-Term Ecological Research; m³, cubic meters; m NGVD 29, meters above National Geodetic Vertical Datum of 1929]

Head calibration (m) (70 targets)				
Mean error			–0.13	
Mean absolute error			0.29	
Root mean squared error			0.44	
Maximum residual			0.96	
Minimum residual			–1.63	
LTER lake stages (m) (5 lakes)				
Mean error			–0.04	
Mean absolute error			0.07	
Root mean squared error			0.08	
Maximum residual			0.06	
Minimum residual			–0.14	
Non-LTER lake stages (m) (23 lakes)				
Mean error			0.25	
Mean absolute error			1.17	
Root mean squared error			1.46	
Maximum residual			4.04	
Minimum residual			–2.05	
Stream flux (m³ d-1)		Observed	Simulated	Percent difference
Mann Creek		5,160	5,197	–1
North Creek		7,110	7,558	–6
Stevenson Creek		7,010	7,194	–3
Allequash Creek		8,610	8,755	–2
Allequash Creek at Trout Lake		23,600	23,323	1
Trout River		81,000	80,994	0.01
Flow path data		Observed	Simulated	Percent difference
Lake plume depth T1-70 (m NGVD 29)		486.50	487.71	–0.2
Lake plume depth T2-90 (m NGVD 29)		473.40	473.43	–0.01
Lake plume depth T5-10 (m NGVD 29)		485.00	486.19	–0.2
Travel time (years)		8.0	8.23	–3

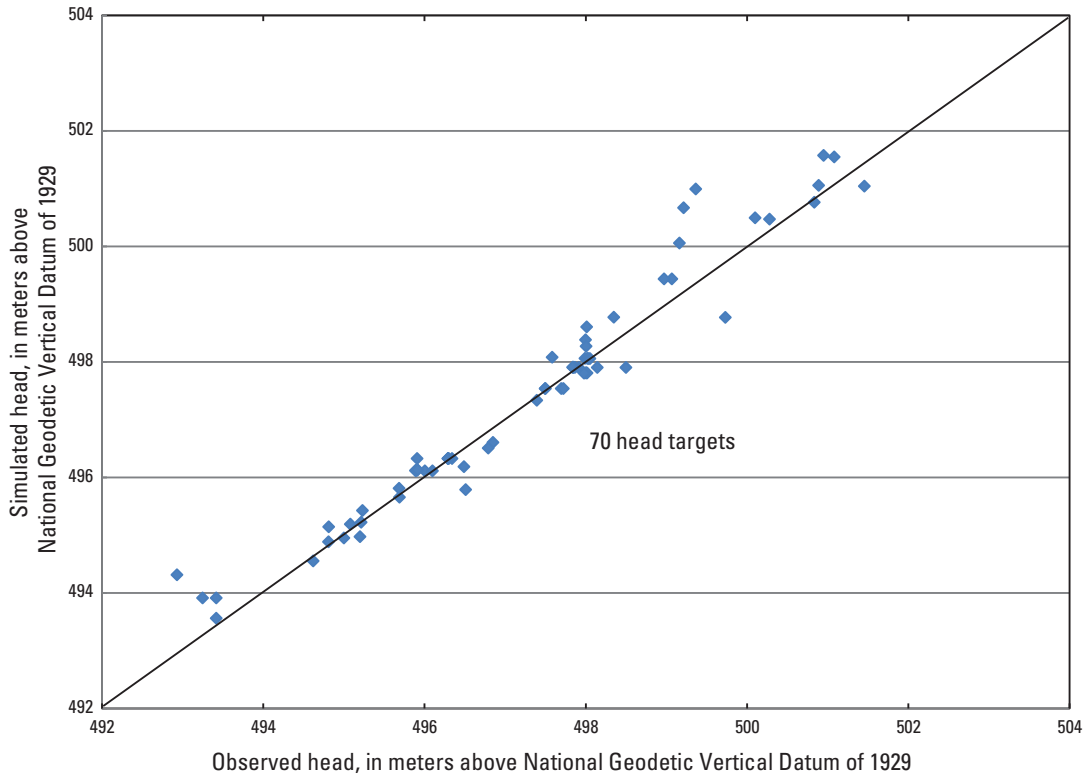


Figure 6-7. Observed heads compared to heads simulated by the optimal sequentially linked model.

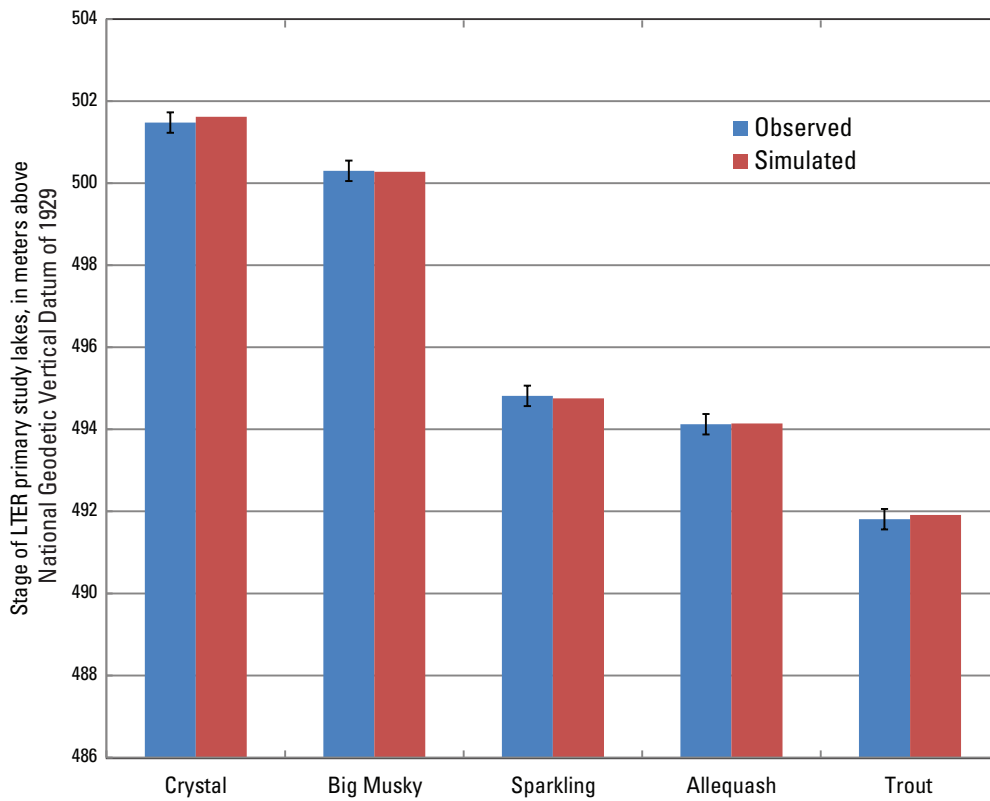


Figure 6-8. Average observed lake stages from the primary Long-Term Ecological Research (LTER) study lakes compared to steady-state lake stages simulated by the optimal sequentially linked model.

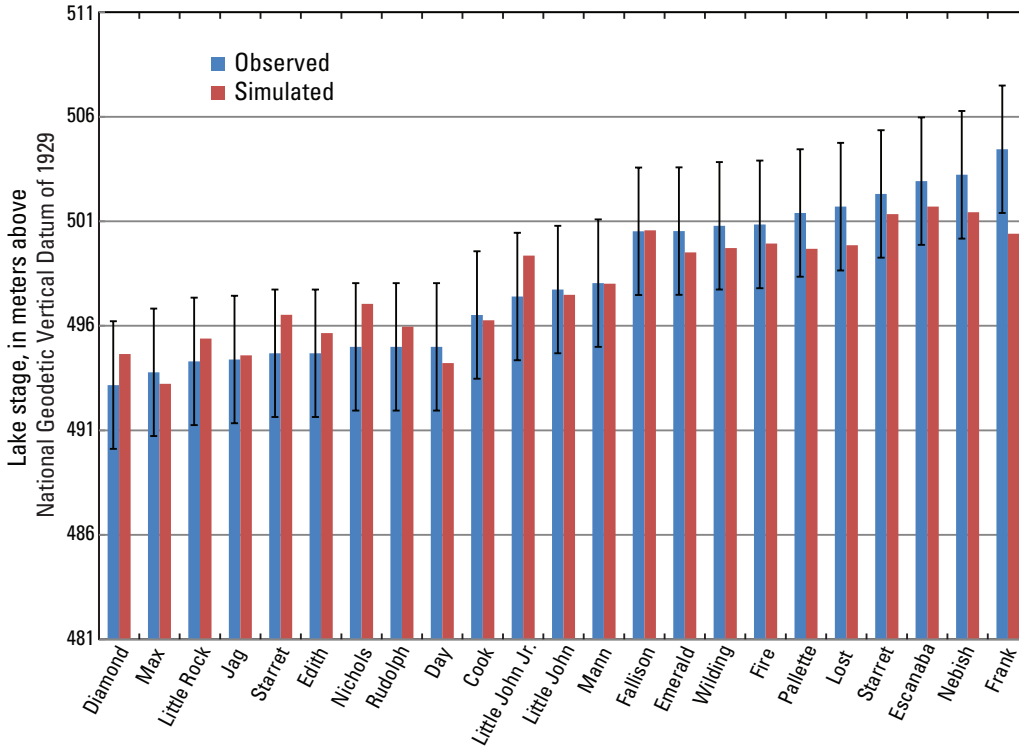


Figure 6-9. Average observed lake stages from other lakes compared to steady-state lake stages simulated by the optimal sequentially linked model.

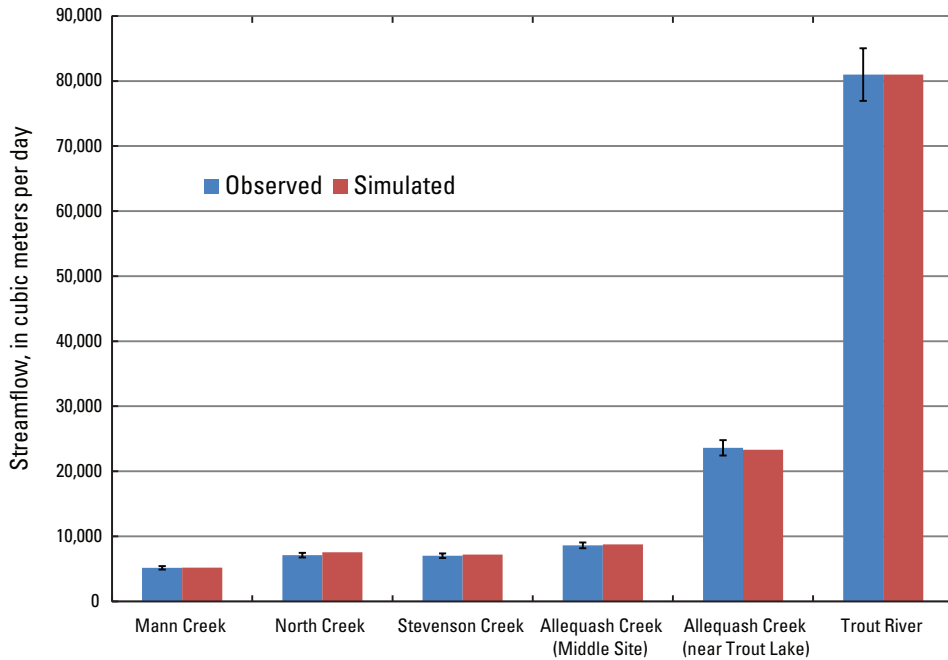


Figure 6-10. Average observed streamflow compared to simulated streamflow.

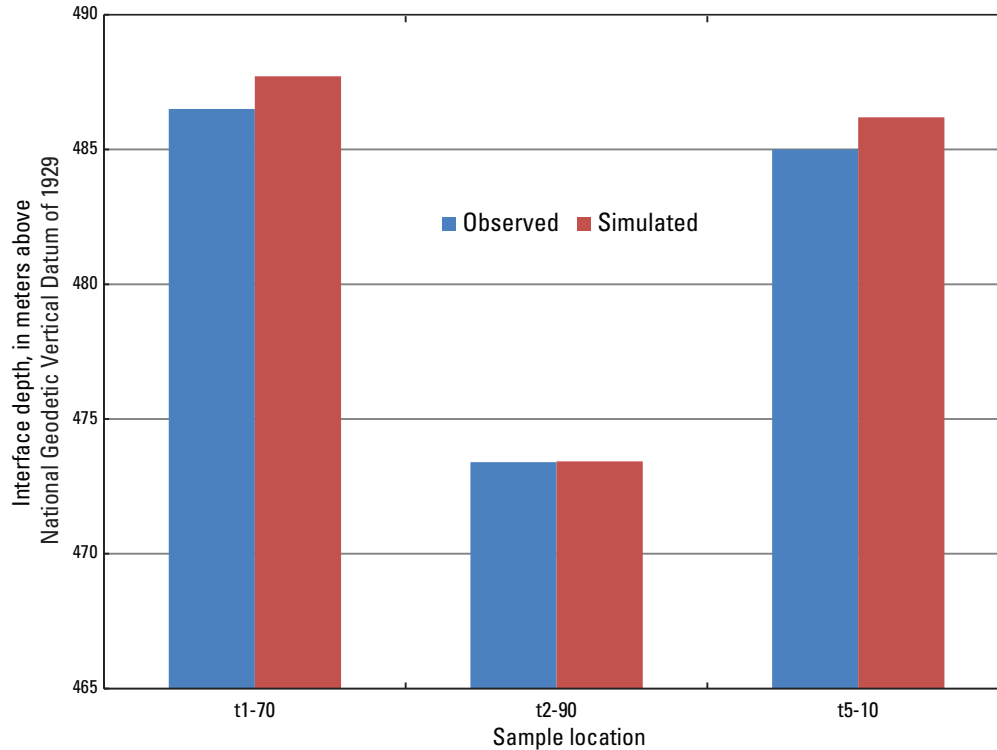


Figure 6–11. Lake-plume interface depth located by using stable isotopes of water (observed) compared to steady-state simulated lake plume interface depth by the optimal sequentially linked model.

Fully Coupled GSFLOW Calibration Results

Potential and actual evaporation, timing and magnitude of snowpack accumulation and snowmelt, and high-resolution evaporation measurements from Sparkling Lake were simulated by using the uncoupled PRMS model calibration (fig. 6–1) and were not affected by subsequent calibration; therefore, these drivers remain adequately simulated in the GSFLOW model after calibration. Observed head, lake stage, and flow characteristics for the Trout Lake Watershed are generally well represented (figs. 6–12 through 6–29). The WEBB study site in the Allequash basin is well simulated from the upper reaches (Allequash Middle Site above Allequash Lake) to below the lake (figs. 6–12 and 6–13, respectively). The other tributary streams in the system are well simulated (figs. 6–14 and 6–15). The outlet of the watershed at the Trout River gage is also well simulated (fig. 6–16), which reflects the importance given to this measurement in the calibration. Simulated groundwater levels generally were similar to timing and magnitudes of observed groundwater levels (figs. 6–17 through 6–22) and reasonably represented mean groundwater level (fig. 6–23). The range of variation in groundwater levels (fig. 6–24) was systematically slightly lower than that in the

observed data, probably a result of spatial averaging over the nodal scale and temporal daily averaging of climate and soil-zone processes. This type of spatial averaging should have less of an effect on observations that integrate many nodes (such as streamflow and lake stage) than on observations involving responses at the node or subnode scale (such as groundwater levels at an individual well). Finally, the slightly lower simulated groundwater levels also result from using a homogeneous unsaturated zone for the model, which precludes preferential-pathway inputs that could increase water levels in the saturated zone. After the initial 10-year spin-up of the coupled model, LTER lake-stage timeseries and mean stage are also well simulated (figs. 6–25, 6–26, and 6–27, panel *A*). Simulated groundwater inflow to the lakes is less well simulated (fig. 6–28), likely, in part, because observation and simulation time periods differed (observed inflows calculated for years prior to 1992; model calibrated to 2000–7 conditions). Similar to the range of variation in groundwater levels, the range of simulated lake stage variation is less than that observed (fig. 6–29), likely reflecting the daily timestep’s imperfect representation of actual storm events; that is, representation of all climate data as daily averages cannot mimic the short-term dynamics of actual climatic events. Long-term average lake stages of non-LTER lakes also were well simulated (fig. 6–27*B* and *C*).

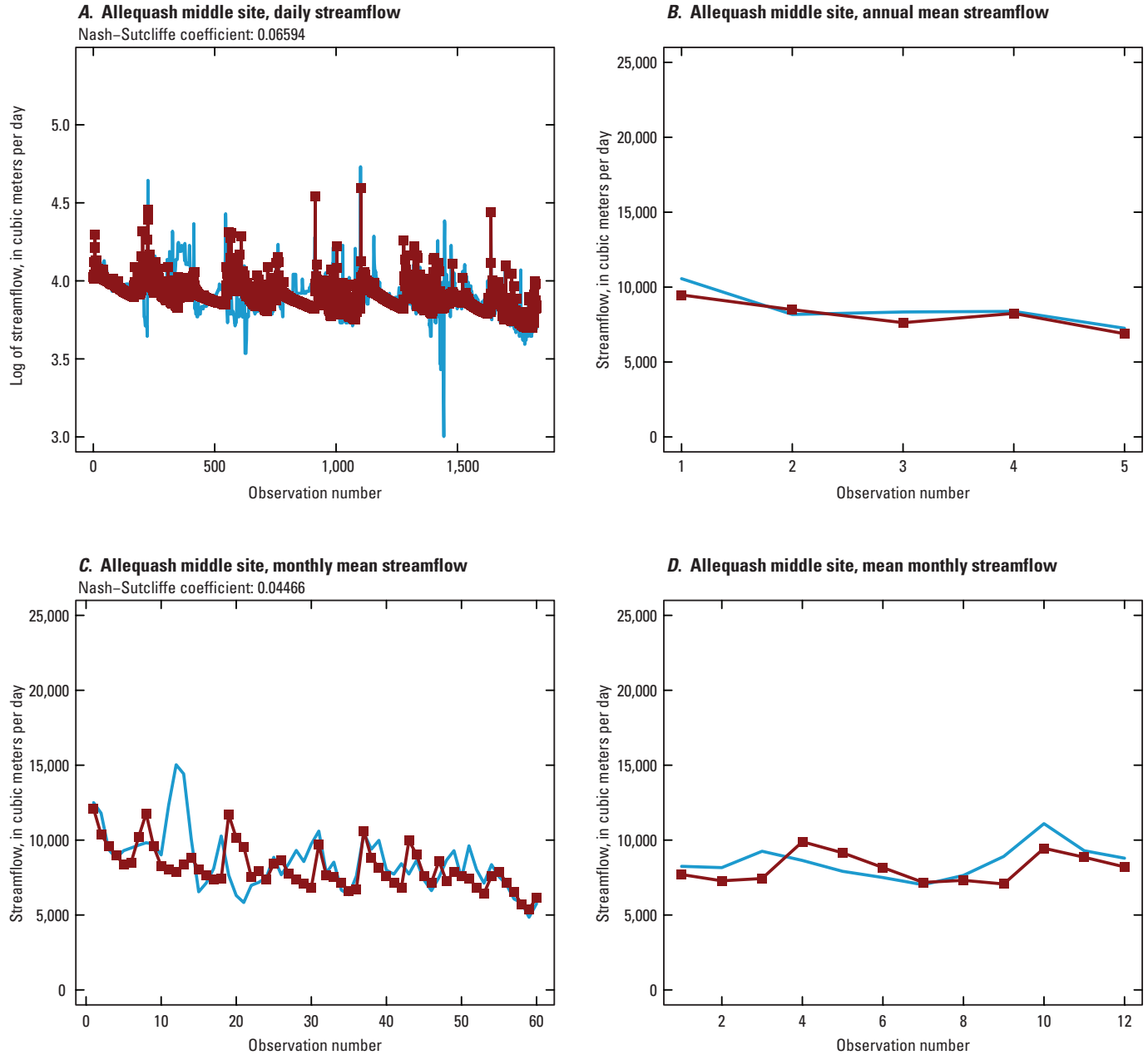


Figure 6–12. Calibration results for 05357206, Allequash Creek at the middle site. *A*, Natural log of daily streamflow. *B*, Annual mean streamflow. *C*, Monthly mean streamflow. *D*, Mean monthly streamflow. Blue lines represent observed data; red lines and symbols are the fully coupled model-simulated equivalent quantity.

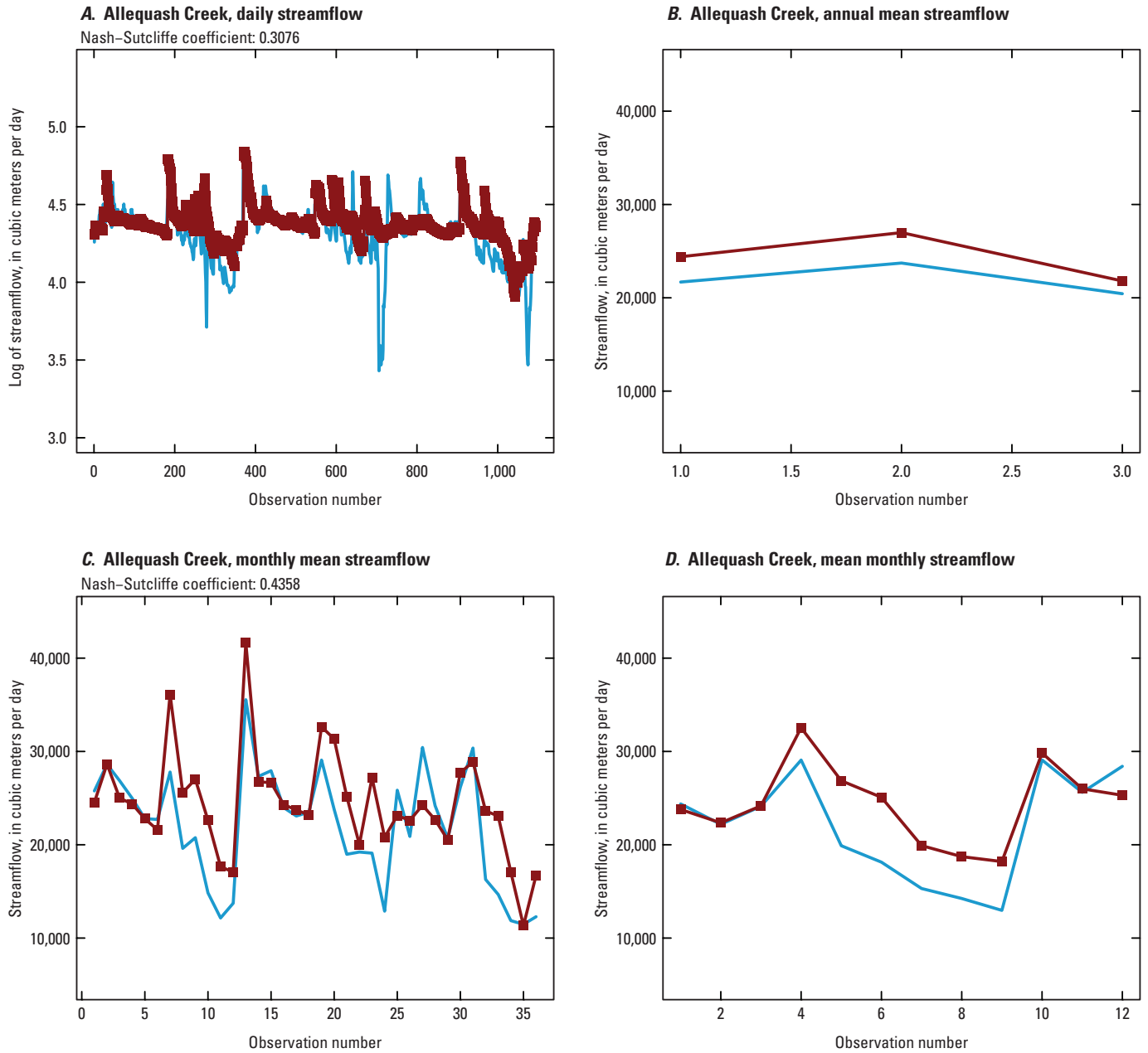


Figure 6–13. Calibration results for 05357215, Allequash Creek at Trout Lake. *A*, Natural log of daily streamflow. *B*, Annual mean streamflow. *C*, Monthly mean streamflow. *D*, Mean monthly streamflow. Blue lines represent observed data; red lines and symbols are the fully coupled model-simulated equivalent quantity.

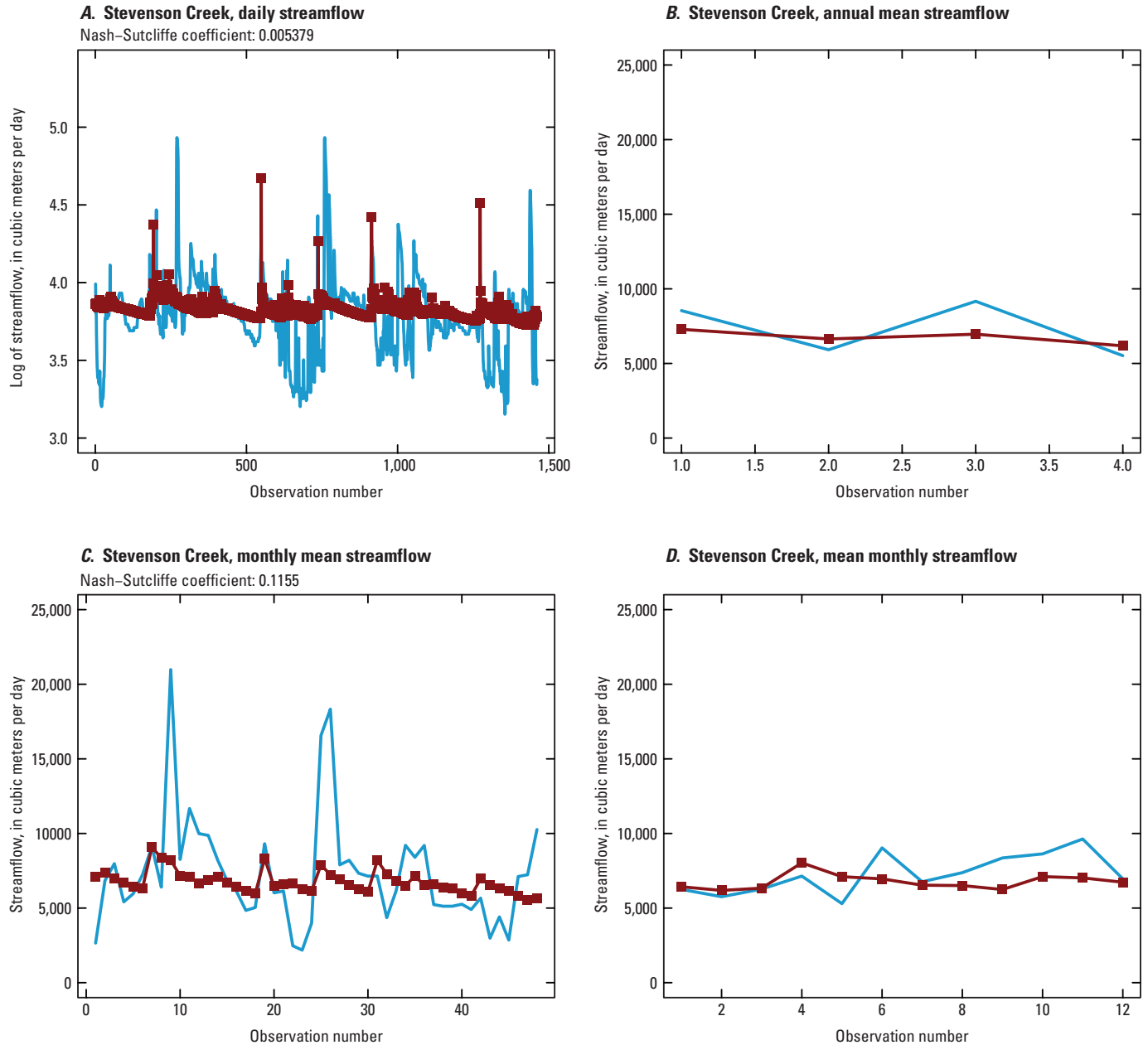


Figure 6-14. Calibration results for 05357225, Stevenson Creek at Trout Lake. *A*, Natural log of daily streamflow. *B*, Annual mean streamflow, *C*, Monthly mean streamflow. *D*, Mean monthly streamflow. Blue lines represent observed data; red lines and symbols are the fully coupled model-simulated equivalent quantity.

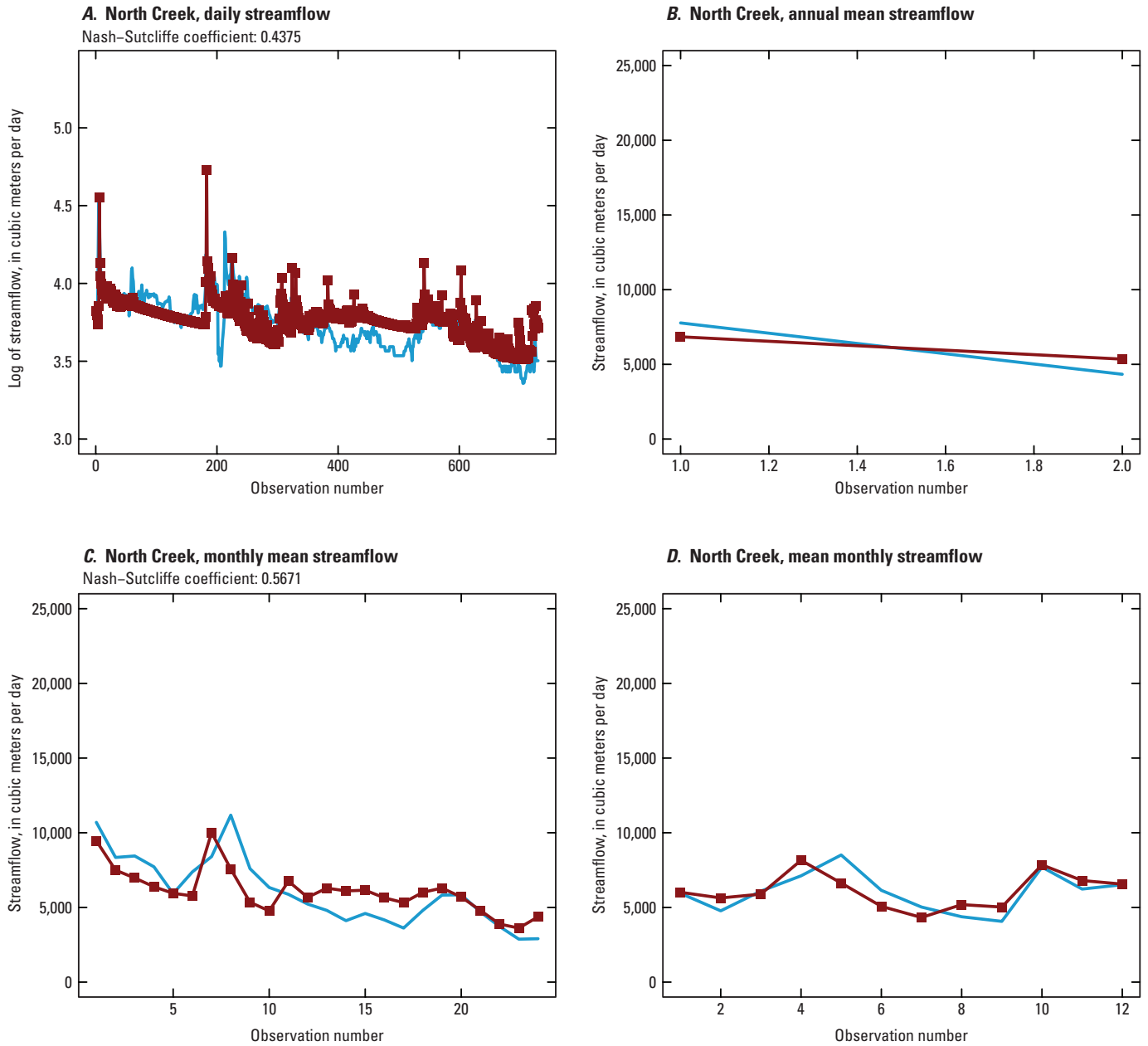


Figure 6–15. Calibration results for 05357230, North Creek at Trout Lake. *A*, Natural log of daily streamflow. *B*, Annual mean streamflow, *C*, Monthly mean streamflow. *D*, Mean monthly streamflow. Blue lines represent observed data; red lines and symbols are the fully coupled model-simulated equivalent quantity.

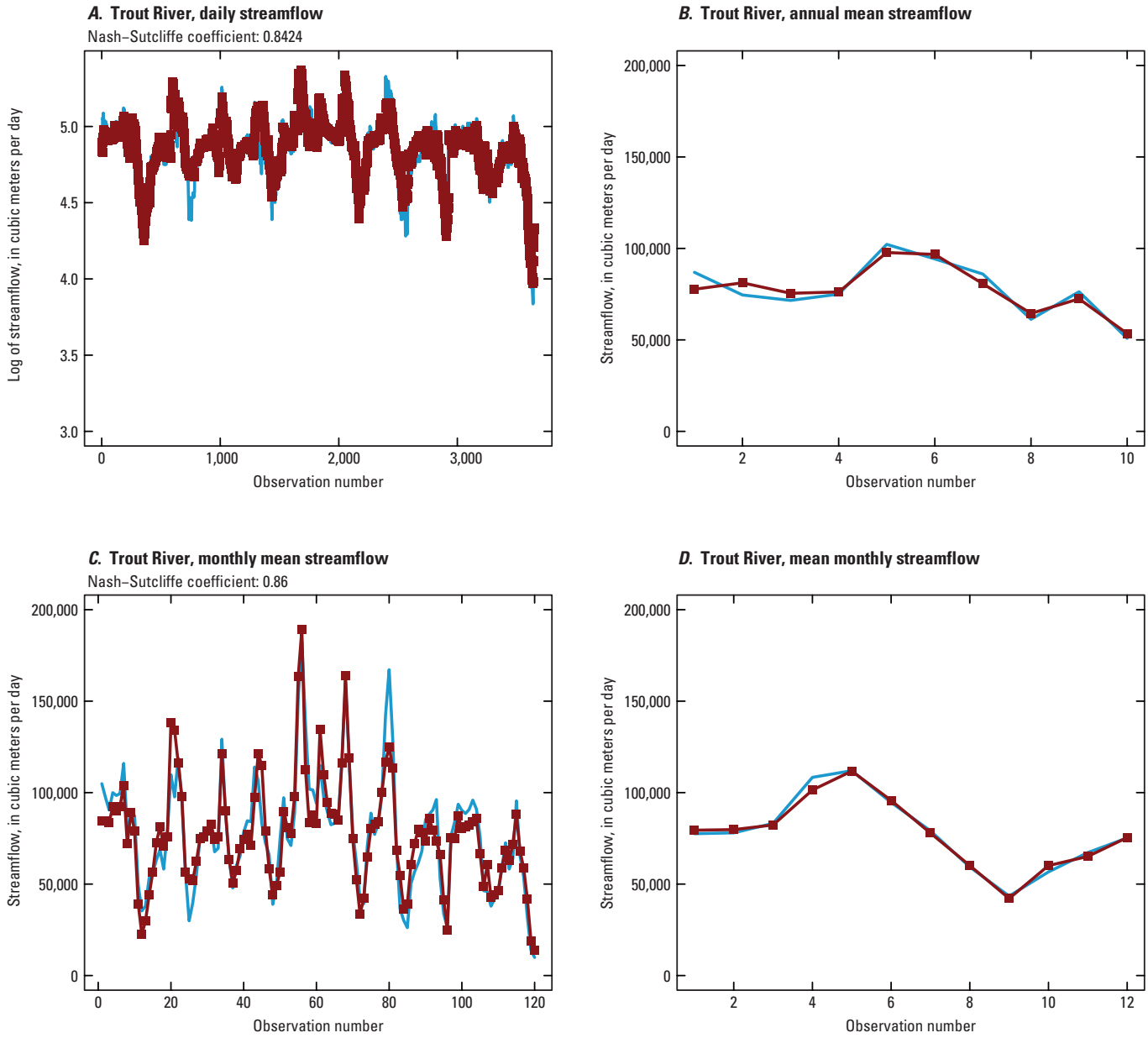


Figure 6-16. Calibration results for 05357245, Trout River at Trout Lake outlet. *A*, Natural log of daily streamflow. *B*, Annual mean streamflow, *C*, Monthly mean streamflow. *D*, Mean monthly streamflow. Blue lines represent observed data; red lines and symbols are the fully coupled model-simulated equivalent quantity.

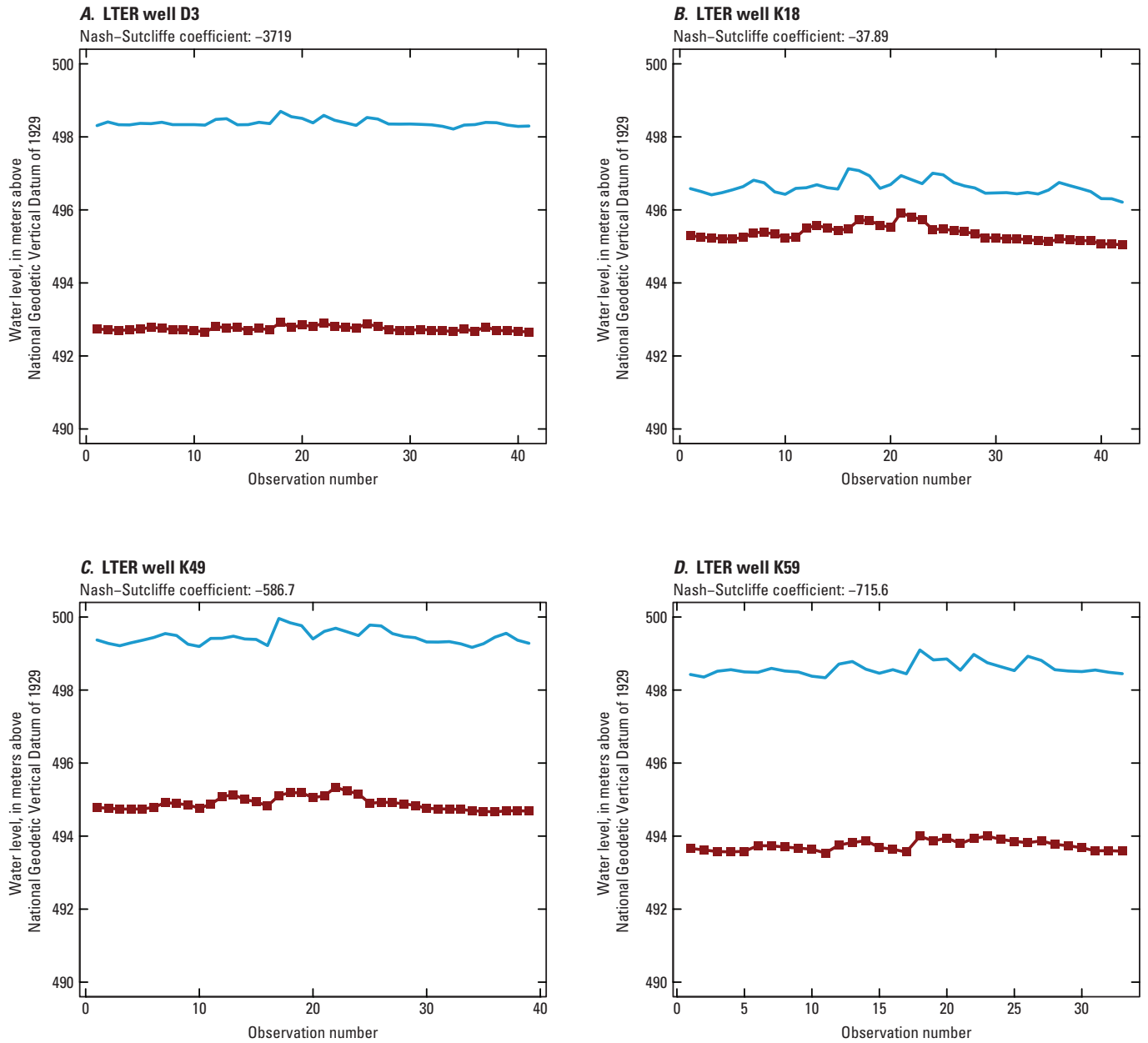


Figure 6–17. Calibration results for Long-Term Ecological Research (LTER) wells. *A*, D3. *B*, K18. *C*, K49. *D*, K59. Blue lines represent observed data; red lines and symbols are the fully coupled model-simulated equivalent quantity.

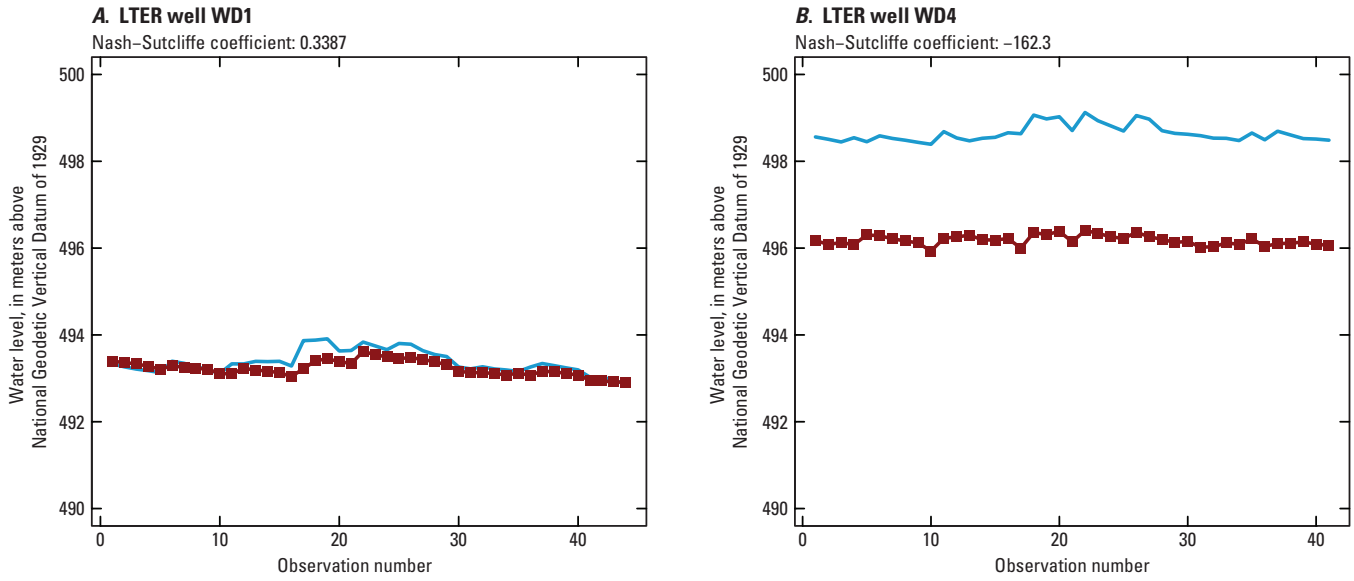


Figure 6-18. Calibration results for Long-Term Ecological Research (LTER) wells. *A*, WD1. *B*, WD4. Blue lines represent observed data; red lines and symbols are the fully coupled model-simulated equivalent quantity.

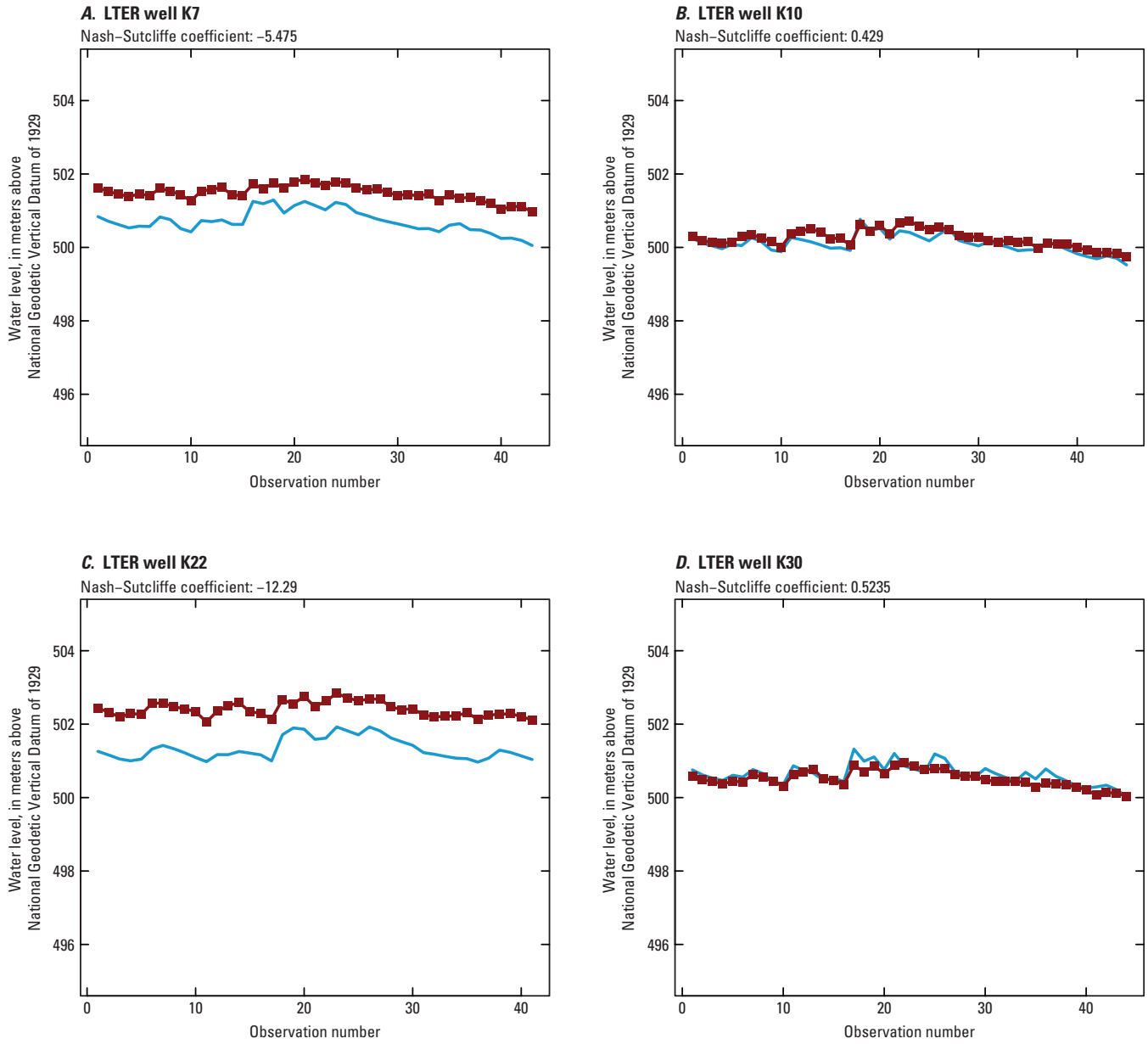


Figure 6–19. Calibration results for Long-Term Ecological Research (LTER) wells. *A*, K7. *B*, K10. *C*, K22. *D*, K30. Blue lines and symbols are observed data; red lines and symbols are the fully coupled model-simulated equivalent quantity.

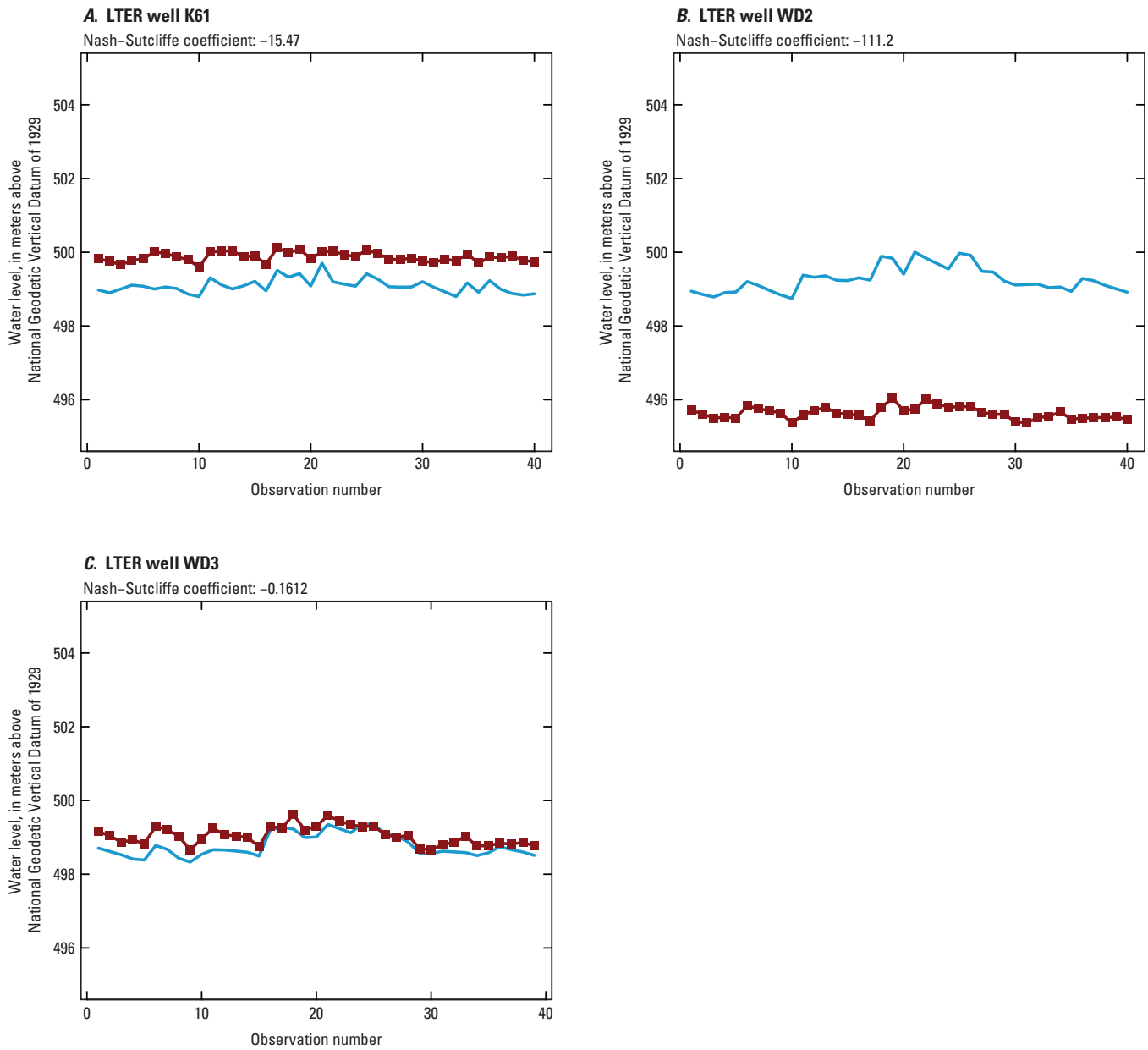


Figure 6–20. Calibration results for Long-Term Ecological Research (LTER) wells. *A*, K61. *B*, WD2. *C*, WD3. Blue lines and symbols are observed data; red lines and symbols are the fully coupled model-simulated equivalent quantity.

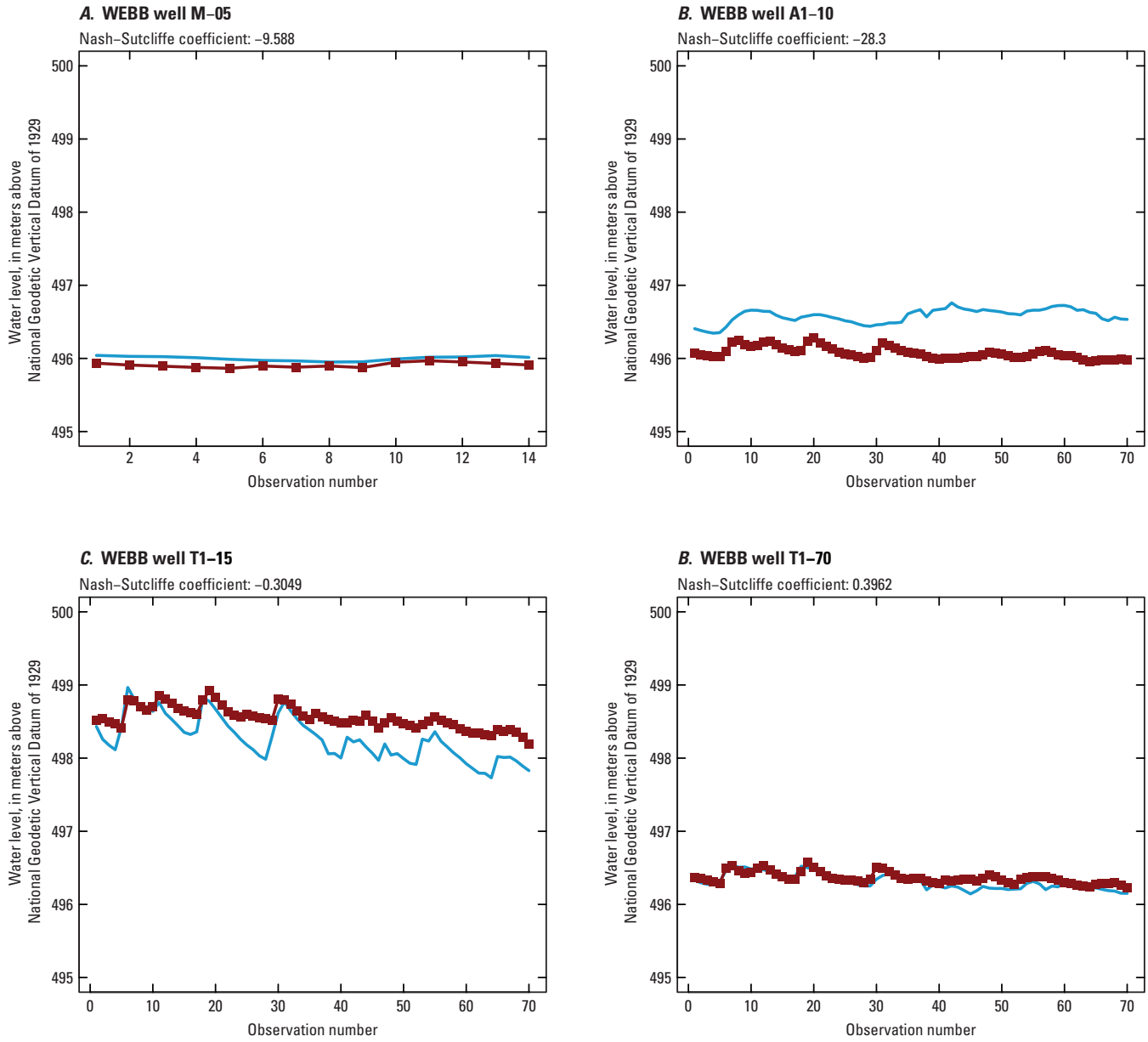


Figure 6–21. Calibration results for Water, Energy, and Biogeochemical Budgets (WEBB) wells. *A*, M-05. *B*, A1-10. *C*, T1-15. *D*, T1-70. Blue lines represent observed data; red lines and symbols are the fully coupled model-simulated equivalent quantity.

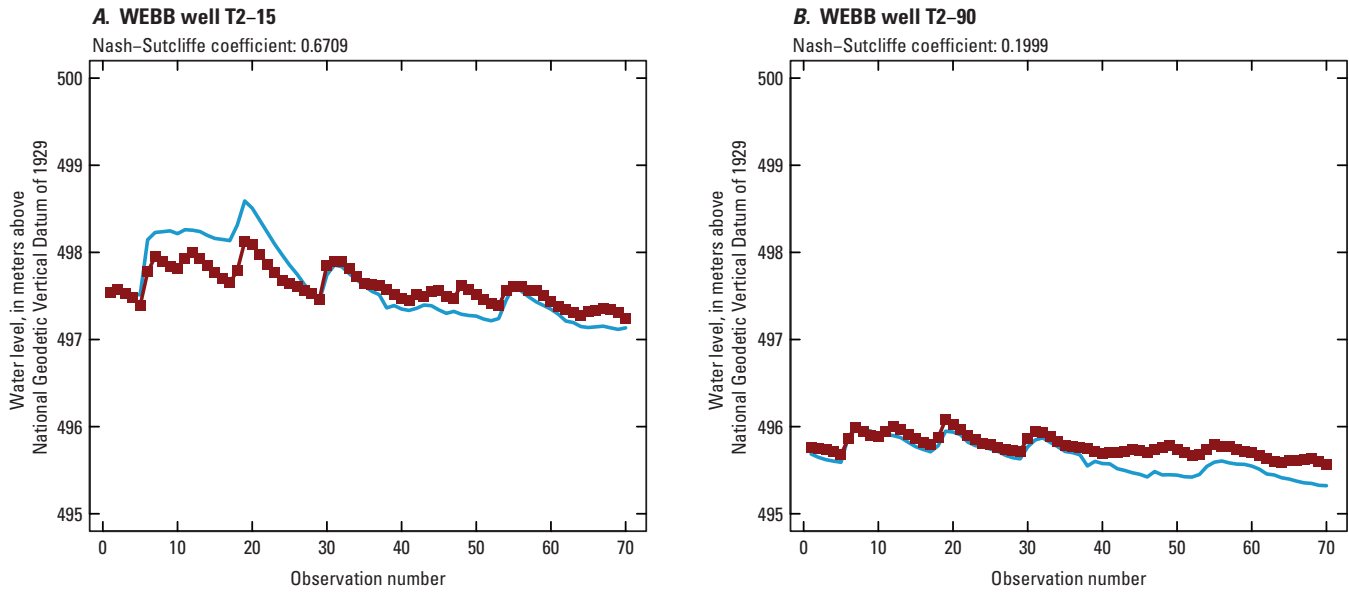


Figure 6-22. Calibration results for Water, Energy, and Biogeochemical Budgets (WEBB) wells. *A*, T2-15. *B*, T2-90. Blue lines represent observed data; red lines and symbols are the fully coupled model-simulated equivalent quantity.

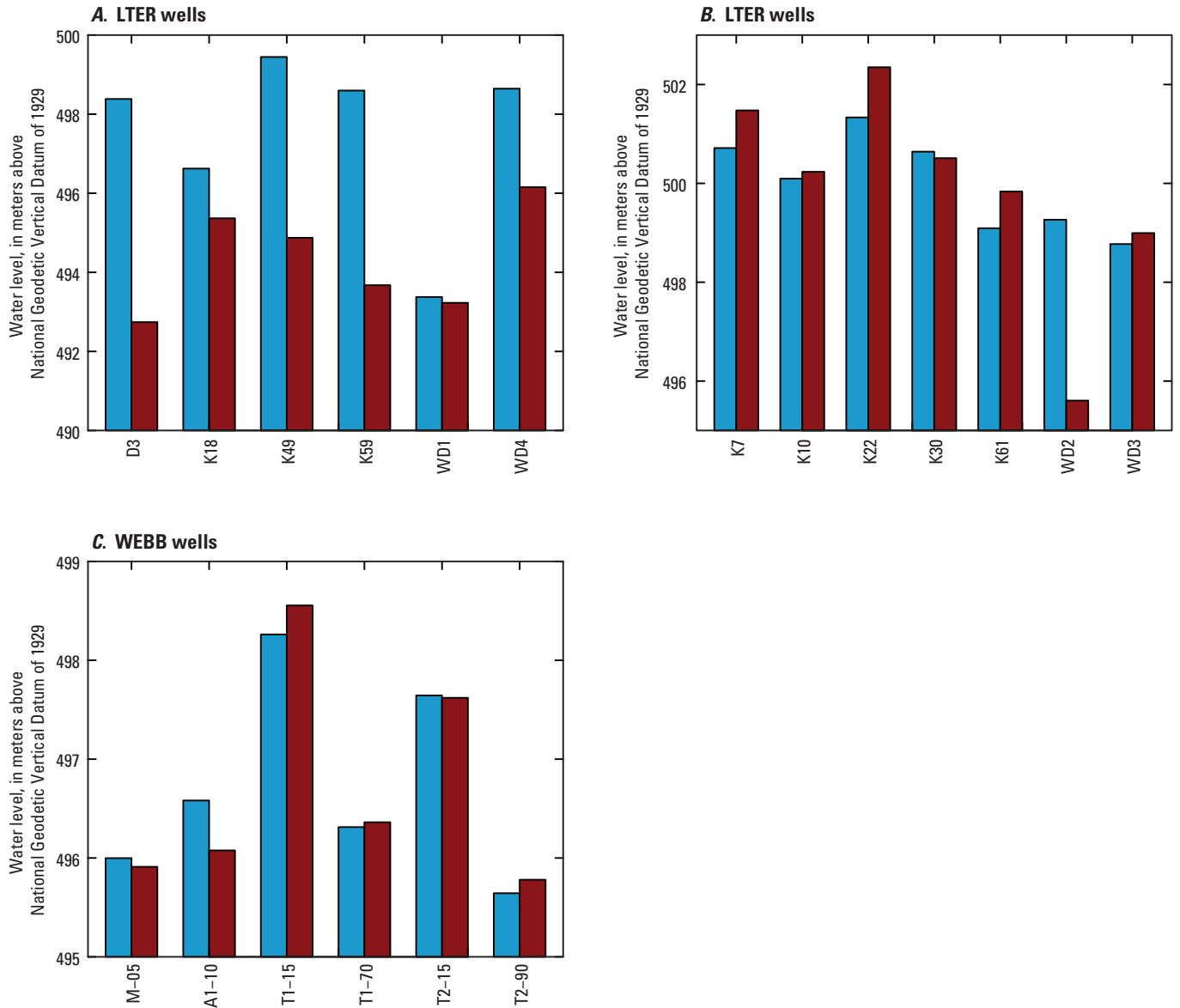


Figure 6-23. Mean water levels. *A* and *B*, Long-Term Ecological Research (LTER) wells. *C*, Water, Energy, and Biogeochemical Budgets (WEBB) wells. Blue bars are observed data; red bars are the fully coupled model-simulated equivalent quantity.

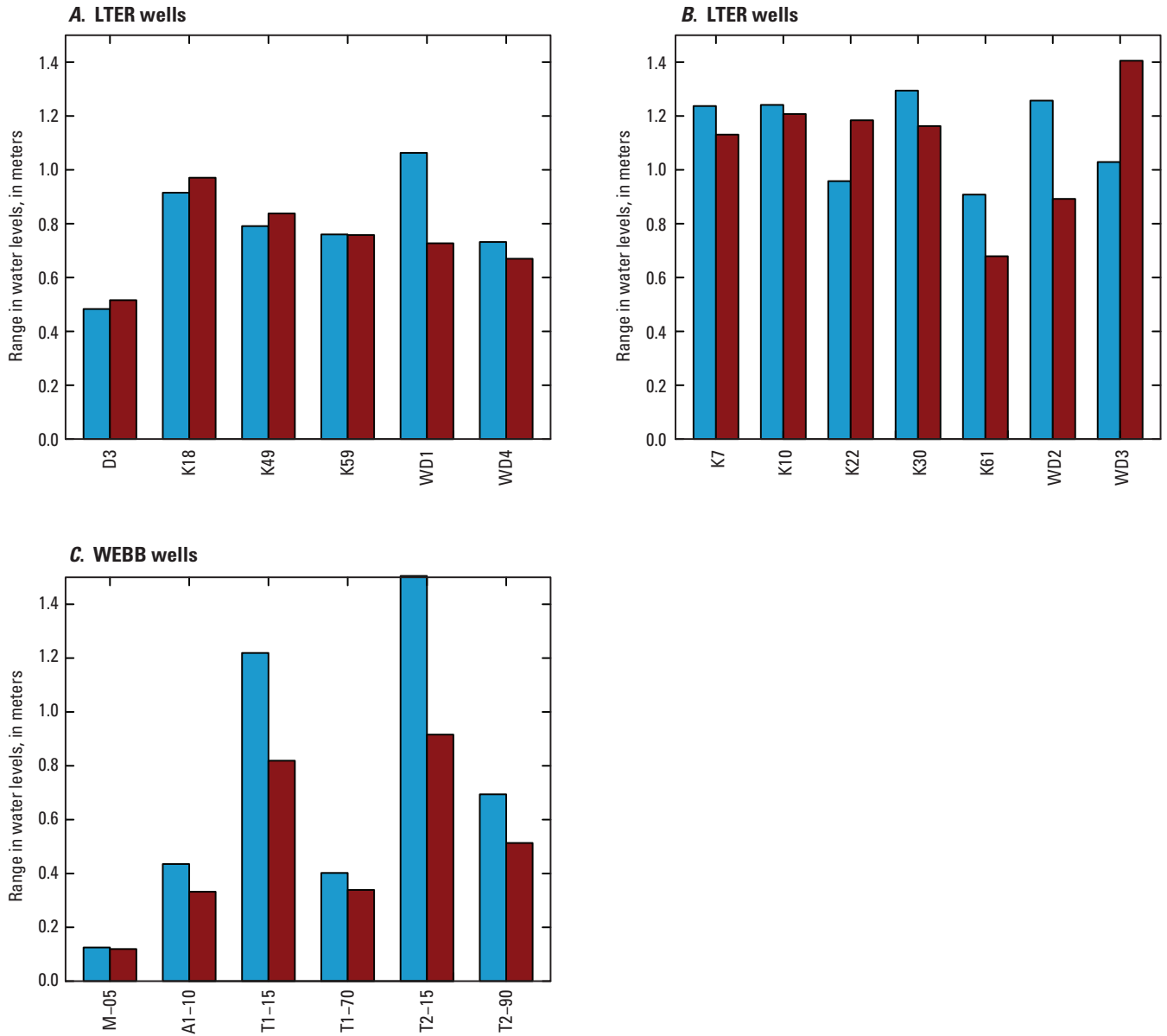


Figure 6–24. Range in water levels. *A*, and *B*, Long-Term Ecological Research (LTER) wells. *C*, Water, Energy, and Biogeochemical Budgets (WEBB) wells. Blue bars are observed data; red bars represent the fully coupled model-simulated equivalent quantity.

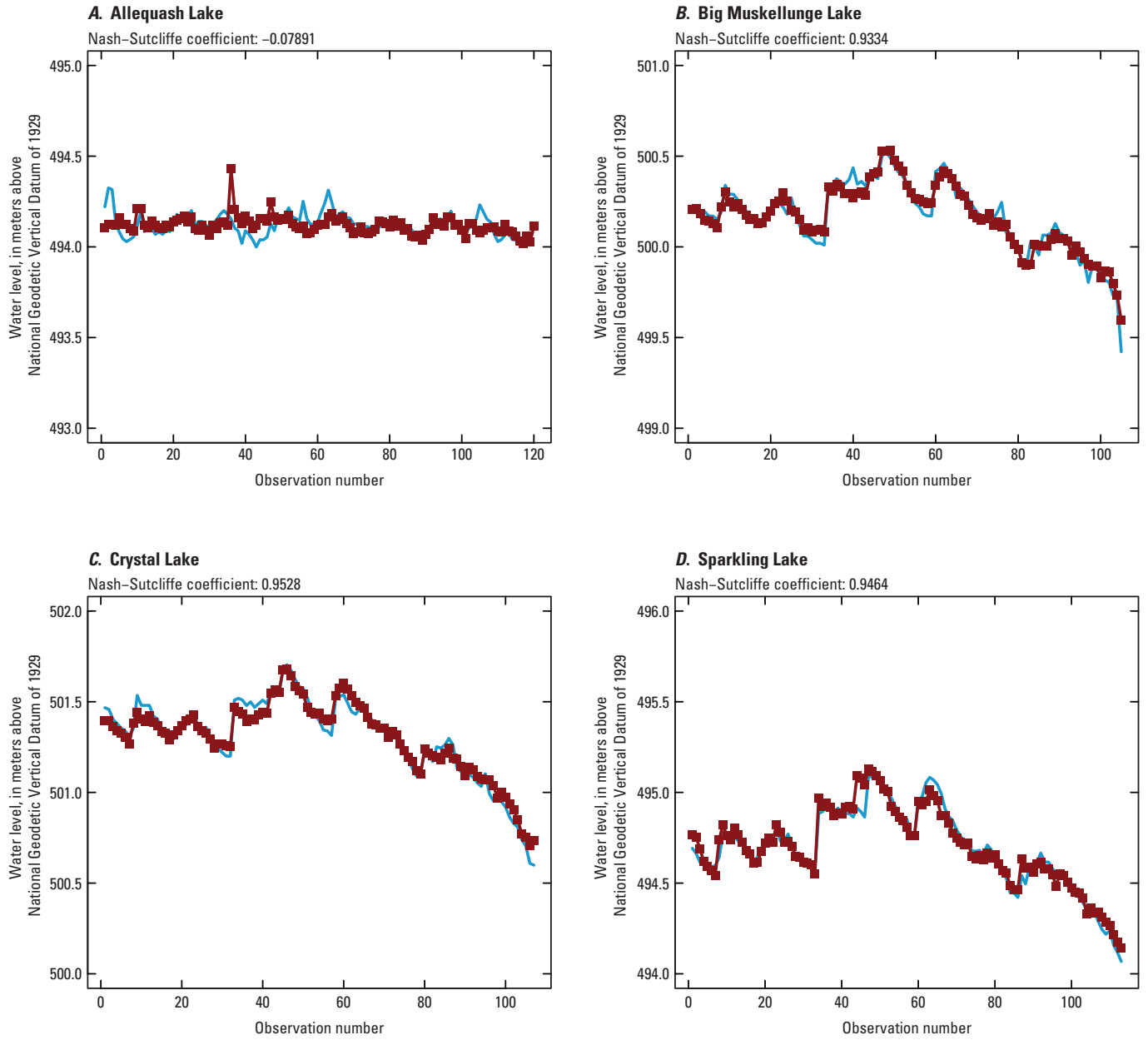


Figure 6–25. Calibration results for lake levels of the Long-Term Ecological Research (LTER) focus lakes. *A*, Allequash Lake. *B*, Big Muskellunge Lake. *C*, Crystal Lake. *D*, Sparkling Lake. Blue lines represent observed data; red lines and symbols are the fully coupled model-simulated equivalent quantity.

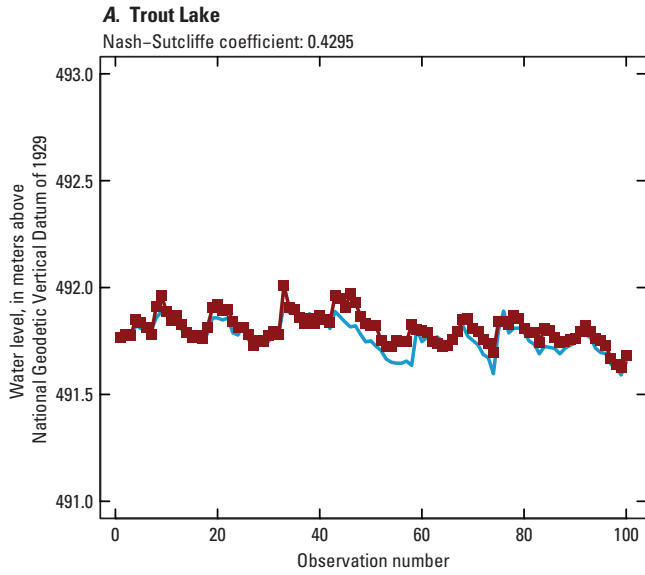


Figure 6–26. Calibration results for lake level of Trout Lake. Blue line represents observed data; red line and symbols are the fully coupled model-simulated equivalent quantity.

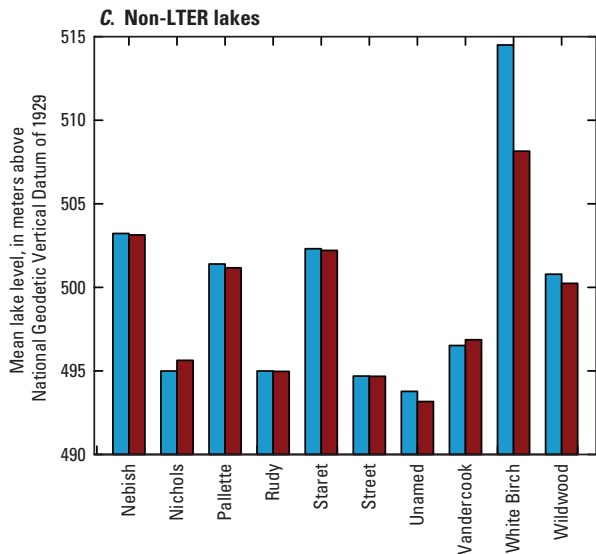
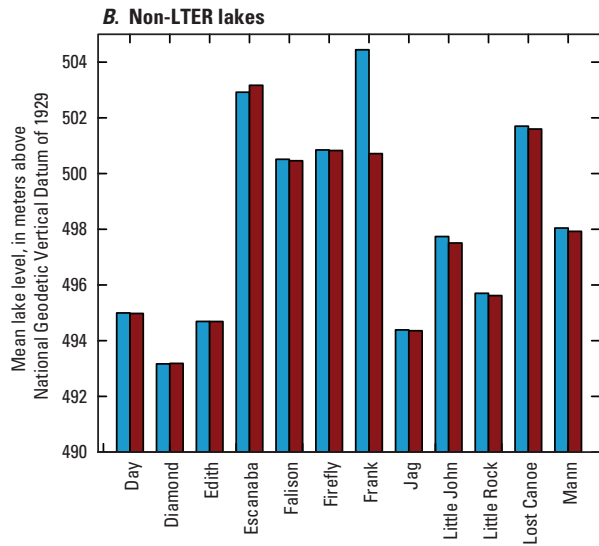
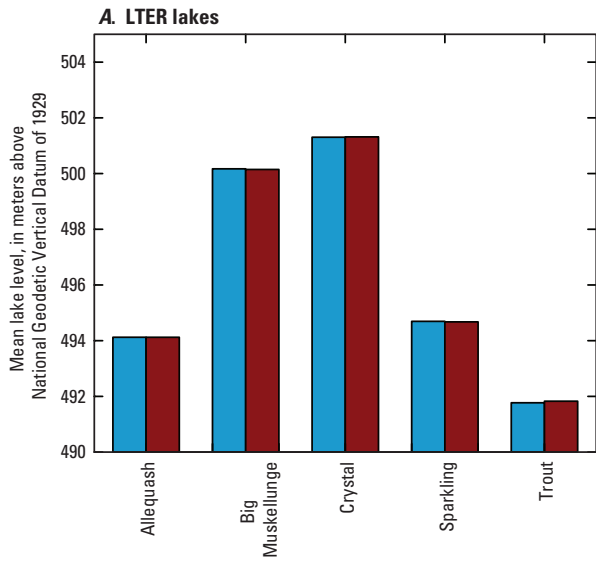


Figure 6–27. Mean lake levels for the Long-Term Ecological Research (LTER) lakes and the remaining lakes in the model domain. Blue bars are observed data; red bars represent the fully coupled model-simulated equivalent quantity.

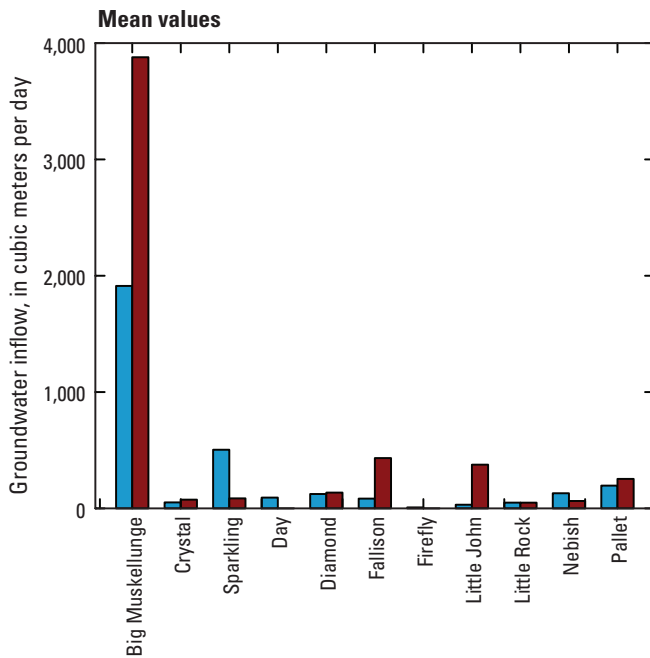


Figure 6-28. Calibration results for average groundwater inflow to selected lakes. Blue bars are observed data; red bars represent the fully coupled model-simulated equivalent quantity.

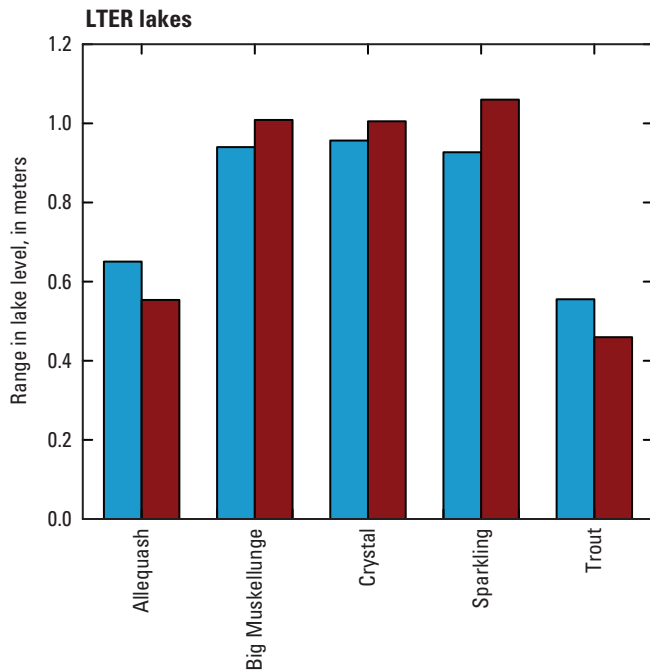


Figure 6-29. Ranges in lake levels for the Long-Term Ecological Research (LTER) lakes. Blue bars are observed data; red bars are the fully coupled model-simulated equivalent quantity.

Results of the study indicate that recharge occurred primarily during the spring snowmelt and late-fall periods—times when plants are in senescence. During the summer months when the plants are active, much of the water infiltrating into the soil is intercepted within the plant root zone.

Hydrologic fluctuations during snowmelt periods also were simulated less well than during other times of the year. The lack of representative frozen-ground processes limits the coupled model’s ability to simulate high snowmelt discharges. This discrepancy during snowmelt occurs even though the other times of the year are reasonably simulated.

As discussed in appendix 3, initially all aquifer hydraulic conductivity values were fixed at optimal values obtained during the sequentially linked calibration in order to reduce the number of parameters included in the long run times of the fully coupled model. However, the calibrated evaporation for Crystal Lake was appreciably higher than for other lakes in the watershed during the initial fully coupled calibration. Given Crystal Lake is a sheltered, small, deep lake with short fetch, this was considered unreasonable. Conceptually, an alternative mechanism to remove water from the lake was to increase groundwater outflow from the lake. In the final fully coupled calibration, layer-wide multipliers for the hydraulic conductivity of the lowest two layers were included in the calibration; choice of these layers was based on the parameter uncertainty analysis for Crystal Lake by Hunt and Doherty (2006). This approach resulted in a slightly higher value of hydraulic conductivity in the lower units (for example, compare table 6-1 to table 6-3) and facilitated enhanced groundwater exchange and reduced the calibrated value for Crystal Lake evaporation to a more reasonable value. The result underscores the need to revise initial model conceptualizations and calibration approaches with the fully coupled model, even after the sequentially linked calibration effort.

Table 6-3. Aquifer hydraulic conductivity statistics after fully coupled model calibration.

[Min, minimum; max, maximum; std, standard; m/d, meters per day; K_h , horizontal hydraulic conductivity; K_v , vertical hydraulic conductivity]

	Min (m/d)	Max (m/d)	Average (m/d)	Std deviation (m/d)	95-percent confidence interval (m/d)	
Layer 1+2						
K_h	1.1	93.2	9.5	3.4	2.7	16.3
K_v	0.3	40.0	3.0	1.3	0.3	5.7
K_h/K_v			3.2			
Layer 3+4						
K_h	1.9	6.9	3.1	0.4	2.3	3.9
K_v	0.4	4.5	0.9	0.2	0.6	1.3
K_h/K_v			3.3			
Layer 5+6						
K_h	2.5	237.6	37.3	16.6	4.1	70.4
K_v	1.0	56.2	10.5	3.8	2.8	18.1
K_h/K_v			3.6			

References Cited

- Attig, J.W., 1985, Pleistocene geology of Vilas County, Wisconsin. Wisconsin Geological and Natural History Survey Information Circular 50, 32 p.
- Doherty, J.E., and Hunt, R.J., 2010, Approaches to highly parameterized inversion—A guide to using PEST for groundwater-model calibration: U.S. Geological Survey Scientific Investigations Report 2010–5169, 60 p.
- Hunt, R.J., and Doherty, J., 2006, A strategy of constructing models to minimize prediction uncertainty, *in* MODFLOW and More 2006—Managing Ground Water Systems. Proceedings of the 7th International Conference of the International Ground Water Modeling Center: Golden, Colo., Colorado School of Mines, p. 56–60.
- Hunt, R.J., Doherty, John, and Tonkin, M.J., 2007, Are models too simple? Arguments for increased parameterization: *Ground Water*, v. 45, no. 3, p. 254–262, doi:10.1111/j.1745-6584.2007.00316.x.
- Hunt, R.J.; Strand, Mac; and Walker, J.F., 2006, Measuring groundwater-surface water interaction and its effect on wetland stream benthic productivity, Trout Lake Watershed, northern Wisconsin, USA: *Journal of Hydrology*, v. 320, p. 370–384.
- Kenoyer, G.J., 1988, Tracer test analysis of anisotropy in hydraulic conductivity of granular aquifers: *Ground Water Monitoring and Remediation*, v. 8, no. 3, p. 67–70. doi:10.1111/j.1745-6592.1988.tb01086.x.
- Pint, C.D., 2002, A groundwater flow model of the Trout Lake Basin, Wisconsin—Calibration and lake capture zone analysis: University of Wisconsin-Madison, M.S. thesis, 123 p.

Publishing support provided by the U.S. Geological Survey
Science Publishing Network,
Columbus Publishing Service Center

For more information concerning the research in this report,
contact the

Director, Wisconsin Water Science Center
U.S. Geological Survey
8505 Research Way
Middleton, WI 53562
<http://wi.water.usgs.gov/>

